

## N O T I C E

THIS DOCUMENT HAS BEEN REPRODUCED FROM  
MICROFICHE. ALTHOUGH IT IS RECOGNIZED THAT  
CERTAIN PORTIONS ARE ILLEGIBLE, IT IS BEING RELEASED  
IN THE INTEREST OF MAKING AVAILABLE AS MUCH  
INFORMATION AS POSSIBLE



"Made available under NASA sponsorship  
in the interest of early and wide dis-  
semination of Earth Resources Survey  
Program information and without liability  
for any use made thereof."

NASA 80-1024a  
CR 154634  
KSC TR 51-3

# INSTITUTE OF FOOD AND AGRICULTURAL SCIENCES

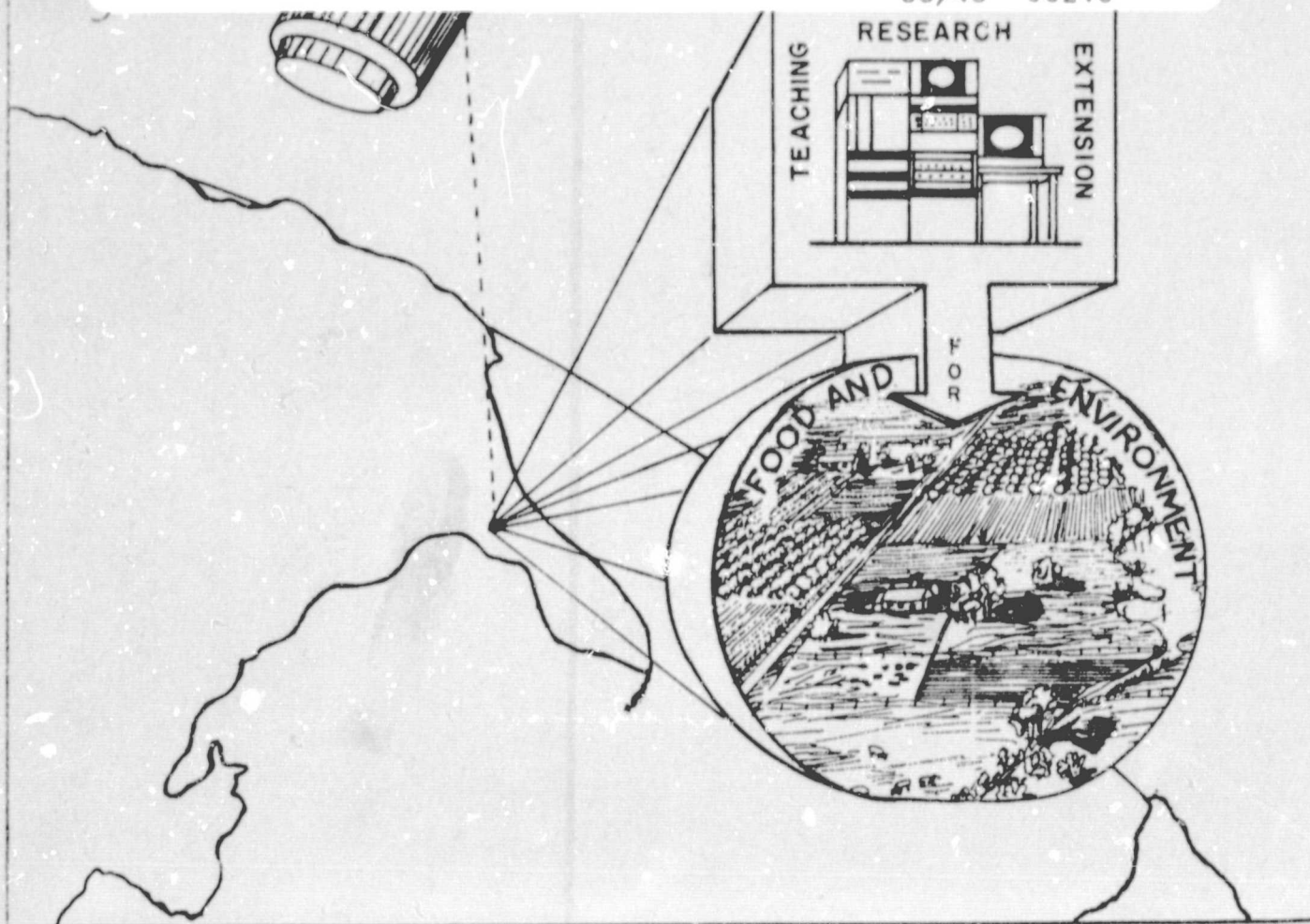
## UNIVERSITY OF FLORIDA

(E80-10246) FLORIDA WATER RESOURCES Final  
Report (Florida Univ.) 325 p HC A14/MF A01  
CSCL 08H

N80-30829

Unclas

G3/43 00246



In Cooperation With:

National Aeronautics and Space Administration  
South Florida Water Management District

FLORIDA WATER RESOURCES - NAS10-9348

Final Report

Original photography may be purchased from  
EROS Data Center

Sioux Falls, SD

April 1980

FLORIDA WATER RESOURCES MANAGEMENT  
RTOP (UPN 177-55-91)

TABLE OF CONTENTS

	<u>Page</u>
1.0 Abstract . . . . .	1.0-1
2.0 Introduction . . . . .	2.0-1
2.1 Florida Water Problem . . . . .	2.0-4
2.2 History of Florida Water Management . . . . .	2.0-6
2.3 Project Origin . . . . .	2.0-7
3.0 Project Description . . . . .	3.0-1
3.1 Task Description . . . . .	3.0-4
3.2 Project Management Team . . . . .	3.0-5
4.0 Project Status . . . . .	4.0-1
5.0 Task Activities . . . . .	5.0-1
5.1 Lake Okeechobee Volume Measurements . . . . .	5.1-1
5.1.1 Background . . . . .	5.1-5
5.1.2 Remote Sensing Data Analysis . . . . .	5.1-5
5.1.3 Water Budget Calculations . . . . .	5.1-9
5.1.4 References . . . . .	5.1-21
5.1-5 Conclusions . . . . .	5.1-22
5.2 Improvement of Conservation Area Water Storage Information . . . . .	5.2-1
5.2.1 Background . . . . .	5.2-5
5.2.2 Remote Sensing Data Analysis . . . . .	5.2-5
5.2.3 Water Budget Calculations . . . . .	5.2-13
5.2.4 References . . . . .	5.2-17
5.2.5 Conclusions . . . . .	5.2-18
5.3 Overland Flow Measurements . . . . .	5.3-1
5.3.1 Remote Sensing Data Analysis . . . . .	5.3-7
5.3.2 Development of Manning's N Data . . . . .	5.3-7
5.3.3 Hydrologic Model Calculations . . . . .	5.3-20
5.3.4 References . . . . .	5.3-87
5.3-5 Conclusions . . . . .	5.3-89
5.4 New Technology for Lake Volume Measurements . . . . .	5.4-1
5.4.1 Collection of Remote Sensing Data . . . . .	5.4-5
5.4.2 Measurements of Volume of East Lake Tohopekaliga . . . . .	5.4-6
5.4.3 Calculation of Lake Volume . . . . .	5.4-9
5.4.4 References . . . . .	5.4-34
5.4.5 Conclusions . . . . .	5.4-35
5.4.6 Appendix I - Program Listing . . . . .	5.4-36

	<u>Page</u>
5.5 Rainfall Estimates from GOES IR Digital Data . . . . .	5.5-1
5.5.1 Introduction . . . . .	5.5-5
5.5.2 Method of Scofield and Oliver . . . . .	5.5-5
5.5.3 Data Analysis . . . . .	5.5-5
5.5.4 Other Methods Using Satellite Data . . . . .	5.5-9
5.5.5 References . . . . .	5.5-12
5.5.6 Conclusions . . . . .	5.5-13
5.6 Evapotranspiration Measurements . . . . .	5.6-1
5.6.1 Remote Sensing Data Collection . . . . .	5.6-6
5.6.2 Evapotranspiration Calculations . . . . .	5.6-7
5.6.3 References . . . . .	5.6-84
5.6.4 Conclusions . . . . .	5.6-87
5.7 Three-Dimensional Aquifer Model . . . . .	5.7-1
5.8 Long Range Plan . . . . .	5.8-1

- 1.0-1 -

1.0 ABSTRACT

The State of Florida has a very different set of hydrological cycle systems which make it unique among the southeastern states. These unique water supply and storage factors within this system contribute to problems within the state concerning the availability of water to meet the expanding competitive needs of the state's urban, industrial, and agricultural communities.

There is a direct conflict created within the state on the demand of water by the various users. In the past the large agricultural demand has not created any problem; however, with the rapid population increases in the state and the new industrial expansion, the user conflict grows daily. This growing conflict between users, coupled with the unique Florida hydrological supply problem, creates a delicate balance between supply and demand which requires specific extensive data bases and models to help water resources managers make realistic decisions concerning their water resources.

The University of Florida, Institute of Food and Agricultural Sciences (IFAS) had been previously working with several of the Florida Water Management Districts, and therefore was familiar with many of their problems. The IFAS had also been working with the National Aeronautic and Space Administration (NASA) Kennedy Space Center Applications Projects Branch (KSC) on remote sensing research projects directed toward applying NASA technology to agricultural problems. With this background IFAS and KSC recognized that many developments in space technology had potential for application to the critical problem of Florida's water resources. Since the South Florida Water Management District (SFWMD) had been in operation for many years and had worked with IFAS on water management data needs in the past, it was decided to develop a joint Water Resources project among IFAS, NASA, and SFWMD. This resulted in the submission of a NASA funded Florida Water Resources Management, Research and Technology Objectives and Plans (RTOP) (UPN 177-55-91) in June of 1977. This project proposal not only included a beginning effort of the development of remote sensing data techniques for the SFWMD, of more significance it required the development of a Long Range Plan. This Long Range Plan would include the cooperation of all five Florida Water Management Districts and culminate in the development of a state-wide Water Resources Management Information System, based on state-of-the-art remote sensing and Automatic Data Processing (ADP) technology, which would provide an adequate data base to help all of the Water Management Districts solve their critical water supply and water use allocation problems. The project was proposed as a five-year research program, however due to NASA funding problems, only one year of the research program was funded. Therefore, the results of the research program can only be considered interim and further research would be required to develop final conclusions.

This one-year research project consisted of seven tasks along with the development of a proposed Long Range Plan required to implement the entire five-year research program which would result in a Florida Water Resources Management Information System that could be used by all of the five Florida Water Management Districts. A condensation of the purpose and results of these technical tasks and the Long Range Planning task are included hereinafter.

A method was developed whereby the water balance budget model results for Lake Okeechobee could be improved by using LANDSAT data to map the complex littoral zone vegetation by combining these plant community data with their

respective transpiration rates. The model results based on this LANDSAT information demonstrated a 94 percent reduction in cumulative lake stage error and a 70 percent reduction in the maximum deviation of the lake stage. To verify its general applicability, the improvements in water volume prediction using this method should be tested in other lake and marshland communities.

In south Florida (SFWMD), large tracts of grassy marshland have been set aside to act as natural water conservation areas. Vast amounts of water stored in the three major conservation areas are questionable because these areas are large, remote, and almost flat. A remote sensing technique using LANDSAT radiance values from Band 5 and Band 7 for October 17, 1976 in Conservation Area 3a were used to correlate with known water depths, thus producing a complete water depth map for the area. Correlation coefficients as high as 0.75 were obtained using this technique. The volume of the storage area was calculated for various stages and compared to conventional data. The results of this comparison showed errors from 0 to 30 percent with the largest error existing between 7.17 and 8.17 ft MSL. Further research is needed to develop this technique for all stage levels and to test it in other conservation areas.

The mapping of the vast Florida wetland areas is a difficult task due to the difficulty of obtaining access to the areas. Also very little research has been done on the flow resistance characteristics of these natural vegetation communities that one value of Manning's N roughness coefficient has frequently been used. A task was undertaken wherein LANDSAT data was used to classify a typical marshland drainage basin, Chandler Slough in the Kissimmee River Basin, into six vegetation categories. Detailed flow measurements were made at various water depths throughout a yearly vegetation growth cycle at some twenty-one test sites throughout the area. From these flow measurements a family of Manning's N flow curves were developed for each complex vegetation test site for various water depths at various growth seasons. These Manning's N curves are being used by the SFWMD to develop better information to deal with water resources problems in marshland vegetated flow areas, such as flood routing, backwater curve computation, channel improvement and scour problems, etc.

The concept of lake volume measurement from satellite surface temperature data is to predict lake volume from the energy balance of the lake. The differential time-rate of change in internal energy of a column in the body of water would be equal to the sum of the exchanges of all energy flux density components. A test of this theory was completed using a typical shallow Florida lake, East Lake Tohopekaliga near St. Cloud. On April 11 and 12, 1978 aircraft thermal scanner data over a 24-hour period was gathered for the lake along with considerable surface and subsurface data using an instrumented boat. Sounding information to calculate actual lake volume was gathered by the SFWMD. Calculations from these data did not adequately predict the average lake depth due to thermal stratification of the lake. Therefore, a stratified lake model (a FORTRAN program called LKVOL) was developed to predict lake depth and volume from measurement of internal energy change and energy flux exchanges. Calculated lake areas and volumes compared to actual values were at best within 10% of each other using the various methods. It does not appear that the procedure as now developed would consistently provide sufficiently accurate results for operational use. More actual test data needs to be gathered to further refine and develop the lake volume model.

3

Present methods of obtaining rainfall amounts over large areas are unsatisfactory because rain gauges are placed far apart and their point records do not reflect true amounts received on the whole ground surface. A method developed by Scofield and Oliver (1977), based on the empirical relationship that in convection cumulus clouds there appears to be a correlation between the cloud top brightness temperatures and the temperature gradient to the amount of rainfall. Software was developed to use half-hourly GOES imageries to measure these temperature relationships by the Scofield and Oliver methods and check the developed rainfall data against ground based radar data (from the University of Miami) and rain gauges. However, due to the lack of coordinated GOES and radar data, adequate correlation was not obtained. Other similar research by Griffith (1978) and Follanshee (1973) does indicate that such methods could provide very useful rainfall data for the Florida Water Management Districts. Further testing of these methods within the Florida climatological regime needs to be accomplished to make such a system operational.

A typical Florida drainage basin, Taylor Creek in south Florida, was chosen to test methods of developing evapotranspiration (ET) values for various vegetation types and climatological conditions using aerial thermal scanner radiation data and ground measured climatological data. Three methods were investigated for calculating ET on a regional basis. All computed sensible heat flux density first, and then computed ET from the energy balance equation. The first was to compute a bulk aerial resistance ( $r_b$ ) from the ground truth sensible heat flux measurement, and from remote sensed surface temperature, and from air temperature. The second method was to develop atmospheric stability-corrected heat transport coefficients to apply in the turbulent boundary layer above the grass surfaces. It was found that the temperature difference in the turbulent layer ( $\Delta T_t$ ) could be accurately calculated from the surface temperature to air temperature difference ( $\Delta T_T$ ). This  $\Delta T_t$  was then used in calculating ET by first calculating the sensible heat flux ( $H$ ). The third method used integrated profile stability corrections. Accurate predictions from this method require the ability to determine the effective height of the heat source ( $Z_H$ ) to apply to the effective source temperature. Once this value was determined, the regional ET calculations were made for the pasture scene. The methodology was tested only over short grass surfaces. Future work is needed on other types of vegetated surfaces to better define effects of wind speed, stability, surface roughness, plant height, leaf area index, and soil moisture conditions on aerial resistances. Comparisons should also be made between ET computed by relatively detailed surface temperature measurements and relatively large-scale pixel temperature measurements.

An evaluation was made of the SFWMD three-dimensional aquifer model to determine the feasibility of using remote sensing techniques to supply a data base for the model. Remote sensing is most applicable in defining parameters which follow the movement of water on the surface, in describing the areal extent of surface conditions (e.g., geology, drainage, vegetation) which might affect both surface flow and flow between surface and groundwater, and in locating direct evidence of links between groundwater and surface water (e.g., free-flowing wells, areas of good drainage). Radar sensors currently under development may soon extend this range below the surface. Further development of this model by the SFWMD should be guided to allow the better use of remote sensing as a data base.

The final goal of the project was to develop a complete Water Resources Management Information System based on the latest state-of-the-art remote sensing and data processing technology and to demonstrate and then implement this system on the various Water Management Districts' computer hardware. To develop a Long Range Plan for accomplishing this goal, a joint NASA, IFAS, and WMD study team was chartered. Major planning meetings were held with four of the five Water Management Districts from the beginning of the project in March 1978 through June 1978, when the FY '80 research proposal was due into NASA Headquarters. From these meetings twelve detailed research tasks were defined. Five major areas of concern that tended to be common to all Water Management Districts were uncovered. These were: Hydrology, Water Use, Environmental, Climatology, and a Data Base Management System. These major areas of concern were the areas wherein the Long Range Plan would concentrate in developing means for meeting all of the common needs of the Water Management Districts which would culminate in a complete Water Resources Management Information System. In August of 1978 notice was received from NASA Headquarters that the proposed five-year research and development program, proposed in June 1978, could not be funded due to limited NASA funds availability. Therefore further development of the Long Range Plan ended and effort was concentrated on documenting the results of the first year's study, depicted in the following detailed report.

- 2.0-1 -

## 2.0 INTRODUCTION

TABLE OF CONTENTS

	<u>Page</u>
2.0 Introduction . . . . .	2.0-1
2.1 Florida Water Problem . . . . .	2.0-4
2.2 History of Florida Water Management . . . . .	2.0-6
2.3 Project Origin . . . . .	2.0-7

FIGURES

<u>Figure No.</u>	<u>Page</u>
2.1-1 Schematic Diagram of the Hydrologic Cycle . . . . .	2.0-5
2.2-1 State of Florida Water Management Districts . . . . .	2.0-8

## 2.1 Florida Water Problem

The State of Florida has a very different set of hydrological cycle (see Figure 2.1-1) systems which make it unique among the southeastern states. These unique water supply and storage factors within this system contribute to problems within the state concerning the availability of water to meet the expanding competitive needs of the state's urban, industrial, and agricultural communities.

Even though the annual rainfall within the state is rather high by comparison to that of other states, the seasonal and geographical characteristics of this rainfall cause considerable problems. The rainfall is primarily convectional which produces varying rainfall patterns across the state. This varied pattern of rainfall can cause some of the areas of the state to experience droughts while other areas are experiencing flooding.

The evapotranspiration function of the unique Florida hydrological cycle causes over 70% of this available rainfall to be lost to the atmosphere. The remaining 30% of the available water from rainfall flows constantly from the inland regions to the surrounding Gulf of Mexico or Atlantic Ocean, either by overland flow or through the aquifers. Florida receives very little water from other geographic areas, therefore it must depend upon capturing what rainfall falls within its boundaries before it runs off.

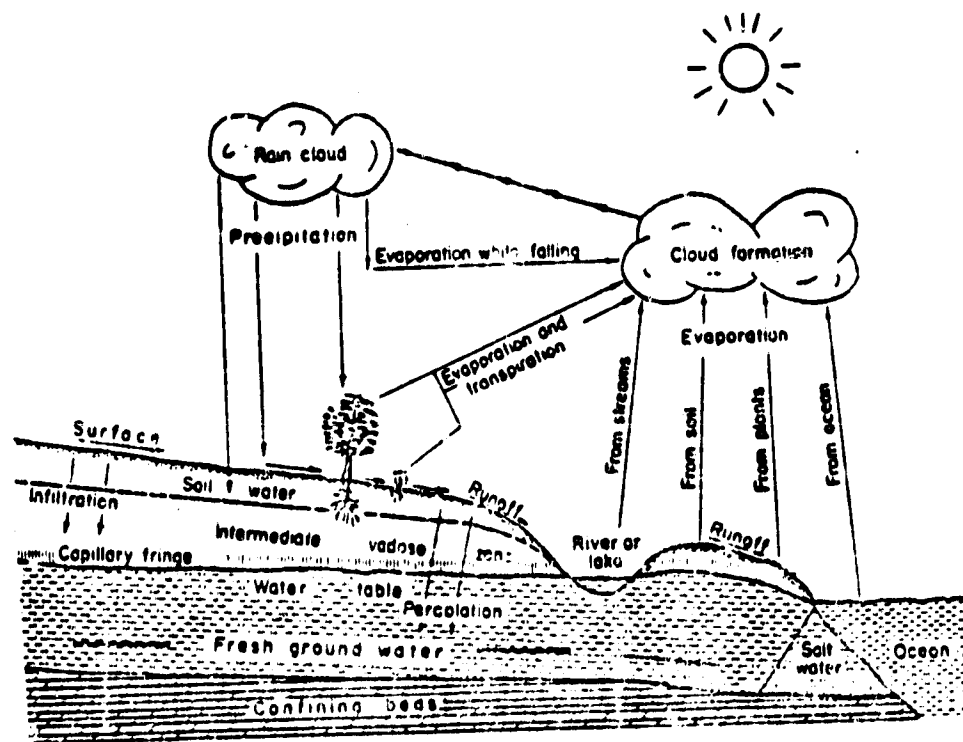
The surface storage of this runoff is complicated by the unique Florida hydrological parameters in that the sandy soil, shallow lake depths, and large flat marshland areas make surface storage of adequate water difficult. The subsurface limestone plateau which underlies most of Florida causes much of this surface water to be rapidly moved to the lower aquifer levels.

Thus much of the fresh water supply must be drawn from the aquifers which are being constantly recharged by rainfall from adjacent geographical areas. Therefore, any withdrawal above the recharge rate can cause excessive aquifer drawdown and the fresh water in the aquifer can become contaminated by the salt water it overlies, not only along the coast, but inland as well.

Much of the available surface water within the state is required to maintain the diverse and sensitive environmental systems such as the estuarine and marshland areas. The terrestrial systems throughout the state depend on established aquifer water table levels for their existence and any significant change may result in vegetation being replaced by other, perhaps less desirable, ecosystems.

All of these problems with the water supply and the natural demand thereon form a critical situation even before the activities of man place demands upon this important resource.

The demands of man on the limited Florida water supply form a complex network of geographical, seasonal, and physical factors that complicate the water use problem. These demands on the Florida water supply consist mainly of urban, industrial, and agricultural usages.



Schematic diagram of the hydrologic cycle

Figure 2.1-1

The rapid urban development of the Florida coastal zones has tended to localize this water demand in an area that, because of the natural hydrological cycle characteristics, does not have an adequate water supply to start with. Thus an even greater impact is placed on the demand of water in these areas than exists from the natural ecosystem.

Some of the high demand industrial requirements, such as the phosphate mining operations, also tend to localize around the central part of the state thus creating an impact on the water supply in that area.

The agricultural demand for water within the state presents the largest of all the water demands. This agricultural demand is not specifically geographically located; however, it does tend to be seasonally specific. This need for agricultural water during specific seasons of the year does impact the other urban and industrial demand on water during these seasons.

Thus there is a direct conflict created within the state on the demand of water by the various users. In the past the large agricultural demand has not created any problem; however, with the rapid population increases in the state and the new industrial expansion, the user conflict grows daily. This growing conflict between users, coupled with the unique Florida hydrological supply problems, creates a delicate balance between supply and demand which require specific extensive data bases and models to help water resources managers make realistic decisions concerning their water resources.

## 2.2 History of Florida Water Management

The management of the water resources within the state of Florida is a rather recent function. In the past the management of water within the state was prompted through flooding within the stream flood plains wherein such flooding interfered with agricultural and residential development. Thus early water oriented legislation enacted by the state was in response to these extreme climatic events.

For example in response to the floods of 1947 and 1948, the State Legislature created the Central and Southern Florida Flood Control District and provided for their local sponsorship and state participation in the vast U.S. Corps of Engineers' Central and Southern Flood Control Project. In 1961, in response to the 1960 hurricane-related floods in the Tampa area, the State Legislature established the Southwest Florida Water Management District for local sponsorship of the U.S. Corps of Engineers' Four River Basin Project.

Since the 1960 flood event, the state of Florida has experienced a completely different hydrologic situation, namely a lack of rainfall. This change in available rainfall was accompanied by a rapidly expanding population, as well as an expanded water use in the industrial and agricultural areas, thus creating a supply and demand problem. In the early 1970's this deficiency became very acute in some areas. Again the State Legislature reacted, but this time it set up a coordinated system of water management districts covering the entire state through the Water Resources Act of 1972. The passage of this act surpassed all of the previous water management laws of the state of Florida in its scope and purpose. In fact, the National Water Commission's Summary of the State Water Laws calls the act probably the most

progressive water management legislation ever enacted by any state. This act created five Water Management Districts (Figure 2.2-1) whose areas of jurisdiction are described around hydrologic not political boundaries. The Act also set down the state's policies as they relate to water resources and established a comprehensive mechanism to carry out these policies.

The newly enacted legislation stated that these novice Water Management Districts (WMD), except for the South Florida Water Management District (SFWMD), were required to develop a Water Use and Supply Development Plan (thorough the year 2020) and immediately accomplish the on-going functions of planning, operations, and regulation of the water resources in their districts. This legislation also empowered them with taxing authority to accomplish their responsibilities.

Thus these newly formed Water Management Districts were immediately faced with the problems of accomplishing all of the administrative functions required of them, but more important they forced the responsibility of allocating a declining water supply over an ever growing and conflicting water demand within the urban, industrial, and agricultural communities. Thus the districts needed to take advantage of every time and cost saving technology available to them.

### 2.3 Project Origin

During the past several years a working relationship has been built up between the NASA Kennedy Space Center Applications Projects Branch (SA-APP) and the University of Florida, Institute of Food and Agricultural Sciences (IFAS), through remote sensing research projects such as the Satellite Freeze Forecast System and several small Regional Applications projects. In 1975, IFAS had completed a study of agricultural water needs within the state, Agricultural Growth in An Urban Age (AGUA), in which they documented the future shortage of agricultural water and the potential impact of agricultural water needs on the rapidly expanding commercial, industrial, and urban needs. The IFAS had been previously working with several of the Florida Water Management Districts, and therefore was familiar with many of their problems. With this background IFAS and KSC recognized that many developments in space technology had potential for application to the critical problem of Florida's water resources. Since the SFWMD had been in operation for many years and had worked with IFAS on water management data needs in the past, it was decided to develop a joint Water Resources project among IFAS, NASA, and SFWMD. This resulted in the submission of a Florida Water Resources Management RTOP (UPN 177-55-91) in June of 1977.

This project proposal not only included a beginning effort of the development of remote sensing data techniques for the SFWMD, of more significance it required the development of a Long Range Plan. This Long Range Plan would include the cooperation of all five Florida Water Management Districts and culminate in the development of a state-wide Water Resources Management Information System, based on state-of-the-art remote sensing and ADP technology, which would provide an adequate data base to help all of the Water Management Districts solve their critical water supply and water use allocation problems.

# STATE OF FLORIDA WATER MANAGEMENT DISTRICTS

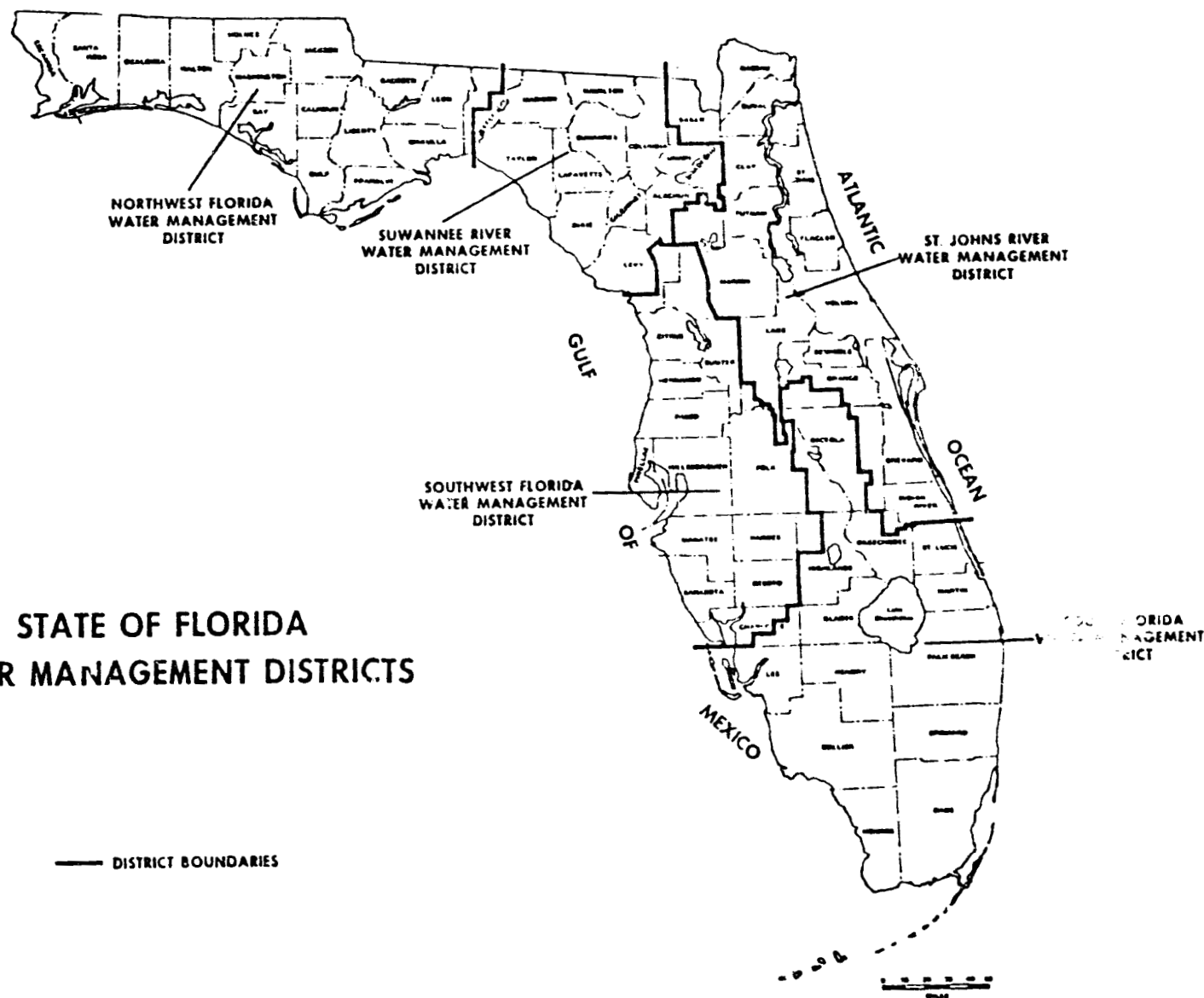


Figure 2.2-1

- 3.0-1 -

### 3.0 PROJECT DESCRIPTION

TABLE OF CONTENTS

	<u>Page</u>
3.0 Project Description . . . . .	3.0-1
3.1 Task Description . . . . .	3.0-4
3.1.1 Lake Okeechobee Volume Measurements . . . . .	3.0-4
3.1.2 Improvement of Conservation Area Water Storage Information . .	3.0-4
3.1.3 Overland Flow Measurements . . . . .	3.0-4
3.1.4 New Techniques for Lake Volume . . . . .	3.0-4
3.1.5 Rainfall Distribution . . . . .	3.0-4
3.1.6 Evapotranspiration Measurements . . . . .	3.0-4
3.1.7 Three-Dimensional Aquifer Model . . . . .	3.0-5
3.1.8 Long Range Planning . . . . .	3.0-5
3.2 Project Management Team . . . . .	3.0-5

FIGURES

<u>Figure No.</u>	<u>Page</u>
3.2-1 Project Management Teams . . . . .	3.0-6

### 3.1 Task Description

For continuity, this section includes a very brief description of the specific tasks defined for the project. A more detailed description of these tasks is included in the Task Activities section of this report.

#### 3.1.1 Lake Okeechobee Volume Measurements

The actual storage volume of available water in Lake Okeechobee is not known to any great accuracy. Therefore, a task was defined to develop a technique using LANDSAT data to better determine the volume of the lake at various stages, based partly on a stage correlation to a classification of vegetation within the lake littoral zone.

#### 3.1.2 Improvement of Conservation Area Water Storage Information

Determining the volume of water stored in the vast marshland conservation storage areas is a very difficult task. A correlation between LANDSAT radiance values and conservation area water depths would assist in solving this problem.

#### 3.1.3 Overland Flow Measurements

Calculating water flows through the marshland areas is a very difficult task since this flow varies widely with respect to water depth and vegetation type. A seasonal vegetation classification using LANDSAT data, correlated to field flow measurements would greatly improve the required flow calculations.

#### 3.1.4 New Techniques for Lake Volume

Much of the fresh water storage in Florida is contained in the thousands of shallow lakes within the state. If an estimate of the volume of these lakes could be obtained from a relationship to their diurnal thermal cycle, thermal data being obtained from satellite, a more cost effective volume measurement would be available.

#### 3.1.5 Rainfall Distribution

Due to the prevalence of convectional rainfall within the state it is very difficult to determine the rainfall distribution throughout a watershed or a water storage area. Techniques developed by NOAA for other areas indicate that information concerning rainfall distribution can be developed using GOES data to measure the change in cloud top temperature. This technique needs to be modified for use with the unique Florida convection rainfall conditions.

#### 3.1.6 Evapotranspiration Measurements

Evapotranspiration constitutes at least 70% of the water budget calculation. Using GOES satellite to obtain a relative measurement of net radiation, the major component in evapotranspiration calculations, better information concerning the areal distribution of evapotranspiration can be obtained.

### 3.1.7 Three-Dimensional Aquifer Model

The determination of the movement of water within aquifers is a very important data need to the SFWMD. The development of such an aquifer model is underway by the SFWMD. Due to the vastness of such aquifers, an easier method is needed to supply such a model with a data base. The SFWMD model will be reviewed to determine if remote sensing can be used to provide a portion of this data base.

### 3.1.8 Long Range Planning

The major need of all Water Management Districts is an adequate current data base to provide information for planning, operation, and regulatory functions that will allow managers to make decisions involving water availability, storage, transportation, usage, and socio-economic impacts. A complete study needs to be made to develop a Long Range Plan which will result in the development of a Water Resources Management Information System (WRMIS) which would use as much remote sensing data as possible.

## 3.2 Project Management Team

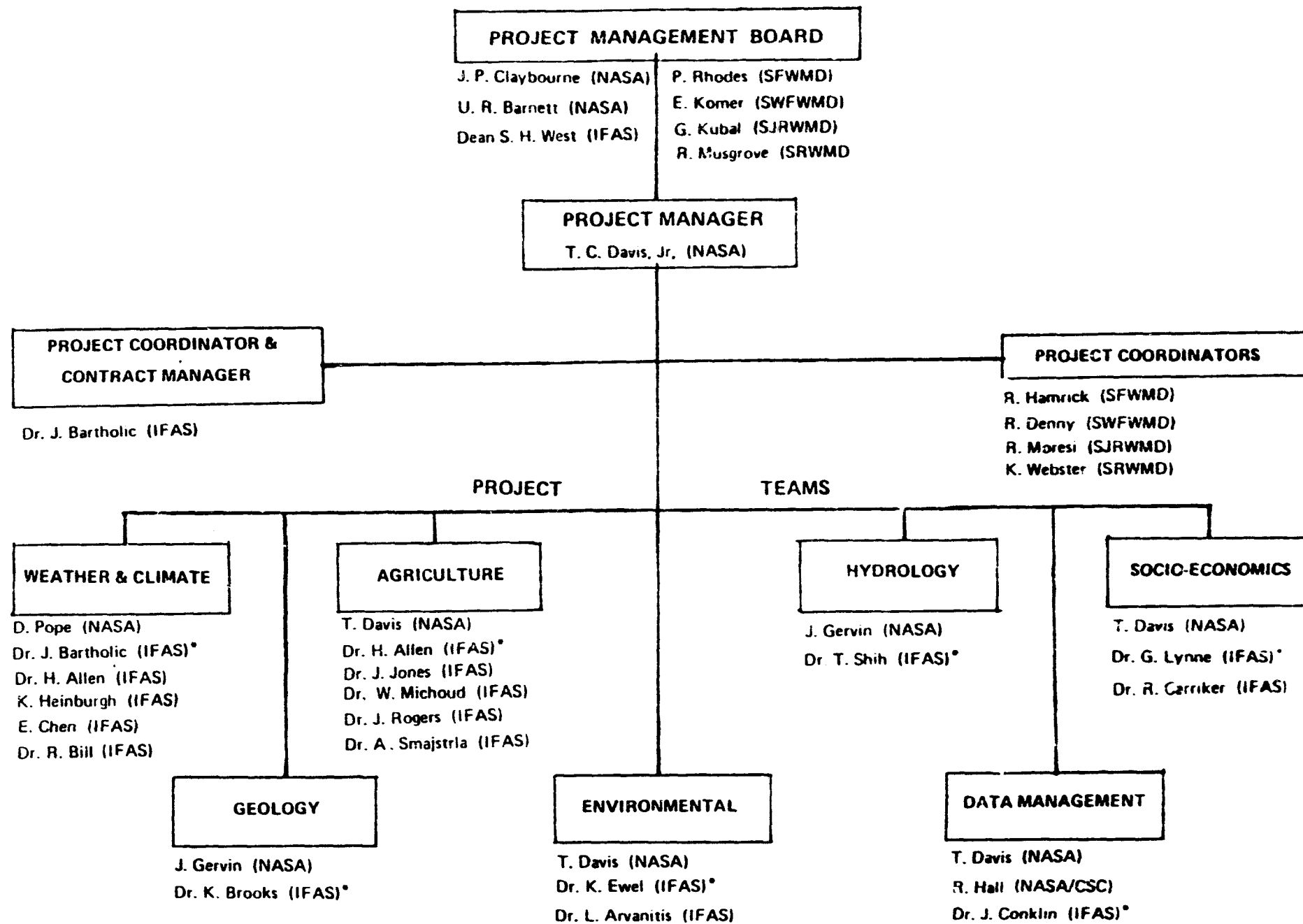
The proposed project was a very complex one, that is the need to determine the requirements of the five Florida Water Management Districts across a vast span of technical disciplines and the fact that these technical disciplines would involve the activities of personnel from the Water Management Districts, IFAS, and NASA. Therefore, a Management Team Concept was developed to assure proper coverage of all of these disciplines, to coordinate the personnel activities and interactions, and to manage the overall project direction. The management structure of this organization, as described below, is delineated in Figure 3.2-1.

A Project Management Board was constituted from senior members of IFAS, NASA, and the Water Management Districts. This Board was responsible for holding project reviews and assuring that the project met the defined technical goals and schedules.

A Project Coordination Team was organized with representatives from the NASA, IFAS, and each cooperating Water Management District. The NASA member of this team had the responsibility, as Project Manager, for the entire project and was also Technical Manager of the IFAS contract. These coordinators were responsible for assuring that adequate study team members were provided from their respective organizations.

Various Project Teams with expertise in the necessary technical disciplines, as delineated in Figure 3.2-1, were formed to accomplish the project tasks. Each team had a team leader who was responsible to his Project Coordinator for completing the assigned tasks.

The IFAS of the University of Florida had demonstrated capability and competence in conducting Florida oriented research in the fields of climatology, agricultural water demands, hydrology, and socio-economic relationships. Also within the confines of the University system, consultation expertise in other disciplines; e.g., computer sciences and geology, was readily available.

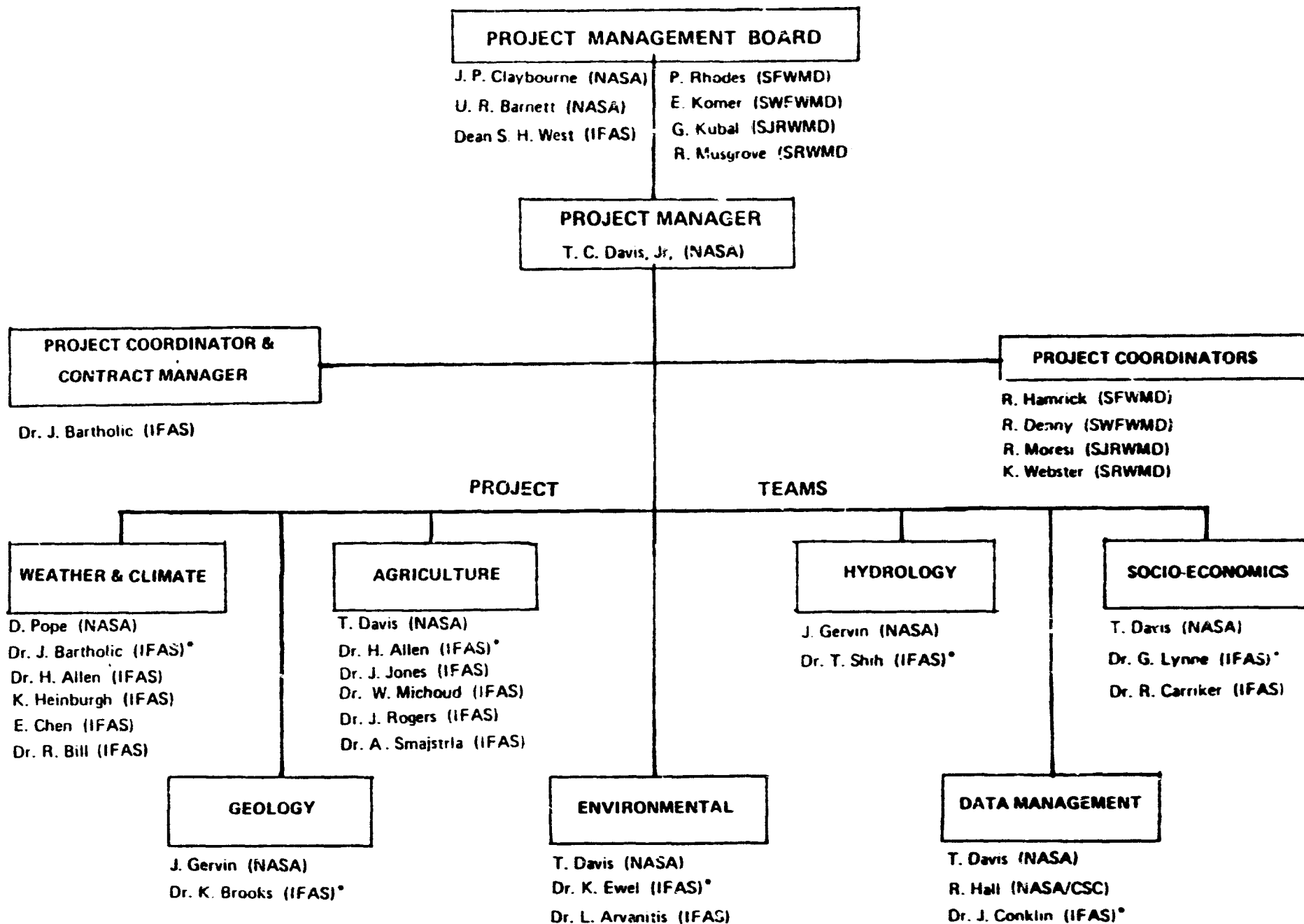


\*Denotes (IFAS) Team Leader

Figure 3.2-1

Therefore a noncompetitive procurement contract was issued to IFAS to support the project with necessary research and consultation personnel.

The project required the joint participation of IFAS, NASA, and the Water Management Districts; therefore, working agreements were initiated between NASA and the Water Management Districts. These agreements were needed to assure that support would be available to the IFAS research and to help the teams develop future task requirements and accomplish the Long Range Planning functions.



\*Denotes (IFAS) Team Leader

Figure 3.2-1

Therefore a noncompetitive procurement contract was issued to IFAS to support the project with necessary research and consultation personnel.

The project required the joint participation of IFAS, NASA, and the Water Management Districts; therefore, working agreements were initiated between NASA and the Water Management Districts. These agreements were needed to assure that support would be available to the IFAS research and to help the teams develop future task requirements and accomplish the Long Range Planning functions.

- 4.0-1 -

4 0 PROJECT STATUS

TABLE OF CONTENTS

	<u>Page</u>
4.0 Project Status . . . . .	4.0-1

FIGURES

<u>Figure No.</u>	<u>Page</u>
4.0-1 Florida Water Resources Management Long Range Schedule . . . . .	4.0-5

The discussions of the FY78 activities of the project need to be prefaced with a discussion of the long range planning of the project envisioned at the project conception and changes that have taken place since that time. Since the project's ultimate goal was to develop a rather complex Water Resources Management Information System based on the latest state-of-the-art remote sensing and automated data processing technology, it was obvious that the development of this system would take several years and involve the activities of a wide variety of disciplines on the part of NASA, IFAS, and the Water Management Districts. Therefore, a tentative overall schedule for completing this effort was developed as depicted in Figure 4.0-1.

For ease of assessment the project was broken down into several areas of major concern. First was the completion of a Long Range Plan which would provide all of the detailed steps necessary to reach the final goal of the implementation of a Water Resources Management Information System on each of the Water Management Districts' computer systems. Since the development of this plan required the assistance of the IFAS personnel and since the FY78 IFAS contract was not signed until March 3, 1978, we were unable to complete the plan prior to the submission of the FY79 study requirements to NASA. Therefore, the Long Range Plan task was also included in the FY79 study proposal. However, since the extension of the study into FY79 was disapproved by NASA the full implementation of the studies necessary to develop a comprehensive Long Range Plan was not completed. The information provided in this report consists only of the findings made up to the time of disapproval of the FY79 follow-on project, i.e., August 1978.

Second, there were Remote Sensing Techniques that needed to be developed to supply data base information for the Water Resources Management Information System. These techniques would primarily be the application of existing remote sensing technology to data base requirements identified by the various Water Management Districts. Eight of these tasks were defined for accomplishment in the FY78 study, several of which would have to be carried over into FY79 and subsequent years due to their complexity. During the FY78 Long Range Plan development phase, eight new Remote Sensing Techniques development and study tasks were identified to begin during the FY79 time frame. Of course, since the FY79 extension of the project was not approved, these tasks were not initiated.

Third, it was observed that various hydrological, agricultural, economic, environmental, and other models would need to be developed to interleave remote sensing and ancillary data into viable tools that could be incorporated into the overall Water Resources Management Information System.

Fourth, it was obvious that considerable basic research, not the responsibility of NASA, would be required to support the development of the models defined under the third function. This joint model development and supportive research needed to be accomplished by the Water Management Districts, primarily in the area of hydraulics; and by IFAS, primarily in the area of agriculture and environmental water functions.

Fifth, there was the need to begin the development of the Data Management System that could provide a viable, flexible, interfacing data base needed to



support the models being developed as well as the other data needs of the Water Management Districts.

Sixth, once the remote sensing data gathering techniques, models, and data base were developed to an adequate point; it would be necessary to begin to integrate these into a viable system on the equipment used by the various Water Management Districts.

Lastly, once the prototype system was operational it would be necessary to test the system under normal operational conditions over a period of time to assure that it would satisfy the needs of each Water Management District. These functions are defined as the Pre-ASVT and ASVT (Application System Verification Test) tasks within the project.

As previously mentioned, the follow-on effort on the project, i.e., FY79 and subsequent years, was not approved in August 1978. Therefore, the only functions to be discussed in this report will be the completion of the FY78 tasks as defined in Section 3.1.

- 5.0-1 -

## 5.0 TASK ACTIVITIES

## 5.1 LAKE OKEECHOBEE VOLUME MEASUREMENT

By

S. F. Shih      Assoc. Prof.

TABLE OF CONTENTS

	<u>Page</u>
5.1 Lake Okeechobee Volume Measurements . . . . .	5.1-1
5.1.1 Background . . . . .	5.1-5
5.1.2 Remote Sensing Data Analysis . . . . .	5.1-5
5.1.3 Water Budget Calculations . . . . .	5.1-9
5.1.3.1 Improvement in Lake Volume Prediction . . . . .	5.1-9
5.1.3.2 Improvement in Water Budget Computation . . . . .	5.1-15
5.1.3.2.1 Water Budget Computation Model . . . . .	5.1-15
5.1.3.2.2 Data Analysis and Model Application . . . . .	5.1-16
5.1.4 References . . . . .	5.1-21
5.1.5 Conclusions . . . . .	5.1-22

FIGURES

<u>Figure No.</u>	<u>Page</u>
5.1.2-1 LANDSAT classification Map of Littoral Zone Vegetation . . . .	5.1-12
5.1.3-1 Relationship Between Lake Stage and Lake Surface Area . . . .	5.1-13
5.1.3-2 Relationship Between Lake Stage and Lake Storage Capacity (Volume) . . . . .	5.1-14
5.1.3-3 Hydrological Data Recording Station in Lake Okeechobee, Florida . . . . .	5.1-17
5.1.3-4 Cumulative Lake Stage Error Based on Conventional and LANDSAT Data . . . . .	5.1-18

TABLES

Table No.	Page
5.1.1-1 Vegetation Association Linked to Evaluations in Lake Okeechobee . . . . .	5.1-6
5.1.2-1 Preliminary Analysis of LANDSAT Images . . . . .	5.1-8
5.1.2-2 Vegetation Classification and Acreage for Evapotranspiration Calculations . . . . .	5.1-10
5.1.2-3 Elevation Acreage for Volume Calculations . . . . .	5.1-11

### 5.1.1 Background

The water balance budget model for Lake Okeechobee contains a positive cumulative error which predicts a water volume approximately 30% greater than the actual volume after a run period of six years. The potential sources of error are those factors which affect lake volume, namely:

- a. water inflow
- b. water outflow
- c. rainfall on the lake
- d. evaporation from the lake.

The movement of water into and out of the lake (a, b) occurs primarily through structures and is carefully measured and recorded. Rainfall on the lake (c) is estimated based on rainfall recorded at stations around the lake and should be fairly accurate. Evaporation from the lake (d) consists of evaporation from the water surface and evapotranspiration from the littoral zone, a complex marsh which comprises 20% of the area within the dikes. The water balance budget model treats the marsh as open water, which tends to overestimate the water volume contained in this area and underestimates the evapotranspiration from it. This would appear to be the most likely source of the water balance error.

In order to eliminate this error, a more accurate estimate of the water distribution within the littoral zone and of the rate of evaporation from it is needed. A SFWMD study of the littoral zone has found that the major vegetation associations are linked to elevation through the hydroperiod (Pesnelli and Brown, 1977) (Table 5.1.1-1). Thus, if the littoral zone vegetation could be classified and mapped from satellite, two major types of information could be provided to the District. First, the acreage of a given plant community and its transpiration rate could be used to give a better estimate of evapotranspiration from the littoral zone. Second, since the plant species are linked to elevation through the hydroperiod, a vegetation classification could provide an approximate map of ground elevations. A factor could be included which takes into account the surface area occupied by each vegetation class (which therefore cannot be open water) to give an effective water surface (Table 5.1.1-1). Thus, the area transgressed by water and the portion of that surface which is open water could be determined for a given lake stage (elevation) based on a satellite vegetation map. This approach seemed to be the most effective way to apply remote sensing techniques to improve the accuracy of the lake water balance budget.

### 5.1.2 Remote Sensing Data Analysis

In order to classify the vegetation of the littoral zone, digital data from the LANDSAT earth-orbiting satellite was analyzed on General Electric's multispectral image analyzer, the Image 100. The Image 100 consists of two tape drives, for inputting and outputting digital data; a CRT screen which display  $(512)^2$  pixels of digital data; a memory for storing and refreshing the displayed image; and a battery of programs capable of measuring, manipulating and highlighting the raw (satellite) data. In the typical classification analysis, an area whose land cover is known from ground observation is located and its spectral characteristics are measured. Then all areas which have similar spectral characteristics are identified and assigned a color

<u>Vegetation</u>	<u>Elevation (ft. MSL)</u>	<u>Effective Water Surface (%)</u>
Waterlily	≤11.0	95
Spikerush (Eleocharis)	11.0-12.4	75
Cattail (Typha)	12.4-13.1	40
Beakrush (Rhynchospora)	13.1-14.6	80
Willow (Salix)	13.2-14.3	40
Wire Cordgrass (Spartina) and Sawgrass	13.1-15.0	30
Mixed Forest	15.0-17.0	-
Mixed Grasses	15.0-17.0	-
Other dry land	15.0-17.0	-

Vegetation Associations Linked to Evaluation in Lake Okeechobee

Table 5.1.1-1

and number code. The similar spectral characteristics are referred to as a signature and the location of those color-coded pixels possessing that signature is displayed on the CRT screen (or mapped on paper) as a theme. The themes can be limited to an area of interest (e.g., within the dikes surrounding Lake Okeechobee). The spectral distribution of a signature can be studied to refine it and identify spectral values that are or are not similar enough to be included in the same signature. Once the signature is finalized, the pixels in the satellite scene which possess that signature (theme) can be counted. In this way, maps and tabulations of areas with similar spectral properties, and presumably similar land cover, can be obtained.

Due to differences in the rate of scan, altitude and other factors, LANDSAT digital data does not precisely represent the relative geographic location of points on the ground. Using nominal values for the satellite, it is possible to correct small areas so that they form a good representation of features on the ground. For the large areas of interest to the Water Management Districts, however, small errors in the nominal values can accumulate to produce large offsets. Consequently, a ground control point correction must be used. In this technique a minimum of seven prominent features are located on the LANDSAT image and on USGS quadrangles. The tape coordinates of these points are read using the Image 100. The latitudes and longitudes are measured from the USGS quadrangles. A computer program performs a least squares fit of these points to develop a transformation matrix. This matrix transforms the old tape coordinates into new ones, oriented north-south with a given pixel size (usually 79m by 79m), and resamples the radiance (spectral) data, providing a LANDSAT scene with no more than 79m RMS error.

The season is extremely important in performing a vegetation classification. Since little satellite work had been done in a marsh as complex as the Lake Okeechobee littoral zone, there was little previous work to guide the analysis.

Consequently, NASA personnel, assisted by SFWMD biologist Gary Pesnell, performed preliminary multispectral classification on fifteen (15) relatively cloud-free dates. These dates included almost every month and spanned several years (Table 5.1.2-1). Vegetation maps prepared by the SFWMD as part of a study of littoral zone plant communities were used as ground truth. The classifications developed during this cursory analysis were then compared for clear definition and accurate representation of the plant communities (Table 5.1.2-1). Late summer (August 8, 1974) appeared to be the best time for distinguishing vegetation but the cumulus clouds associated with Florida's summer convection pattern obscured some of the data. Two back-up dates were chosen in late spring (May 5, 1975 and April 11, 1976).

A thorough vegetation classification was then performed on the Image 100. The ground truth maps were used to locate training sites for the major marsh vegetation communities, including cattail, willow, beak rush, spike rush, wire cordgrass, and mixed grasses. In some places clouds covered the vegetation so that it could not be classified. If a cloud was small and entirely contained within one of the vegetation communities, it was simply added to that vegetation class. When a cloud was so large that it overlapped two or more vegetation classes, LANDSAT data from another date (May 5, 1975) was used to classify the vegetation in that area. After this vegetation classification was completed, less than 1% of the area within the dikes remained unclassified. The

Date	Average Lake Stage (ft. MSL)	Vegetation Definition			Additional Comments
		Willow	Cattail	Beakrush	
1/30/76	13.2	poor	fair	poor	
2/27/74	13.5	poor	fair	fair	
3/4/73	12.8	good	poor	burn scar	clouds
3/22/73	12.8	fair	poor	burn scar	
4/9/73	13.0	good	poor	burn scar	
+4/11/76	12.7	fair	fair	fair	
+5/5/75	11.9	good	fair	fair	
5/26/76	12.4	poor	poor	poor	high gain, clouds
6/2/73	12.2	good	fair	fair	clouds
6/15/74	11.1	fair	poor	poor	clouds
*8/8/74	15.2	good	good	good	clouds
10/19/74	15.5	poor	fair	good	
11/4/76	14.6	poor	poor	good	
11/29/73	14.4	poor	poor	fair	
12/30/74	14.6	poor	fair	poor	striping

\*Primary date selected

+Back-up dates

### Preliminary Analysis of LANDSAT Images

Table 5.1.2-1

surface area occupied by each vegetation group (Table 5.1.2-2) was distributed equally throughout its elevation range (Table 5.1.2-3) to give the additional surface area associated with each increase in elevation. This data represents the remote sensing-based estimate of the lake surface area (and hence water volume). A typical LANDSAT Image 100 classified littoral zone vegetation map is shown in Figure 5.1.2-1.

This data will be used in the water balance budget model to develop improved estimates of lake volume and the improvement over conventional methods will be evaluated.

### 5.1.3 Water Budget Calculations

#### 5.1.3.1 Improvement in Lake Volume Prediction

The surface area occupied by each vegetation group (Table 5.1.2-2) was distributed equally throughout its elevation range (Table 5.1.2-3) to give the additional surface area associated with each increase in elevation. These data represent the remote sensing-based estimate of the lake surface area (Figure 5.1.3-1).

At a lake stage of 11.0 ft MSL, below the littoral zone, the lake surface estimates based on remote sensing and conventional data are quite similar (approximately 339,000 acres). With increasing elevation, the lake surface area derived from LANDSAT imagery is less than the area obtained through conventional means by 27,509 acres at 12.4 ft MSL, 15,290 acres at 13.1 ft MSL, 33,183 acres at 14.6 ft MSL, and 16,804 acres at 15 ft MSL (Figure 5.1.3-1).

Consequently, the lake storage capacity as a function of lake stage based on remotely sensed data also differed from the values used previously. The equation used to calculate the increase in lake volume associated with a small increase in lake stage was:

$$V_{s+0.01} = V_s + 0.01 [1/2 (A_s + A_{s+0.01})] \quad (5.1.3-1)$$

where

$V_{s+0.01}$  = lake storage volume at lake stage  $s + 0.01$  ft, in acre ft;

$V_s$  = lake storage volume at lake stage  $s$  ft, in acre-ft;

$A_{s+0.01}$  = lake surface area at lake stage  $s + 0.01$  ft, in acres; and

$A_s$  = lake surface area at lake stage  $s$  ft, in acres.

The resulting differences between the conventional and remotely sensed lake storage capacities were 42,898 acre-ft, 36,901 acre-ft, 88,150 acre-ft, and 98,078 acre-ft for 12.4, 13.1, 14.6, and 15.0 ft MSL, respectively, as shown in Figure 5.1.3-2.

<u>Vegetation</u>	<u>Area (Acres)</u>
Water	33,513
Waterlily	662
Spikerush	14,536
lallall	30,999
Beakrush	14,509
Willow	12,598
Wire Cordgrass and Sawgrass	9,734
Mixed Forest	1,509
Mixed Grasses	9,337
Other Dry Land	11,537
Unclassified	2,109
Total Area Within Dike	446,042

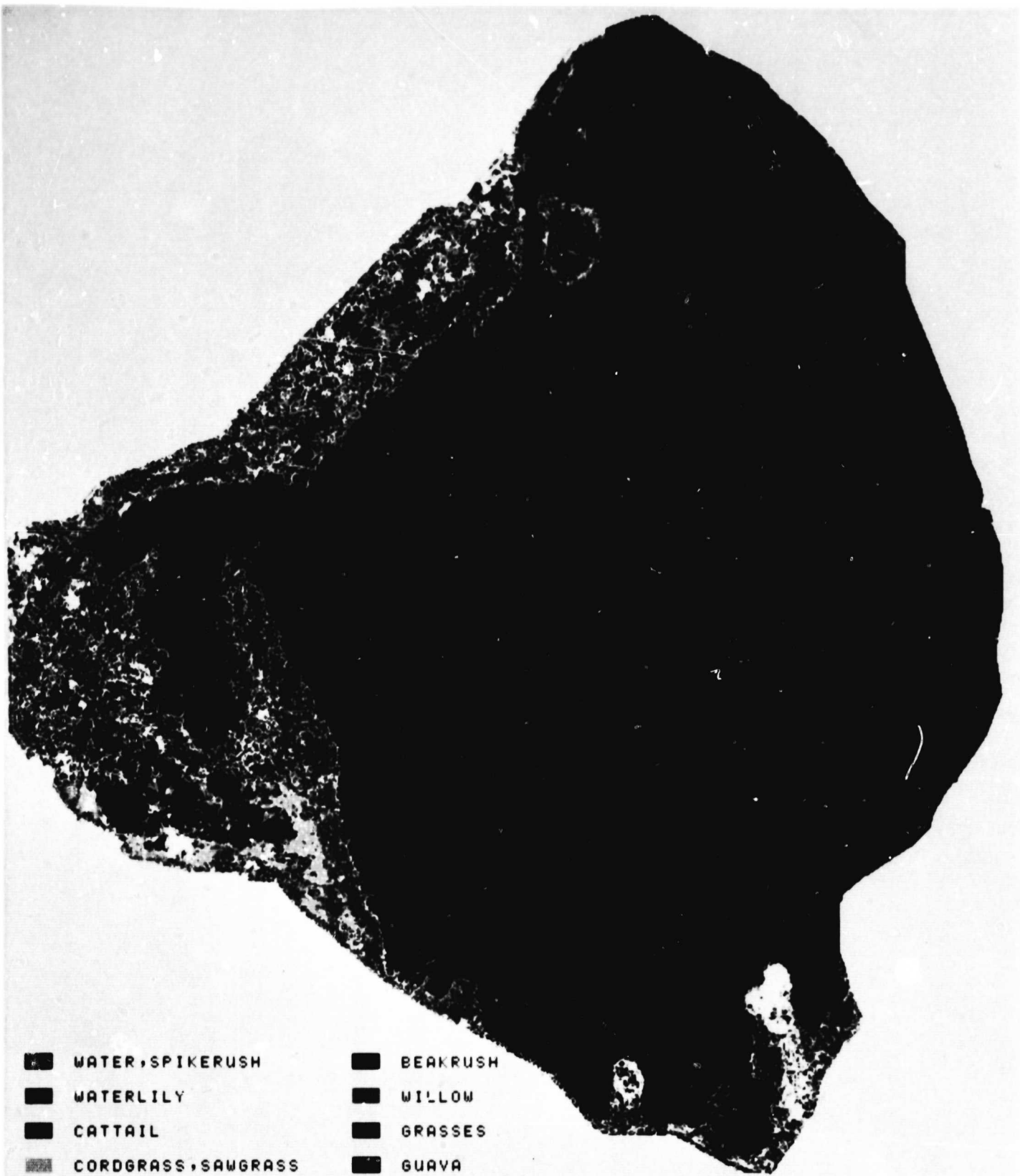
Vegetation Classification and Acreage for Evapotranspiration Calculations

Table 5.1.2-2

<u>Vegetation</u>	<u>Elevation (ft. MSL)</u>	<u>Total Lake Surface (Acres)</u>	<u>Effective Water Surface (Acres)</u>
Water, Waterlily	0.0 - 11.0	339,175	339,142
Spikerush	11.0 - 12.4	14,536	10,902
Cattail	12.4 - 13.1	30,999	12,399
Beakrush	13.1 - 14.6	14,509	11,607
Willow	13.2 - 14.3	12,598	5,039
Wire Cordgrass and Sawgrass	13.1 - 15.0	9,734	2,920
Mixed Forest and Grasses and Other Dry Land	15.0 - 17.0	22,382	-
Unclassified		2,109	-
Total		446,042	382,009

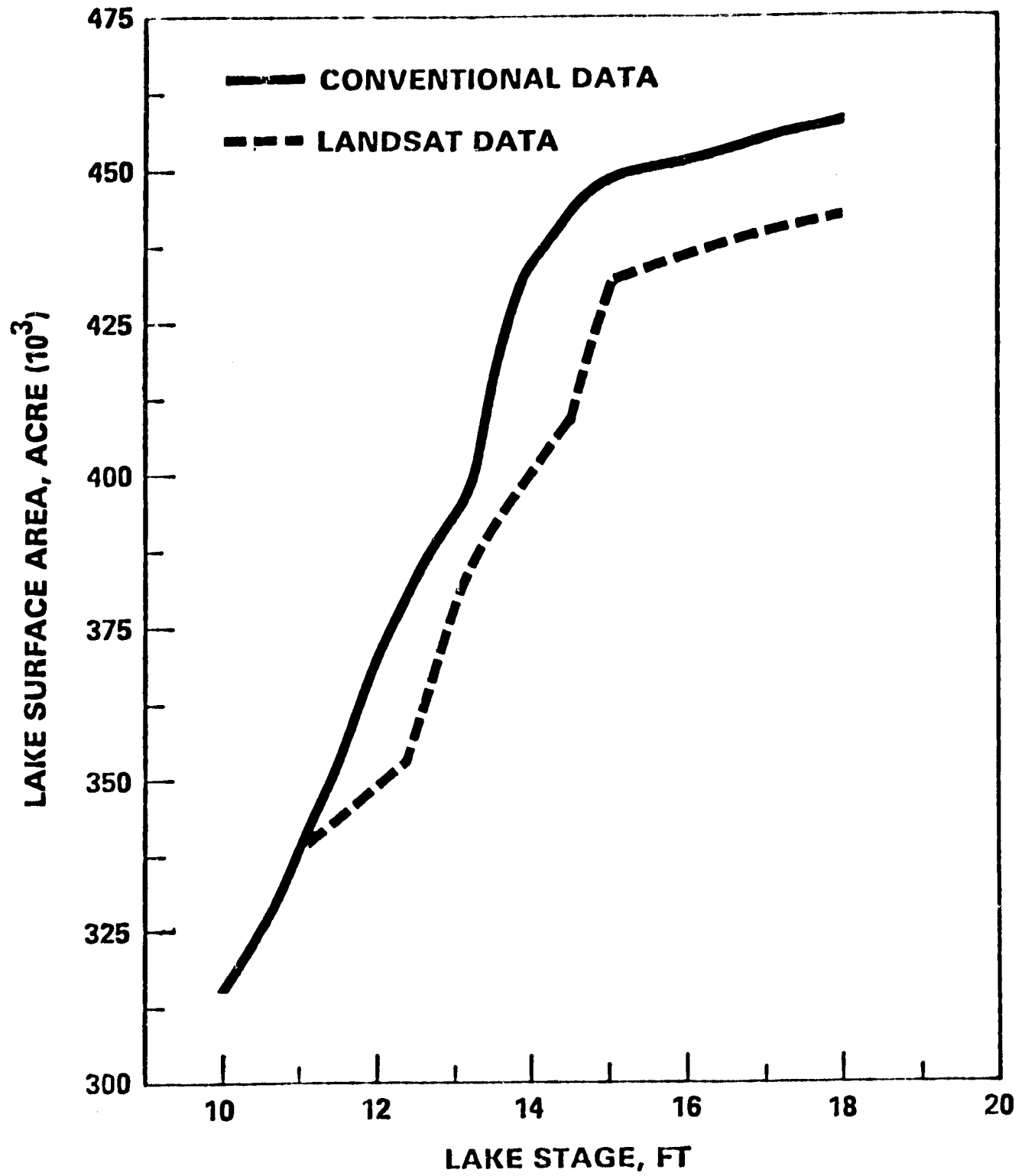
Elevation Acreage for Volume Calculations

Table 5.1.2-3



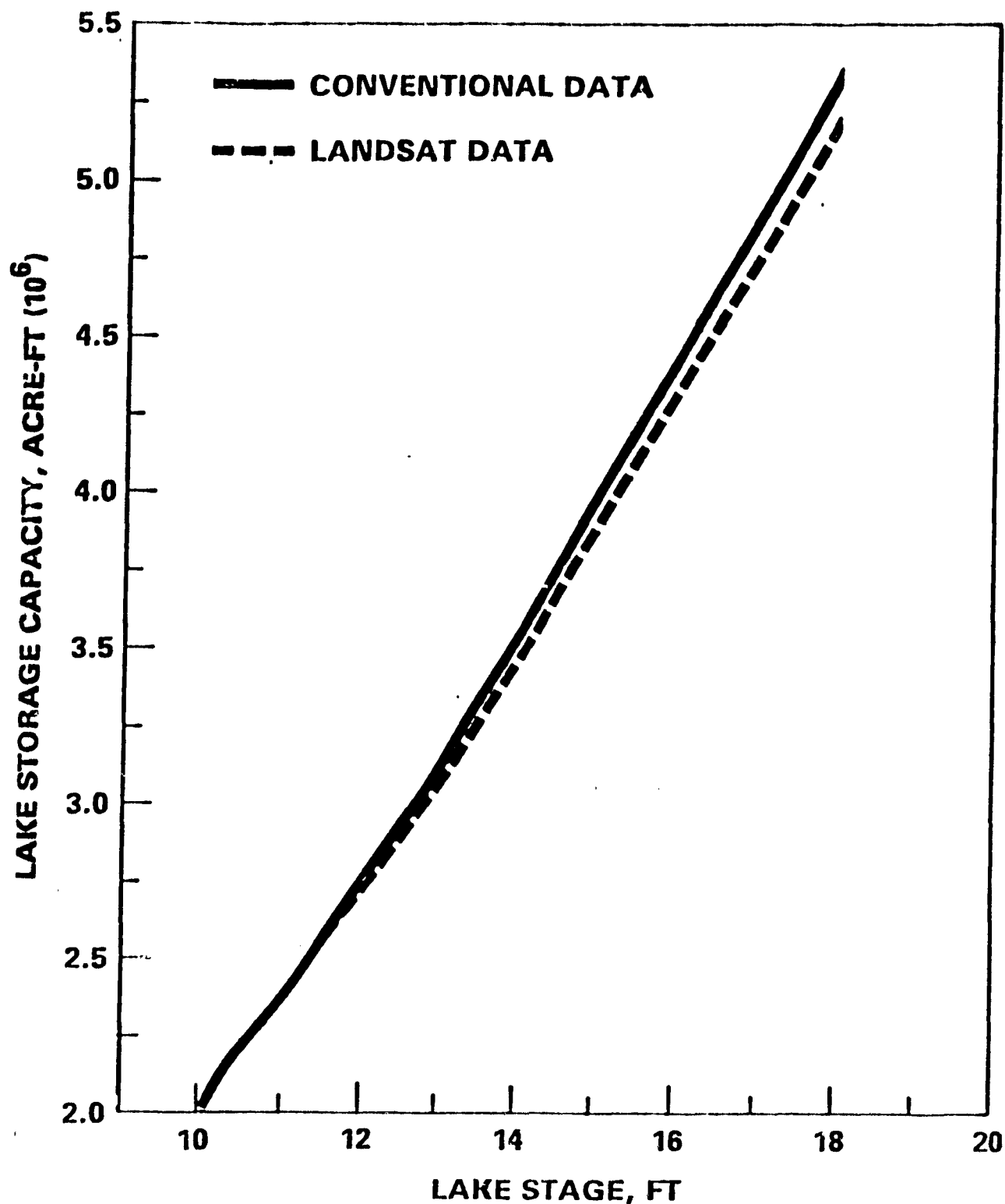
## LAKE OKEECHOBEE VEGETAT:

Figure 5.1.2-1 LANDSAT Classification Map of Littoral Zone Vegetation



Relationship Between Lake Stage and Lake Surface Area

Figure 5.1.3-1



Relationship Between Lake Stage and Lake Storage Capacity (Volume)

Figure 5.1.3-2

### 5.1.3.2 Improvement in Water Budget Computation

#### 5.1.3.2.1 Water Budget Computation Model

The water budget (or water balance) computation is a method based on the continuity of flow within the lake. According to the water balance equation provided by Linsley et al. (1958), the basic budget equation may be written as:

$$S = I + P - O - E - SP \quad (5.1.3-2)$$

where

S = Reservoir content change;

I = Inflow;

P = Precipitation;

O = Outflow, or total runoff;

E = Evaporation; and

SP = Seepage.

Theoretically, equation 5.1.2-2 may be used without reference to any marshes contained within the lake. Practically, however, most shallow lakes do contain substantial marshes, which transpire a significant amount of water from the lake. Therefore, based on the continuity equation, water budget computation for a shallow lake at time t (t month) may be modified as follows, incorporating the component of evapotranspiration:

$$V_t = V_{t-1} + I_t + R_t - O_t - E_t - ET_t - SP_t \quad (5.1.3-3)$$

where

$V_t$  = Storage at the end of t month;

$V_{t-1}$  = Storage at the end of (t-1) month;

$I_t$  = Inflow during t month;

$R_t$  = Rainfall during t month;

$E_t$  = Evaporation from water surface during t month;

$ET_t$  = Evapotranspiration from marsh zone during t month;

$O_t$  = Outflow during t month; and

$SP_t$  = Seepage during t month.

As equation 5.1.3-3 shows, there are two important zones involved, the water surface and marsh zones. The most difficult elements to measure are the  $E_t$  and  $ET_t$ . In general, the evaporation pan is the most widely used instrument for evaporation measurement today. The evaporation from the lake water surface can be expressed as:

$$E = X \cdot PE \quad (5.1.3-4)$$

where

$E$  = Evaporation from lake water surface;

$PE$  = Evaporation from evaporation pan; and

$X$  = Pan evaporation coefficient.

The evapotranspiration from the marsh zone is difficult to measure but can be determined indirectly by relating it to evaporation from the lake water surface, i.e.,

$$ET = k \cdot E \quad (5.1.3-5)$$

where

$ET$  = Evapotranspiration from marsh zone;

$k$  = Evapotranspiration coefficient; and

$E$  = Evaporation from lake water surface.

Based on a study by Meyer and Hull in 1969, the estimated seepage around Lake Okeechobee is approximately 0.9 cfs per mile per foot of the head between the lake and borrow canal. This is a negligible amount when compared to the total volume of the lake. Therefore, the seepage term was not included in calculations based on equation 5.1.3-3.

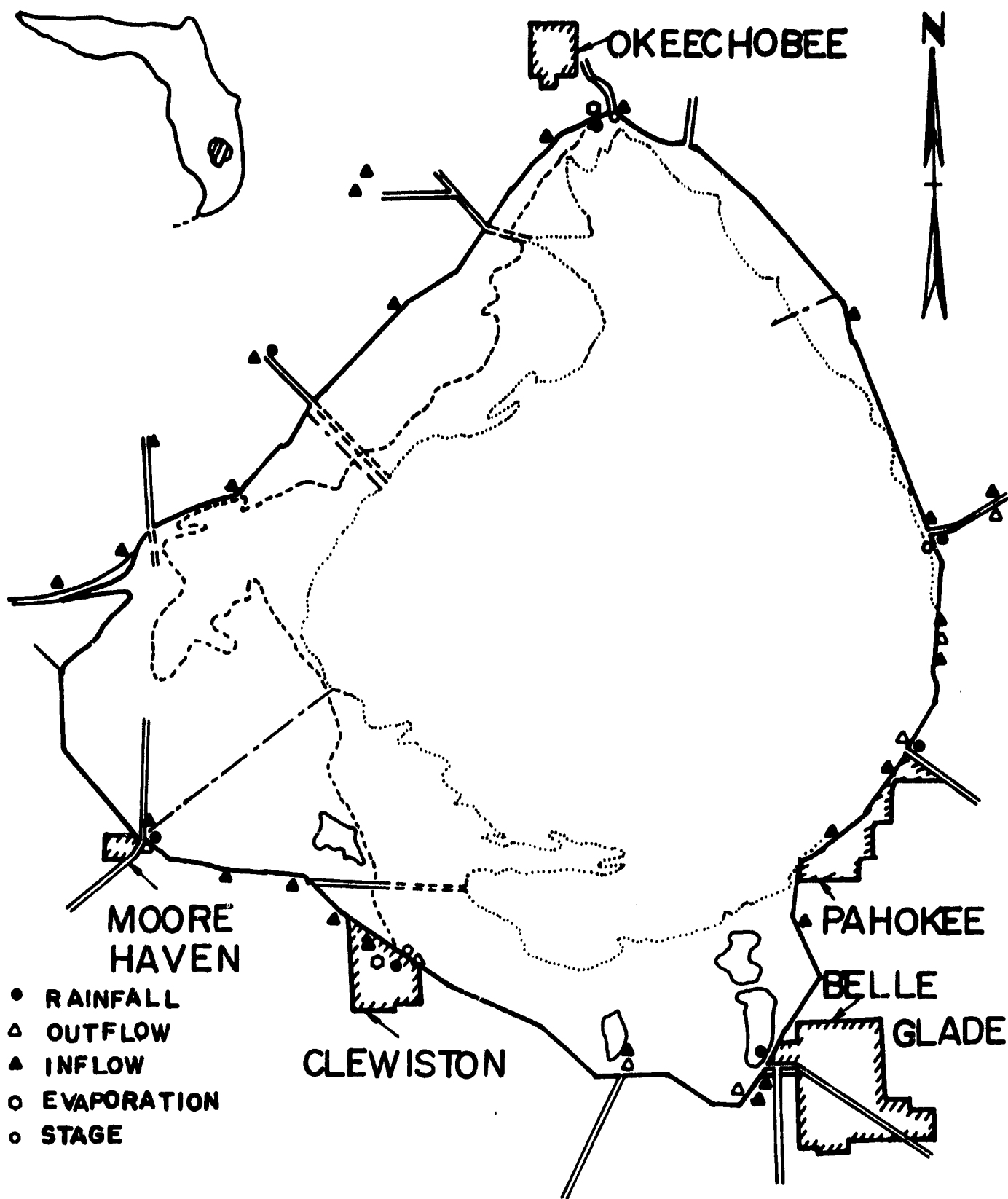
#### 5.1.3.2.2 Data Analysis and Model Application

The location of recording stations for rainfall, evaporation, inflow, outflow, and stages for the Lake Okeechobee are shown in Figure 5.1.3-3.

The recorded data from the period 1952-77 as shown in the Corps of Engineers monthly Lake Okeechobee water budget report were used in this study to compare water budget calculations based on conventional and remotely sensed lake volume data.

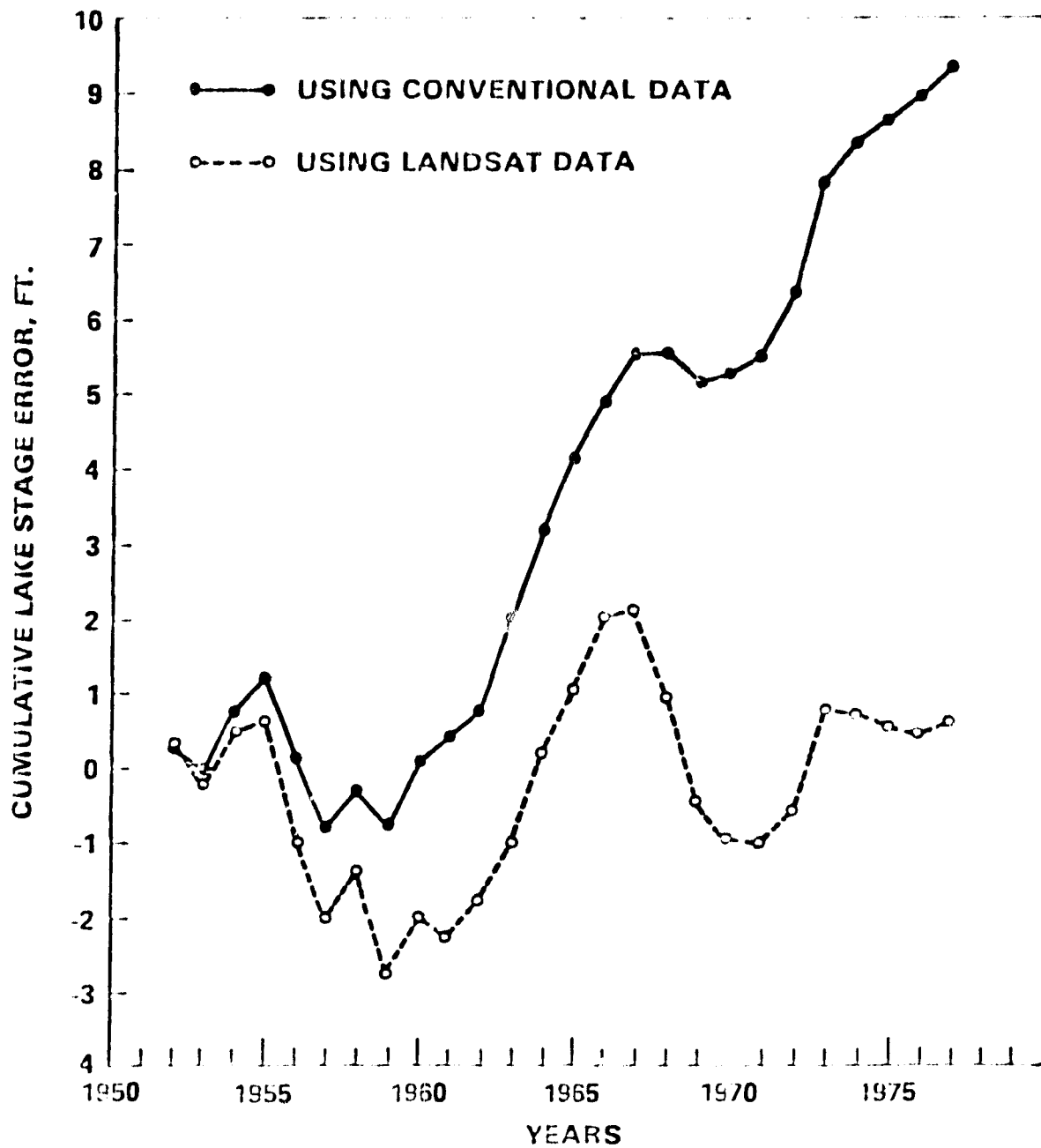
Water Balance Computation Based on Conventional Data: The historical record data, including cumulative error during the 26-year period, human computation error and estimation for missing data, were examined. The lake volume was computed based on the water balance equation provided by the Corps of Engineers (COE):

$$V_t = V_{t-1} + R_t + I_t - X \cdot PE_t - O_t \quad (5.1.3-6)$$



Hydrological Data Recording Stations in Lake Okeechobee, Florida

Figure 5.1.3-3



Cumulative Lake Stage Error Based on Conventional and LANDSAT Data

Figure 5.1.3-4

The terms used in equation 5.1.3-6 are the same as those described in equations 5.1.3-3 and 5.1.3-4. The model described by equation 5.1.3-6 is designated as water budget computation using conventional data.

The monthly Lake Okeechobee water budget data, which includes rainfall, pan evaporation, inflow, outflow, and lake stage, were summarized from the Corps of Engineers monthly water budget report for the period 1952-77 (COE, 1952-77). The monthly water budget computed by COE was based on the model given in equation 5.1.3-6 using 0.865 for the pan evaporation coefficient. The results of stage deviations between historical record and computed stage are shown in Figure 5.1.3-4. The cumulative error was 9.33 ft. over 26 years. This 9.33 ft. of stage is equivalent to 4 million acre-ft. of storage water, which is comparable to the volume of the lake at its normal stage of 15 ft. While the error for an individual year is not extremely large, its unpredictable nature makes reliable water volume predictions, on which water management decisions must be based, much more difficult. Moreover, it is obvious that the water budget for Lake Okeechobee is out of balance.

Water Balance Computation Based on LANDSAT Data: The lake volume data and the evapotranspiration rate developed from LANDSAT data were used in the model computation. After the seepage term is removed from equation 5.1.3-3, it may be rewritten as:

$$V_t = V_{t-1} + R_t + I_t - X \cdot PE_t - X \cdot ET_t - O_t \quad (5.1.3-7)$$

The model given in equation 5.1.3-7 is designated as water budget computation using LANDSAT data. The difference in cumulative errors between the model computation using conventional and remote sensing data was then investigated.

Before performing the lake volume computation, two parameters must be determined: the evapotranspiration coefficient  $k$  for the marsh and the area of marsh zone at different lake stages. The evapotranspiration (ET) for most marsh zone species is not available. Fortunately, Clayton (1949) in a 7-year ET study of sawgrass at the Agricultural Research and Education Center in Belle Glade, Florida, reported an ET of 69 inches/year for sawgrass. The average evaporation for the lake as reported by COE (1952-77) was 57.4 inches/year. Therefore, the evapotranspiration coefficient  $k$  given in equation 5.1.3-5 is  $69/57.4 = 1.2$  for sawgrass. This value will be used as a best estimate for the other vegetation species in this preliminary investigation since evapotranspiration measurements are not yet available for most of them.

Ihle (1978) reported a total surface area within the dikes of 446,080 acres, which is similar to the value of 446,042 acres used in the remote sensing measurements. However, he did not examine the lake and marsh surface areas as a function of water surface elevation. Using LANDSAT data, this information is now available and is presented in Table 5.1.2-3. The majority of the littoral zone lies between 11.5 and 15 ft. MSL.

After checking and correcting some obvious known errors, the original monthly water budget computations were rerun using conventional and LANDSAT data. The cumulative errors based on conventional and remotely sensed data

are plotted in Figure 5.1.3-4. As this figure shows, there are large differences between the two models. Choosing 0.865 as the typical pan evaporation coefficient, the cumulative error reached 9.33 ft. by the end of 1977 for conventional data and 0.54 ft. for the remotely sensed data. This represents a reduction of about 94 percent in the cumulative error over the 26-year test period. The maximum deviation of cumulative errors was found to be 2.85 ft. in 1959 for computations based on LANDSAT data and 9.33 ft in 1977 for the conventional method. The maximum deviation of cumulative errors was thus reduced about 70 percent by using the new information derived by analyzing LANDSAT data. This represents a substantial improvement in the accuracy of lake volume predictions achieved through the use of remotely sensed data. Traditional hydrological modeling and precise ground measurements also formed an essential part of this integrated approach to a water resources management problem.

#### 5.1.4 References

- Clayton, B. S., 1949. Water Control Investigation. University of Florida Agricultural Experiment Stations Project 89 Progress Report.
- Corps of Engineers, 1952-77. Monthly Water Budget Report for Lake Okeechobee. Department of the Army.
- Gervin, J. C., and S. F. Shih, 1979. Improvements in Lake Volume Predictions Using LANDSAT Data, in Satellite Hydrology, American Water Resources Association.
- Ihle, Hans, 1978. Area of Lake Okeechobee. South Florida Water Management District Memorandum Report 7-LO-90.
- Linsley, R. K., Jr., M. A. Hohler, and J. L. H. Paulthus, 1958. Hydrology for Engineers. McGraw-Hill.
- Meyer, F. W., and J. E. Hull, 1969. Seepage Test in L-D1 Borrow Canal at Lake Okeechobee, Florida. U. S. Geological Survey Information Circular 59.
- Pesnell, Gary L., and Robert T. Brown, III, 1977. The Major Plant Communities of Lake Okeechobee, Florida, and Their Associated Inundation Characteristics as Determined by Gradient Analysis. South Florida Water Management District Technical Publication 77-1.
- Shih, S. F., 1976. Modified Methodology Used to Compute the Water Balance of Lake Okeechobee. South Florida Water Management District Memorandum Report 9-8-1.

#### 5.1.5 Conclusions

Using LANDSAT data, the vegetation in Lake Okeechobee's complex littoral zone was classified multispectrally to provide a data base for determining two types of information. First, the acreage of a given plant community as measured by satellite could be combined with its transpiration rate to give a better estimate of evapotranspiration from the littoral zone. Second, the surface area occupied by plants (which therefore could not be considered open water) was used to adjust the vegetation acreage giving an effective water surface area as a function of lake stage. Based on this information, more detailed representations of evapotranspiration and total water surface (and hence total lake volume) can be made.

The model results based on information derived from satellite demonstrated a 94 percent reduction in cumulative lake stage error and a 70 percent reduction in the maximum deviation of the lake stage. As more detailed information on evapotranspiration coefficients for individual marshland species becomes available, an even greater reduction in error may be achieved. However, these results represent the application of this remote sensing technique to only one lake. To verify its general applicability, the improvements in water volume prediction using this method should be tested in other lake and marshland communities.

The techniques presented here could be applied to a wide variety of water resources management needs.

5.2 IMPROVEMENT OF CONSERVATION AREA WATER STORAGE INFORMATION

By

S. F. Shih      Assoc. Prof.

TABLE OF CONTENTS

	<u>Page</u>
5.2 IMPROVEMENT OF CONSERVATION AREA WATER STORAGE INFORMATION . . . . .	5.2-1
5.2.1 Background . . . . .	5.2-5
5.2.2 Remote Sensing Data Analysis . . . . .	5.2-5
5.2.3 Water Budget Calculations . . . . .	5.2-13
5.2.3.1 Storage Capacity Prediction . . . . .	5.2-13
5.2.3.2 Improvement Application of Water Quantity Receiving Model . .	5.2-13
5.2.4 References . . . . .	5.2-17
5.2.5 Conclusions . . . . .	5.2-18

FIGURES

<u>Figure No.</u>	<u>Page</u>
5.2.2-1 Selection Factors for Available LANDSAT Scenes . . . . .	5.2-6
5.2.2-2 The Everglades Conservation Areas . . . . .	5.2-7
5.2.2-3 Water Depth Map in Conservation Area 3a . . . . .	5.2-10
5.2.3-1 Relationship Between Stage and Storage Capacity in Conservation Area 3a . . . . .	5.2-15

TABLES

Table No.	Page
5.2.2-1 Correlation of LANDSAT Radiance with Water Depth for Conservation Area 3a . . . . .	5.2-9
5.2.2-2 Water Surface and Volume in Conservation Area 3a . . . . .	5.2-12
5.2.3-1 Elevation Acreage for Volume Calculation in Conservation Area 3a . . . . .	5.2-14

### 5.2.1 Background

In south Florida large tracts of grassy marshland have been set aside to act as natural water retention areas. Similar to the Everglades, these areas consist of wet prairies broken by elevated ridges of trees called tree islands. These areas are diked and most flow into and out of them is controlled by pumps and structures.

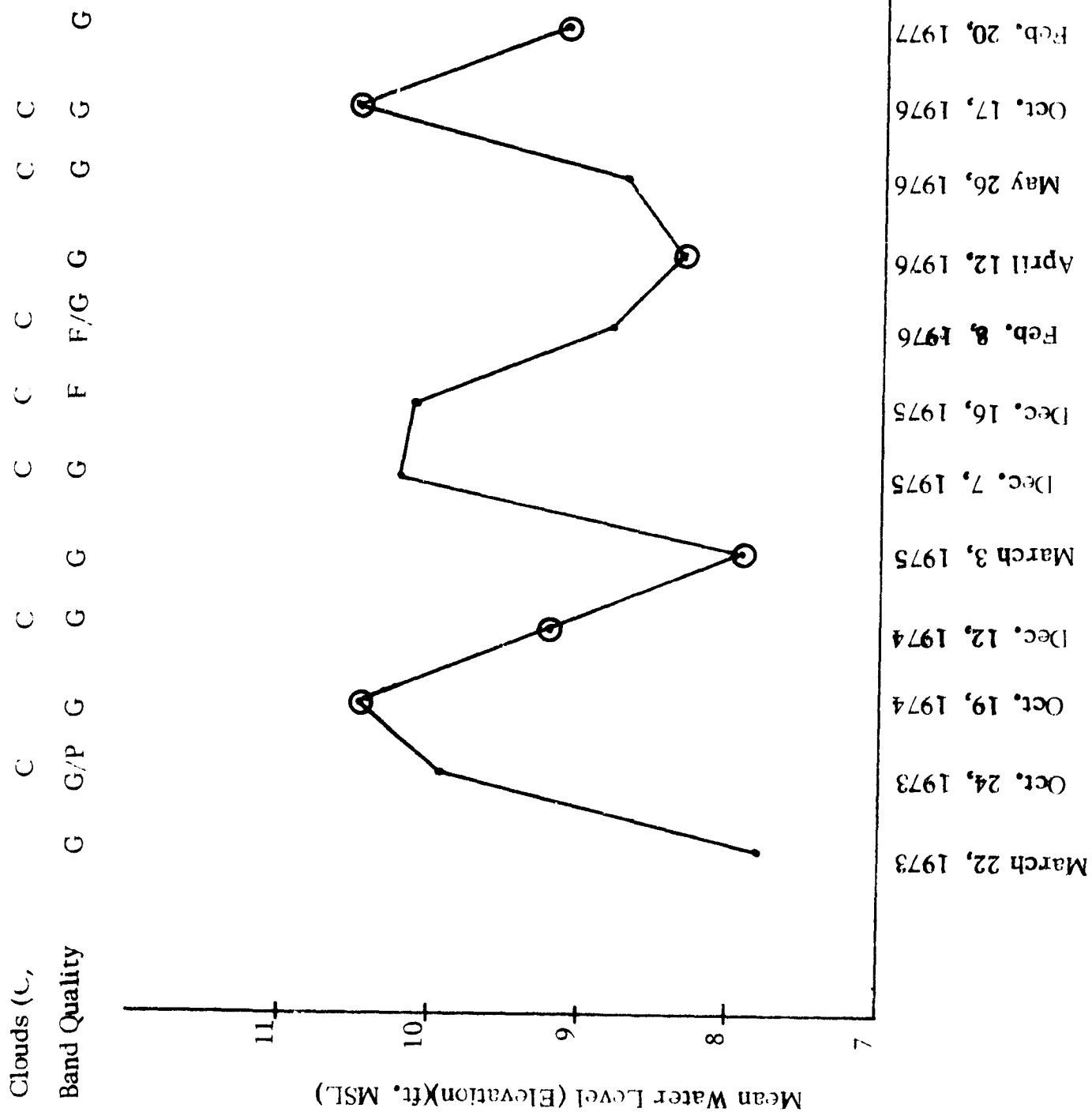
Vast amounts of water stored in the three major conservation areas flow slowly from the agricultural region south of Lake Okeechobee to the Everglades and finally to the Gulf of Mexico. The SFWMD has only limited knowledge of the total amount of water and its distribution and flow pattern because these areas are large, remote, and almost flat. Models describing the movement of water in these areas use arbitrarily selected nodal points to simulate this sometimes reversible water flow. If remote sensing data could be used to provide water depths or approximate elevation contours, the calculation of water volume in the conservation areas and the simulation of water flow through them could be improved.

In previous studies Aaron Higer, of the USGS, tried to relate LANDSAT radiance to water depths in Conservation Area 1 with some success. In more recent unpublished work, he had investigated the correlation between LANDSAT radiance and water depths in Conservation Area 3a on two dates using 100 field measurements. He had achieved good correlations but, because of the manpower required to gather field measurements, this technique would not be practical as an operational tool.

Consequently, NASA decided to examine water depths in Conservation Area 3a on a number of dates ranging from minimum to maximum but to use only existing water depth gauging stations and if necessary a few supplemental field measurements. The method to be applied would involve correlating LANDSAT radiance and water depth using an automated computer technique. In this manner water depth distribution could be mapped routinely and possibly ground elevation information might be inferred from this. If successful it was planned to test this technique in Conservation Areas 1 and 2 in subsequent years of the project.

### 5.2.2 Remote Sensing Data Analysis

Twelve relatively cloud-free LANDSAT tapes representing the full range of water levels, from minimum to maximum, were identified (Figure 5.2.2-1). From these, two sets of three dates, each set covering a minimum to maximum cycle, were selected for more intensive study. Sets of consecutive dates were chosen to minimize the likelihood that long term changes in vegetation distribution would affect the data analysis. SFWMD then provided water elevation data, ground elevations, and latitudes and longitudes for the eighteen water depth stations in Conservation Area 3a. The water depth was obtained by subtracting ground elevation from water elevation. Unfortunately, some of the stations were not truly representative of water depths within the conservation area. Some recorded water depth in canals, or were affected by pumping, or were separated from the conservation area by dikes. Eliminating these stations reduced the usable number of stations to the eight shown in Figure 5.2.2-2. This indicated a need for additional gauging stations and/or supplemental field measurements to truly test the technique. If the project were to



Selection Factors for Available Landmark Scenes

Figure 5.2.2-1

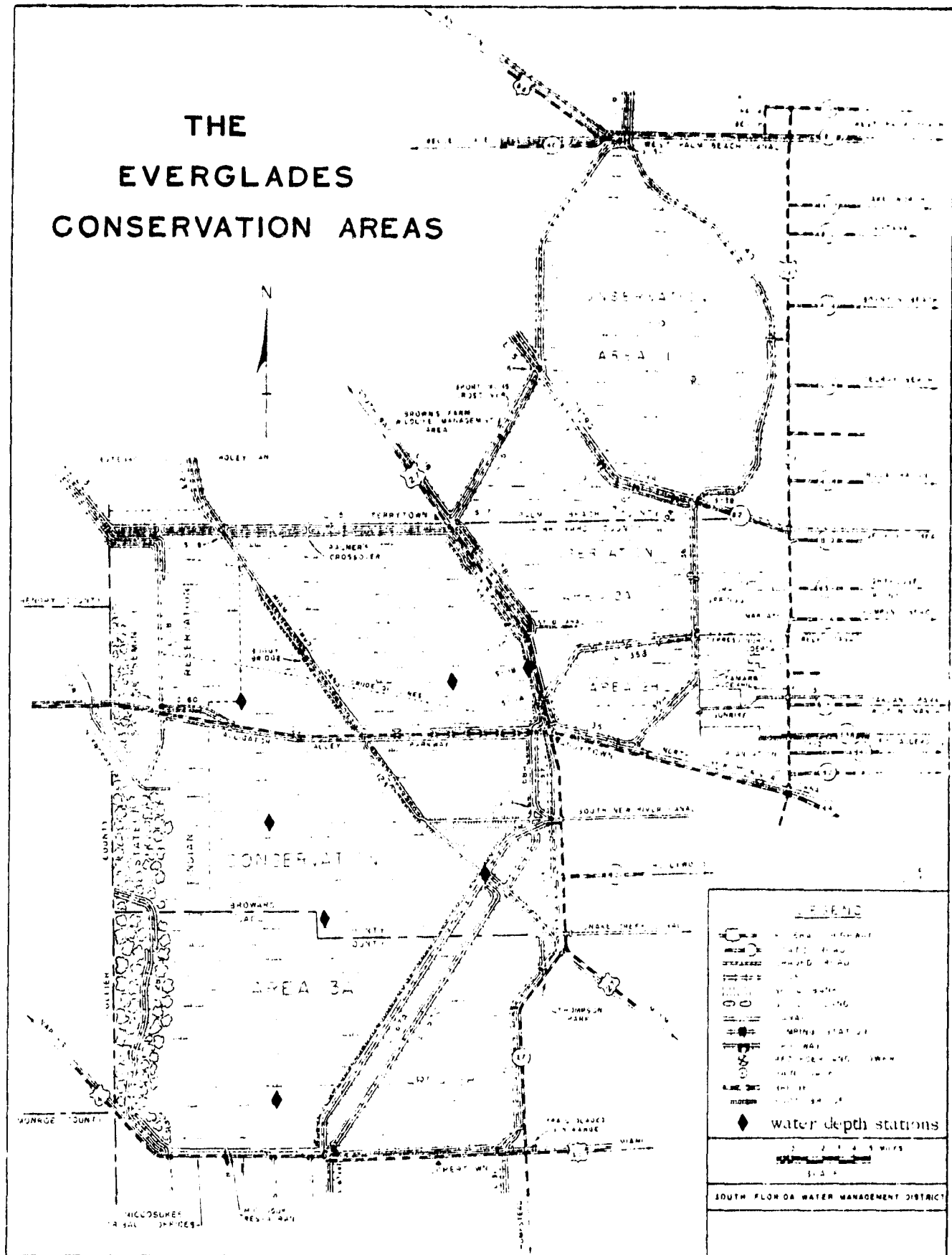


Figure 5.2.2-2

continue for another year, supplemental water depth measurements would be made to improve the correlation.

Meanwhile, a preliminary test of the technique was performed with the existing historical data. After examining each date carefully, it was found that there was very little water in the conservation area on the two days of minimum water level. Therefore, these dates were removed from the test, leaving four dates representing medium and high water levels. The Image 100 was used to develop a geometric correction matrix for the four remaining dates, using the method described in Section 5.1.2. This matrix was used to locate the water depth stations on the LANDSAT tape from their latitudes and longitudes since very few landmarks or other distinct features are available in a marsh. The Image 100 was then used to measure the LANDSAT radiance of the four pixels closest to each gauging station on each date. If a cloud or data drop obscured the gauge location, the nearest group of clear pixels was used. A multiple regression analysis was performed for each date relating water depth, as measured by the gauging stations, to the LANDSAT radiance as measured on the Image 100. All four bands and each possible combination of two bands were used (Table 5.2.2-1). The four band combinations and some of the two band combinations produced acceptable correlations but the small number of samples cast doubt on the reliability of the predicted relationships. In an attempt to obtain a more reliable relationship, the radiance values from different dates were normalized to be radiometrically equivalent to each other using minimum and maximum measurements of the LANDSAT radiance, including open ocean and very bright (urban) sites on each of the dates. Radiance values from these normalized images were regressed against their respective water depths in the same manner as for each individual date. The resulting correlations were not high enough to be considered reliable, however.

To demonstrate the type of product that could be produced using this technique, a map of water depths was generated using the Band 5-Band 7 relationship for October 17, 1976 (Figure 5.2.2-3). This date was chosen for its range of water depths and good correlation in a two-band combination (for ease in hand calculation). Similar maps could be produced based on all four bands for this and other dates using a simple computer algorithm. The areas occupied by each water depth were measured automatically on the Image 100 and combined to calculate the estimated water storage volume in the conservation area on that date (Table 5.2.2-2).

The position of the nodal points in the water quantity receiving model will be reviewed and the water volumes predicted for various water levels will be compared to those calculated from the LANDSAT imagery. However, since only one date was classified based on only seven ground data points, the accuracy and reliability of the remote sensing based data is limited. This information may also be useful in selecting locations for additional water depth stations in the conservation area.

Landsat Bands	DATES				Normalized, All Dates
	Oct. 19, 1974	Dec. 12, 1974	Oct. 17, 1976*	Feb. 20, 1977	
Bands 4 - 7	.97	.98	.83	.91	.45
Bands 4 & 5	.40	.60	.74	.73	.40
Bands 4 & 6	.03	.60	.64	.69	.38
Bands 4 & 7	.36	.49	.70	.78	.37
Bands 5 & 6	.19	.84	.71	.54	.43
Bands 5 & 7	.28	.73	.75*	.57	.43
Bands 6 & 7	.70	.51	.56	.60	.17

\* One apparently anomalous point removed

⊙ Correlation for regression equation used to produce map in Figure 5.2.2-3

Correlation of Landsat Radiance with Water Depth for Conservation Area 3a

Table 5.2.2-1

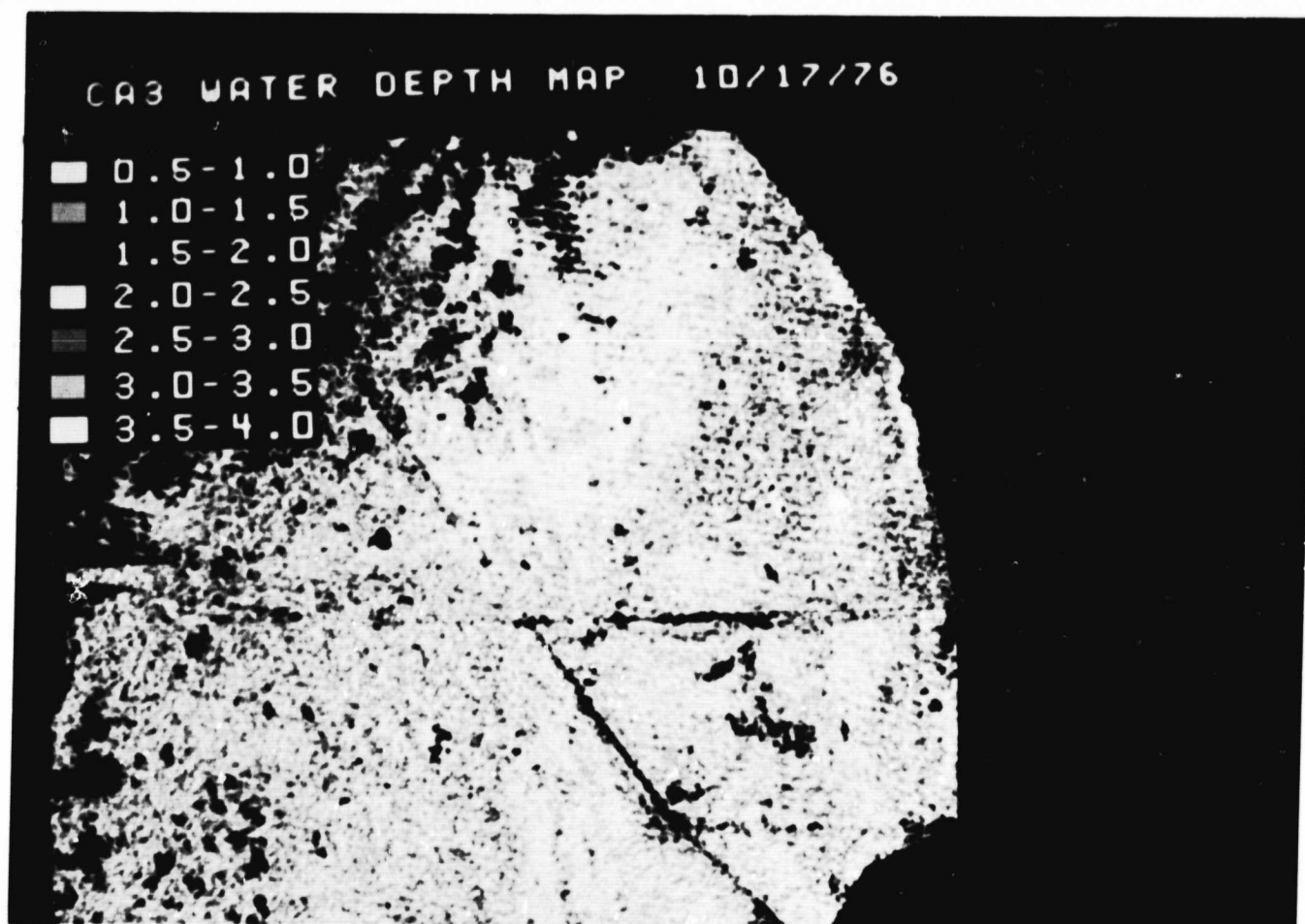


Figure 5.2.2-3A Upper Section of Conservation Area 3a Water Depth Map  
(LANDSAT Bands 5 and 7).

ORIGINAL PAGE IS  
OF POOR QUALITY

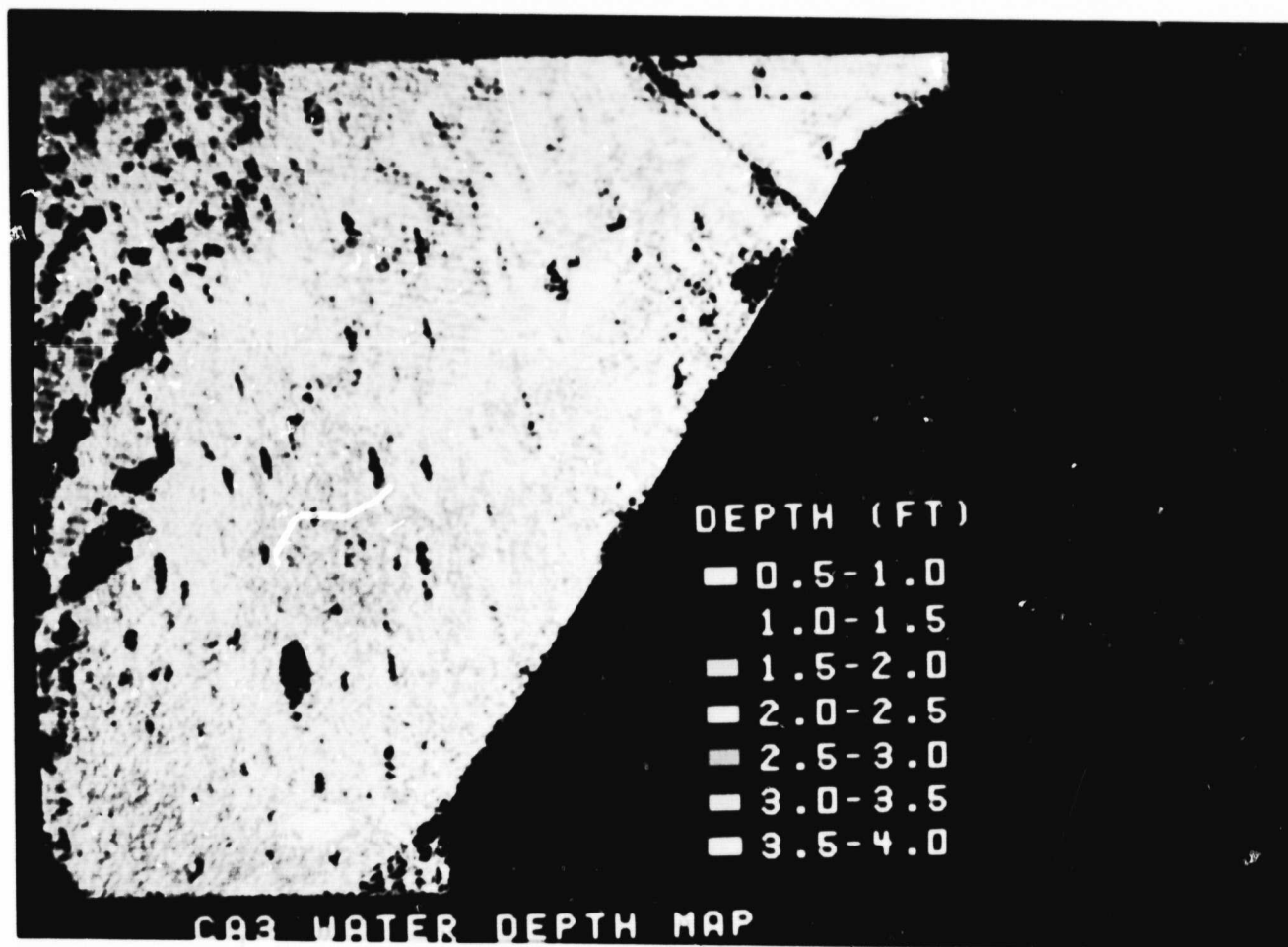


Figure 5.2.2-3B Lower Section of Conservation Area 3a Water Depth Map  
(LANDSAT Bands 5 and 7).

Water Depth	Water Surface in (hectares)                      (Acres)	
0.5 - 1.0	9067	22404
1.0 - 1.5	31297	77336
1.5 - 2.0	41671	102969
2.0 - 2.5	42353	104653
2.5 - 3.0	21471	53055
3.0 - 3.5	7094	17350
3.5 - 4.0	4910	12134

Estimated Water Volume: 776,930 Acre-feet

Based on data for Oct. 17, 1976, using relationship and map indicated in Table 5.2.2-1 and Figure 5.2.2-3, respectively.

Water Surface and Volume in Conservation Area 3a

Table 5.2.2-2

### 5.2.3 Water Budget Calculations

#### 5.2.3.1 Storage Capacity Prediction

The water surface area occupied by each water depth (Table 5.2.2-2) was used to compute the storage capacity in Conservation Area 3a. The stage recorded on October 17, 1976 was 10.42 ft MSL. This elevation was used as a bench mark to compute the relationship between stage elevation and water surface area. Before computing the storage capacity, the water surface area associated with each increase in elevation needs to be computed based on the water surface area related to water depth as given in Table 5.2.2-2. As Table 5.2.2-2 shows, the surface areas are undefined when the water depth is either shallower than 0.5 ft or deeper than 4 ft. Thus, two assumptions should be made. First, the water surface area between 0 and 0.5 ft of water depth is near zero. Second, the water surface area at the water depth of 4 ft. is assumed to be the same as the water surface area in between 3.5 and 4.0 ft of water depth because the conventional data shows that there is some water stored below the 4 ft. water depth. Based on those two assumption and 10.42 ft of the recorded stage, the water surface areas related to stage elevation were computed and the results are listed in Table 5.2.3-1.

The storage capacity as a function of stage can be computed based on the remotely sensed data as listed in Table 5.2.3-1. The method as defined in Equation 5.1.2-1 is used to calculate the increase in volume associated with a small increase in stage. The initial volume at stage 6.42 ft is 18,160 acre-ft which was obtained from the conventional data. The resulting differences between the conventional and remotely sensed storage capacities were 81, 40, 20, 29, 37, 26, and 7 thousands acre-ft for the stage at 10.17, 9.67, 9.17, 8.67, 8.17, 7.67, and 7.17 ft MSL, respectively, as shown in Figure 5.2.3-1. These differences are approximately equivalent to the errors of 10, 6, 5, 11, 23, 30 and 19% of the conventional data in the same order of stages. There seems to be a large error existing between 7.17 and 8.17 ft MSL stages.

As the remotely sensed data developed in Section 5.2.2 indicated, the number of ground recorded stage sites is not large enough to draw a final conclusion. However, using the Band 5-Band 7 relationship for October 17, 1976, the correlation coefficient between LANDSAT radiance and water depth has been found to reach 0.75. In other words, this technique is quite encouraging to detect the water depth. If this is the case, three recommendations can be made. First, there might have been an error in the conventional data in the relationship between stage and storage. Second, in between the stages around 7 and 8 ft MSL, the storage volume is extensively reduced as compared with the conventional data. The reason for this reduction should be investigated further. Third, the storage capacity computed from the remotely sensed data is always less than from the conventional data. This implies that the volume of water stored in the Conservation Area 3a has been overestimated in the conventional data. Therefore a correct relationship between stage and storage should be established as soon as possible.

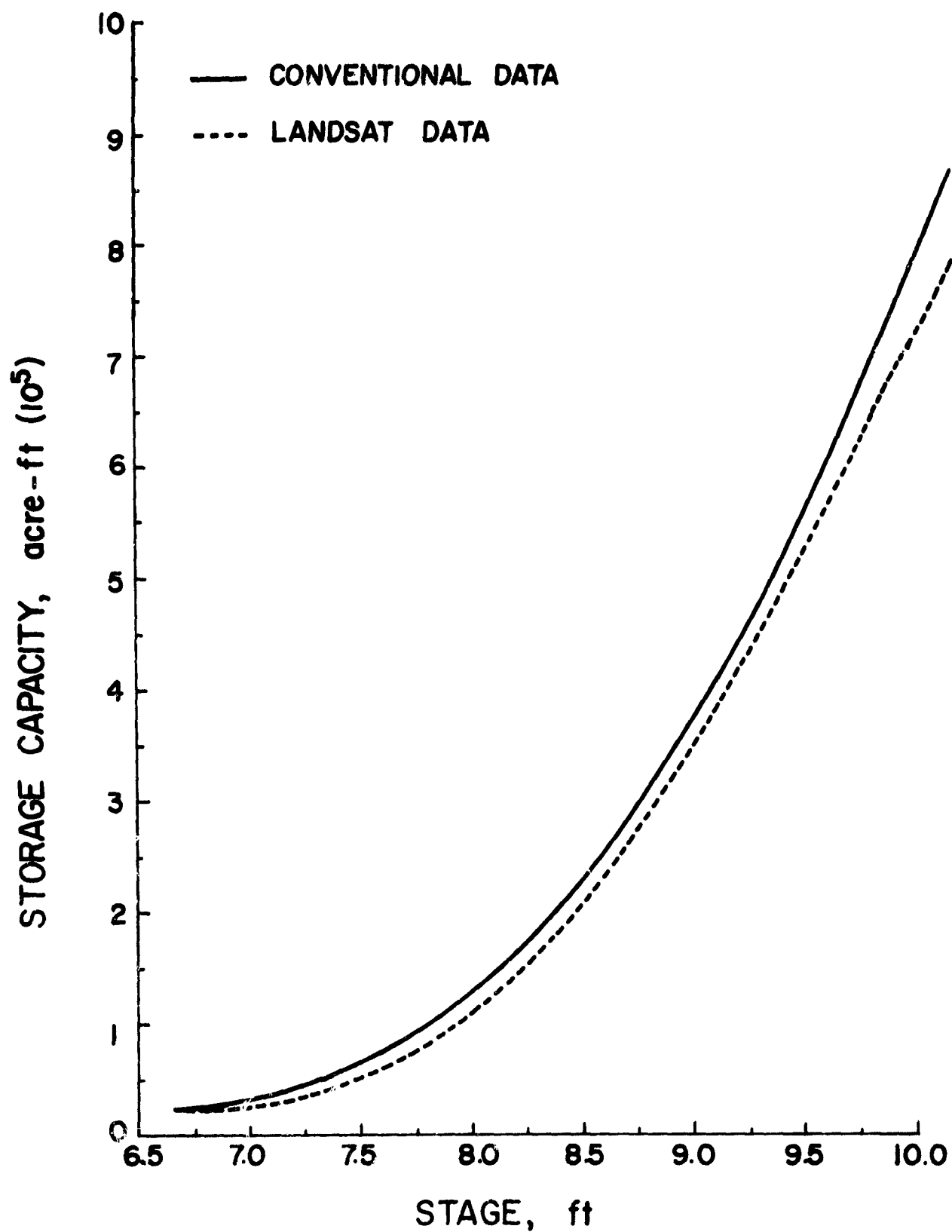
#### 5.2.3.2 Improvement Application of Water Quantity Receiving Model

The Conservation Area in south Florida has been considered as one of the major water storage areas to provide a water supply for the Everglades National

Elevation (ft. MSL)	Total Water Surface Area (Acres)
9.92 - 10.42	389,901
9.42 - 9.92	389,901
8.92 - 9.42	367,477
8.42 - 8.92	290,161
7.92 - 8.42	187,192
7.42 - 7.92	82,539
6.92 - 7.42	29,484
6.42 - 6.92	12,134
- 6.42	12,134

Elevation Acreage for Volume Calculation  
in Conservation Area 3a

Table 5.2.3-1



Relationship Between Stage And Storage Capacity in Conservation Area 3a.

Park and Lower East Coast (LEC). Due to the increasing water demand of the area, additional backpumping of the surplus runoff from the LEC area into the Conservation Areas has been considered as one of the several alternative plans (SFWMD, 1977). The Receiving Water Quantity (EPA, 1971) model has been adapted and modified by Lin and Shih (1979) to be applicable in the Conservation Areas to investigate the possible impact of additional inflow under various backpumping cases. Modification of the model included Manning's roughness coefficient, depth of flow, width of hypothetical channels through marsh areas, rainfall input, seepage rate, etc.

The Receiving Water Quantity model requires a nodal point and grid system to represent the prototype water receiving body. Therefore, a network system representing the general flow pattern of the water body is set up for each study area. For each channel, the input requires a junction number at both ends of the channel section, length, width, average depth of the channel, and Manning's N coefficient. For each node, the input requires an assigned junction number, initial water surface elevation, bottom and minimum elevation, junctions x- and y- coordinates in the system, surface area, etc. There are three major problems encountered in the Receiving Water Quantity Model Application. First, the node point is selected based on the water depth, vegetation characteristics, inflow, outflow, rain gage, and computer storage core capacity, etc. But, some of the parameters are very difficult to estimate. Second, the average depth, and Manning's N coefficient which is a function of vegetation and water depth, are very difficult to evaluate in hypothetical channels. Third, the initial water surface elevation, bottom and minimum elevation in each node are very unreliable based on the conventional data. As the technique presented in this study and the results shown in Figure 5.2.2-3, the remotely sensed data is a very promising method to solve these three difficult problems. The vegetation distribution, water depth in different locations, water stage, water surface and ground elevation all can be drawn from the remotely sensed data. This technique should be encouraged and studied further in the future.

#### 5.2.4 References

Environmental Protection Agency, 1971. Storm Water Management Model. EPA Report No. 11024, Doc: 07-10.

Lin, S.T., and S.F. Shih, 1979. Modified Water Quantity Receiving Model for Florida Conservation Areas. Water Resources Bulletin, Vol. 15(1):155-166.

South Florida Water Management District, 1977. Water Use and Supply Development Plan. Vol. 111A, Lower East Coast Planning Area, Technical Exhibits. "I-K", West Palm Beach, Florida.

### 5.2.5 Conclusions

In south Florida, large tracts of grassy marshland have been set aside to act as natural water retention areas. Similar to the Everglades, these areas consist of wet prairies broken by elevated ridges of trees called tree islands. These areas are diked and most water flow into and out of them is controlled by pumps and structures. Vast amounts of water stored in the three major conservation areas are questionable because these areas are large, remote, and almost flat. The South Florida Water Management District has only limited knowledge of the total amount of water and its distribution and flow pattern. The Receiving Water Quantity (RWQ) model describing the movement of water in these areas uses arbitrarily selected nodal points to simulate this sometimes reversible water flow. Thus, the remote sensing technique was initiated to provide water depths and the water volume in the conservation areas.

LANDSAT radiance values from Band 5 and Band 7 for October 17, 1976 in Conservation Area 3a were used to correlate with the water depths. The results showed that the correlation coefficient is as high as 0.75. Thus, an alphanumeric map of water depth was generated and the water surface area corresponding to water depth was computed. Consequently, the volume of storage was computed. The results showed that this technique is a very promising tool for helping the storage volume computation and RWQ model application. The improvement of LANDSAT data analysis technique and ground truth data collection are recommended for further study in the future.

### 5.3 OVERLAND FLOW MEASUREMENTS

By

S. F. Shih      Assoc. Prof.

G. S. Rahi      Res. Assoc.

## TABLE OF CONTENTS

	<u>Page</u>
5.3 OVERLAND FLOW MEASUREMENTS . . . . .	5.3-1
5.3.1 Remote Sensing Data Analysis . . . . .	5.3-7
5.3.2 Development of Manning's N Data . . . . .	5.3-7
5.3.2.1 Effect of Vegetation on Manning's N . . . . .	5.3-7
5.3.2.2 Information on Vegetation in Chandler Slough . . . . .	5.3-12
5.3.2.3 Selection and Vegetation of Test Sites . . . . .	5.3-15
5.3.3 Hydrologic Model Calculations . . . . .	5.3-20
5.3.3.1 General Consideration and Techniques Used . . . . .	5.3-20
5.3.3.2 Determination of Slope . . . . .	5.3-20
5.3.3.3 Models Application . . . . .	5.3-21
5.3.3.3.1 Determination of Manning's N . . . . .	5.3-21
5.3.3.3.2 Determination of Vegetation Density . . . . .	5.3-21
5.3.3.4 Results and Discussions . . . . .	5.3-22
5.3.3.4.1 Flow Resistance Trends at Different Sites . . . . .	5.3-23
5.3.3.4.1.1 Variations in N Values with Depth . . . . .	5.3-23
5.3.3.4.1.2 Weighted N Values Versus Total Flow Depth . . . . .	5.3-30
5.3.3.4.1.3 Flow Resistance Values Versus Depth as Related to Predominant Vegetation . . . . .	5.3-30
5.3.3.4.2 Relations Between Flow Retardance Values and Vegetation Density . . . . .	5.3-38
5.3.3.4.3 Flow Resistance and Vegetation as Related to Time . . . . .	5.3-46
5.3.3.4.4 Roughness Coefficient and Vegetation Density Values Calculated from November, 1978 Data . . . . .	5.3-46
5.3.3.4.5 Roughness Coefficient and Vegetation Density Values Calculated from June, 1979 Data . . . . .	5.3-48
5.3.3.4.6 Roughness Coefficient and Vegetation Density Values Calculated from July, 1979 Data . . . . .	5.3-49
5.3.3.5 Appendix . . . . .	5.3-51
5.3.4 References . . . . .	5.3-87
5.3.5 Conclusions . . . . .	5.3-89

# FIGURES

<u>Figure No.</u>	<u>Page</u>
5.3.1-1 Vegetation Communities of Chandler Slough . . . . .	5.3-8
5.3.1-2 Chandler Slough Vegetation Map, April 11, 1976 . . . . .	5.3-9
5.3.2-1 Location of Sampling Sites in Site . . . . .	5.3-16
5.3.2-2 Relative Location of Subsites in a Given Site . . . . .	5.3-19
5.3.3-1 Relation Between 'N' Values and Depth for Site 1 (Sub- sites 1, 2, 4, 5, 6, 9, 11) . . . . .	5.3-24
5.3.3-2 Relation Between 'N' Values and Depth for Site 1 (Sub- sites 3, 7, 8, 10, 12, 13) . . . . .	5.3-25
5.3.3-3 Relation Between 'N' Values and Depth for Site 2 (All Subsites) . . . . .	5.3-27
5.3.3-4A Relation Between 'N' Values and Depth for Site 3 (Subsites 1-5) . . . . .	5.3-28
5.3.3-4B Relation Between 'N' Values and Depth for Site 3 (Subsites 6-9) . . . . .	5.3-29
5.3.3-5 Relation Between 'N' Values and Depth for Site 4 (Subsites 1-4) . . . . .	5.3-31
5.3.3-6 Relation Between 'N' Values and Total Depth (All 4 sites) . . .	5.3-32
5.3.3-7 Relation Between Averaged 'N' Values for Different Vegetation Classes and Depth for Site 1 . . . . .	5.3-33
5.3.3-8 Relation Between Different Vegetation Classes and Depth for Site 2 . . . . .	5.3-34
5.3.3-9 Relation Between Average 'N' Values for Different Vegetation Classes and Depth for Site 3 . . . . .	5.3-35
5.3.3-10 Relation Between Averaged 'N' Values for Different Vegetation Classes and Depth for Site 4 . . . . .	5.3-36
5.3.3-11 Overall Relation Between 'N' Values and Depth for Different Types of Vegetation for all Sites . . . . .	5.3-39
5.3.3-12 Relation Between 'N' Values and Vegetation Density for Site 1 (Subsites 1, 2, 4, 6, 12) . . . . .	5.3-40
5.3.3-13 Relation Between 'N' Values and Vegetation Density for Site 1 (Subsites 7, 8, 9, 11) . . . . .	5.3-41

<u>Figure No.</u>	<u>Page</u>
5.3.3-14 Relation Between 'N' Values and Vegetation Density for Site 1 (Subsites 3, 10, 13) . . . . .	5.3-42
5.3.3-15 Relation Between 'N' Values and Vegetation Density for Site 3 (Subsites 1, 2, 3, 8) . . . . .	5.3-43
5.3.3-16 Relation Between 'N' Values and Vegetation Density for Site 3 (Subsites 4, 5, 6, 7, 9) . . . . .	5.3-44
5.3.3-17 Relation Between 'N' Values and Vegetation Density for Site 4 (Subsites 1, 2, 3, 4) . . . . .	5.3-45
5.3.3-18 Flow Retardance Values (for Surface Flow) as a Function of Time . . . . .	5.3-47

TABLES

<u>Table No.</u>	<u>Page</u>
5.3.3-1A Manning's N Values Calculated from Water Flow Data Measured on Aug. 22, 1978 (Using Dye Method) . . . . .	5.3-52
5.3.3-1B Manning's N Values Calculated from Water Flow Data Measured on Sept. 25, 1978 (Using Flowmeter and Dye Methods) . . . . .	5.3-53
5.3.3-1C Manning's N Values Calculated from Water Flow Data Measured on Oct. 17, 1978 (Using Flowmeter and Dye Methods) . . . . .	5.3-57
5.3.3-1D Manning's N Values Calculated from Water Flow Data Measured on Nov. 29, 1978 (Using Dye Method) . . . . .	5.3-61
5.3.3-1E Manning's N Values Calculated from Water Flow Data Measured on June 29, 1979 (Using Flowmeter Method) . . . . .	5.3-63
5.3.3-1F Manning's N Values Calculated from Water Flow Data Measured on June 29, 1979 (Using Dye Method) . . . . .	5.3-65
5.3.3-1G Manning's N Values Calculated from Water Flow Data Measured on July 23, 1979 (Using Flowmeter Method) . . . . .	5.3-66
5.3.3-1H Manning's N Values Calculated from Water Flow Data Measured on July 23, 1979 (Using Dye Method) . . . . .	5.3-70
5.3.3-2A Vegetation Density Values Calculated from Water Flow Data Measured on Aug. 22, 1978 (Using Dye Method) . . . . .	5.3-71
5.3.3-2B Vegetation Density Values Calculated from Water Flow Data Measured on Sept. 25, 1978 (Using Flowmeter and Dye Methods). . . . .	5.3-72
5.3.3-2C Vegetation Density Values Calculated from Water Flow Data Measured on Oct. 7, 1978 (Using Flowmeter and Dye Methods). . . . .	5.3-76
5.3.3-2D Vegetation Density Values Calculated from Water Flow Data Measured on Nov. 29, 1978 (Using Dye Method) . . . . .	5.3-80
5.3.3-2E Vegetation Density Values Calculated from Water Flow Data Measured on June 29, 1979 (Using Flowmeter Method) . . . . .	5.3-81

<u>Table No.</u>	<u>Page</u>
5.3.3-2F Vegetation Density Values Calculated from Water Flow Data Measured on June 29, 1979 (Using Dye Method) . . . . .	5.3-83
5.3.3-2G Vegetation Density Values Calculated from Water Flow Data Measured on July 23, 1979 (Using Flowmeter Method) . . . . .	5.3-84
5.3.3-2H Vegetation Density Values Calculated from Water Flow Data Measured on July 23, 1979 (Using Dye Method) . . . . .	5.3-86

### 5.3.1 Remote Sensing Data Analysis

A substantial portion of the water transport in south Florida is by overland flow, much of it through natural vegetation. So little research has been done on the flow resistance characteristics of these natural vegetation communities that one value of Manning's N is frequently used to represent all of them in all seasons. If a more detailed representation of the resistance to flow of natural vegetation could be developed, it would greatly improve the accuracy of water flow simulation. Unfortunately, most groundbased mapping methods would be prohibitively expensive. A comparable remote sensing technique would be less detailed, both in terms of plant species delineation and geographic representation, but its cost would be acceptable.

Therefore, it was decided to classify a typical marshland drainage basin in south Florida using LANDSAT data. Chandler Slough, a site in the Kissimmee River Basin, was selected. It had already been well ground-truthed as part of another study (Federico, et al., 1978), was readily accessible as was required for flow measurement, and contained a variety of vegetation species characteristic of the marshlands of south Florida.

The first task in performing the vegetation analysis was to select the proper season. James F. Milleson, a SFWMD biologist familiar with the site, identified the major vegetation communities and their seasonal growth patterns. He provided two vegetation maps of the area with different species groupings (Figure 5.3.1-1) as well as black-and-white aerial photographs at scales of 1:24,800 and 1:4,800. Based on this information, classification during the winter season was not attempted due to lack of plant growth. No completely cloud-free scenes were available for summer. A preliminary Image 100 vegetation classification was performed on cloud-free spring and fall scenes from various years. It was determined that little change had occurred in this area in recent times. The LANDSAT scene recorded on April 11, 1976, was found to give the best vegetation definition. A detailed multispectral training was then performed to get the best possible plant discrimination. The vegetation discrimination was found to be most closely linked to radiance in Bands 5 and 6, possibly due to striping on Band 7. A map showing six vegetation categories was prepared with the help of Jim Milleson. The area of major flow was identified and the proportion of each vegetation category in that area was measured. This data and the accompanying map (Figure 5.3.1-2) were provided in selecting sites at which to make the seasonal flow measurements from which Manning's N values would be calculated.

### 5.3.2 Development of Manning's N Data

#### 5.3.2.1 Effect of Vegetation on Manning's N

Determination of flow resistance coefficient 'N' as a function of depth is very important in dealing with water resources problems (especially of the vegetated flow areas), such as flood routing, backwater curve computation, channel improvement and scour problems, etc. Understanding the flow resistance trends for a particular flow system would help the water resources planner to be able to develop better water management systems in the area.

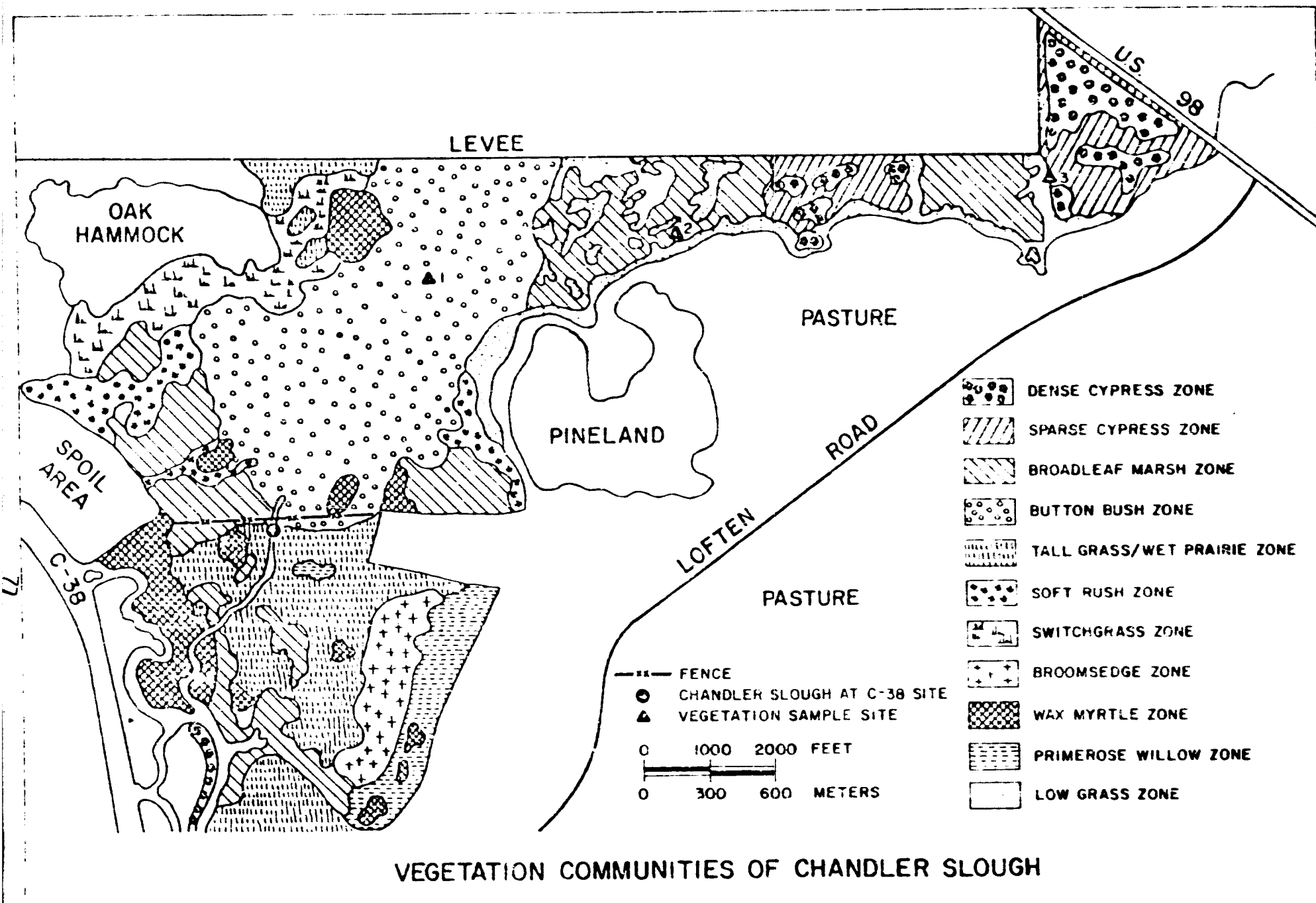
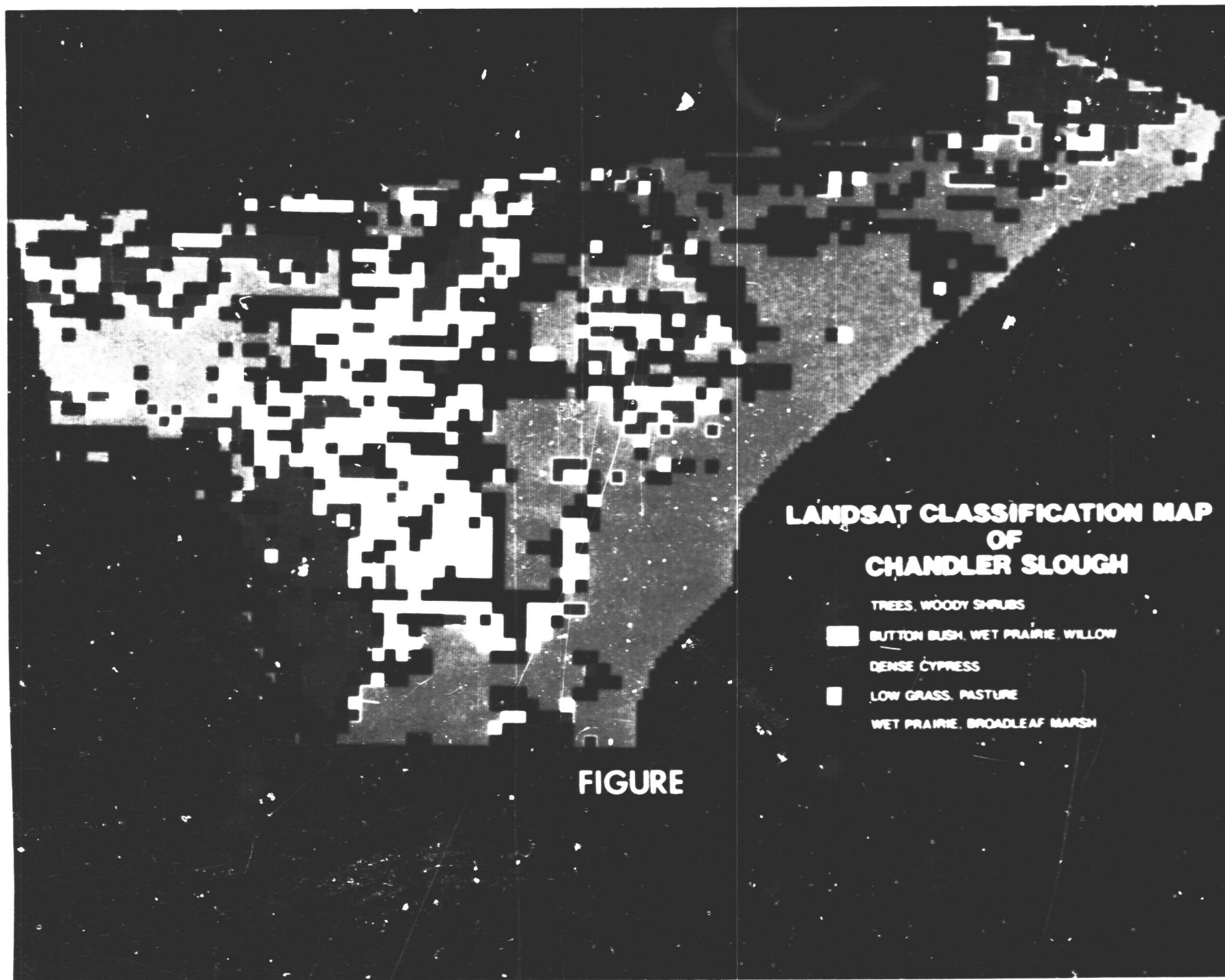


Figure 5.3.1-1



ORIGINAL PAGE IS  
OF POOR QUALITY

However, the value of this coefficient among other factors is very significantly affected by the vegetation. Flow resistance through a given vegetated area is a function of many variables including flow velocity, distribution of vegetation vertically and laterally, roughness of the channel boundary, and structural and hydrodynamical properties associated with the stems and leaves of the plants. The effect of aquatic weeds in retarding flow can be quite pronounced in channels with small depth and low velocities. Unfortunately, little is known about the variations in flow resistance values in heavily vegetated channels, except for some grassed waterways. Some of the pertinent findings reported in literature about flow retardance and vegetation relations are described briefly as follows:

Bogart (1949) measured flow retardance coefficient values in North New River canal in the Everglades area after the canal was infested with thick water hyacinth growth. He found that on the average 'N' in vegetated canals increased 2.5 times as compared to the original value the canal was designed for and this resulted in 40% reduction in the carrying capacity of the canal. The roots of plants make the sides and bottom of the canal very rough. He also reported that water hyacinth and other plant roots cause a surprisingly large amount of friction loss by inducing turbulence in the water and with complete hyacinth cover, a canal becomes in effect a closed conduit without any free water surface.

Flow retardance coefficients were reported for several row-planted crops by Ree (1958). He found that Manning's N values were related to the product of velocity and hydraulic radius when velocities were large enough to displace the vegetation. N values for wheat ranged up to 0.17 and height and quality of the wheat had greater effect than did a change in row spacing from 7" to 14". These values for tall sorghum and short sorghum were 0.15 and 0.11, respectively. Swanson and Peterson (1960) obtained lower velocities and higher coefficients of retardance in waterways grassed with brome grass, Kentucky 30 fescue, reed canarygrass, and switchgrass. Fenzl (1962) investigated the effect of vegetation density on the flow characteristics using a dimensional analysis for conditions of uniform flow in a simulated vegetated channel.

In their studies on flow retardance by channel weeds, Stephens et al. (1963) worked out flow retardance coefficients for channels in southeast Florida and found large channels (with or without aquatic weed infestation) that had hydraulic radii exceeding 20' generally have N values between 0.024 and 0.031. In moderate-size channels having cross-sectional areas between 100 and 2000 sq. feet, Manning's N values were less than 0.036 with light vegetative growth, between 0.036 and 0.052 for moderate growth, and exceeded 0.052 with heavy growth. Under conditions of infestation by submersed and emergent aquatic weeds, N values increased exponentially as the product of velocity and hydraulic radius decreased.

Graf (1966) developed a mathematical equation relating the frictional behavior of a cross-section in a water course to its velocity profiles. Field, as well as laboratory data, confirmed his theory. N values obtained in test flumes were comparatively quite high in relation to other waterways. Das and Huggins (1971) studied the effect of rainfall on the resistance in channels with shallow flow and found that friction factor for rough surface increases at a given rainfall intensity and Reynolds number as the slope increases.

Leutheusser and Chisholm (1972) measured an N value of 0.225 in an open channel with steep and heavily vegetated sideslopes in Toronto, Canada. Overton, et al. (1972) conducted studies to optimize resistance coefficients for large bed element streams in Utah. They tried to relate the Darcy-Weisbach resistance coefficient and location of the plane of effective zero velocity to the roughness intensity, the width of channels, and the mean size of the material. They found that roughness intensity did not adequately explain the variation of the resistance coefficient in laboratory roughnesses, however spacing of the roughness elements was a more important factor. The streamflow regime appeared to arrange the large bed elements in an optimal way. They also reported that roughness intensity values between 0.1 and 0.2 were realistic for laboratory simulation of large bed element streams.

Kuowen and Unny (1973), using flexible plastic strips to simulate a vegetative channel lining, studied the variation of relative roughness with the stiffness of vegetation. They observed three basic flows (erect, wavy, and prone) and their plot of friction coefficient versus the Reynolds number showed the friction factor primarily to be a function of relative roughness for the erect and wavy regimes. Thompson and Roberson (1976) developed an analytical model to get solutions for resistance and other flow parameters caused by discrete roughness selected to simulate flow conditions in vegetative channels. They calculated the conveyance factor as a function of flow depth and found that the conveyance factor values in general were higher for fully submerged vegetation as compared to the partially submerged vegetation.

Petryk and Bosmajian III (1975) presented a flow resistance model for unsubmerged vegetation conditions and the model was used to predict N value in terms of vegetation density, hydraulic radius, and the Manning bottom roughness value without the vegetation. In case of a uniform density of vegetation with height as in case of heavily treed flood plains, the N value increased in proportion to the  $2/3$  power of hydraulic radius. It was assumed that the flow occurred through heavily vegetated areas where the total shear force on the channel boundary is negligible compared to total drag force on the vegetation. The important component in the model was the vegetation density. The computed variation in vegetation density was found to be a function of height because the analyzed data agreed with the physical plant descriptions through which the flow occurred. Preliminary computation of water surface profile gave N values as high as 0.4 in heavily vegetated flood plains. They extended the model to already established USDA data for different row crops as well as other heavily vegetated flow conditions and found in general there was direct relation between the N value and the vegetation density and depth. In submerged test conditions, the N value decreased as velocity x hydraulic radius value increased. The decrease in N value was associated with increase in plant bending. This relation was not considered valid in case of protruding vegetation. They found that under vegetation conditions where foliage mainly consisted of bush and weeds, the vegetation density increased rapidly with depth along with N value. The rapid increase in vegetation density was considered to be due to increased branching and leaf density with height for the measured flow depths. In areas covered with large trees, the main obstruction to flow occurs due to tree trunks and lower branches. The degree of leaf cover and its obstruction to flow is limited in each case because of heavily shaded conditions over the flow depth. In such cases, the photographs and analytical results showed that

the vegetation density relatively remained constant with flow depth while N value increased with depth.

Chen (1976) evaluated friction coefficient for shallow flows over turf surfaces and found that the coefficient for laminar flow on the turf surface is a few orders of magnitude higher than that on glued-sand or concrete surface. In general the coefficient value increased with bed slope but decreased with Reynolds number (or discharge if the water temperature was constant). He found a linear relationship on log-log paper between conveyance value and bed slope for Kentucky blue grass and Bermuda grass.

Most of these studies have dealt with the effects of vegetation on flow characteristics and flow retardance coefficient in general. However, very little work has been reported in literature about the N value dependence on vegetation density under different types of vegetation especially in a very slow water flow system like marshland or slough. Seasonal changes, vertical and lateral vegetation distribution, flow depth, types of plant communities and their inter-relations all effect the estimation of flow retardance coefficient. This complicates the prediction of N value that could be successfully used in backwater profile computations and other such calculations. The present studies initiated would help in understanding the effect of diverse vegetation conditions on the flow parameters including flow retardance coefficient.

#### 5.3.2.2 Information on Vegetation in Chandler Slough

In areas where water flows through vegetation, density and types of vegetation have an important bearing on the flow characteristics, quality and quantity of water moving through the flow system. This is especially true of a marsh area since fresh water marshes are considered to be among the most productive for plant communities even in the temperate zone and may be two or more times as productive as the terrestrial system (Jervis, 1969). High productivities of emergent marshes are attributable to ample supplies of water and nutrients from upland drainage areas, lack of grazing by animals, species adapted to wet land environments (Auclair et al., 1976), a longer growing season (Keefe, 1972), and better moderated temperatures as compared to the adjacent terrestrial plant communities. Information on vegetation is very essential to characterize the flow patterns in Chandler Slough and to interpret the flow data in terms of cause and effect relations.

Chandler Slough constitutes a very diverse wetland system where not only diversity in types of vegetation and their abundance, but seasonal changes in composition and biomass production intriguingly complicate the flow patterns in the marshy area.

Vegetation maps of the predominant plant species in Chandler Slough were prepared using aerial photography (Highlands County Tax Assessor's Office-Watson and Company, Tampa, Florida (1966)); Mark Hurd Aerial Surveys, Inc., Minneapolis, Minnesota (1972); U.S. Department of Agriculture, ASCS (1974) to help differentiate various major plant communities and to approximate area occupied by them. Ground truthing of these communities included a record of various species and their abundance. A brief description of each major plant species was prepared from field notes and observations. Based on vegetation sampling in Chandler Slough, eleven major plant species were identified which

could be grouped into broad nine groups (Federico, et al., 1978). About 40% of the marsh was occupied by button bush (Cephalanthus occidentalis), and about 20% by broad leaf marsh including species like pickerel weed (Pontederia lanceolata), arrowhead (Sagittaria lancifolia), and water hyacinth (Eichhornia crassipes), etc. The other seven plant communities all had area less than 10% occupied by them. A map of major plant species identified and their area of occurrence is given in Figure 5.3.1-1.

Environmental studies conducted by Federico, et al. (1978) and Shih, et al. (1978) during years 1974-76 in Chandler Slough indicated that the vegetation growth followed a cyclic trend consistent with seasons of the year. Most of the plants in Chandler Slough are perennial, and the above ground portions die back during the winter. However, new growth is initiated from persistent underground roots and rhizomes before surface water flows through the marsh. About 34 different species were collected during the course of studies mentioned earlier. The most abundant emergent species include Pontederia lanceolata, Cephalanthus occidentalis, Sagittaria lancifolia, Panicum hemitomon, Mikania scandens, with Ludwigia repens as the submergent species. Eichhornia crassipes is the significant member of the Chandler Slough flora during the wet season.

February is assumed to be the beginning of the growth season with end of April to middle of June as the most productive period. Growth rate slows in mid summer though vegetation still looking lush, it starts declining significantly in October and biomass production stay declined through the winter months. Federico et al. (1978) have reported that minimum standing crop occurred in February which ranged from 48.8 to 95.9 g/m<sup>2</sup> while maximum biomass occurred in August which ranged from 300 to 716.3 g/m<sup>2</sup>. Plant detrital mass is the highest in February and exceeds the macrophyte biomass from the previous October.

The vegetation classes developed using the LANDSAT data, described in Section 5.3.1, were used to select test sights for flow measurements. These vegetation classes, depicted in Figure 5.3.1-2, are described as follows:

1. Wax myrtle that includes woody shrubs, dense woody shrubs and trees. The predominant species in this group is the large tree-like shrub called wax myrtle (Myrica cerifera). It forms dense stands that often occupy an elevated knoll. The canopy becomes complete that eliminates most understory vegetation from this association.
2. Buttonbush. The central portion of Chandler Slough is dominated by buttonbush plants which are one to two meters tall. It generally grows in association with species like Sagittaria lancifolia, maiden-cane (Panicum hemitomon), and climbing hempweed (Mikania scandens),

etc. Buttonbush density averages about 0.25 plants/m<sup>2</sup>. In the fall and winter season the plant remains without leaves. Marsh vegetation between the buttonbush plants include pickerel weed (P. lanceolata), cut grass (Leersia hexandra), prairie iris (Iris hexagona), and false maidencane (Sacciolepis striata), etc.

3. Transition, improved pasture and low grass pasture. The southern part of the slough is dominated by aquatic tall grasses like torpedo grass (Panicum repens) or maidencane (Panicum hemitomon). Other grass species include broom sedge (Andropogon sp.), cutgrass (L. hexandra), and false maidencane (Sacciolepis striata). Less tall plants consist of Aster spp. aromatic figwort (Bacopa caroliniana), coinwort (Centella asiatica), Cyperus haspan, white top sedge (Dichromena latifolia), and pennywort (Hydrocotyle umbellata), etc. Patches of pickerel weed, arrowhead, primrose willow, bulrush, wax myrtle and Thalia geniculata are scattered in this zone.

Some area is also infested with switchgrass (Spartina bakerii) in western part of the slough and in the buttonbush zone. The grass grows in spreading clumps up to two meters in height. Climbing hempweed is found growing on switchgrass at some places.

Besides, there are slight ridges and small knolls in Chandler Slough which support a ground cover of small grasses, sedges, and herbaceous plants. These areas are grazed by cattle during the dry season. When water levels rise during rainy season the vegetation shifts to a more aquatic community that is characterized by smartweed, pickerel weed, and submergents like aromatic figwort and Hydrochloa carolinensis. There is some area located west of the major tall grass/wet prairie associations which is infested with broomsedge (Andropogon sp.).

4. Broadleaf Marsh. Considerable area is dominated by several broadleaf aquatic plants which include pickerel weed, arrowhead, and Thalia geniculata. Smartweed is usually present, cattail (Typha sp.), primrose willow (Ludwigia peruviana), and bulrush occur occasionally. Submergents such as willow and aromatic figwort are usually present.
5. Dense Cypress Vegetation area. This area contains bald cypress (Taxodium distichum) which has a density of about one tree per five meter squared. Several species of epiphytes including Tillandsia spp. and Encyclia tampensis (butterfly orchid), grow on the cypress. Other large plants include pop ash (Fraxinus caroliniana), buttonbush (Cephalanthus occidentalis). There is some low growing vegetation except during the summer and autumn when water hyacinth (Eichhornia crassipes) becomes abundant. Some open water areas have smartweed (Polygonum sp.).

In some places bald cypress is also present but it is less dense and is intermixed with occasional cypress heads. Low growing vegetation is of similar type as in case of dense cypress vegetation area.

Cyperus articulatus, buttonbush, prairie iris and several species of submergent plants are also present.

### 5.3.2.3 Selection and Vegetation of Test Sites

An attempt was made to select sites in areas under each of the major vegetation categories on basis of their relative abundance and area occupied by them for making flow velocity measurement and subsequent 'N' values determinations. Four such sites were selected in vegetated areas occupied by predominant plant communities such as; (i) broadleaf marsh, wet prairie (transition); (ii) buttonbush, wet prairie, willow; (iii) improved and unimproved pasture, low grass; and (iv) woody shrubs and tress, etc. All these plant community groups together occupy about 90% of the area of the slough.

At each site, subsites were selected on basis of presence or absence of protruding vegetation, different predominant species of vegetation and abundance of a particular local species alone or in combination with other species. General description of the vegetation in sites and subsites where flow measurements were taken is given below. Location of the sites in the slough is indicated in Figure 5.3.2-1.

Site 1. This site is located in the broadleaf marsh (transition) type of vegetation group area. Approximately 20% of the slough area is infested with this type of vegetation. Broadleaf marsh vegetation is very succulent and lushy type and the growth in general is affected by seasons with peak during wet season. The peripheral vegetation is buttonbush and woody shrub type. The most abundant vegetation occupying about 40% of the total area of the slough is buttonbush. At this particular site the general effects on flow result from this type of vegetation whereas local vegetation affects the flow measurement at a particular location or subsite. Thus, this site represents the two most abundant categories of vegetation.

Emergent species including water hyacinth, pickerel weed, buttonbush, and arrowhead were locally present. A thick mat of water hyacinth was covering a large spot in relatively deeper water area with gradually grading into other species of vegetation like pickerel weed alone and in combination with buttonbush, and other vegetations. The site was selected with a view to see effect of two main groups of vegetation alone and in combination on flow resistance coefficient at different depths and different locations. Buttonbush during the fall and winter months does not bear leaves and only woody stems stand out affecting the flow velocity. During the month of October water level had already receded by about 17-20 cm as compared to water level in September. The local vegetation is given as:

Subsite 1. Infested with thick water hyacinth vegetation that floats on the surface with roots anchoring the plant near the water surface. Thick

# CHANDLER SLOUGH VEGETATION MAP

APRIL 11, 1976

The map shows a series of parallel lines representing the slough's boundaries and internal features. Various symbols like dots, dashes, and circles are scattered throughout, corresponding to the legend. Circles 1, 2, 3, and 4 highlight specific points of interest along the slough.

- @ DENSE CYPRESS
- 8 TREES, WOODY SH
- o BUTTONBUSH, WE
- PRAIRIE, PRIMR
- / BROADLEAF HARS
- UNIMPROVED PAS
- LOW GRASSES &
- IMPROVED PASTU

85-

- @ DENSE CYPRESS
- 8 TREES, WOODY SHRUBS
- 0 BUTTONBUSH, WET PRAIRIE, PRIMROSE WILLOW
- / BROADLEAF HARSH
- UNIMPROVED PASTURE
- LOW GRASSES & IMPROVED PASTURE

Figure 5.3.2-1

surface mat cuts off any light making the place unsuitable for any submerged growth. This type of vegetation creates another plane where water velocity approaches near zero producing conduit type of flow instead of open channel flow. The vegetation appeared to be about 1 to 1.25 m tall.

Subsite 2. This subsite lies in predominantly pickerel weed area where water depth is comparatively less as compared to subsite 1. The area has some intermingled buttonbush and some submerged vegetation.

Subsite 3. This is again in water hyacinth area, though water depth is comparatively a little less. The subsite lies between 1 and 2.

Subsite 4. This subsite is further down in the same direction as subsite 3. Medium pickerel weed growth and woody stems of buttonbush stand in between giving relatively free and exposed water surface. Some submerged vegetation is also present.

Subsite 5. This is located in area adjacent to subsite 4 on the outward side. Predominant vegetation is pickerel weed about medium tall. About 30 - 40% dried woody buttonbush and shrub stems are also present. The subsite also has spots with no surface but submerged growth.

Subsite 6. This subsite lies next to subsite 5. Medium high pickerel weed plants have good dense population. Drying buttonbush plants without leaves stand intermingled.

Subsite 7. This subsite lies in front of stage recorder again in deep water hyacinth area. The purpose of selecting this site was to compare flow velocity under dense hyacinth cover at different depths and then with other type of local vegetation.

Subsite 8. This subsite is on the opposite side of the other 1 through 6 subsites. The area has a good proportion of buttonbush mixed with pickerel weed. The objective was to study effect of pickerel weed mixed with buttonbush on the flow resistance values.

Subsite 9. This subsite is located in buttonbush with little pickerel weed and some submerged vegetation. This would give the effect of buttonbush predominantly on 'N' values. Dry vegetation was giving withering appearance in the month of October.

Site 2. This site is located in the low grass group area on one side surrounded by broadleaf marsh and buttonbush, and on the other open water containing submerged vegetation. The vegetated area has tall and dense growing plants. Deep inside pickerel weed plants are very tall and well developed. This also has a zone where tall trees are standing. The site was selected to study flow patterns in low vegetation area, mixed vegetation and tall tree and shrub type of plants, increasing flow depths, and changing vegetation density. Vegetation at subsites and reason for their selection are as follows:

Subsite 1. Scattered spots of vegetation are present with mostly open water space containing submerged weeds. The place was considered to be

good for low depth open water, flow without much emergent vegetation. Some creeper branches were present on the surface.

Subsite 2. Next to subsite 1 in direction of increasing vegetation density. Low growth vegetation grades into medium growth, mixed type of vegetation. Very few woody plants were present. This place provided spot for studying effects of increasing vegetation density on the flow resistance values.

Subsite 3. This subsite lies further down on denser side of subsite 2. Medium to tall plants containing 30 - 40% pickerel weed with some submergent and bent plants and very little dry shrub population. This subsite was selected to get ideas about flow patterns in mixed vegetation with increased density.

Subsite 4. This subsite has relatively denser top story vegetation and contains tall and very developed pickerel weed. Thin stemmed trees and woody plants with relatively deeper flow depth was suited for studies under tree and bushy type of vegetation.

Subsite 5-6. They were on the opposite side of subsite 1 through 4 in decreasing vegetation density area. Submerged weed growth was present. During the month of October no free water was noticed. The subsite was selected to study flow resistance trends in low and very thin vegetation growth area.

Site 3. This site is located in area surrounded by unimproved pasture. The local vegetation is very succulent broad leaf marsh type. Because of short type of peripheral vegetation, this place was selected to study the role of local vegetation on the flow characteristics of the area. The spots where flow measurements were made had thick pickerel weed which was medium in height and had constituted about 90% of the local weed population. There were only 2-3 trees present in the nearby area. Subsites 1, 2, and 3 were selected on the basis of vegetation density. Subsite 1 was located in the most dense with subsites 3 and 2 in less dense locations. The site had very little open water space.

Site 4. This site is located in area surrounded by tall trees, dense woody shrubs, etc., which constitutes a significant vegetation group present in the slough. This type of vegetation has a larger effect on the general flow patterns of water which are conditioned by local vegetation if any present. The local vegetation where flow measurements were made was water hyacinth. The vegetation made a thick mat over the surface and though the water was relatively deeper than at other sites, the flow appeared to be slow even under the mat due to outside peripheral vegetation effects. Three subsites were selected, one with very thick cover, another an open water spot surrounded on two sides by hyacinth, and third a spot in less dense hyacinth vegetation. This site was selected to study the effect of local vegetation density on the flow patterns of the area surrounded by tall woody vegetation.

General location of subsites in a site in relation to instrumentation ports or landing places is given in Figure 5.3.2-2.

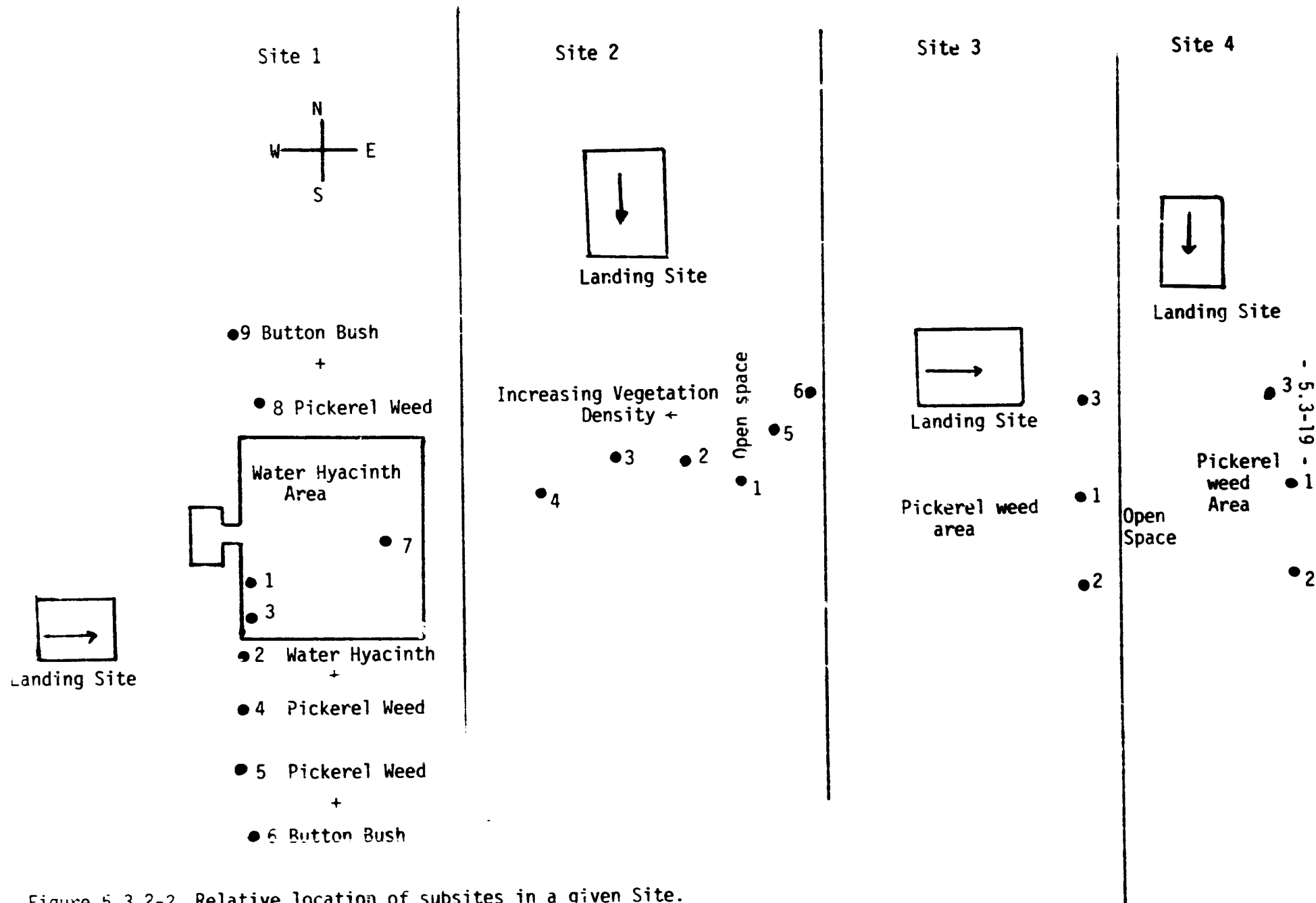


Figure 5.3.2-2. Relative location of subsites in a given Site.

### 5.3.3 Hydrologic Model Calculations

#### 5.3.3.1 General Considerations and Techniques Used

In making the flow measurements, precautions were taken to keep disturbance in water to a minimum to evaluate the flow in natural conditions. The helicopter at each site was landed at least 70 m away from the area where the flow measurements were intended to be made. The helicopter engine was shut off and enough waiting period was maintained before starting measurements until water currents induced by helicopter landing had died down. While making actual flow measurements using either of the two techniques given below, walking and all other activities affecting the flow were stopped. The techniques used were (a) water current meter and (b) Fluorescein Dye method.

- a. Water Current Meter Technique: An electromagnetic water current meter called Velmeter (developed by Cushing Engineering, Inc.) was used to make speedy flow velocity measurements. Flow velocity profile was developed along the flow depth at ten-centimeter depth intervals at different sub-sites. The sensor of the flow meter was dipped in water to the indicated mark at a given location and was rotated if necessary to get positive velocity readings on both channels of the current meter indicating correct orientation of the electrode in the direction of flow. Proper response time adjustment was made depending on the flow velocity at a given depth and location. Velocity readings from both channels were recorded and the composite velocity was calculated. Depth of the flow was measured with meter stick. The current meter could not be used for measuring flow velocity at the surface since it had to be dipped in water to a certain depth for its proper operation. The meter gave flow velocity reading at 20 cm depth and below. The flow meter was checked time and again against the dye technique for its calibration during the course of all flow measurements.
- b. Fluorescein Dye Technique: The technique was used for surface water flow velocity measurements. Initial flow measurements were started with this method.

Powdered fluorescein dye was injected at a particular location and its path was noticed downstream as a function of time. The time the dye took to pass through the measured distance was noted and flow velocity was computed. Average depth of flow over the dye path and slope of the area were also measured.

#### 5.3.3.2 Determination of Slope

Gradient of flow in Chandler Slough at each site, needed to compute  $N$  values at a particular location, was determined by surveying the sites in two ways and then finding the average elevations at adjacent sites.

- a. At each site, elevations were taken in direction of flow at particular distance interval (short intervals for steep changes and long intervals for smooth changes in slope) and general elevation of the site was computed by averaging the elevations measured excluding any ditches and bumps at the bottom of flow.

b. A contour elevation map had already been prepared to scale by surveying the bottom of the Slough. Elevation for a given site was obtained from the line passing through the central part of the given site.

Slope was determined by getting the difference in average elevations between adjacent sites and dividing that difference by the distance calculated from the map between the two neighboring sites. Slope thus computed was used in calculations for site with lower elevation.

### 5.3.3.3 Models Application

#### 5.3.3.3.1 Determination of Manning's N

The roughness coefficient N was calculated using the modified Manning's flow formula (Shih, et al., 1978), i.e.

$$N = \frac{1.486}{V} D^{2/3} S^{1/2} \quad (5.3.3-1)$$

where

V = velocity of flow, ft/sec

D = the depth of flow, ft

S = slope of the energy gradient, ft/ft.

The hydraulic radius in the original Manning's flow equation was modified by the depth of flow in the marsh because the wet perimeter in marsh flow is very close to the width of marsh.

Flow velocity and depth data, collected at different subsites, and slope calculated for each site were used to calculate N values at each location in a specific site. Flow velocity determined by using fluorescein dye technique constituted the surface flow whereas the current meter readings were used to calculate N values at lower depths.

#### 5.3.3.3.2 Determination of Vegetation Density at Different Depths

Vegetation density at different depths in each location was calculated to study the effect of vegetation growth on the flow resistance parameter and to see if the flow resistance could be related to and interpreted in terms of type of local vegetation. The relationships used to calculate vegetation density is as given by Petryk and Bosmajian (1975):

$$\begin{aligned} \text{Vegetation density} &= \frac{\sum_{i=1}^n C_d \times A_i}{AL} = \frac{2gS}{V^2} \quad (5.3.3-2) \\ &(\text{ft}^2/\text{ft}/\text{ft}^2 \text{ i.e. vegetation} \\ &\text{occupied area per unit flow} \\ &\text{length per unit area of flow}) \end{aligned}$$

where

$C_d$  = the drag coefficient for vegetation

$A_i$  = the projected area of the  $i$ th plant in the direction of flow ( $ft^2$ )

$A$  = cross-sectional area of flow ( $ft^2$ ),

$n$  = total number of plants

$l$  = length of the channel reach being considered

$S$  = bed slope of the channel  $ft/ft$

$V$  = flow velocity  $ft/sec$

$g$  = acceleration due to gravity  $ft/sec^2$

In the above relation it is assumed that the velocity is constant over the depth interval being considered, and the  $N$  value for flow without vegetation is small and can be neglected in relation to flow resistance induced by vegetation.

#### 5.3.3.4 Results and Discussions

Type of vegetation, its growth characteristics, hydraulic behavior of the whole plant and its component tissues, its lateral and vertical distribution, depth of flow, fluctuating levels of water, and seasonal variations are some of the very crucial factors that affect the flow characteristics of a vegetated flow system. Unfortunately, not much information is available on the retardance coefficient (Manning's  $N$  values) in heavily vegetated channels except for some grassed water ways. Chocking aquatic weeds at some places produce thick large mats of vegetation on the surface that not only causes considerable reduction in water carrying capacity of the system but alters open channel flow to enclosed or conduit type of flow (Bogart, 1949). General and local thick protruding and/or submerged vegetation of the area causes water to follow tortuous path that complicates the driving head and flow velocity relations thus making it hard to get meaningful flow retardance coefficient values that are needed to predict the water flow relations of a densely vegetated flow system.

Flow resistance coefficients ( $N$  values) at different depths in Chandler Slough were determined from the velocity data using Manning's formula. Since the flow velocities were determined to be low in general and did not appear to be large enough to displace vegetation,  $N$  values versus depth (instead of velocity x hydraulic radius) plotting method was used to study and evaluate trend of flow retardance values in the marsh land flow.

General trends: The flow retardance values in general are relatively larger than those reported in literature for canals and other vegetated water ways because of impeded water flow induced by dense vegetation. At all sites tested,  $N$  values varied widely both horizontally and vertically because of

wide differences in vegetation and flow depth at a particular time. Type of general vegetation (broad group) of the area affected the overall resistance values, whereas local vegetation, its abundance, and its relation to the adjacent type of local vegetation significantly affected the N values at a particular location. No singular trend of N values was evident at any of the four sites investigated in relation to depth or lateral distance. Local vegetation, based on its growth characteristics and its abundance alone and in proportion with other species, gave the following general trends of computed N values in relation to depth at all sites as interpreted from flow velocity data collected in the month of September, 1978: (a) N values decreased sharply with depth and then became consistent forming an 'L' type curve. This is true of thick surface mat spots indicating an additional plane of velocity approaching zero a little below the surface thus making closed channel flow system for the water flowing below the dense vegetation cover; (b) flow resistance increased with depth indicating reduction in effective depth of flow at the bottom; (c) flow resistance values first decreased to a minimum and then increased with depth forming 'J' type of curve, (d) N value first increased to a maximum and then decreased with lower depths giving an inverted 'V' type of relationship, and finally Manning N values slightly increased with depth (or remained fairly constant). This is true of open spot or free surface water place that has some submerged vegetation near the bottom. Flow response was observed to be complex where more than one type of vegetation was growing in combination.

Details of different types of vegetation at various sites and subsites are given in the previous section 5.3.2.

#### 5.3.3.4.1 Flow Resistance Trends at Different Sites

##### 5.3.3.4.1.1 Variations in N Values with Depth

Flow resistance coefficient values, computed for different subsites in a given site, were plotted as a function of depth. For sake of convenience in plotting and interpretation of trends, subsites were grouped on basis of magnitude of computed N values. The flow resistance values computed from September, 1978 data are given in Figures 5.3.3-1 and 5.3.3-2 for Site 1. Only September data were plotted to study the depth relations because (1) in October the water level had receded significantly and flow velocity was measured in most cases only at one water depth (and very rarely two or three) and (2) in August the flow meter was not working properly and the dye technique could only be used to measure surface flow. Site 1 is infested with both emerged and submerged vegetation. In general the N values are very high as compared to N values reported in literature. High values were found either a little below surface (20-25 cm depth) or at the bottom of the flow depending on the type of vegetation. Generally flow resistance varied 4-5 fold at a particular location, however, in extreme one case the maximum N was observed at 25 cm below the water surface and the value was about 15 fold the minimum value of N found near the bottom over a flow depth of 65 cm. In locations with 40 cm flow depth, N values in general varied less with depth except in one or two cases where the maximum N value observed at bottom was about 8-9 fold the minimum value calculated at 25 cm below the surface. Laterally, the retardance values varied 3-5 folds up to a depth of 30-35 cm but about 10 cm below

Figure 3.1. 4. Relationship Between  $W$  Values and Depth for Site 1.  
(Sept. 25, 1978) Subsites 1, 2, 4, 5, 6, 9, 11

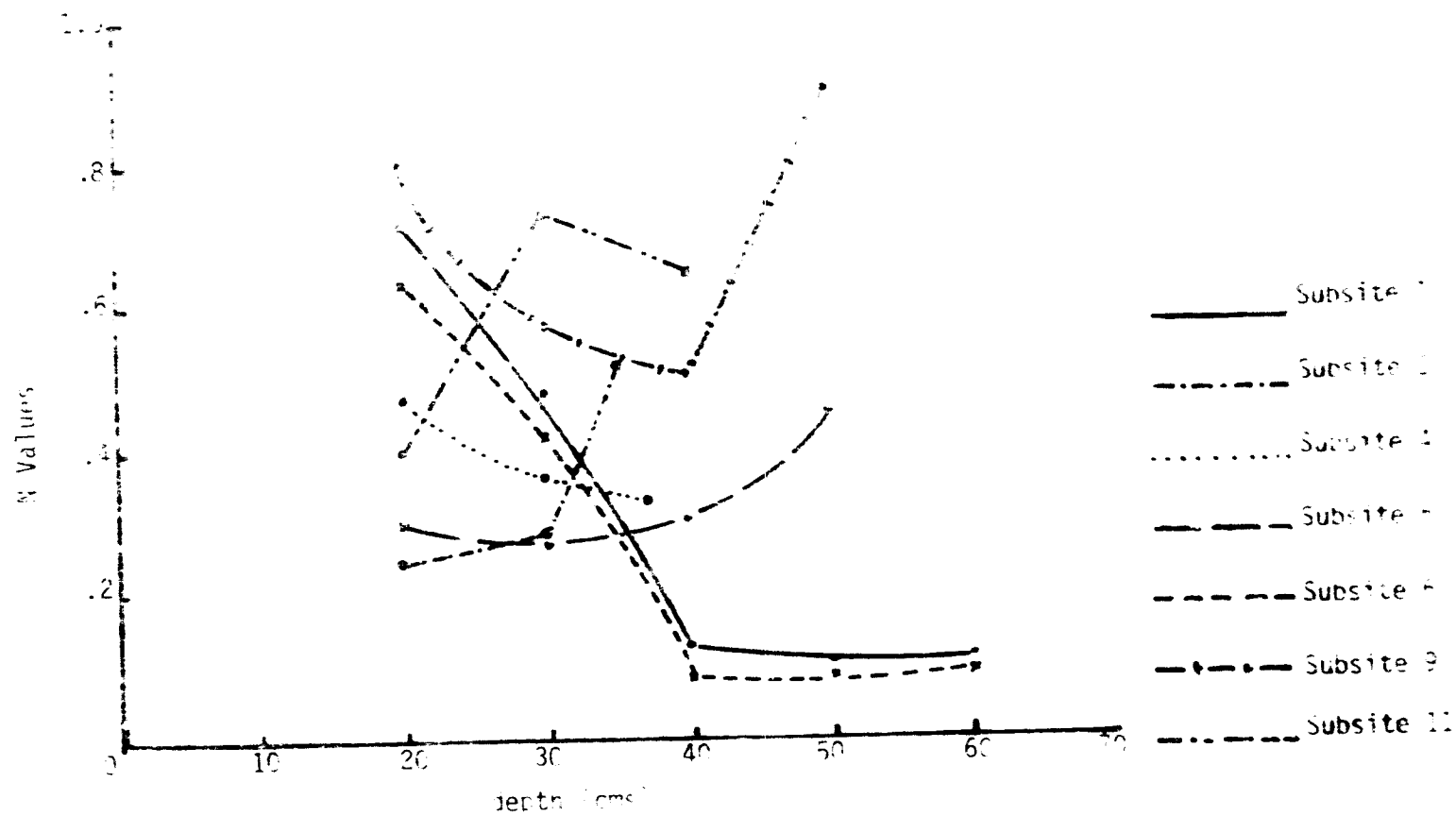
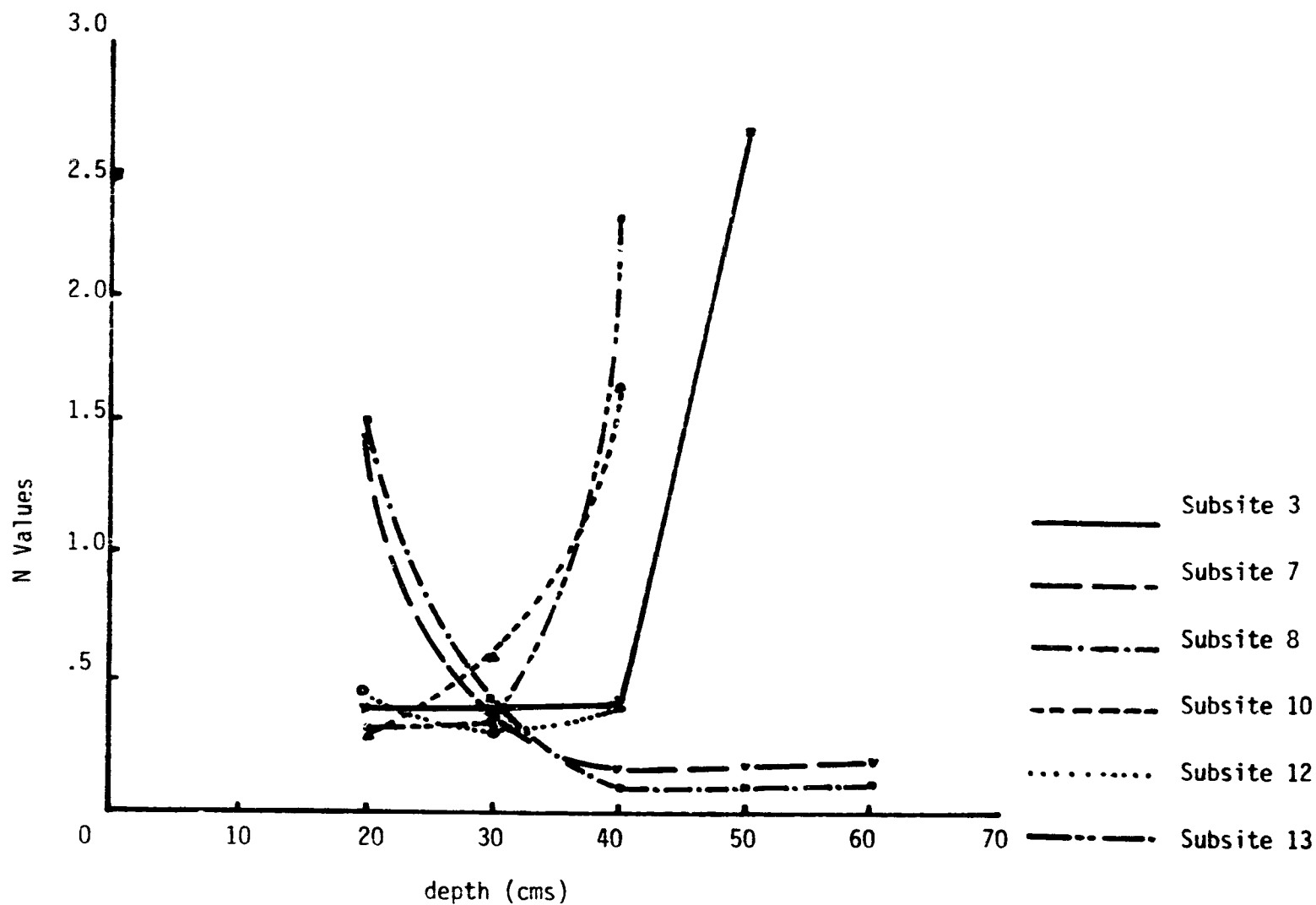


Figure 5.3.3-2. Relation Between 'N' Value and Depth for Site 1.

(Sept. 25, 1978) Subsites 3, 7, 8, 10, 12, 13



this depth the maximum value was about 30 times the minimum N value considering all locations where flow velocity was measured in this site. However, the lateral minimum N value at this depth of 40-45 cm was computed for a total flow depth of 65 cm with pickerel weed vegetation medium dense whereas the maximum value was observed at the bottom and having pickerel weed plus dry buttonbush relatively denser vegetation. The flow depth varied from 40-70 cm over the locations sampled. Decrease in N value with depth was characteristic of water hyacinth type of vegetation that protrudes through water, forms a thick covering over the surface, and its roots anchor at or little below the water surface. The thick matly cover at the top shuts off much of the sunlight that restricts growth of any submerged vegetation, thus creating conditions favorable for relatively faster flow under its cover.

Increase in N value with depth was indicated by the vegetation that anchors at the bottom, may or may not protrude through the water surface, and forms no thick cover at the surface which is typical of vegetation like pickerel weed and buttonbush, etc. Where the two categories of vegetation were growing in combination, trend of N values was affected by the relative abundance and distribution pattern of each type present.

The main reason for relatively higher general N value is the broadleaf marsh and buttonbush types of vegetation the site 1 is surrounded with, which would have predominant effect on impeding the overall flow through the area. In addition the local vegetation with its density has a marked influence in reducing the flow at a particular spot. Except in a few extreme cases the N values were about 1-3 times the maximum value of .4 reported by Petryk and Bosmajian (1975) for heavily vegetated flood plains.

The N values computed for site 2 are plotted in Figure 5.3.3-3. It is largely an open water space having submerged type of vegetation and some emerged vegetation. Maximum depth of water was recorded to be about 40-45 cm. The N values in general are of about the same magnitude that were found at lower depths in locations with water hyacinth vegetation in site 1. Relatively lower N value could be due to tree type general vegetation and less density of local vegetation. N values in the open water flow area with little emerged vegetation were of about the same magnitude as reported by Graf (1966) from Swiss data on ETH-Zurich experiments in test flumes and reported by Ree (1958) for row crops. However, in areas with relatively dense vegetation values were about two to three folds the values in open water space at the same depth and about 10 cm below. Vertically also the values varied two to three times over the entire site. The subsite 3 infested with pickerel weed mixed with shrubs and thin trees had a deeper flow of about 40-45 cm.

The flow retardance values for data from site 3 are given in Figure 5.3.3-4. The site locally has a thick growth of pickerel weed that constitutes about 90% of the total vegetation population. General surrounding vegetation comprises low unimproved pasture and broadleaf marsh with very little tree or tall vegetation. In general N values varied from 1-4 times the maximum reported by Petryk and Bosmajian (1975) for the heavily vegetated flood plains with mostly in the range of .4 to .8 and about 1 1/2 - 7 times the values reported by Leutheusser and Chisholm (1972) in an open channel steep and with heavily

Figure 5.3.3-3. Relation Between 'N' Values and Depth for Site 2. (Sept. 25, 1978) All Subsites.

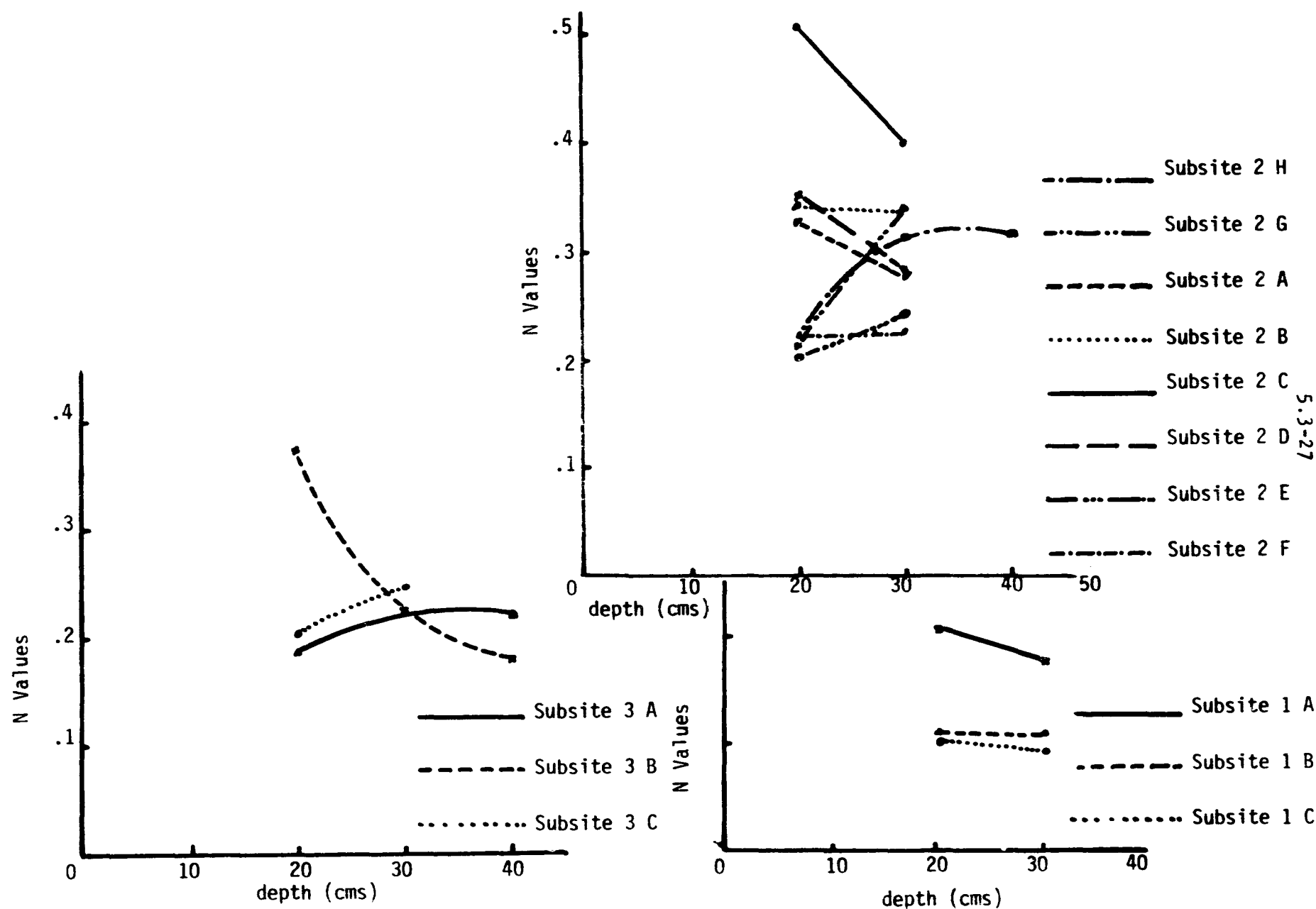


Figure 5.3.3-4A. Relation Between 'N' Values and Depth for Site 3.

(Sept. 25, 1978) Subsites 1 - 5.

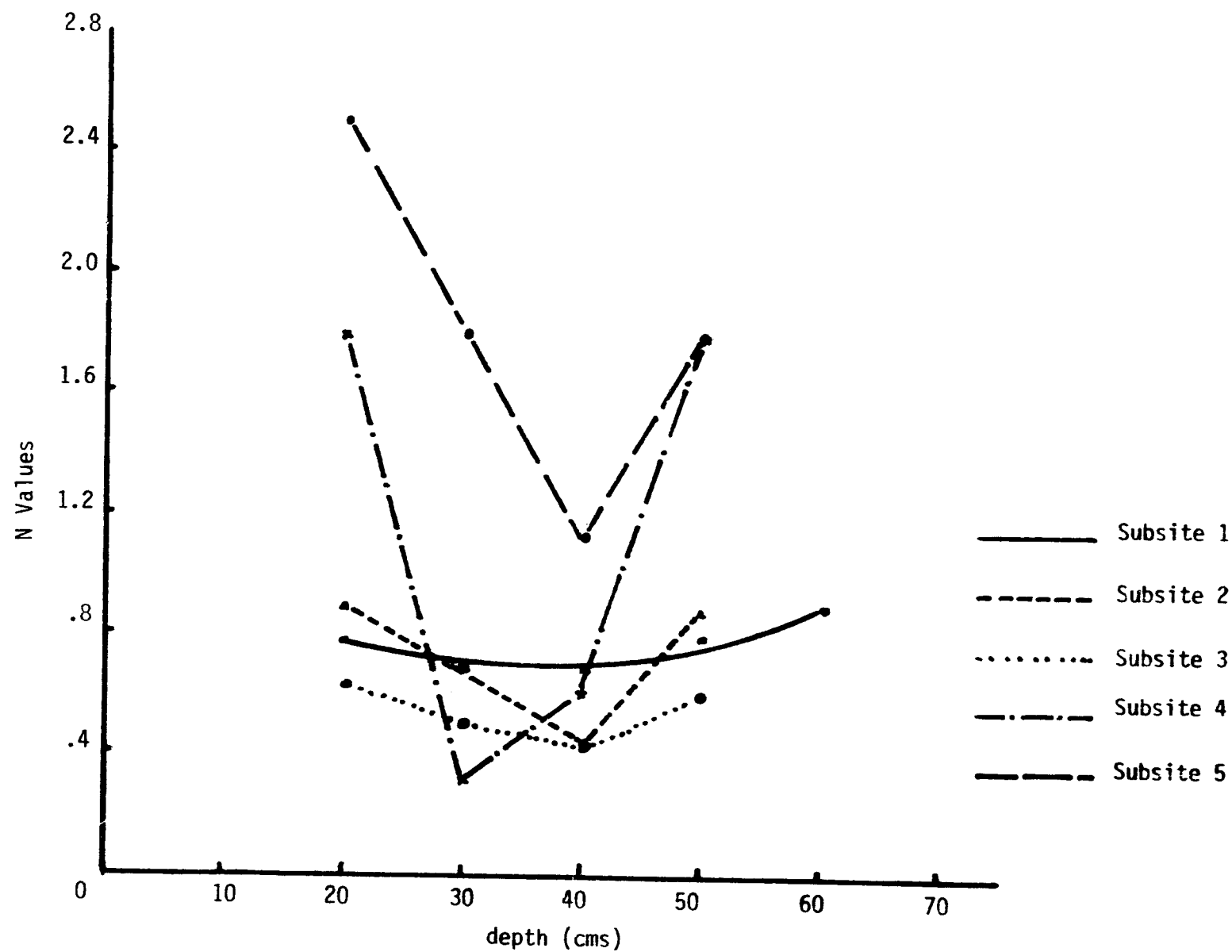
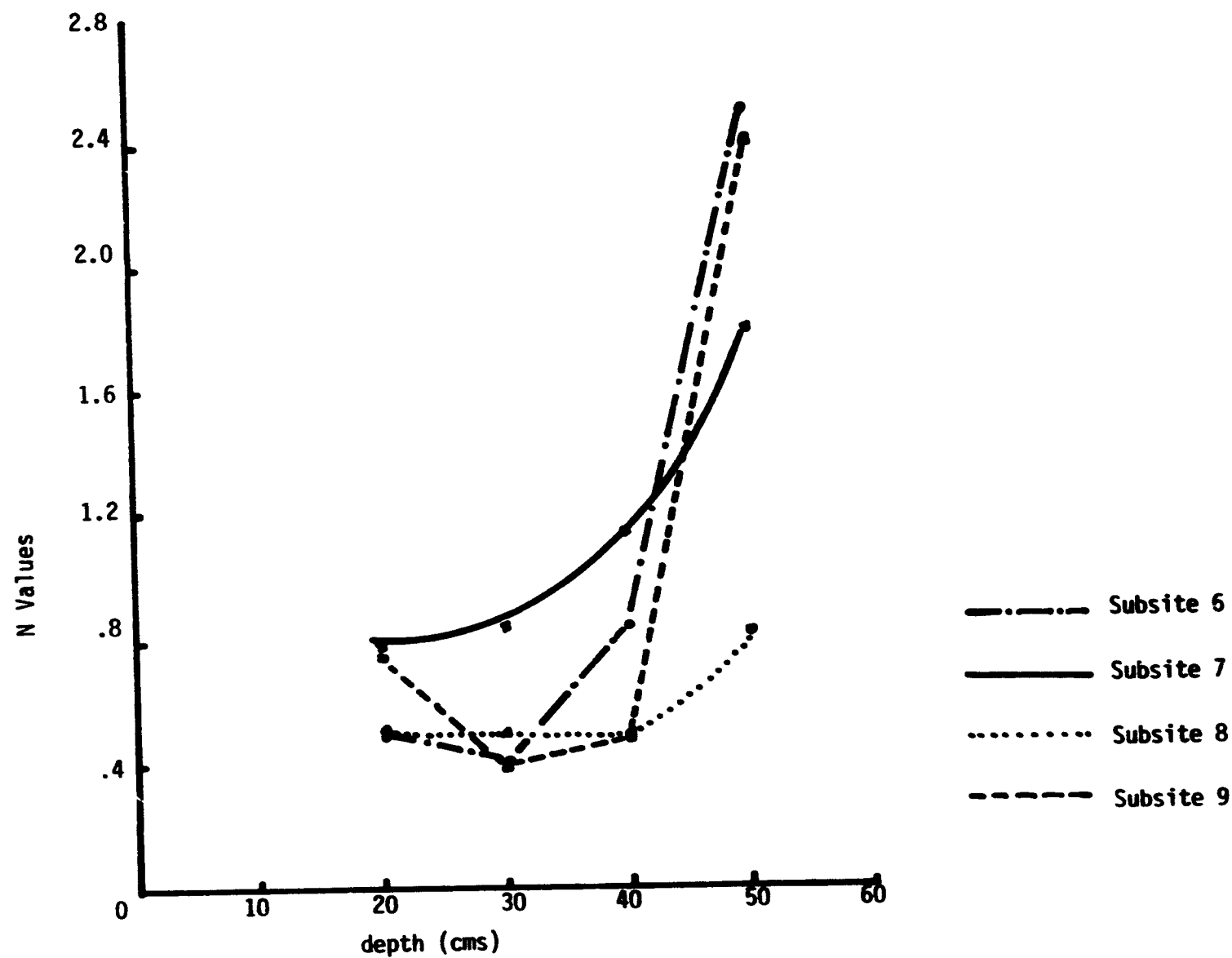


Figure 5.3.3-4B. Relation Between 'N' Values and Depth for Site 3.

(Sept. 25, 1978) Subsites 6 - 9.



vegetated sideslopes in Toronto, Canada. Generally the flow retardance coefficient increased 1-2 folds with depth at a particular location and varied about 3-5 folds at different locations for the same depth depending on density of vegetation.

The N Values versus depth for site 4 are plotted in Figure 5.3.3-5. The predominant local emerging vegetation is thick water hyacinth with some open water space infested with submerged and floating creeper type of vegetation. The computed N values are the largest in this site. In some cases the flow velocity was so low that the current meter could not measure it. The site is surrounded by dense woody shrubs and trees type vegetation which significantly effect the overall flow rate and then the local water hyacinth vegetation considerably diminishes the driving force. This combination of vegetation is the main reason the flow resistance is about the same all along the depth of flow and does not decrease as observed in site 1. Bogart (1949) has reported a maximum N value of 0.055 for this type of vegetation for the surface flow in canal in the Glades area. The computed N values are about 30-80 times the values reported by him in the densely vegetated location and about 10-20 times in the open waterspace adjacent to the vegetated area. The N values computed for different locations varied quite a bit vertically and the maximum N value was observed to be about eight times larger than the minimum obtained at 40 cm depth when all the subsites are considered in this site. Water depths in this area varied from 65 to 78 cm.

#### 5.3.3.4.1.2 Weighted N Values Versus Total Flow Depth

The flow retardance values computed for different depths were weighted to get an average for a given location and these averaged N values are plotted as a function of total depth of flow in Figure 5.3.3-6. In site 1, the resistance values showed an increase towards the middle which was probably due to predominate influence of local water hyacinth vegetation that anchors a little below the water surface leaving somewhat free space below. Weighted N values varied between .35 to .75 which is about 1-2 times the maximum values reported for heavily vegetated flood planes (Petryk and Bosmajian, 1975). Site 2 indicates an overall increase in N value with depth with the 45 cm bottom value about three times the value found at about 25 cm depth. In site 3, the first decrease and then abrupt increase in N value over 58-60 cm flow depth is due to mixed vegetation response. The values varied between .55 to 1.95. In site 4 increasing trend of N value with depth up to a certain distance indicative of water hyacinth type of vegetation in deep water. The weighted N value in open water space was about five times the value in the adjacent densely vegetated area. Computed N values for all sites are given in Tables 5.3.3-1A, 5.3.3-1B and 5.3.3-1C, in Appendix for August, September and October, respectively.

#### 5.3.3.4.1.3 Flow Resistance Values Versus Depth as Related to Predominant Vegetation.

To study the effect of predominant type of local vegetation on flow resistance along the depth of flow, the locations with visibly similar type of vegetation were grouped in each site and the average N value was computed and plotted as a function of depth. These relations for sites 1, 2, 3, and 4, are given in Figures 5.3.3-7, 5.3.3-8, 5.3.3-9 and 5.3.3-10, respectively. Each

Figure 5.3.3-5. Relation Between 'N' Values and Depth for Site 4.

(Sept. 25, 1978) Subsites 1 - 4.

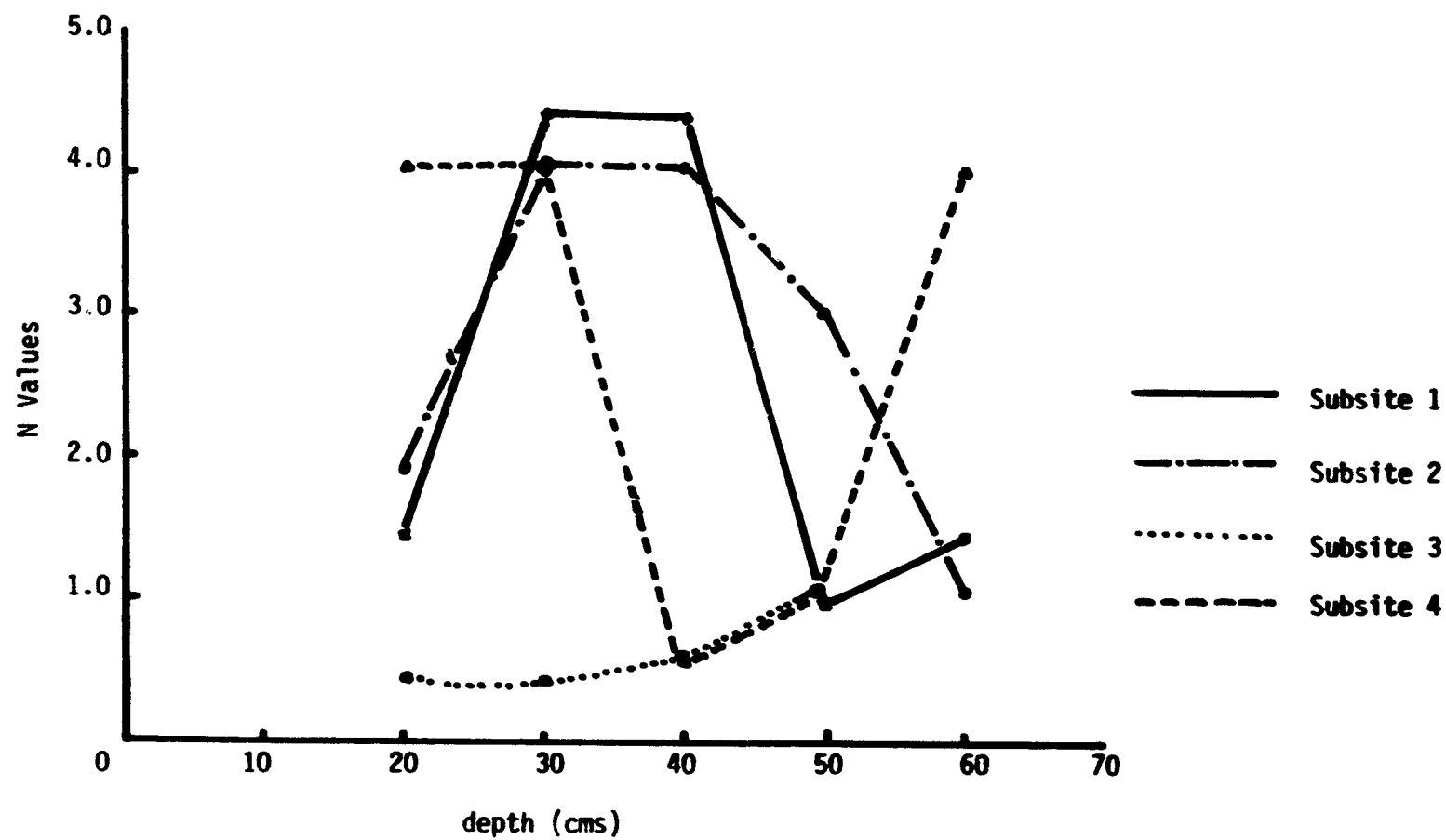


Figure 5.3.3-6. Relation Between Weighted 'N' Values and Total Depth.

(Sept. 25, 1978) All 4 Sites.

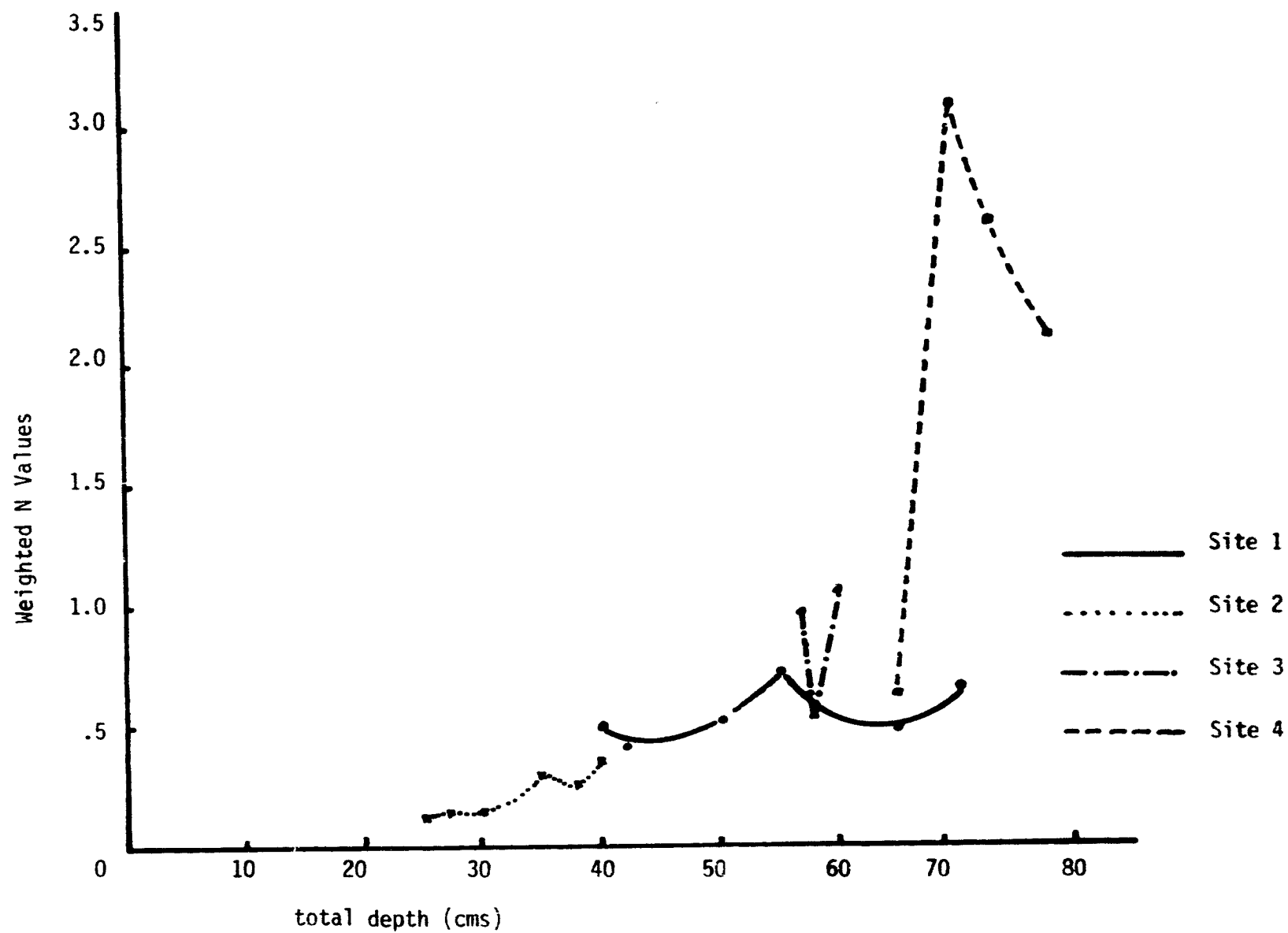


Figure 5.3.3-7. Relation Between Averaged 'N' Values for Different Vegetation Classes and Depth for Site 1.

(Sept. 25, 1978)

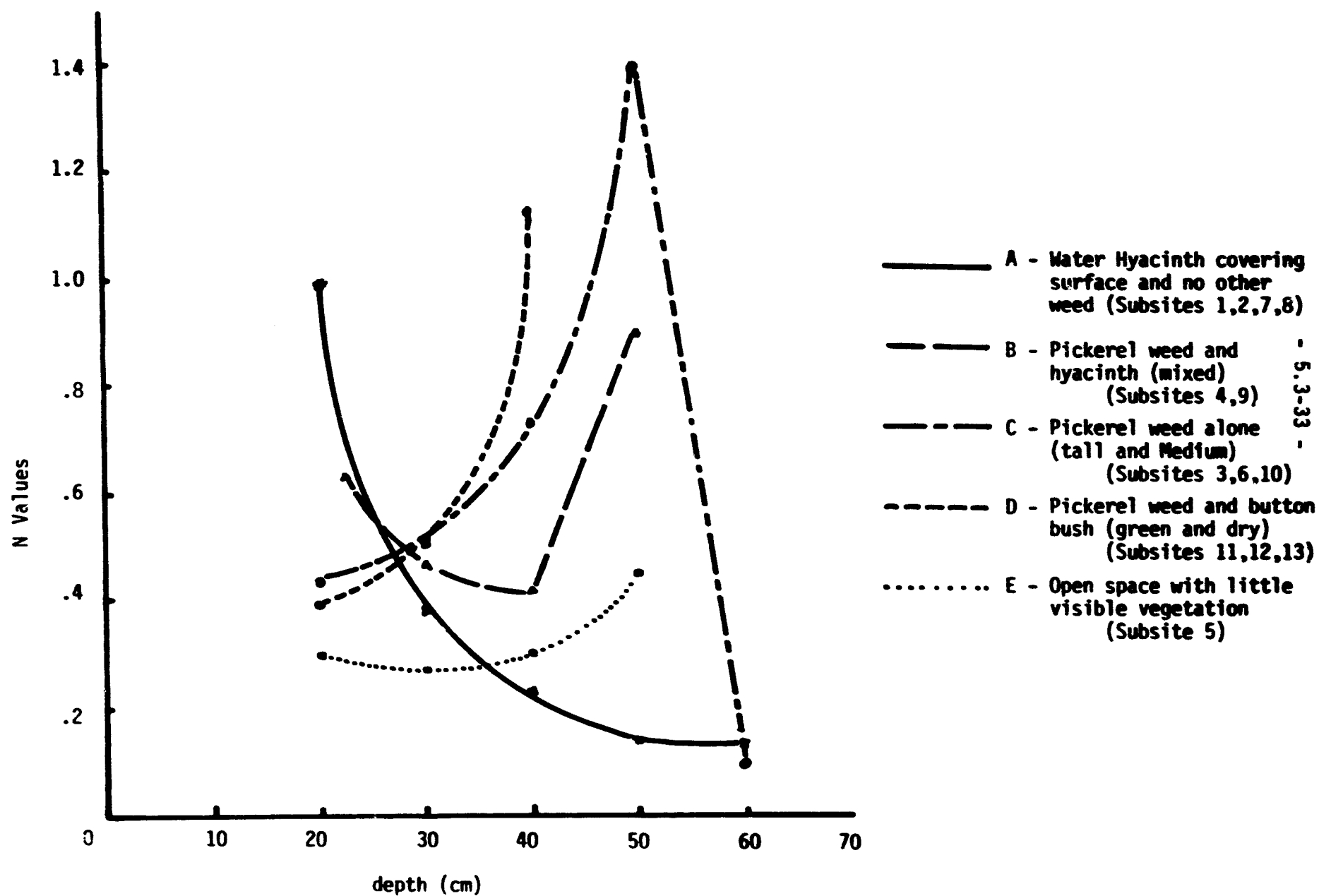
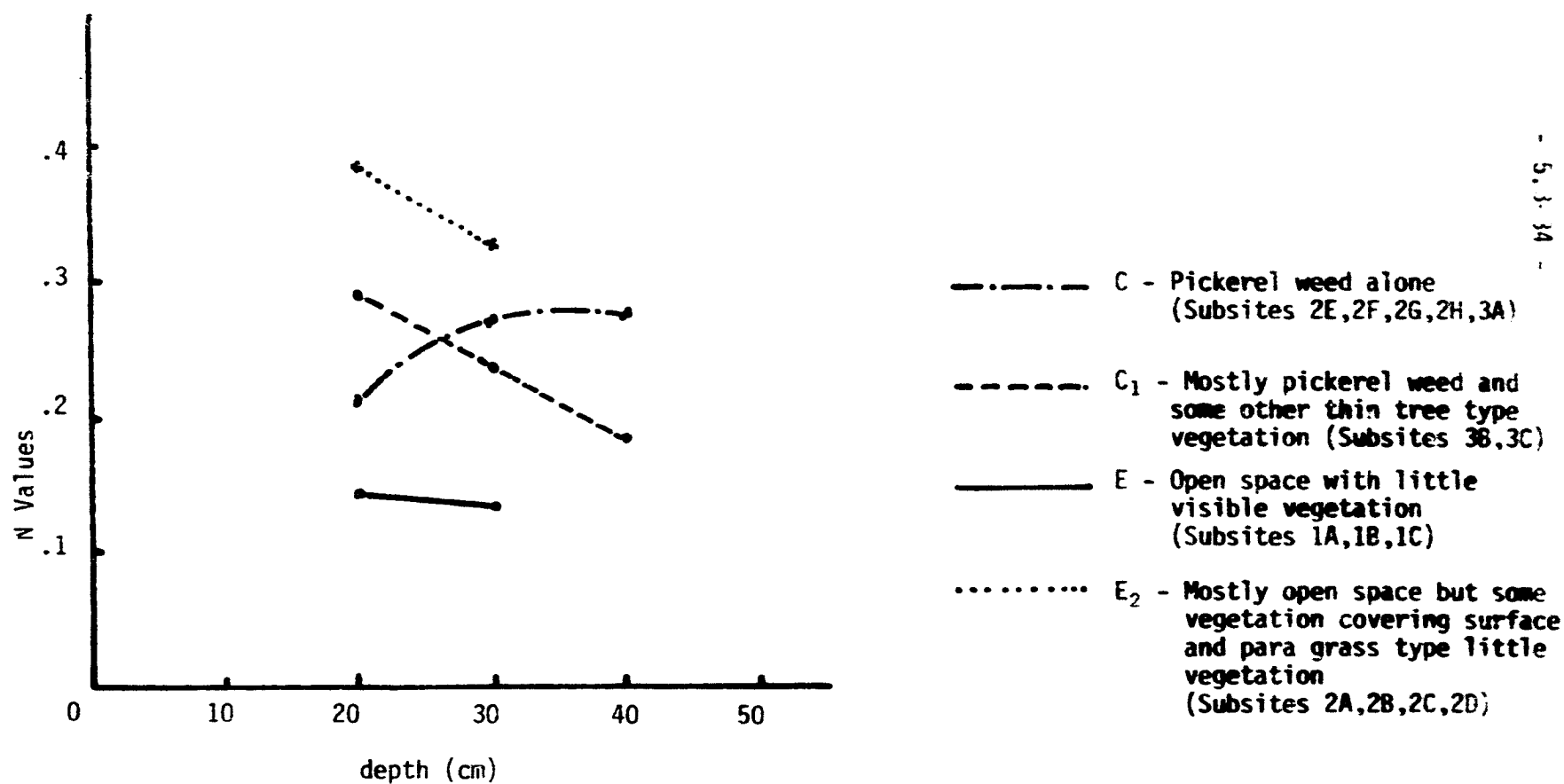


Figure 5.3 3-8.

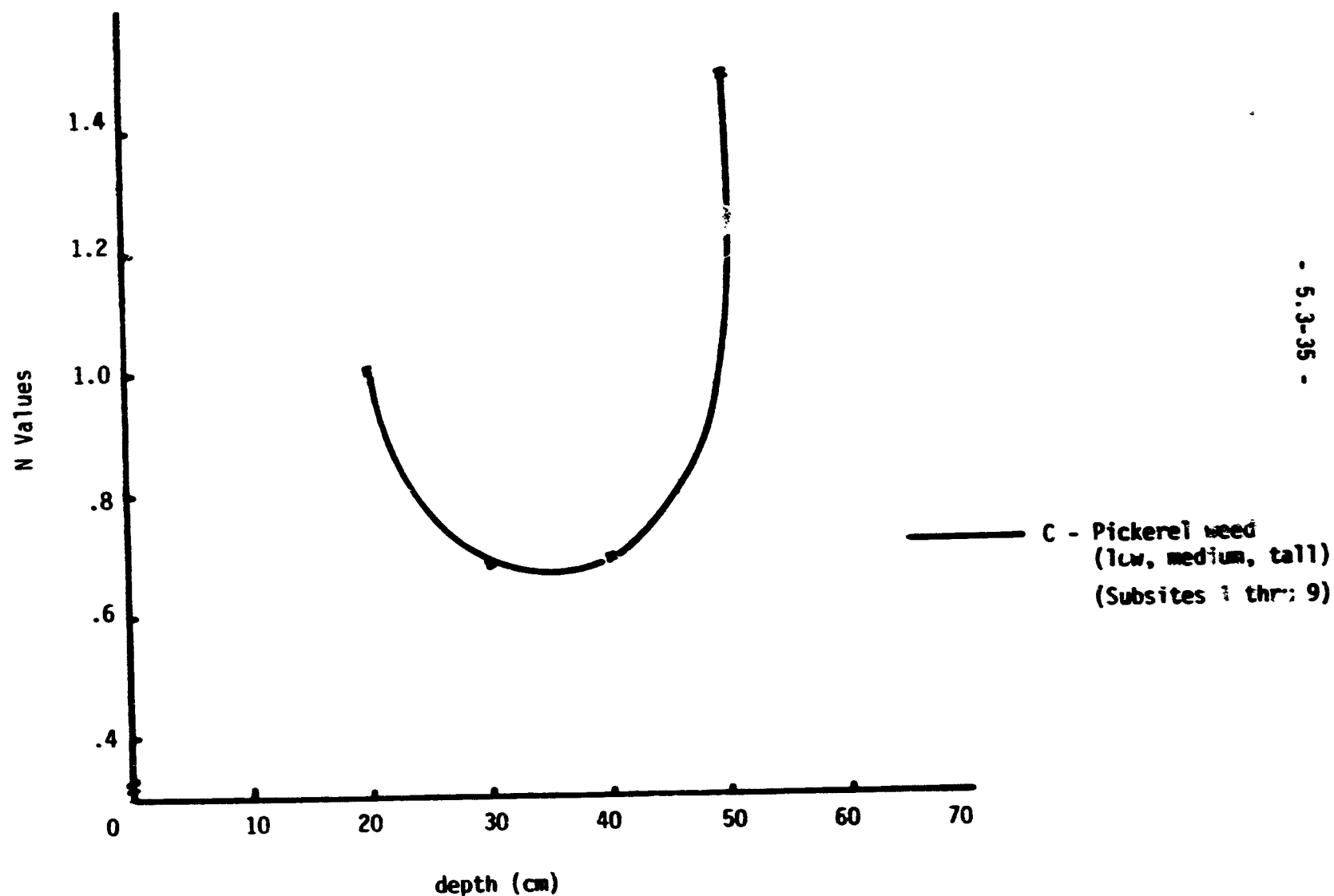
Relation Between 'N' Values for Different Vegetation Classes and Depth for Site 2. (Sept. 25, 1978).



5.3.34

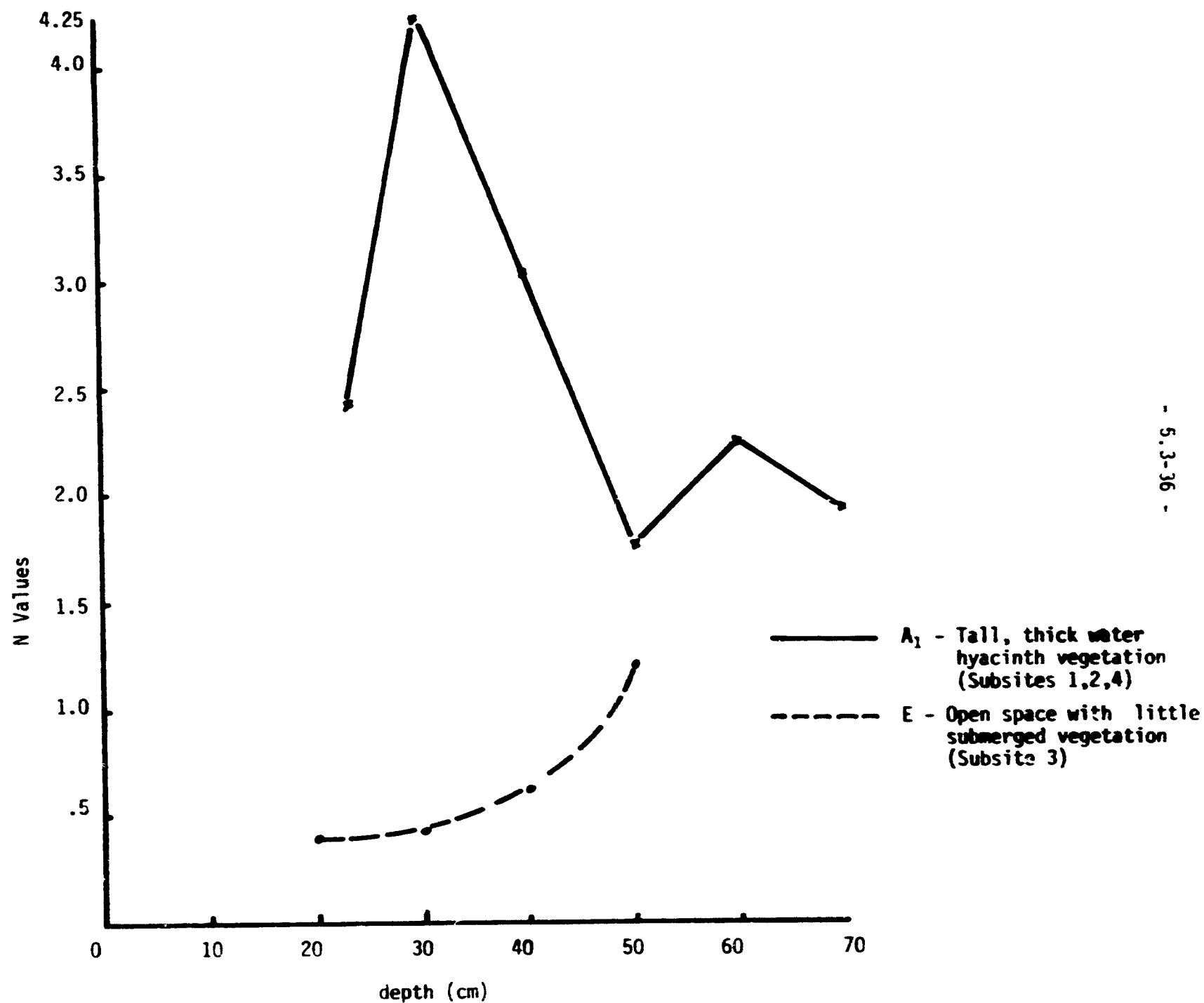
163

Figure 5.3.3-9.  
Relation Between Averaged 'N' Values for Different Vegetation Classes and Depth for Site 3. (Sept. 25, 1978).



lation Between Averaged 'N' Values for Different Vegetation Classes and Depth for Site 4.

(Sept. 25, 1978).



predominant vegetation group gave a distinct trend of N values in relation to depth.

As indicated in Figure 5.3.3-7, vegetation in site 1 was classified into 5 groups, namely

- A - Water hyacinth no other major weed
- B - Pickerel weed and water hyacinth mixed
- C - Pickerel weed no other major weed
- D - Pickerel weed and buttonbush
- E - Open water space with submerged vegetation.

In case of group A vegetation the N values were maximum near the surface at about 25 cm depth which decreased with depth and the minimum values were found at the bottom at a flow depth of 60-70 cm. The maximum N values here were about 2 1/2 times the maximum value reported in literature for heavily vegetated flood plains (Petryk and Bosmajian, 1975) and the minimum values were of about the same magnitude as reported by Ree (1958) for row crops like sorghum and wheat. For vegetation groups C and D, the N values started with value close to .4 at 25 cm depth and then increased with depth about three times at a depth of 50-55 cm that is close to the bottom. Vegetation group B produced 'V' type of curve because of the two different types of vegetation groups with heavily vegetated flood plains values at 35-45 cm depth. Open water space with little emerged vegetation but containing submerged weed growth gave relatively smaller N values as compared to any other vegetation group. The N values increase a little with depth in this case.

In site 2, four vegetation groups were formed such as: C - pickerel weed alone and no other major weed; C1 - predominantly pickerel weed mixed with some thin trees scattered; E - open water space with little visible vegetation but submerged vegetation present; and E2 - mostly open water space but with thinly scattered emerged vegetation. No flow depth at this site was more than 40-45 cm. N values with predominantly pickerel weed vegetation were of about the same magnitude as reported by Leutteusser and Chisholm (1972) for an open channel steep and with heavily vegetated sideslopes. In typical pickerel weed situation values increased with depth and in other cases they decreased. Slight decrease in N values with depth is also evident in case of open water space area where the N values were about the same order as reported for row crop like sorghum (Ree, 1958). In open water space with slight-emerged vegetation the flow resistance values were almost doubled in magnitude.

Figure 5.3.3-9 indicates the trend of N values as a function of depth where the predominant local vegetation is dense pickerel weed. The relation produces a 'J' type curve with the minimum N values in between depth of 25 and 45 cm. These values varied about 1 1/2 to 3 1/2 times the maximum N value reported for heavily vegetated flood plain.

In Figure 5.3.3-10 for site 4, the vegetation was classified into two groups such as A - tall thick water hyacinth and E - open water space with

submerged vegetation and adjacent to water hyacinth area. The N values under thick hyacinth increased to a maximum up to 30 - 35 cm depth and decreased rapidly indicating less resistance at lower depth due to relatively free space for flow. The values varied from 5 to 7 1/2 folds the maximum N value reported in literature. In open water space adjacent to the vegetated area, the N value increased with depth due to flow impedance caused by submerged vegetation.

Finally the flow retardance values for subsites with visibly similar type of vegetation for all sites are combined and averaged for a given depth. These averaged N values are given in Figure 5.3.3-11. The figure clearly indicates the trend of flow resistance values as related to the predominant type of local vegetation present in the Slough. The relations support the trends depicted in preceding figures for vegetation groups in each site.

#### 5.3.3.4.2 Relations Between Flow Retardance Values and Vegetation Density

To study the effect of vegetation growth in general on the flow retardance values, vegetation density at each depth at each location was calculated and flow resistance values were plotted against the vegetation density. Calculated vegetation density was a relationship developed from flow velocity data with the assumptions that flow velocity is uniform over the depth interval used and flow retardance value without vegetation is negligible as compared to calculated N value for vegetated area in the slough. Vegetation density, calculated as an area occupied by vegetation per unit area of flow per unit length of flow path is expressed on relative basis. The values differed very widely from location to location and with depth at the same location. The vegetation density data for different sites are given in Appendix. The studies indicated that the vegetation density (as expected) was very very high near the surface where water hyacinth was growing and the values, though larger, were comparable with the vegetation density values calculated for pickerel weed and buttonbush mixed vegetation found at the bottom of flow for site 1 and 3. Vegetation density values for 1 and 4 were in extremes from very low to very high, whereas in case of site 3 the values were intermediate and for site 2 they were generally low.

The computed N values versus vegetation density data are plotted in Figures 5.3.3-12 through 5.3.3-17 for all sites except site 2. The reason site 2 was not included was that most of the flow velocity data were confined to one depth and very rarely to two depths because of less deep water. Vegetation density and N values plots indicate that there is a direct relation between the two which varies from linear to curvilinear types of trends with most curves indicating curvilinear response in N values against vegetation density which could probably be due to hydrodynamical behavior of the local vegetation. N values versus vegetation density relations for subsite 9 (Figure 5.3.3-13), 3, and 13 (Figure 5.3.3-14) in site 1, and subsites 1 and 8 (Figure 5.3.3-16) in site 3 are straight line type relations and all other relations are curvilinear. Local vegetation description given for different subsites indicate that straight line type of direct relation between N values and vegetation density was observed where the vegetation was stiff, tall, and/or mixed. Curvilinear type of response can be explained on the basis that since most of the local vegetation is succulent and lush type, with relatively larger flow velocity and less density the vegetation can bend and there

Figure 5.3.3-11.

Overall Relation Between 'N' Values and Depth for Different Types of Vegetation for All Sites.

(N Values averaged for all sites for a given class at a given depth). (Sept. 25, 1978).

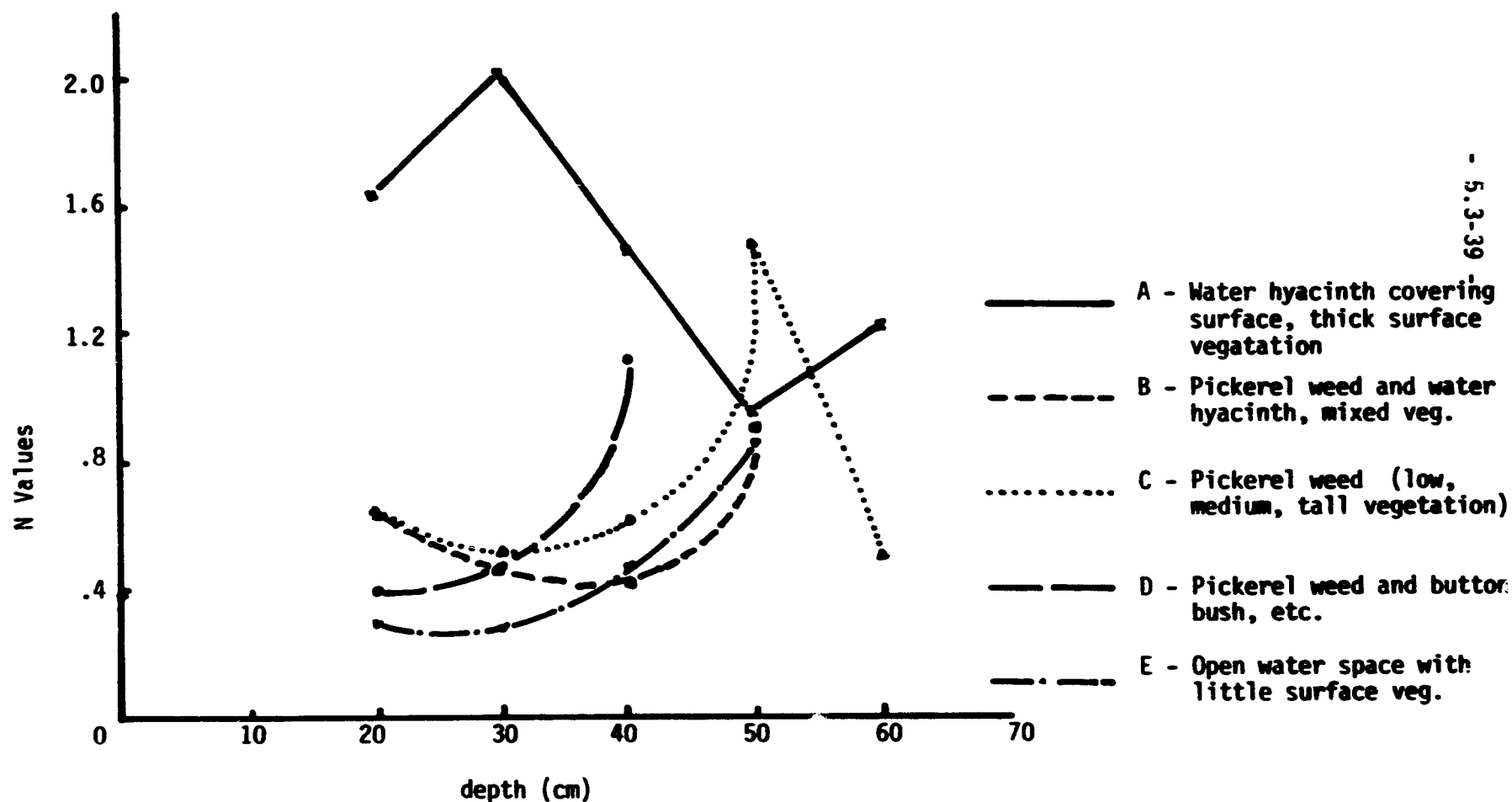


Figure 5.3.3-12.

Relation Between 'N' Values and Vegetation Density for Site 1. (Sept. 25, 1978). (Subsites 1,2,4,6,12),

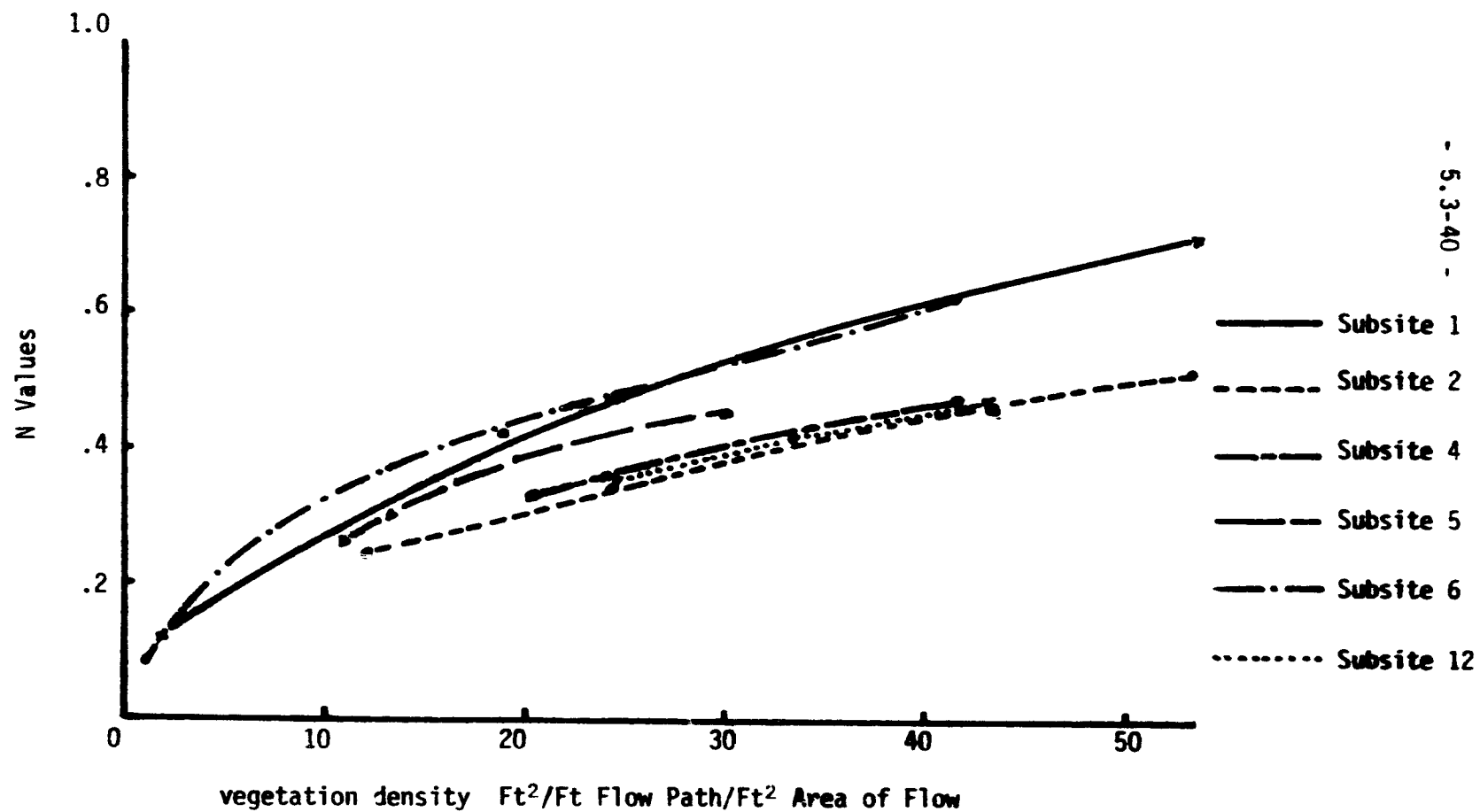


Figure 5.3.3-13.

Relation Between 'N' Values and Vegetation Density for Site 1. (Sept. 25, 1978). (Subsites 7,8,9,11).

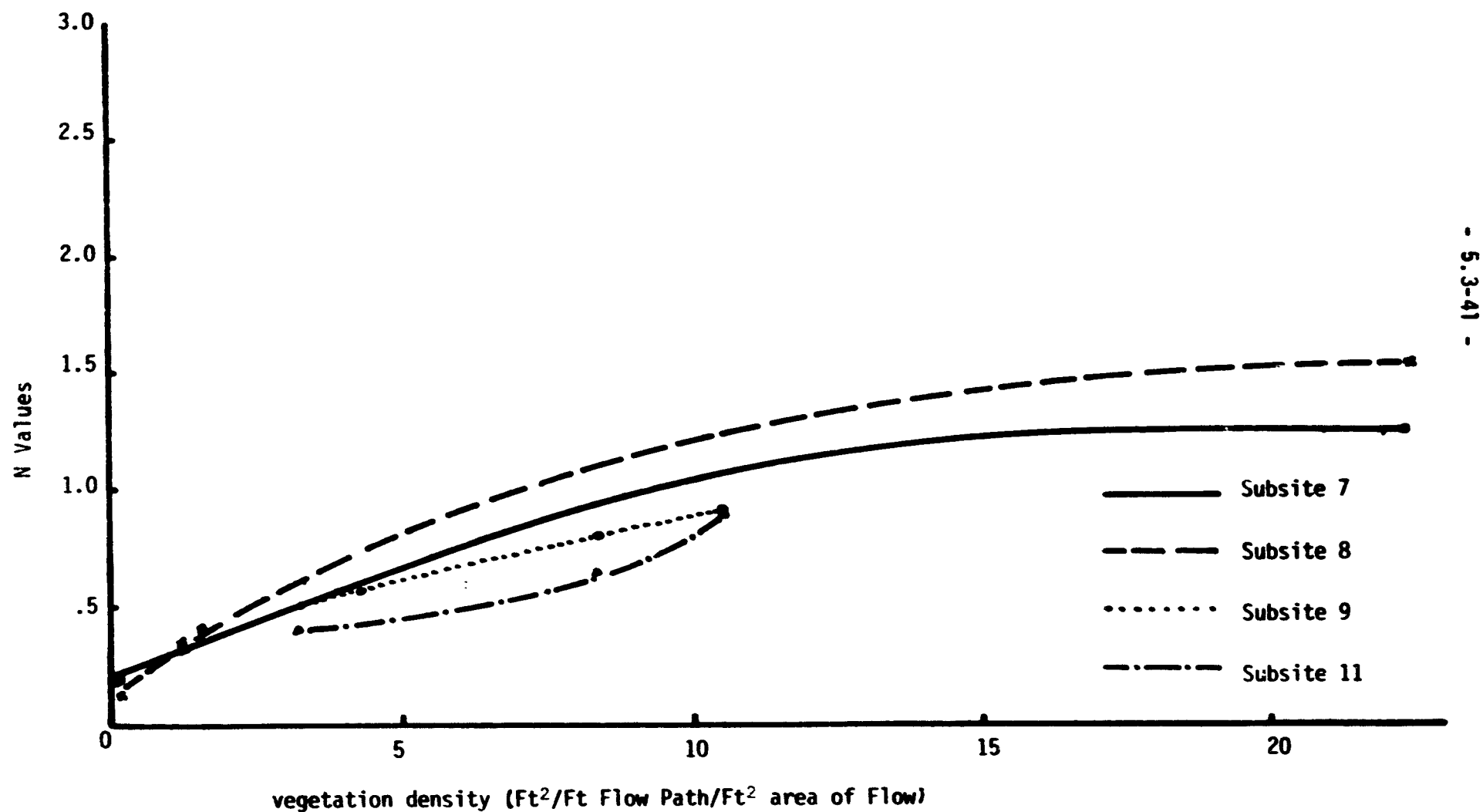


Figure 5.3.3-14.  
Relation Between 'N' Values and Vegetation Density for Site 1. (Sept. 25, 1978). (Subsites 3,10,13).

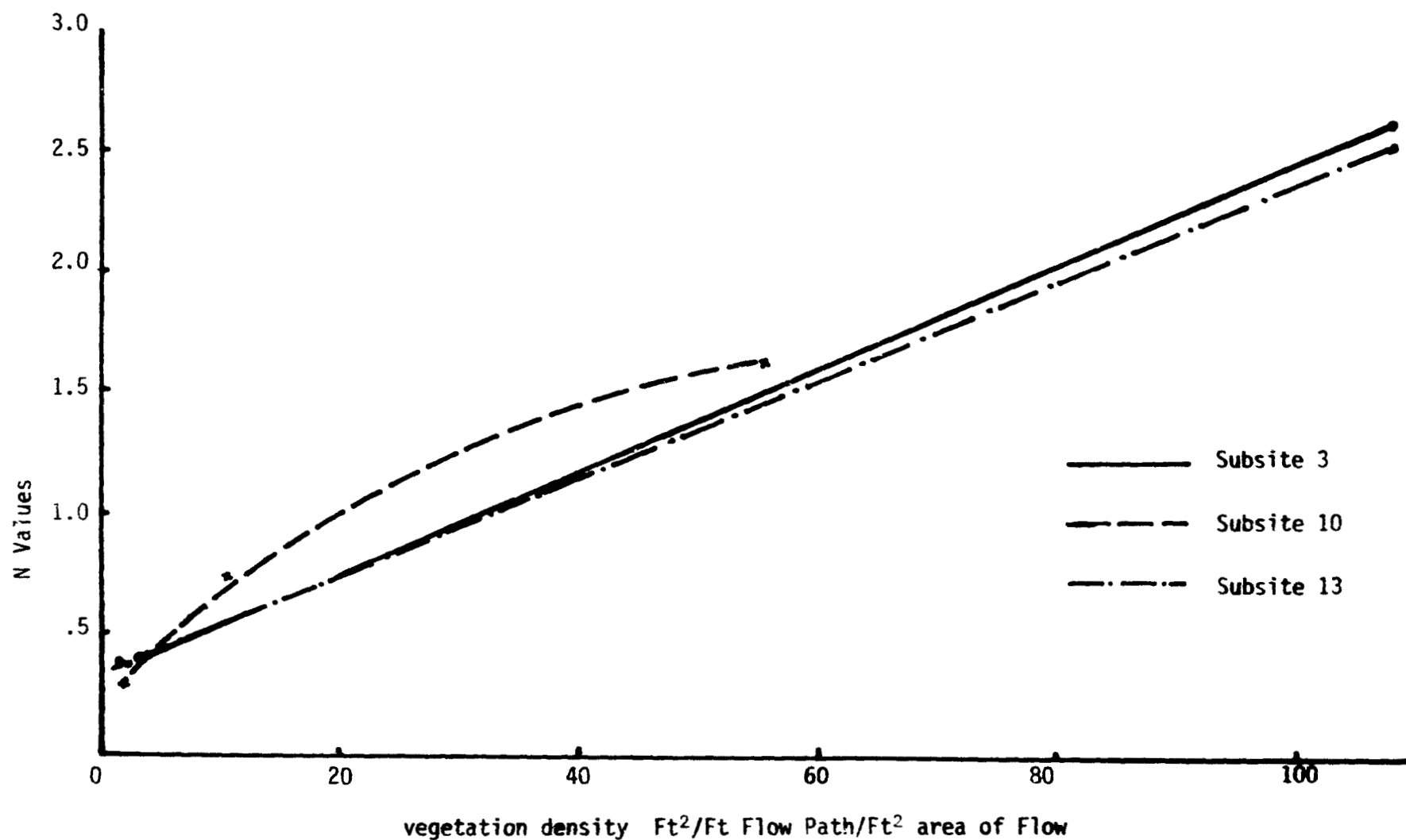


Figure 5.3.3-15.

Relation Between 'N' Values and Vegetation Density for Site 3. (Sept. 25, 1978). (Subsites 1,2,3,8).

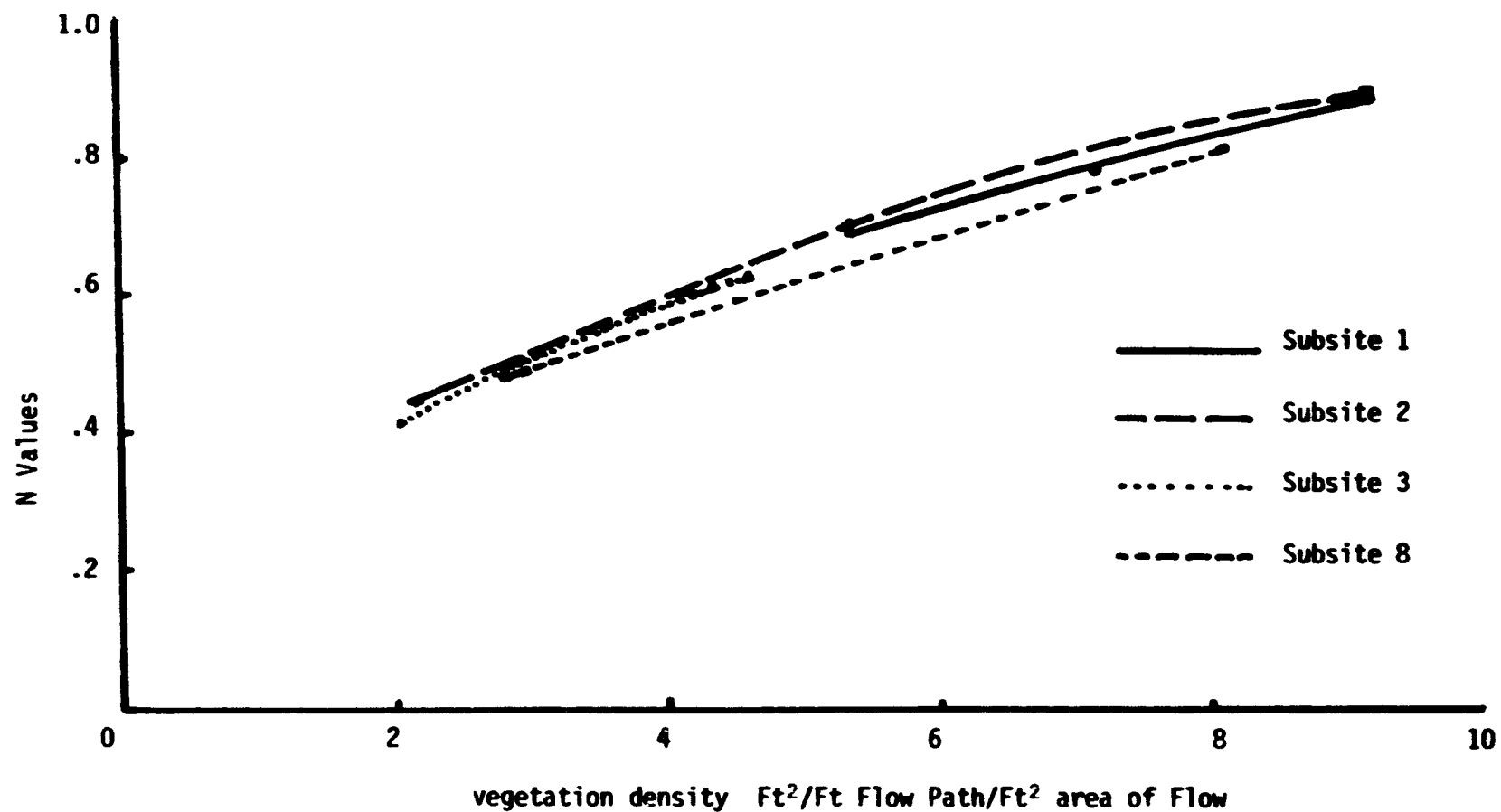


Figure 5.3.3-16.  
Relation Between 'N' Values and Vegetation Density for Site 3. (Sept. 25, 1978). (Subsites 4,5,6,7,9).

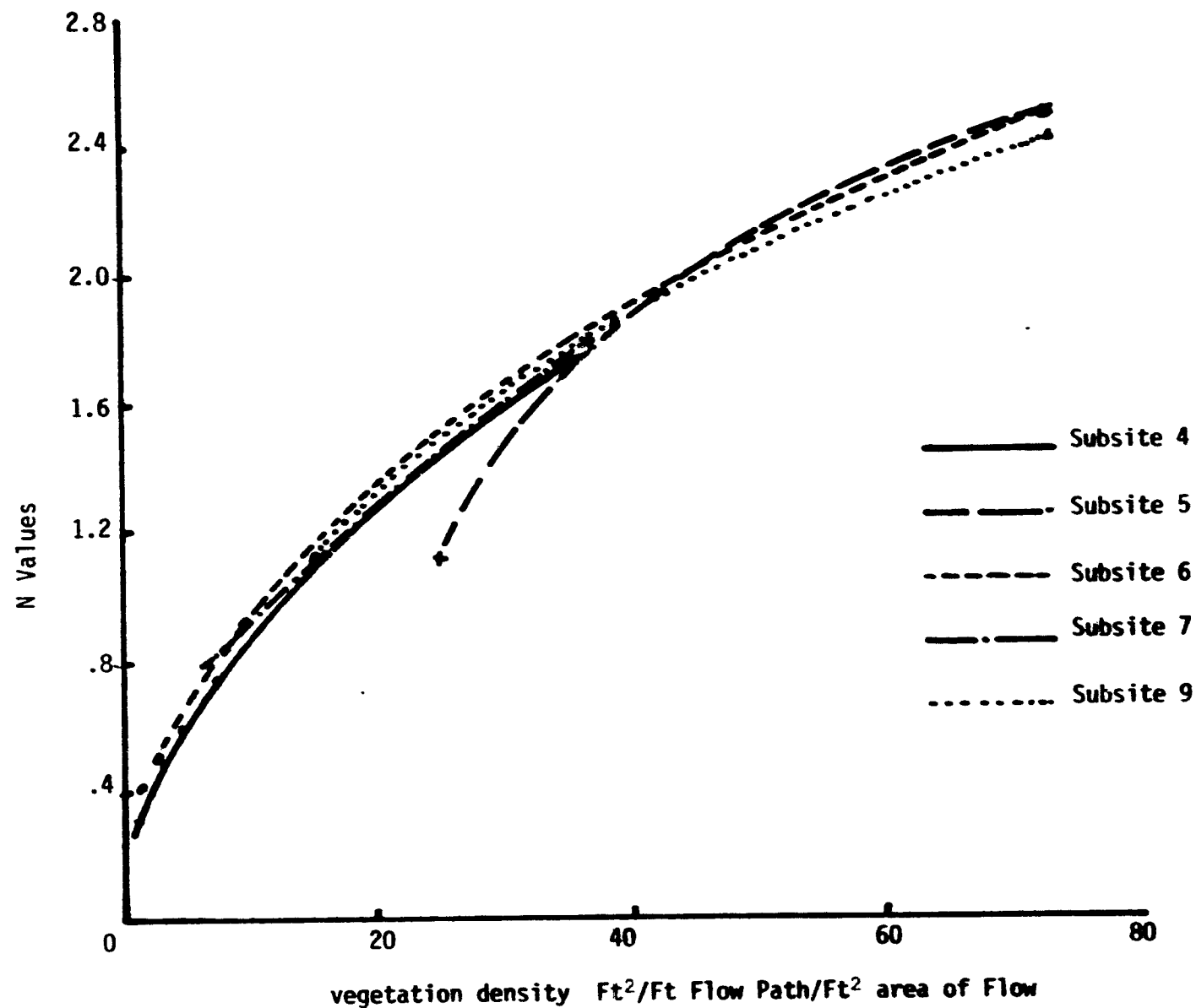
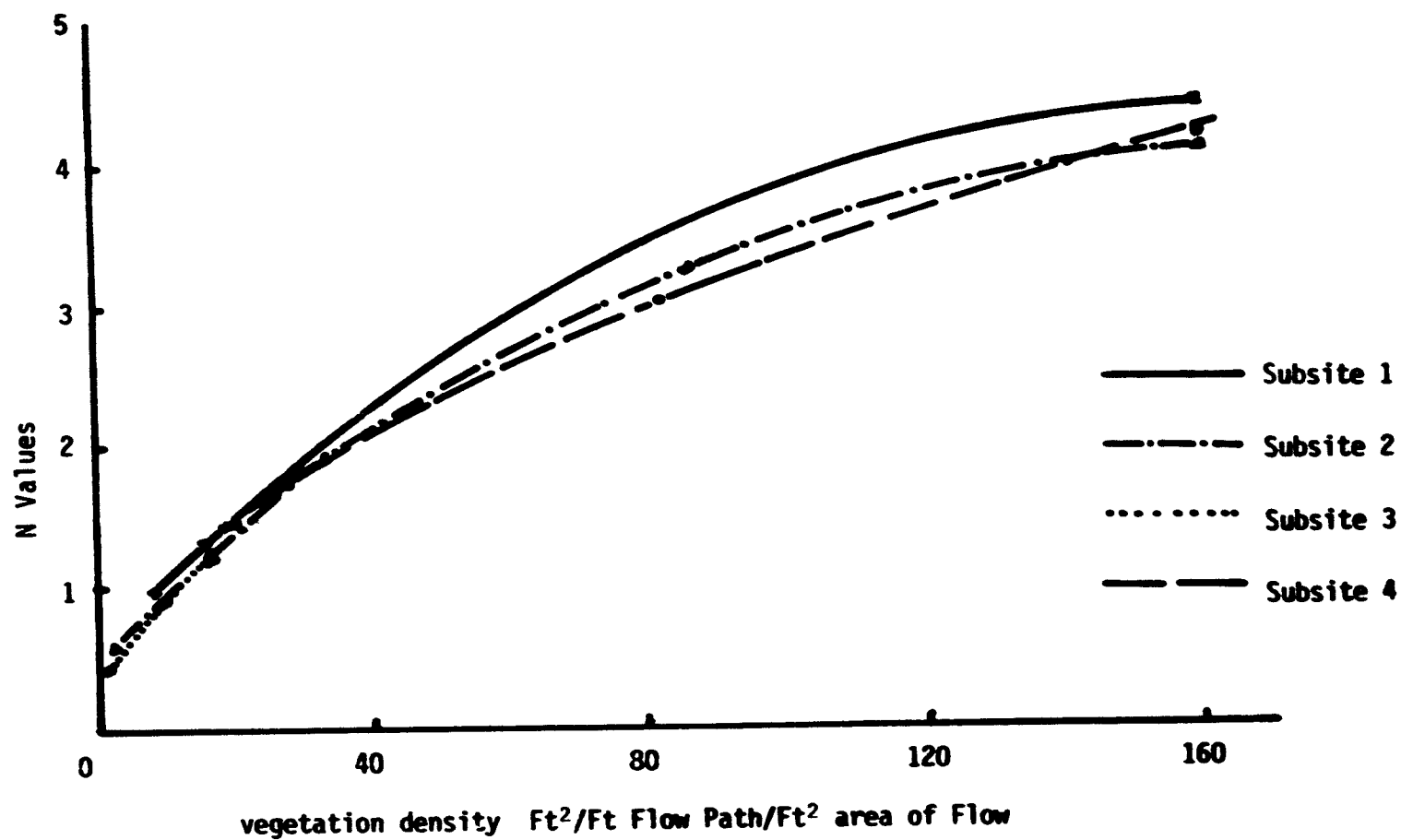


Figure 5.3.3-17. Relation Between 'N' Values and Vegetation Density for Site 4. (Sept. 25, 1978). (Subsites 1,2,3,4).



is less force of retardance exerted but as flow velocity decreases and density becomes more, the retardance force becomes larger and larger and approaches a maximum in thick full matty canopy.

Calculated vegetation density data for all sites is given in Tables 5.3.3-2A, 5.3.3-2B and 5.3.3-2C in Appendix for August, September and October, respectively.

#### 5.3.3.4.3 Flow Resistance and Vegetation as Related to Time

From the data collected over a period of three months it is hard to make any interpretations as to the effect of time on flow resistance. For one reason or the other the flow velocity data could not be collected as a function of depth on all the three dates. In August the flow meter was not working alright, and in October the water level had receded sufficiently and few places even did not have free water. However, surface flow measurements were taken using the dye technique at all the three times. Computed N values for surface flow in general do indicate an increase in N values as the time progresses from rainy to fall season. This, of course, is related to the receding water level and decreased flow depth. Decreasing water level results in over all reduction in general flow rate and then general increase in vegetation density with depth impedes the flow further. That gives an increasing trend in N values with time over this particular period, from August to October. That is true for effect of time on vegetation density at the surface too. Relation for any location in site 4 is not plotted because data could not be collected for surface flow in the month of September because of rain at the time of this particular measurement. Flow resistance values for surface flow are plotted as a function of time in Figure 5.3.3-18.

#### 5.3.3.4.4 Roughness Coefficient and Vegetation Density Values Calculated from November 1978 Data

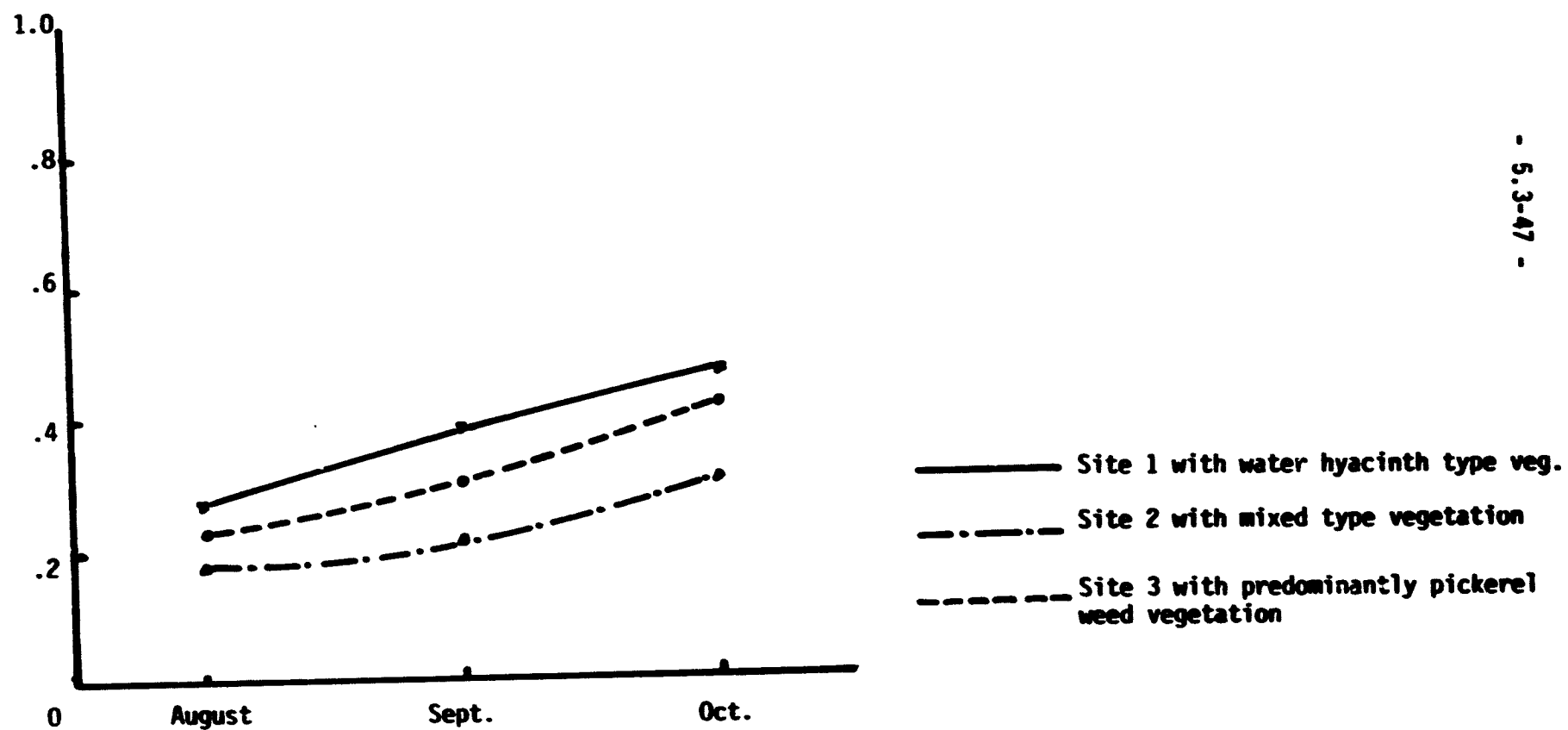
In this trip, made in the end of November, water level was observed to have receded significantly. Among all the sites, site 2 in general had shallower water depth than any other site at any time. This time, most of area in site 2 where measurements were usually made, had dried up and the originally deeper spots had little water moving extremely slow. Because of shallow water depth all over, water current meter was not used. Instead, wherever possible flow velocity was measured using the dye technique at different subsites in a given site except site 2.

Floating type of vegetation like water hyacinth had settled at the bottom. At some places growth of short water hyacinth had appeared. Some of the vegetation like pickerel weed and buttonbush in particular, appeared withering. Factors like (i) shallow depth of water, (ii) vegetation density, (iii) bent and detached vegetation, (iv) bottom surface roughness of the slough, and (v) more resistive hydraulic behavior of the plant parts (bottom parts close to the ground are stiffer; they do not bend, and when water passes they offer more resistance) all contributed significantly to impede the flow. At some places large depressions had made the water stagnant.

The calculated N and vegetation density values from November water flow data are given in Tables 5.3.3-1D and 5.3.3-2D in Appendix, respectively.

Figure 5.3.3-18.

Flow Retardance Values (for surface flow) as a Function of Time. (Three months' data.)



The flow retardance values in general are of about the same magnitude as indicated by previous measurements made by using dye technique. There is a slight increase in N values in general as a function of time (Figure 5.3.3-18) and November data further supports it. At subsite 1 in site 1 where dye measurements were made most of the times, the N values went up a little with time with November values being the highest. Among other subsites, namely 5, 6, and 9, the November N values are not very different from that of October values. Similar type of trend of none to slight increase in November N values for surface flow measurements at different locations infested with sparse to dense vegetation has been observed for sites 3 and 4 as compared to October values. Relation of N values obtained from dye measurements did not give any consistent trend with respect to flow resistance values calculated from water current meter flow data taken earlier at the same depth. That is, no particular relation was observed in N values computed first from meter flow data at a particular subsite at some depth and then from the other method later when water level receded to this depth and dye measurement had to be made.

A large increase in November vegetation density values computed from dye technique velocity data has been noticed as compared to August data for subsite 1 in site 1 and most of the subsites in sites 3 and 4. There is a general increase in vegetation density values in relation to time with the largest values obtained in November. This is true for vegetation density values obtained from surface flow measurements using dye technique. However, vegetation density values calculated from current meter flow velocity data at 20 cm and other depths were generally larger as compared to the values obtained from surface flow measurements even after the water level had receded to the lower level giving the same depth of water from the bottom in both cases.

#### 5.3.3.4.5 Roughness Coefficient and Vegetation Density Values Calculated from June 1979 Data (marsh zone stage = 29.34 ft. MSL)

'N' values obtained from water flow data collected in June followed the same pattern in relation to type of vegetation and its density as observed last year. The values showed more consistent relation with a particular species of vegetation. Flow resistance values in general were in the same range and indicated the same general trend as was obtained from water flow data collected in October last year (1978). During that time the vegetation growth was on decline after peak period of growth, whereas during this time (i.e. June 1979), the aquatic vegetation is still growing but growth rate is slow due to unusually dry weather pattern. Water depth in slough in general was shallow and was of about the magnitude as in October last year. A few interesting changes were observed in the vegetation patterns that subsequently affected flow resistance values. Some of these changes were:

- 1) Vegetation Establishment Drift. Last year, some places did not have much protruding vegetation, that is, some places had open water spots. But this time most of those places were filled up with water hyacinth, pickerel weed, and other aquatic weeds. This was particularly true of site 2 which had lot of open space containing shallow water depth with very sparse vegetation on one side last year, but this time it was filled with most medium high pickerel weed mixed with other type of vegetation. Very dense and tall water hyacinth had given way to short and dense growth of this weed at site No. 4. This resulted in the differences of flow retardance values determined at these places.

- 2) Less location to location difference in 'N' values was observed for a particular type of vegetation since rain and temperature conditions permitted more uniform vegetative growth of selected species. The flow retardance values were more typical of a particular type of vegetation.
- 3) This time, effect of defoliants was also observed. Site 1, a section with mainly pickerel weed and buttonbush mixed vegetation, had been sprayed. The area had only dry stems of mostly buttonbush standing in close vicinity of natural vegetation. The 'N' values in nonsprayed areas were more than double those measured in sprayed areas.
- 4) As measured previously, 'N' values increased with depth up to about 20 cm and then the 'N' value below this depth was smaller, indicating less restricted flow below the water hyacinth root concentration zone. In the case of pickerel weed and other types of vegetation, 'N' values increased with depth. Because of shallow depth of water, flow resistance values in some cases could not give very distinct trend with depth.

Calculated 'N' values are given in Tables 5.3.3-1E and 5.3.3-1F of the Appendix for measurements made by using flow meter and dye technique, respectively.

Vegetation density values were also calculated from the velocity data collected at different locations in relation to type of vegetation. The calculated data are given in Tables 5.3.3-2E and 5.3.3-2F of the Appendix. In general, vegetation density values also confirmed the response of type of vegetation to flow, based on the anchoring and rooting patterns of a particular type of vegetation. Vegetation density values associated with water hyacinth decreased with depth, whereas an opposite trend was observed in the case of pickerel weed alone or pickerel weed and water hyacinth in combination. Vegetation density values were almost of the same magnitude as determined from last year's data.

#### 5.3.3.4.6 Roughness Coefficient and Vegetation Density Values Calculated from July 1979 Data

Water level in the slough had increased by about 16 cm as compared to water level observed in end of June. Vegetation in general was also noticed to have proliferated. Flow retardance values indicated an increasing trend. Water flow measurements, made in the surface 10 cm or so using flow meter or dye technique, gave higher N values at some places in spite of higher water levels. This was probably because the protruding as well as submerged vegetation had also flourished with excess water and favorable temperatures. Calculated N values obtained from flow meter as well as dye technique are given in Tables 5.3.3-1G and 5.3.3-1H of the Appendix.

In site 1, flow resistance values were little smaller in locations where water hyacinth was growing as compared to values obtained for June. Whereas, these values in pickerel weed area had become larger with time and depth of water. In sprayed defoliated area the flow resistance values were almost of the identical magnitude. However, in the nonsprayed area adjacent to the sprayed area, the N values had increased in magnitude probably because of the more luxuriant vegetative growth during the summer season. Roughness

coefficient values in open water space surrounded by vegetative areas showed decrease with time and depth of water.

In site 2, dye measurements indicated increase in the N values for July dates. Values in general were typical of pickerel weed type vegetation. Shallow depths and submerged vegetation gave relatively larger flow resistance values.

At site 3, water flow measurements indicated the same magnitude of flow resistance as observed earlier.

Flow measurements obtained from dye technique showed increase in the flow resistance in the thick water hyacinth vegetation areas in site 4. Floating type vegetation had formed a more dense covering at the surface.

Vegetation density values calculated from the water flow data are given in Tables 5.3.3-2G and 5.3.3-2H of the Appendix. These values were typical of the various types of vegetation. For water hyacinth, the vegetation density values decreased up to a certain depth, and then increased near the bottom whereas for other type of vegetation and open water spaces, vegetation density values increased with depth. Magnitude of vegetation density values impeding the flow of water relatively was less as compared to values obtained from June data.

- 5.3-51 -

5.3.3.5 APPENDIX

Table 5.3.3-1A. Manning's "N" Values Calculated from Water Flow Data Measured on Aug. 22, 1978 (using Dye Method).

Site & Location	Flow Depth (cm)	$S^{1/2}$ Value Used	Calculated 'N' Values	Type of Vegetation
1 1	50	.0130	.271	Tall thick hyacinth vegetation
2	58	.0130	.357	Pickere1 weed
3	60	.0130	.316	Pickere1 weed
4 1	63	.0328	.841	Open space
2	60	.0328	.870	Open space
2 1	44	.0125	.155	Open water with some below surface veg. mixed w/pickere1
2	48	.0125	.180	Open water with some below surface veg. mixed w/pickere1
3	49	.0125	.111	Tall pickere1 weed
4	61	.0125	.088	Open water, no surface vegetation
5	39	.0125	.149	Aquatic weed, thin-stemmed vegeta- tion and some open space
3 1	56	.0107	.231	Pickere1 weed

Table 5.3.3-1B. Manning's 'N' Values Calculated from Flow Data Measured on Sept. 25, 1978 (using Flowmeter and Dye Methods).

Site & Location	Flow Depth (cm)	S <sup>1/2</sup> Value Used	Calculated 'N' Values at Depths (cm)						Type of Vegetation	
			20	30	40	50	60	Ave.		
1	1	65	.0130	.711	.477	.128	.103	.115	.400	Hyacinth vegetation covering surface, no other weeds
	2	40	.0130	.244	.286	.515 at 35cm			.303	Hyacinth vegetation covering surface, no other weeds
	3	50	.0130	.384	.378	.440	2.687		.737	Pickere1 weed tall vegetation
	4	42	.0130	.469	.357	.328 at 37cm			.419	Pickere1 weed/hyacinth mixed
	5	50	.0130	.299	.269	.299	.448		.315	Not much hyacinth, some open spots
	6	65	.0130	.628	.421	.088	.087	.094	.348	Pickere1 weed, not very tall
	1*	50	.0130	.378					.378	Hyacinth, pickere1 weed mixed
1	7	65	.0130	1.455	.348	.179	.188	.183	.698	Very thick hyacinth
	8	70	.0130	1.529	.415	.111	.111	.102	.659	Very thick hyacinth
	9	55	.0130	.795	.572	.502	.895		.720	Hyacinth, pickere1 weed mixed
	10	40	.0130	.297	.724	1.654 at 35cm			.632	Pickere1 weed area
	11	40	.0130	.399	.724	.643 at 35cm			.506	Pickere1 weed, button bush
	12	40	.0130	.463	.346	.406 at 35cm			.430	Pickere1 weed, button bush green
	13	40	.0130	.326	.326	2.316 at 35cm			.699	Pickere1 weed, button bush dry

(Continued)

Table 5.3.3-1B. (Continued)

Site & Location	Flow Depth (cm)	S <sup>1/2</sup> Value Used	Calculated 'N' Values at Depths (cm)							Type of Vegetation
			20	30	40	50	60	Ave.		
4	1	78	.0158	1.464	4.393	4.393	.976	1.464	2.112	Thick water vegetation, tall growth
	2	73	.0158	1.910	4.200	4.200	3.002	1.314	1.910	Thick water vegetation, tall growth
	3	65	.0158	.427	.427	.618	1.216		.628	Open water space, little below surface vegetation
	4	70	.0158	4.087	4.087	.560	1.277	4.087	3.081	Hyacinth, thick vegetation
2	1a	30	.0125	.207	.178				.202	Open water area with small aquatic weeds below surface
	1b	30	.0125	.116	.117				.116	50% weeds
	1c	30	.0125	.103	.096				.102	Open, no surface covering weeds
	1d	27	.0125	.186					.186	Not much weeds
	4a	27	.0125	.120					.120	25% pickerel weed, some small weeds
	4b	27	.0125	.110					.110	20% pickerel weed and sporadic small weeds
	4c	25	.0125	.122					.122	Small pickerel weed, mixed veg.
	4d	25	.0125	.084					.084	Shallow water, small pickerel weed and mixed vegetation
	4e	25	.0125	.163					.163	Shallow water, small pickerel weed and mixed vegetation
	*1c	27	.0125	.074					.074	Open water with some below surface weeds
near	*4c	25	.0125	.114					.114	Small pickerel weed, mixed veg.
near	*4e	25	.0125	.211					.211	Small pickerel weed, mixed veg.

(Continued)

Table 5.3.3-1B. (Continued)

Site & Location	Flow Depth (cm)	S <sup>1/2</sup> Value Used	Calculated 'N' Values at Depths (cm)						Type of Vegetation	
			20	30	40	50	60	Ave.		
2a	35	.0125	.328	.281				.316	Small veg. covering surface	
2b	35	.0125	.339	.334				.338	Small veg. covering surface	
2c	35	.0125	.509	.399				.478	Surface covered with small thin-stemmed weeds	
2d	35	.0125	.351	.283				.332	Surface covered with small thin-stemmed weeds	
2e	35	.0125	.200	.240				.211	Tall pickerel weed	
2f	35	.0125	.221	.226				.222	Pickerel weed, thick vegetation	
2g	38	.0125	.215	.342				.258	50% pickerel weed and thin-stemmed plants	
2h	40	.0125	.223	.318	.318			.259	75% pickerel weed vegetation	
3a	40	.0125	.186	.223	.223			.200	Relatively tall pickerel weed mixed	
3b	40	.0125	.371	.223	.180			.307	Relatively tall pickerel weed mixed	
3c	40	.0125	.206	.245				.276	Relatively tall pickerel weed mixed	
3	1	60	.0107	.780	.694	.694	.780	.892	.789	90% pickerel weed, thick vegetation and some hyacinth
	2	60	.0107	.892	.694	.438	.892		.764	"
	3	60	.0107	.624	.499	.416	.609		.557	"
	4	60	.0107	1.784	.312	.609	1.784		1.294	"

(Continued)

Table 5.3.3-1B. (Continued)

Site & Location	Flow Depth (cm)	S <sup>1/2</sup> Value Used	Calculated 'N' Values at Depths (cm)						Type of Vegetation
			20	30	40	50	60	Ave.	
5	60	.0107	2.497	1.784	1.135	2.497		.971	90% pickerel weed, thick vegetation and some hyacinth
6	60	.0107	.499	.416	.832	2.497		.971	"
7	60	.0107	.780	.832	1.135	1.784		1.072	"
8	58	.0107	.488	.488	.479	.814		.551	"
9	57	.0107	.754	.396	.483	2.414		.959	"
1* near	60	.0107	.301					.301	90% pickerel weed and some hyacinth, rained, too
3* near	60	.0107	.333					.333	"

\*Using dye method.

Table 5.3.3.1C. Manning's 'N' Values Calculated from Water Flow Data Measured on Oct. 17, 1978 (using Flowmeter and Dye methods).

Site Subsite & Locations	Flow Depth (cm)	S <sup>1/2</sup> Value Used	Calculated 'N' Values at Depths (cm)					Type of Vegetation	Temp
			Surface	20	30	40	50		
1	1	47	.0130	.716	.153	.092		Water hyacinth, thick veg. covering surface. About 100 cm tall.	22°
	1'	47	.0130	.183	.122	.086			
	2	23	.0130	1.601				Pickere! weed lodged (dying down) and some dry button bush.	
	2'	25	.0130	.846					
	3	41	.0130	1.070	.187	.781		Water hyacinth, thick veg. like subsite 4 <sub>1</sub>	
	3'	41	.0130	.471	.277	.138			
	4	25	.0130	.277				Button bush and some open water (and submerged weeds) and some pickere! weed (dying vegetation)	
	4'	25	.0130	.206					
	4''	25	.0130	.332					
	5	25	.0130	.197				Pickere! weed, less lodged, medium height and dry button bush	
	5'	25	.0130	.212					
	6	25	.0130	.339				Thick pickere! weed, less button bush dry.	
	6'	25	.0130	.769					

(Continued)

Table 5.3.3.1C. (Continued)

Site Subsite & Locations	Flow Depth (cm)	S <sup>1/2</sup> Value Used	Calculated 'N' Values at Depths (cm)						Type of Vegetation	Temp
			Surface	20	30	40	50	60		
6''	25	.0130		.846					Not much foliage dry button bush and submerged vegetation.	
6'''	47	.0130	.	1.209						
1*	47	.0130	.460						As in Subsite 4 <sub>1</sub>	
2*	25	.0130	.245						As in Subsite 4 <sub>2</sub>	
3*	25	.0130	.557						As in Subsite 4 <sub>3</sub>	
4*	25	.0130	.204						As in Subsite 4 <sub>4</sub>	
4*	25	.0130	.206						As in Subsite 4 <sub>4</sub>	
5*	25	.0130	.158						As in Subsite 4 <sub>5</sub>	
6*	25	.0130	.195						As in Subsite 4 <sub>6</sub>	
7	45	.0130		5.101	.224	.130			Thick water hyacinth covering	
1 8	25	.0130		3.385					Pickerel weed very thick and button bush. (Similar to 4 <sub>2</sub> and 4 <sub>6</sub> )	
8'	25	.0130		.605						
8''	25	.0130		1.209						
8'''	25	.0130		1.693						
9	25	.0130		.282					Dry button bush, very little pickerel weed and some submerged vegetation.	

(Continued)

Table 5.3.3.1C. (Continued)

Site Subsite & Locations	Flow Depth (cm)	S <sup>1/2</sup> Value Used	Calculated 'N' Values at Depths (cm)					Type of Vegetation	Temp
			Surface	20	30	40	50		
	9'	25	.0130		.139				
	9''	25	.0130		.339				
	9'''	25	.0130		.145				
	7*	45	.0130	1.165					
	8*	25	.0130	.190					
	9*	25	.0130	.106					
2	* 1	6.5	.0125	.074				Some spotty veg. and submerged veg. and very few grass type vegeta- tion.	
	* 1	6.0	.0125	.071					
	* 2	13	.0125	.301				Mixed veg. and white flower plants and pickerel weed, some dying down button bush type veg.	29°
	* 3	15	.0125	.214				Some plants w/white flowers dying down veg. & submerged	
	* 4	15	.0125	.227				Dying down veg. & pickerel weed, some submerged veg.	
	* 4	20	.0125	.090				Relatively deep water and very tall & developed pickerel weed + drying small tall tree stems.	

(Continued)

Table 5.3.3.1C. (Continued)

Site Subsite & Locations	Flow Depth (cm)	S <sup>1/2</sup> Value Used	Calculated 'N' Values at Depths (cm)						Type of Vegetation	Temp
			Surface	20	30	40	50	60		
3	1*	35	.0107	.415					Thick pickerel weed (med. height lodged plants, dying down vegetation 90% pickerel weed	24°
	2*	35.3	.0107	.428						
	3*	30	.0107	.477						
4	1	35	.0158	1.839					Thick water hyacinth all covered and submerged vegetation.	24°
	1'	35	.0158	2.575						
	1''	35	.0158	1.287						
	1*	35	.0158	.696					Thick water hyacinth veg. all surface covered. Not much surface veg. Some submerged vegetation.	
	2*	35	.0158	.572 (with vegetation)						
	3*	35	.0158	.362 (without vegetation)						

\*Using dye technique.

Table 5.3.3-1D. Manning's N Values Calculated From Water Flow Data Measured on Nov. 29, 1978 (Using Dye Method).

Site and Subsite	Average Flow Depth (CM)	S <sup>1/2</sup> Value Used	Calculated Velocity ft/sec	Calculated N Value	Type of Vegetation	Temp. °C	Remarks
1 Between 1 and 3 (subsites)	35	.0130	.036	.588		22	
Between 2 and 4 (subsites)	18	.0130	.097	.140			
1 <sub>5</sub>	14	.0130	.078	.147			
1 <sub>6</sub>	14	.0130	.095	.121			
1 <sub>9</sub>	15	.0130	.069	.175			
2	At subsites 1, 2, 5, and 6 water had completely dried and at subsites 3 and 4 very little (1 - 2 cm) water was standing.						
3 1	16	.0107	.019	.545			
3 2	16	.0107	.032	.323			
3 3	16	.0107	.036	.287			
4 1	14	.0158	.042	.333		24	Open water
1	20	.0158	.030	.591			In open water space
(Continued)							

Table 5.3.3-1D. (Continued)

Site and Subsite	Average Flow Depth (CM)	S <sup>1/2</sup> Value Used	Calculated Velocity ft/sec	Calculated N Value	Type of Vegetation	Temp. °C	Remarks
4 1	20	.0158	.024	.739			In vegetation
4 2	20	.0158	.051	.348			Open water space
4 2	13	.0158	.047	.283			Open water space

Table 5.3.3-1E. Manning's N Values Calculated from Water Flow Data Measured on June 29, 1979 (Using Flowmeter Method).

Site, Subsite & Location	Average Flow Depth (cm)	Slope Value Used	Calculated N Value at Depth (cm)			Type of Vegetation
			10	20	30	
1 1	35	.000169		.189	.141	Open water space surrounded by water hyacinth vegetation. Area adjacent to defoliated area that was sprayed and had only tall, thin, and dry stems of button bush standing. Some pickerel weed mixed.
2	35			.424	.165	Water hyacinth thick vegetation.
2'	35			.665	.285	Inside the thick water hyacinth vegetation plants about 6-8" tall flowering and covering the surface.
2"	35			.311	.144	Water hyacinth vegetation, bottom not much rough.
3	25			.423		Water hyacinth somewhat dense vegetation shallow uneven depth of water.
3'	25			.339		"
4	16		.121			Sprayed area, dry defoliated plants of button bush.
5	16		.141			
6	16		.251			No succulent vegetation causing resistance to flow.
6'	16		.107			Last year, this area was full of button bush and pickerel weed vegetation.
4'	16		.251			Non sprayed area with natural vegetation. Mostly medium tall plants of pickerel weed.
5'	16		.491			
6"	16		.217			Flow was restricted here. These subsites are the same where last years' subsites 4, 5, and 6 were located.
7	35		.294		.424	Open water space surrounded by water hyacinth thick vegetation.
7'	15		.098			"
7"	35		.706		.706	In water hyacinth thick vegetation area adjacent to open water space.

(Continued)

Table 5.3.3-1E. (Continued)

Site, Subsite & Location	Average Flow Depth (cm)	Slope Value Used	Calculated N Value at Depth (cm)			Type of Vegetation
			10	20	30	
1	8		.312			Medium tall pickerel weed and some dry button bush plants.
	8'		.217			
	9		.177			Medium Tall pickerel weed some dry button bush and very rare water hyacinth. Vegetation similar to old 8 and 9 subsites. There were dense bushes at some places.
	9'		.196			
2	1	.000156	Water was shallow to make any flow meter readings.			Previously there was no vegetation in much of the area at this site. However, now pickerel weed and other small grasses were present in abundance everywhere.
3	1	.0001145	.733	1.467		Thick pickerel weed making up about 95% of the vegetation with little water hyacinth mixed. Dense vegetation same as last year.
	1'		.489	.667		
	1"		.407	.407		
	2		.407	.733		
	2'		.407	.407		
	2"		.733	1.048		Thick pickerel weed vegetation mixed with some water hyacinth.
	3		.407	.667	1.467	
	3'		.349	.524	.407	
	3"		.733	.667	1.467	
	4		Flowmeter did not work, probably due to battery problem			Thick hyacinth vegetation with dense covering over the water surface in most of the area. Last year there was some open water space which had disappeared this time.

Table 5.3.3-1F. Manning's N Values Calculated from Water Flow Data Measured on June 29, 1978 (Using Dye Method).

Site and Subsite		Average Flow Depth (cm)	N Values	Type of Vegetation	Remarks
1	4	45	.116	Sprayed area with defoliated plants. Dry stems standing (mostly button bush).	Flow was relatively faster. These subsites are similar to former 4, 5, 6 subsites.
	4'	16	.253	Nonsprayed area. Tall pickerel weed thick vegetation intermixed with water hyacinth water movement quite slow.	
	7	35	.178	Large open water space though surrounded by water hyacinth on all sides.	
	7'	32	.224	Next to open water space. Measurements done in 6-7" tall water hyacinth forming thick mat over the surface.	
	8	25	.168	Tall mixed vegetation of pickerel weed and button bush. Some places plants were in group obstructing flow.	
	8'	22	.134		
2	1	10	.268	Pickerel weed, thin grasses, and bushes, etc. mixed vegetation. Shallow water.	Before there was no vegetation at many places in this site.
	2	10	.268		
3	1	26	.376	Pickerel weed about 95% with very small proportion of water hyacinth mixed.	Same type of vegetation as last year.
	2	31	.482		
4	1	29	.370	10-11" tall water hyacinth covering the surface all over.	No open water space.
	2	24	.439		
	3	35	1.123	Very dense cover of water hyacinth restricting flow of water.	All area was covered with vegetation.

Table 5.3.3-1G. Manning's N Values Calculated from Water Flow Data Measured on July 23, 1979 (Using Flowmeter Method).

Stage Recorder Reading at Site 1 = 29.50 feet m.s.l.

Site Subsite and Location	Flow Depth cm	Slope	Calculated 'N' Value at Depth (cm)					Type of Vegetation	Remarks
			10	20	30	40	50		
1 1	45	.000169	.112	.112	.250	.250		In water hyacinth before open water space in direction of flow not very dense water hyacinth.	
1 2	45		.250	.250	.178	.250		Open water space adjacent to thick water hyacinth vegetation.	
2'	35		.150	.212	.150			Open water spot, shallow depth, in the same vicinity as the previous location.	
3	45		.250	.250	.159	.079		In water hyacinth, thick vegetation east of the second location plants about 10-12" tall.	
3'	35		.212	.212	.212			Thick water hyacinth same vegetation as above.	
3"	45		.501	.250	.178	.069		Repeat of above, thick water hyacinth.	
4	45		.250	.352	.125	.125		Another location in thick water hyacinth area with 10-12" high plants.	
5	35		.510	.118	.189			Defoliated area with button bush dry plants. Area surrounded on two sides by open water space.	Old.
1 6	32		.141	.399	.200			Defoliated area, no green vegetation, dry button bush plants.	Old subsite #2.
6'	20		.130	.130				Defoliated area dry plants.	Old subsite #3.

(Continued)

Table 5.3.3-1G. (Continued)

Site Subsite and Location	Flow Depth cm	Slope	Calculated 'N' Value at Depth (cm)					Type of Vegetation	Remarks
			10	20	30	40	50		
7	25		.238	.151	.339			In sprayed, defoliated area, no leafy vegetation, only dry stems, same in groups.	Old sub-site #4
7'	25		.094	.094	.151			Sprayed area, no leafy vegetation scattered stems.	Repeat of above.
7"	20		.103	.103				Sprayed and defoliated area.	"
8	20		.252		.204			Sprayed area somewhat scattered dry plants.	Same as old subsite #5.
8'	25		.076	.094	.339			"	Repeat of above.
8"	20		.094	.292				Defoliated area.	"
9	20		.292	.347				Defoliated area with groups of leafless plants scattered around.	Old subsite No. 6.
9'	20		.205	.205				"	Repeat of above.
9"	20		.146	.096				Defoliated area with slope.	Repeat of above.
1 10	25		.769	.470				Pickereel weed green vegetation, adjacent to sprayed area.	
10'	25		.313	.470				Dense pickereel weed mostly and some button bush.	
10"	25		.252	.405				Dense pickereel weed, on low sides surrounded by water hyacinth and defoliated area.	
10"	25		.564	.564				Same as above.	
11	25		.846	.846				Dense pickereel weed vegetation.	

(Continued)

Table 5.3.3-1G. (Continued)

Site Subsite and Location	Flow Depth cm	Slope	Calculated 'N' Value at Depth (cm)					Type of Vegetation	Remarks
			10	20	30	40	50		
11'	25		.564	.564				Pickere1 weed area surrounded by water hyacinth and defoliated area.	
12	45		.250	.112	.112	.125		Open water space surrounded by water hyacinth.	Dye measure- ment made here.
12	35		.112	.112	.089			Open water space close to water hyacinth.	Near above location.
12'	25		.089					Open water space shallow depth.	"
13	25		.313	.264				Pickere1 weed and button bush, green vegetation.	Same as old 8-9-10 sub- sites.
13'	25		.564	.339				Pickere1 weed and very little button bush green vegetation.	
13"	25		.297 .197	.403 .238				Mostly pickere1 weed and not much button bush.	"
13"	25		.376	.470				Mostly pickere1 weed, some dead plants and leaves lying on the surface.	
2	1	.000156	.579					Pickere1 weed mostly 3-4" tall	
	2		.579					thick vegetation. Small plants	
	3		.579					intermingled.	
	4		.322					Took a number of measurements at	
	5		.214					at different locations all had	
	6		.289					about the same type of vegeta-	
	7		.322					tion.	

(Continued)

Table 5.3.3-1G. (Continued)

Site Subsite and Location	Flow Depth cm	Slope	Calculated 'N' Value at Depth (cm)					Type of Vegetation	Remarks
			10	20	30	40	50		
8	4		.386						
9	4		.386						
3	35	.0001145	.872	.872	.484			95% of pickerel weed dense vegetation 3-4' (above water) tall plants.	
3	30	.0002496	Flowmeter was not working when reached here.					Very thick water hyacinth vegetation.	

Table 5.3.3-1H. Manning's N Values Calculated from Water Flow Data Measured on July 23, 1979 (Using Dye Method).

Site and Subsite	Flow Depth (cm)	Slope	N Value	Type of Vegetation	Remarks
1 12	19	.000169	.050	Open water space surrounded by water hyacinth.	Flowmeter data gave higher N values. "
12'	19		.044	Adjacent to open water space in direction of flow.	
10	24		.510	Pickereel weed area dense vegetation.	
8	24		.141	Defoliated area, no leafy vegetation, some dry button bush plants standing.	
2 1	15	.000156	.330	Pickereel weed dense vegetation with small plants near the surface.	
3	35	.0001145	.601	95% pickereel weed dense vegetation.	
4 1	30	.0002496	.704	Thick water hyacinth vegetation. Plants about 10-12" tall.	
2	33		.917	Thick water hyacinth vegetation. Dense mat near the water surface.	

Table 5.3.3-2A. Vegetation Density Values Calculated from Water Flow Data Measured on Aug. 22, 1978  
(Using Dye Method)

Site & Location	Flow Depth (cm)	Slope	Vegetation Density	Type of vegetation
1 1	50	.000169	1.104	Tall, thick hyacinth
2	58	.000169	1.570	Pickere1 weed
3	60	.000169	1.174	Pickere1 weed
3 1	56.5	.0001145	.678	Pickere1 weed
4 1	63	.00025	1.811	Open space, some submerged weed
2	60	.00025	2.066	Open sapce, some submerged weed
2 1	44	.00015625	.427	Open water and grass-type mixed with pickere1 weed
2	49	.00015625	.496	Open water and grass-type mixed with pickere1 weed
3	61.5	.00015625	.140	Open water and grass-type mixed with pickere1 weed
4	39.5	.00015625	.159	Open water, no vegetation
5	23	.00015625	.943	Aquatic submerged weed and open space

Table 5.3.3-2B. Vegetation Density Values Calculated from Water Flow Data Measured on Sept. 25, 1978  
(Using Flowmeter and Dye Methods).

Site & Location	Flow Depth (cm)	Slope	Vegetation Density at Depth (cm)						Ave.	Type of Vegetation
			20	30	40	50	60	70		
1	1	65	.000169	5.341	2.409	.169	108.16	.140	2.493	Hyacinth veg. covering surface, no other weed
	2	40	.000169	1.198	1.649	5.341			2.059	Hyacinth veg. covering surface, no other weed
	3	50	.000169	2.207	2.146	2.907	108.16		18.193	Pickereel weed tall veg.
	4	42	.000169	4.158	2.409	2.030			3.373	Pickereel/hyacinth mixed
	5	50	.000169	1.335	1.082	1.335	3.004		1.535	Not much hyacinth, some open
	6	65	.000169	4.158	1.87	.082	.079	.094	1.926	Pickereel weed, not very tall
	1	50*	.000169	2.146					2.146	Hyacinth, pickereel mixed
	7	65	.000169	22.347	1.278	.338	.374	.353	8.955	Very thick hyacinth
	8	70	.000169	22.347	1.649	.117	.119	.099	8.272	Very thick hyacinth
	9	55	.000169	8.346	4.326	3.329	10.563		7.106	Hyacinth, pickereel mixed weed
	10	40	.000169	1.778	10.563	55.184			13.439	Pickereel weed area
	11	40	.000169	3.215	10.563	8.346			5.555	Pickereel weed, button bush
	12	40	.000169	4.326	2.409	3.329			3.780	Pickereel, green button bush

(Continued)

Table 5.3.3-2B. (Continued)

Site & Location	Flow Depth (cm)	Slope	Vegetation Density at Depth (cm)						Ave.	Type of Vegetation	
			20	30	40	50	60	70			
4	13	40	.000169	2.146	2.146	108.16			22.024	Pickere1, dry button bush	
	1	78	.00025	17.78	--	160.	160.	7.901	17.78	73.759	Thick hyacinth, tall growth
	2	73	.00025	33.058	--	--	81.633	15.625	33.058	72.341	Thick hyacinth, tall growth
	3	65	.00025	1.932	1.932	4.031	15.625			27.600	Open water space, little below surface veg.
2	4	70	.00025	160.	160.	3.0	15.625			111.790	Hyacinth, thick vegetation
	1a	30	.00015625	1.262	.943					1.209	Open water area, small aquatic weeds below surface
	1b	30	.00015625	.401	.406					.402	50% weeds
	1c	30	.00015625	.316	.274					.309	Open, no surface cov. veg.
2	1d	27	.00015625	1.181						1.181	Not much weeds
	4a	27	.00015625	.489						.489	25% pickere1, some small weed
	4b	27	.00015625	.411						.411	20% pickere1, sporadic weed
	4c	25	.00015625	.565						.565	Small pickere1, mixed veg.
	4d	25	.00015625	.266						.266	Small pickere1, mixed veg.
	4e	25	.00015625	1.00						1.00	Small pickere1, mixed veg.

(Continued)

Table 5.3.3-2B. (Continued)

Site & Location	Flow Depth (cm)	Slope	Vegetation Density at Depth (cm)						Ave.	Type of Vegetation
			20	30	40	50	60	70		
near	1c	27*	.00015625	.187					.187	Open water with some be- low surface weeds
	4c	25*	.00015625	.489					.489	Small pickerel weed and mixed vegetation
	4e	25*	.00015625	1.687					1.687	Small pickerel weed and mixed vegetation
	2a	34	.00015625	2.687	1.984				2.501	Small veg. covering surface
	2b	35	.00015625	2.778	2.687				2.752	Small veg. covering surface
	2c	35	.00015625	6.250	3.845				5.563	Surface covered with small grass-type weed
	2d	35	.00015625	2.973	1.929				2.675	Surface covered with small grass-type weed
	2e	35	.00015625	.961	1.384				1.082	Tall pickerel weed
	2f	35	.00015625	1.181	1.235				1.196	Pickerel, thick vegeta- tion
	2g	38	.00015625	1.000	2.520				1.188	50% pickerel, some grass
	2h	40	.00015625	1.000	2.041	2.041			1.534	75% pickerel weed vege- tation
	3a	40	.00015625	.694	1.000	1.000			.809	Relatively tall growth
	3b	40	.00015625	2.778	1.000	.650			2.046	Pickerel weed, mixed veg.
	3c	40	.00015625	.857	1.208				.989	Pickerel weed, mixed veg.

(Continued)

Table 5.3.3-2B. (Continued)

Site & Location	Flow Depth (cm)	Slope	Vegetation Density at Depth (cm)						Ave.	Type of Vegetation
			20	30	40	50	60	70		
3	1	60	.0001145	7.156	5.654	5.654	7.156	9.346	6.929	90% pickerel weed
	2	60	.0001145	9.346	5.654	2.255	9.346		7.253	Thick weed, some hyacinth
	3	60	.0001145	4.580	2.931	2.035	4.359		3.729	Thick weed, some hyacinth
	4	60	.0001145	37.384	1.145	4.359	37.384		24.464	Thick weed, some hyacinth
	5	60	.0001145	73.294	37.384	15.139	37.384		47.704	Thick weed, some hyacinth
	6	60	.0001145	2.931	2.035	8.142	73.274		18.522	Thick weed, some hyacinth
	7	60	.0001145	7.156	8.142	15.139	37.384		15.281	Thick weed, some hyacinth
	8	58	.0001145	2.931	2.931	2.817	8.142		3.942	Thick weed, some hyacinth
	9	57	.0001145	7.156	1.969	2.931	73.274		18.190	Thick weed, some hyacinth
3 near 1*	60	.0001145	1.064						1.064	90% pickerel weed, some hyacinth
near 5*	60	.0001145	1.303						1.303	90% pickerel weed, some hyacinth

\*Using dye method.

Table 5.3.3-2C. Vegetation Density Values Calculated from Water Flow Data Measured on Oct. 17, 1978  
(Using Flowmeter and Dye Methods).

Site, Subsite, & Location	Flow Depth (cm)	S Value Used	Calculated Vegetation Density at Depth (cm)						Type of Vegetation
			Surface	20	30	40	50	60	
1	1	47	.000169	8.346	.383	.139			
	1'	47	.000169	.544	.241	.120			
	2	23	.000169	108.16					
	2'	25	.000169	27.04					
	3	41	.000169	22.347	.681	.540			
	3'	41	.000169	4.326	1.497	.370			
	4	25	.000169	2.907					
	4'	25	.000169	1.609					
	4''	25	.000169	4.158					
	5	25	.000169	1.462					
	5'	25	.000169	1.690					
	6	25	.000169	4.326					
	6'	25	.000169	22.347					

(Continued)

Table 5.3.3-2C. (Continued)

Site, Subsite, & Location	Flow Depth (cm)	S Value Used	Calculated Vegetation Density at Depth (cm)						Type of Vegetation
			Surface	20	30	40	50	60	
6''	25	.000169		27.04					
6'''	25	.000169		55.184					
7	45	.000169		110.356					
8	25	.000169		110.356					
8'	25	.000169		13.800					
8''	25	.000169		55.184					
8'''	25	.000169		108.16					
9	25	.000169		3.004					
9'	25	.000169		.727					
9''	25	.000169		4.326					
9'''	25	.000169		.790					
1 1*	47	.000169	3.449						
2*	25	.000169	2.272						
3*	41	.000169	5.341						

(Continued)

Table 5.3.3-2C. (Continued)

Site, Subsite, & Location	Flow Depth (cm)	S Value Used	Calculated Vegetation Density at Depth (cm)					Type of Vegetation	
			Surface	20	30	40	50		60
	4*	25	.000169	1.570					
	4*	25	.000169	1.609					
	5*	25	.000169	.945					
	6*	25	.000169	1.429					
	7*	45	.000169	23.400					
	8*	25	.000169	1.365					
	9*	25	.000169	.422					
2	1*	6	.00015625	1.235					
	1*	6	.00015625	1.262					
	2*	13	.00015625	8.163					
	3*	15	.00015625	3.429					
	4*	15	.00015625	3.845					
	4'*	15	.00015625	.411					
3	1*	35	.0001145	4.154					

(Continued)

Table 5.3.3-2C. (Continued)

Site, Subsite. & Location	Flow Depth (cm)	S Value Used	Calculated Vegetation Density at Depth (cm)					Type of Vegetation	
			Surface	20	30	40	50		60
	2*	35.3	.0001145	4.359					
	3*	35	.0001145	6.729					
4	1*	35	.00025	11.687					
	2*	35	.00025	7.901					
	3*	35	.00025	3.265					
	1'	35	.00025		81.633				
	1''	35	.00025		160.00				
	1'''	35	.00025		40.00				

\*Using dye technique.

Table 5.3.3-2D. Vegetation Density Values Calculated from Water Flow Data Measured on  
Nov. 29, 1978 (Using Dye Method).

Site and Subsite	Flow Depth (cm)	Slope ft/ft	Vegetation Density	Type of Vegetation	Remarks
1 1 <sub>1-3</sub>	35	.000169	8.346		
1 <sub>2-4</sub>	18	.000169	1.150		
1 <sub>5</sub>	14	.000169	1.778		
1 <sub>6</sub>	14	.000169	1.198		
1 <sub>9</sub>	15	.000169	2.272		
3 1	16	.0001145	20.299		
2	16	.0001145	7.156		
3	16	.0001145	5.654		
4 1	14	.00025	9.070		Open water
1	20	.00025	17.778		Open water
1	20	.00025	27.778		In vegetation
2	20	.00025	6.151		Open water
2	13	.00025	7.243		Open water

Table 5.3.3-2E. Vegetation Density Values Calculated from Water Flow Data Measured on June 29, 1979  
(Using Flowmeter Method).

Site & Location	Average Flow Depth (cm)	Slope	Vegetation density at depth (cm)			Type of Vegetation
			10	20	30	
1 1	35	.000169		.862	.481	Open water space surrounded by water hyacinth. Area adjacent to sprayed region where the plants were defoliated.
2	35			4.326	.660	Water hyacinth thick vegetation.
2'	32			12.018	2.207	Inside thick vegetative area covered with water hyacinth.
2"	32			4.326	.927	Thick water hyacinth vegetation with somewhat smooth bottom surface.
3	25			6.760		Thick water hyacinth with uneven bottom sprayed area has dry defoliated plants of button bush.
3'	25			4.326		At one section too many dry plants mixed with submerged vegetation. Nonsprayed area with natural vegetation, mostly medium tall pickerel weed.
4	16		1.000			
5	16		1.365			
6	16		4.326			
6'	16		.790			
4'	16		4.326			
5'	16		12.018			
6"	16		3.215			
1 7	35		2.086	4.326		Open water space surrounded by thick water hyacinth.
7'	15		1.126			Thick water hyacinth vegetation area.
7"	35		12.018	12.018	12.018	
8	17		6.132			Pickerel weed of medium height mixed with some dry button bush.
8'			3.215			"
9	16		2.146			"
9'	16		2.641			

(Continued)

Table 5.3.3-2E. (Continued)

Site & Location	Average Flow Depth (cm)	Slope	Vegetation density at depth (cm)			Type of Vegetation
			10	20	30	
3	1	.0001145	18.320	73.280		Thick pickerel weed about 95% in proportion with very little water hyacinth. Dense vegetation.
	1'		8.142	15.140		
	1"		5.654	5.654		
	2		5.654	18.320		
	2'		5.654	5.654		
	2"		18.320	37.388		Thick pickerel weed mixed with very little water hyacinth.
	3		5.654	15.140	73.280	
	3'		4.154	9.347	5.654	
	3"		18.320	15.140	73.280	

Table 5.3.3-2F. Vegetation Density Values Calculated from Water Flow Data Measured June 29, 1979  
(Using Dye Method).

Site and Location		Average Flow Depth	Slope	Vegetation Density	Type of Vegetation
1	4	45	.000169	.963	Defoliated button bush plants with some pickerel weed.
	4'	16		3.850	Natural vegetation of pickerel weed and button bush adjacent to sprayed area.
	7	35		.764	Open water space surrounded by thick water hyacinth vegetation.
	7'	32		1.365	Water hyacinth vegetation 6-8" tall plants.
	8	25		1.975	Pickerel weed tall and button bush vegetation mixed.
	8'	22		2.030	"
2	1	10		9.183	Thick pickerel weed with small grasses covering the surface.
	2	10		9.183	
3		26		5.075	Thick pickerel weed about 95% in proportion with medium height.
		31		6.729	
4	1	29		4.294	Thick water hyacinth vegetation forming a mat over surface.
	2	24		7.551	
	3	35		30.202	

Table 5.3.3-2G. Vegetation Density Values Calculated from Water Flow Data Measured on July 23, 1979  
(Using Flowmeter Method).

Site, Subsite & Location	Flow Depth (cm)	Slope	Calculated Vegetation Density at Depth (cm)				Type of Vegetation
			10	20	30	40	
1 1	45	.000169	.216	.216	1.082	1.082	Water hyacinth area before open water space.
2	45		1.082	1.082	.544	1.082	Open water space next to thick water hyacinth vegetation.
2'	35		.544	1.082	.544		Open water space (surrounded by water hyacinth) next to defoliated area.
3	45		1.082	1.082	.433	.108	Thick water hyacinth 10-12" tall plants.
3'	35		1.082	1.082	1.082		" deeprooted.
3"	45		4.326	1.082	.544	.082	Thick water hyacinth.
4	35		1.082	2.146	.270	.270	Water hyacinth somewhat shallow rooted.
5	35		.544	.334	.862		Open water area near defoliated button bush section.
6	32		.544	4.326	1.082		Defoliated button bush section, no leafy vegetation.
6'	20		.862	.862			Sprayed, defoliated area.
7	25		2.146	.862	4.326		Defoliated area, dry button bush plants present in groups.
1 7'	25		.334	.334	.862		Sprayed, defoliated area not much surface vegetation.
7"	20		.544	.544			"
8	20		3.215	2.146			Sprayed area but some submerged vegetation.
8'	25		.216	.332	4.326		Open water space in defoliated area but some submerged vegetation.
8"	25		.334	3.215			Defoliated button bush area.
9	20		4.326	6.132			Groups of defoliated button bush plants.
9'	20		2.146	2.146			Sprayed area.
9"	20		1.082	.481			Sprayed area.

(Continued)

Table 5.3.3-2G. (Continued)

Site, Subsite & Location	Flow Depth (cm)	Slope	Calculated Vegetation Density at Depth (cm)				Type of Vegetation
			10	20	30	40	
10	25		22.347	8.346			Pickere1 weed dense vegetation, nonsprayed area adjacent to sprayed area.
10'	25		3.709	8.346			Dense pickere1 weed vegetation.
10"	25		3.215	8.346			Dense pickere1 weed with decaying plants at surface.
10"	25		12.018	12.018			"
11	25		27.040	27.040			"
11'	25		12.013	12.018			"
12	45	.000169	1.082	.216	.216	.270	Open water space surrounded by water hyacinth.
12	45		.216	.216	.135	.334	"
12'	25		3.709	2.641			Pickere1 weed and some button bush.
12"	25		12.018	3.215			Thick pickere1 weed mostly.
13	25		4.326	1.365			Thick pickere1 weed vegetation and some button bush.
13'	25		3.329	6.132			"
13"	25		1.462	2.146			Pickere1 weed and button bush.
13"	25		5.341	8.346			Thick pickere1 weed and other vegetation.
2 1	15		24.96				Pickere1 weed dense vegetation, mixed with small protruding as well as submerged vegetation.
2 2	15		24.96				
2 3	15	.000156	24.96				
2 4	15		7.704				
2 5	15		3.424				
2 6	15		6.241				
2 7	15		7.704				Pickere1 weed plants about 3-4' tall (above the water surface).
2 8	15		11.093				
2 9	15		11.093				
2 10	15		7.704				
3	35	.0001145	18.32	18.32	5.654		95% pickere1 weed dense vegetation.
4	30	.0002496	No flowmeter readings				Thick water hyacinth vegetation.

Table 5.3.3-2H. Vegetation Density Values Calculated from Water Flow Data Measured on July 23, 1979  
(Using Dye Method).

Site Subsite & Location	Average Flow Depth (cm)	Slope	Calculated Vegetation Density	Type of Vegetation	Remarks
1	19	.000169	.137	Open water space surrounded by water hyacinth.	
	19		.105	In water hyacinth area adjacent to open water space.	
	24		4.694	Pickerel weed area dense vegetation.	
	24		.790	Defoliated area with button bush dry stems.	
2	15	.000156	8.150	Thick pickerel weed area with submerged vegetation. Shallow water.	
3	35	.0001145	8.713	95% pickerel weed area.	
4	30	.0002496	14.669	Thick water hyacinth vegetation plants 10-12" tall.	
	33		21.913	Thick water hyacinth forming mat on surface.	

#### 5.3.4 References

- Auclair, A.N.D., A. Bouchard, and J. Pajaczkowski, 1976. Plant Standing Crop and Productivity Relation in a Scirpus-Equisetum Wetland, Ecology, 57, 941-952.
- Bogart, D.B., 1949. The Effect of Aquatic Weeds on Flow in Everglades Canals, Soil Sci. Soc. of Florida, Proc. 9:32-52.
- Chen, C., 1976. Flow Resistance in Broad Shallow Grassed Channels, Journal of Hydraulic Div., ASCE, 102:307-322.
- Das, K.C., and L.F. Huggins, 1971. Effect of Rainfall on the Resistance in Channels with Shallow Flow. Paper presented at 1971 Annual meeting of ASAE at Washington State University, Pullman, Washington, Paper No. 71-211.
- Federico, A.C., J.F. Milleson, P.S. Miller, and M. Rosen, 1978. Environmental Studies in the Chandler Slough Watershed, South Florida Water Management District Tech. Publication #78-2.
- Fenzl, R.N., 1961. Hydraulic Resistance of Broad Shallow Vegetated Channels. Ph.D. thesis presented to University of California, at Davis, California in 1962.
- Graf, W.H., 1966. On the Determination of the Roughness Coefficient in Natural and Artificial Waterways. Int'l Assoc. of Sci. Hydrology XI Annee No. 1:59-68.
- Jervis, R.A., 1969. Primary Production in the Freshwater Marsh Ecosystem of Troy Meadows, New Jersey, Bull Torrey Bot. Club, 96:209-231.
- Keefe, C.W., 1972. Marsh Production: A Summary of Literature, Contr. Mar. Sci., 16:163-181.
- Kouwen, N. and T.E. Unny, 1973. Flexible Roughness in Open Channels. Journal of Hydraulic Divn. ASCE 99:713-728.
- Leutheusser, H.J., and W.O. Chisholm, 1972. Extreme Roughness of Natural River Channels. Paper presented at ASAE Hydraulics Div'n specialty conference, held at Cornell University, Ithica, New York, August 1972.
- Long, R.W., and O. Lakela, 1971. A Flora of Tropical Florida, University of Miami Press, Coral Gables.
- Overton, D.E., H.E. Judd, and C.W. Johnson, 1972. Optimizing Resistance Coefficients for Large Bed Element Streams. Report from Utah Water Research Laboratory, College of Engineering, Utah State University, Logan, Utah.
- Petryk, S., and G. Bosmajian III, 1975. Analysis of Flow Through Vegetation. Journal of Hydraulics Div'n. ASCE, 101:871-884.
- Ree, W.O., 1958. Retardation Coefficients for Row Crops in Diversion Terraces. Trans. Am. Soc. Agr. Eng., 1:78-80.

- Shih, S.F., A.C. Federico, J.F. Milleson, and M. Rosen, 1978. Sampling Program for Evaluating Upland Marsh to Improve Water Quality. Trans. of Amer. Soc. Agri. Engr., Vol. 22(4):828-833.
- Stephens, J.C., R.D. Blackburn, D.F. Seaman, and L.W. Welden, 1963. Flow Retardance by Channel Weeds and Their Control. Journal Irr. and Drainage Div'n. ASCE, 89:31-53.
- Swanson, N.P., and E.O. Peterson, 1960. Vegetated Waterways for Disposal of Irrigation Waste Water and Runoff from Rainfall. Paper presented at Winter meeting of Am. Soc. Agr. Eng. held at Memphis, Tenn., December 1960.
- Thompson, G.T., and J.A. Roberson, 1976. A Theory of Flow Resistance for Vegetated Channels. Trans. of Am. Soc. Agr. Eng., 19:288-293.

### 5.3.5 Conclusions

In the past, one value of the roughness coefficient has frequently been used to represent the flow resistance characteristics of an entire natural wetland throughout the year. To improve the simulation of water flow through these natural vegetation communities, LANDSAT imagery and in situ flow measurements were combined to produce a more detailed representation of flow resistance. The vegetation in a typical marshland drainage basin in south Florida was classified into six categories using LANDSAT data. Flow measurements were then performed at characteristic sites in the basin. The measurements were taken at various depths during months of significant flow to examine the effect of seasonal growth. This information was then combined with the areal distribution of the vegetation as measured by satellite to more accurately simulate resistance to water flow in a natural marshland drainage basin as a function of depth and season.

Two types of vegetation based on their rooting mechanism were selected namely; a) Floating type of surface rooted like water hyacinth, and b) Bottom rooted like pickerel weed. Flow velocity at different locations representing typical vegetation was determined using electromagnetic water current meter and dye technique. Areas with floating type vegetation alone gave flow resistance values that started high with shallow depth in the beginning of growth season and as the flow depth increased with time and onset of rainy season the values decreased with water level rise up to about 30-35 cm below the surface and then formed a maximum in the root zone. Maximum flow resistance values ranged about 5-6 fold the minimum values over a flow depth of 40-60 cm. Flow resistance values below water surface increased and formed a maximum with a peak in the vegetative growth and then decreased with decline in vegetation. Prime growth values varied 2 to 3 times the initial or decay time values in the root zone. However, in bottom rooted vegetation, flow resistance increased with vegetative growth and during and after peak growth period the values stayed high. Peak growth values varied 1 1/2 to 2 times the starting values near the water surface. The favorable effect of increase in flow depth is completely masked by vegetation. This was supported by the vegetation density values calculated at different depths. The flow resistance values showed consistent curvilinear relationships with vegetation density. Flow resistance values in general were higher than reported for any overland flow measurements. The values were as high as 0.7 in the root zone.

LANDSAT data can determine vegetation types. Accurate flow retardance coefficients depend on knowledge of vegetation density and water depth. Future efforts could be directed toward remote sensing methods of estimating those parameters.

#### 5.4 NEW TECHNOLOGY FOR LAKE VOLUME MEASUREMENTS

Contributed by:

R. A. Sutherland	Res. Assoc.
R. G. Bill, Jr.	Res. Assoc.
L. H. Allen, Jr.	Assoc. Prof. and Soil Scientist, USDA
J. F. Bartholic	Prof., Principal Investigator

TABLE OF CONTENTS

	<u>Page</u>
5.4 New Technology for Lake Volume Measurements . . . . .	5.4-1
5.4.1 Collection of Remote Sensing Data . . . . .	5.4-5
5.4.1.1 Equipment . . . . .	5.4-5
5.4.1.2 Test Site Location . . . . .	5.4-5
5.4.1.3 Data Gathering Mission . . . . .	5.4-5
5.4.2 Measurements of Volume of East Lake Tohopekaliga . . . . .	5.4-6
5.4.3 Calculation of Lake Volume . . . . .	5.4-9
5.4.3.1 Theory . . . . .	5.4-9
5.4.3.2 Volume of East Lake Tohopekaliga from Remote Sensed Surface Temperatures . . . . .	5.4-12
5.4.3.3 Lake Volume Model (LKVOL) . . . . .	5.4-13
5.4.3.3.1 Geometry Calculations . . . . .	5.4-13
5.4.3.3.2 Lake Volume Model Description . . . . .	5.4-16
5.4.3.3.3 Summary of Equations . . . . .	5.4-17
5.4.3.3.3.1 Truncated Cone Geometry . . . . .	5.4-17
5.4.3.3.3.2 Fluxes of H, $\mu E$ , and Rn . . . . .	5.4-17
5.4.3.3.3.3 Temperature Profile and Lake Internal Energy . . . . .	5.4-19
5.4.3.4 Results of Lake Volume Model . . . . .	5.4-20
5.4.3.4.1 Program Output Description . . . . .	5.4-20
5.4.3.4.2 Model Predictions of Lake Tohopekaliga . . . . .	5.4-22
5.4.3.4.3 Sensitivity Analysis . . . . .	5.4-22
5.4.3.4.4 Water Temperature Profiles . . . . .	5.4-30
5.4.3.4.5 Model Predictions for Lake Okeechobee . . . . .	5.4-30
5.4.4 References . . . . .	5.4-34
5.4.5 Conclusions . . . . .	5.4-35
5.4.6 Appendix I - Program Listing . . . . .	5.4-36

FIGURES

<u>Figure No.</u>	<u>Page</u>
5.4-1 Bottom contours of East Lake Tohopekaliga based on old U.S. Army Corps of Engineers' data . . . . .	5.4-8
5.4-2 Bottom contours of East Lake Tohopekaliga based on January-February 1979 depth finder soundings . . . . .	5.4-10
5.4-3 Surface temperature from aircraft remote sensing at two times on April 11-12, 1978 . . . . .	5.4-14
5.4-4 Geometry for lake volume calculations. Measured areas were from contour map . . . . .	5.4-15
5.4-5 Plot of flux energies and stored energies from volume calcu- lation program. Depth is incremented until two energies are equal . . . . .	5.4-23
5.4-6 Plots of lake temperature profiles. Smooth curve is theoretical function; dots are data . . . . .	5.4-31

TABLES

<u>Table No.</u>	<u>Page</u>
5.4-1 East Lake Tohopekaliga areas and volumes at each contour elevation from Figures 5.4-1 and 5.4-2 . . . . .	5.4-7
5.4-2 Output of lake volume model for test case. Wind from second data set and temperature from first data set . . . . .	5.4-21
5.4-3 a. Input parameters, data, and fluxes from first data set for East Lake Tohopekaliga volume calculations. b. Volume calculation results . . . . .	5.4-24
5.4-4 a. Input parameters, data, and fluxes from second data set for East Lake Tohopekaliga volume calculations. b. Volume calculation results . . . . .	5.4-26
5.4-5 Energy fluxes and depth calculations for different sky temperatures for East Lake Tohopekaliga . . . . .	5.4-29
5.4-6 a. Input parameters, data, and fluxes for Lake Okeechobee volume calculations from GOES satellite sensed surface temperatures. b. Volume calculation results . . . . .	5.4-32

#### 5.4.1 Collection of Remote Sensing Data

##### 5.4.1.1 Equipment

In collecting the remotely sensed data for the lake volume measurements, KSC utilized the following equipment.

a. Electronic Scanner: A Daedalus DS-1250 Scanner with two thermal channels (3 to 5 microns and 8 to 14 microns).

b. Aircraft: Twin engine Beechcraft C45H with 450 horsepower Pratt and Whitney engines and a cruise speed of 160 knots. Range is 600 nautical miles, ceiling is 12,000 feet and maximum useful equipment payload is 1079 pounds.

##### 5.4.1.2 Test Site Location

The test site for the development of the new volume technique was East Lake Tohopekaliga near St. Cloud, Florida. The test lake was approximately 4.6 miles in diameter and is located at the following coordinates on the following quadrangle:

East Lake Tohopekaliga 81°17'30" W      St. Cloud North  
28°17'30" N

##### 5.4.1.3 Data Gathering Mission

A ground data gathering mission was completed on April 11 and 12, 1978. During this time period three flight missions were completed using three thermal scanner flight lines over the lake for each mission. The following are the times and altitudes of the thermal flights:

<u>Flight Times</u>	<u>Aircraft Altitude</u>	<u>Black Body Range</u>
April 11, 1978 - 1500	8,000 ft.	60 - 78° F
April 11, 1978 - 2400	8,000 ft.	60 - 78° F
April 12, 1978 - 0500	5,000 ft.*	60 - 78° F

\*(Due to low clouds the aircraft altitude was lowered to prevent interference with the clouds.)

In addition to the scanner data acquired by the KSC aircraft, at KSC's request the state of Florida Department of Transportation completed a photographic mission over the test side with color infrared film (Kodak 2443) at a scale of 1:24,000 taken on April 4, 1978, at 1200 EST.

An instrumented boat was used on East Lake Tohopekaliga for data collection from 1500 EST April 11 to 1530 EST April 12, 1978. Wind speed, wind direction, and air temperature were measured at a height of 3 m above the water. Air from this height was sampled and pumped to a dewpoint hygrometer to measure the specific humidity of the air. Water temperature was measured at depths of 0.1, 0.3, 1.0, 2.0, and 3.0 m in the lake and at 0.3 m in the lake bottom with copper-constantan thermocouples connected to a multipoint recorder with an ice-point reference junction.

Wind speeds were moderate to low. The mean wind speed during the period was 3.0 m/s, with a maximum and minimum hourly average of 5.3 m/s and 1.7 m/s, respectively. The wind was primarily from the south or southwest.

Dewpoint temperature was relatively constant during the observation period. A minimum value of 15.6°C occurred at 1530 EST on April 12. The maximum value of 20.6°C was maintained between 2000 EST on April 11 and 0730 EST on April 12. The minimum air temperature, 20.8°C, was reached at 0530 EST on April 12.

The mean water temperature at 10 cm below the surface was 24.9°C as measured by copper-constantan thermocouple, and the mean surface temperature was 23.4°C as measured by radiation thermometry. The lake bottom temperature was 23.9°C.

Hourly wind speed, surface temperature, and net radiation are given in tables in Section 5.4.3.4.2.

During January and February 1979, the South Florida Water Management District completed a set of grid (N - S and E - W) depth finder soundings on the lake so that new bottom contour maps and stage-volume relationships could be obtained. (This was accomplished since the only set of depth measurements on the lake were taken by the U.S. Army Corps of Engineers some twenty years previous and did not represent the current lake bottom contours.)

#### 5.4.2 Measurements of Volume of East Lake Tohopekaliga

Bottom elevation contours of East Lake Tohopekaliga were available from U.S. Army Corps of Engineers depth measurements (Figure 5.4-1) with a shoreline elevation of 56 feet msl. The areas within each of these contours were computed using a Hewlett-Packard<sup>1</sup> Model No. 9864A digitizer system with a Model No. 9830A Programmable Calculator. The volumes (V) were computed by considering each 1-foot interval to be approximated by the frustrum of a cone.

$$V = \frac{\pi}{3} Z (r_2^2 + r_2 r_1 + r_1^2) \quad (5.4-1)$$

where

$$r_2^2 = \frac{A_2}{\pi}; \quad r_1^2 = \frac{A_1}{\pi}; \quad r_2 r_1 = \frac{(A_2 A_1)^{1/2}}{\pi}$$

A<sub>2</sub> and A<sub>1</sub> are the top and bottom areas, respectively, of the contours of the lake depth interval, Z. Each of the volumes of the 1-foot depth intervals were summed to give cumulative lake volume. Table 5.4-1 shows the areas and volumes of water computed from Figure 5.4-1. The total area was 42.55 X 10<sup>6</sup> m<sup>2</sup> and the total volume was 116 X 10<sup>6</sup> m<sup>3</sup>.

---

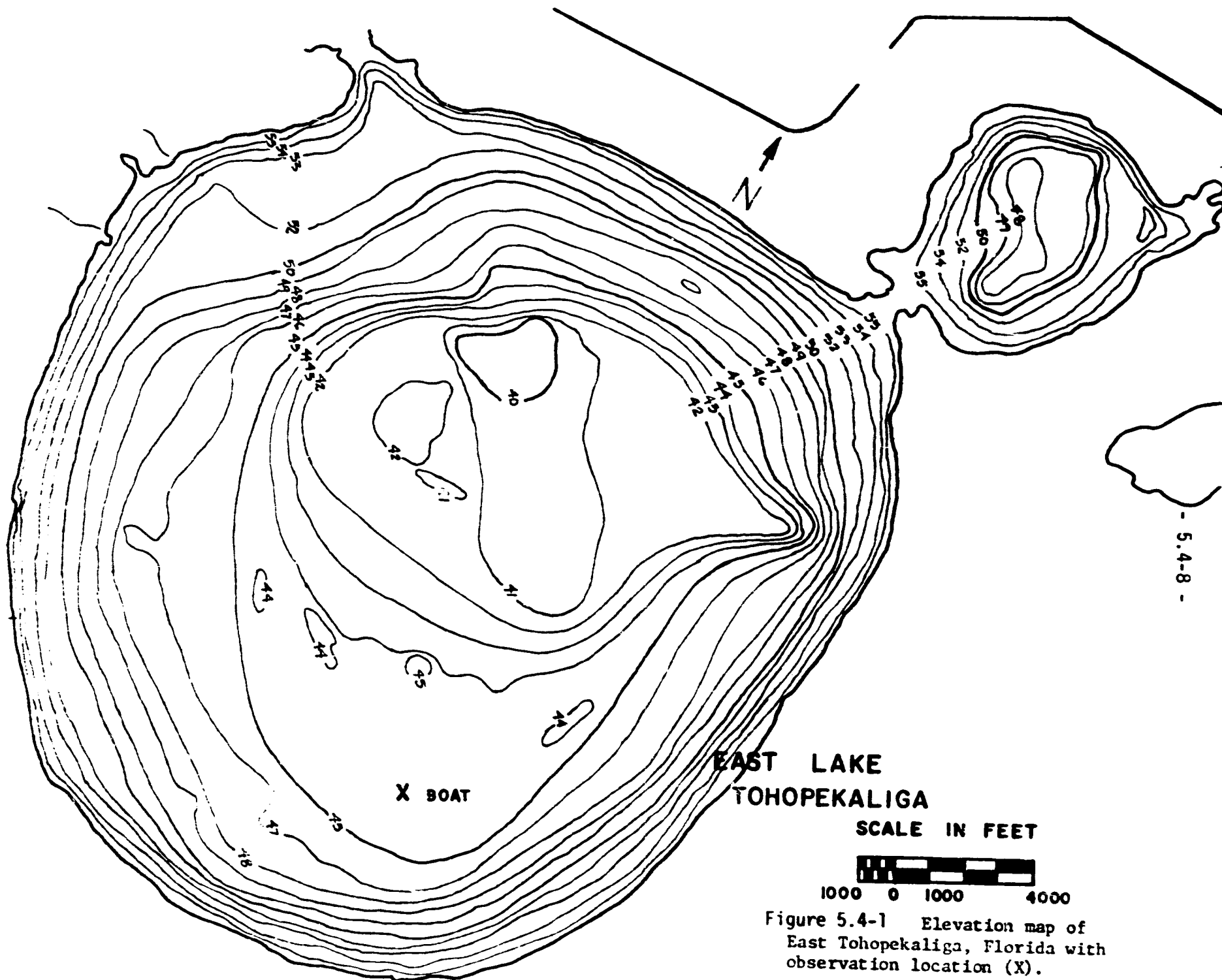
<sup>1</sup> Mention of proprietary products is for the convenience of the reader only, and does not constitute endorsement or preferential treatment by NASA or the University of Florida.

Table 5.4-1. East Lake Tohopekaliga areas and volumes at each contour elevation from Figure 5.4-1 and 5.4-2.

Elevation (ft)	Data from Figure 5.4-1			Data from Figure 5.4-2		
	Contour Area (X 10 <sup>6</sup> ft <sup>2</sup> )	Layer Volume (X 10 <sup>6</sup> ft <sup>3</sup> )	Cumulative Volume (X 10 <sup>6</sup> ft <sup>3</sup> )	Contour Area (X 10 <sup>6</sup> ft <sup>2</sup> )	Layer Volume (X 10 <sup>6</sup> ft <sup>3</sup> )	Cumulative Volume (X 10 <sup>6</sup> ft <sup>3</sup> )
57				472	462	4231 <sup>2</sup>
56	458	449	4096 <sup>2</sup>	(452) <sup>1</sup>	444	3769
55	441	432	3647	(433)	423	3327
54	424	412	3215	(414)	405	2904
53	400	385	2803	(396)	387	2499
52	371	362	2418	378	362	2155
51	(353) <sup>1</sup>	344	2056	347	332	1753
50	336	324	1712	318	303	1421
49	312	298	1388	288	274	1118
48	284	268	1090	261	234	844
47	253	233	822	208	187	610
46	214	194	589	167	147	423
45	175	143	395	127	112	276
44	114	103	252	97	88	164
43	93	86	149	79	57	76
42	79	50	63	37	17	19
41	26	13	13	3	2	2
40	4	-	0	1	-	0

<sup>1</sup>Values in parentheses were estimated.

<sup>2</sup>Cumulative volumes computed from layer volumes, which were computed from equation 5.4-1. Total areas and volumes in metric units were 42.55 X 10<sup>6</sup> m<sup>2</sup> and 116 X 10<sup>6</sup> m<sup>3</sup> from Figure 5.4-1 data and 43.85 X 10<sup>6</sup> m<sup>2</sup> and 120 X 10<sup>6</sup> m<sup>3</sup> from Figure 5.4-2 data. Average depths (from equation 5.4-5 were 2.72 m (8.94 ft) and 2.73 m (8.97 ft) for the two data sets, respectively.



The depth finder soundings collected by the South Florida Water Management District from seven N-S soundings on January 16-18, 1979, and from seven E-W soundings on January 18-19, January 30-31, and February 6-7, 1979, were plotted as an overlay on a 7.5-minute series U.S. Geological Survey topographic map (St. Cloud North Quadrangle). From this overlay, a bottom contour map at 1-foot intervals was drawn (Figure 5.4-2) by carefully estimating depths. Cross-over points on the grid were usually in close agreement after slight lake level corrections for the January 30-31 and February 6-7, 1979 surface elevation data. The elevation averaged 57.03 feet msl on January 16-19 and 56.68 feet msl on January 30-February 7, 1979. No bottom contours could be drawn from the 52-foot elevation to the 57-foot shoreline contour because the soundings did not come that close to shore. The USGS topographic map gave the lake elevation as 57 feet msl. Since the outflow from the lake is controlled by a water control structure, this elevation is probably reasonably constant. These latter bottom contours (Figure 5.4-2) appear slightly different from the early East Lake Tohopekaliga contours (Figure 5.4-1), but certain similarities exist. Table 5.4-1 also shows the bottom contour areas and volumes computed from the January-February 1979 soundings. The total area was  $43.85 \times 10^6 \text{ m}^2$  and the total volume was  $120 \times 10^6 \text{ m}^3$ .

Based on the earlier bottom contour data which covered only up to the 56-foot shoreline contour, the lake appears to have decreased in volume by about 8% below this 56-foot contour (from  $116 \times 10^6 \text{ m}^3$  to  $107 \times 10^6 \text{ m}^3$ ). However, the January-February 1979 depths were determined with respect to the 57-foot contour lake level. The volume of water in the lake ( $120 \times 10^6 \text{ m}^3$ ) appears to have increased by about 3% due to a higher lake level. However, we do not have any way of determining how accurately the contours were drawn.

The average depth for each of the volume determinations was computed from the total areas and total volumes. The values were 2.72 m (8.94 ft) and 2.73 m (8.97 ft) for the contours from Figures 5.4-1 and 5.4-2, respectively.

### 5.4.3 Calculation of Lake Volume

#### 5.4.3.1 Theory

The concept of lake volume measurement from satellite surface temperature data is to predict lake volume from the energy balance of the lake. The differential time-rate of change in internal energy of a column in the body of water would be equal to the sum of the exchanges of all energy flux density components. This can be written as:

Change in Internal Energy = Sum of energy flux densities

$$\frac{d}{d\tau} \int_0^S C T(Z) dZ = R_n + H + \lambda E + G \quad (5.4-2)$$

where  $R_n$  = net radiation flux density  
 $H$  = sensible heat flux to or from atmosphere  
 $\lambda E$  = latent heat flux to atmosphere (evaporation)  
 $\lambda$  = heat of vaporization  
 $E$  = vapor flux to atmosphere

- 5.4-10 -

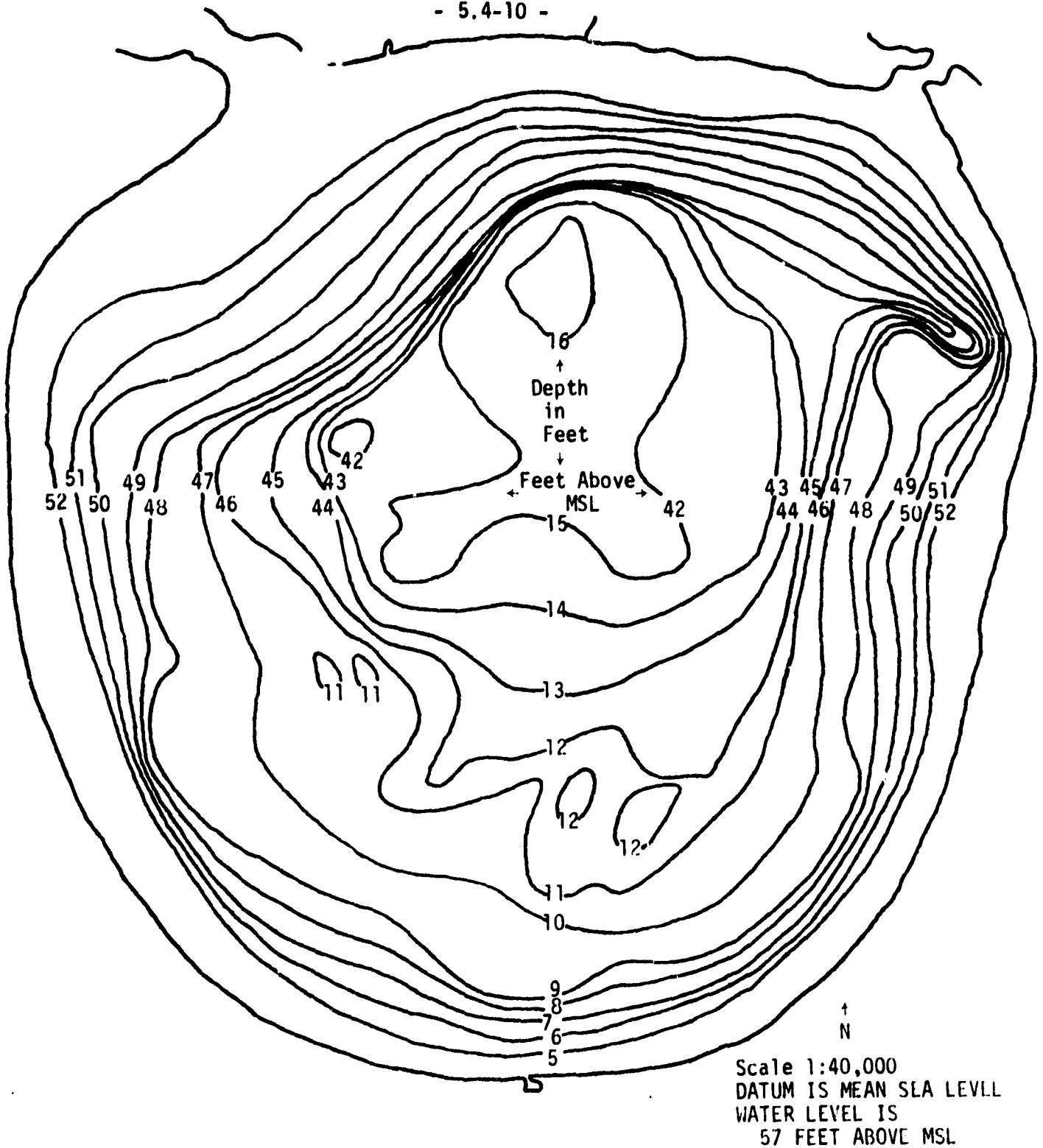


Figure 5.4-2. Bottom contours of East Lake Tohopekaliga based on January-February 1979 depth finder soundings.

G = heat flux to or from bottom  
 $\tau$  = time  
 C = volumetric heat capacity of water  
 T = water temperature  
 Z = depth.

The equation can also be written in finite thickness element form over a given time interval (integrated with respect to time) as:

$$\sum_{i=1}^n C(\Delta T)_i \Delta Z_i = \sum_{\tau} (R_n + H + \epsilon E + G) \quad (5.4-3)$$

where i = depth interval index of summation

n = number of depth increments

$\Delta T$  = water temperature change from initial time to final time (over total time interval).

In general, the heat flux through the bottom of a lake would be small compared to the other fluxes, so the term (G) can be dropped for simplicity. Also since most lakes would not have uniform area from top to bottom, the change in internal energy in equation 5.4-3 would need to be weighted by the area of each slice.

$$\frac{1}{A} \left( \sum_{i=1}^n C \Delta T_i a_i \Delta Z_i \right) = \sum_{\tau} (R_n + H + \epsilon E) \quad (5.4-4)$$

where A = total area

$A_i$  = average area of each depth increment.

The average depth,  $\bar{D}$ , could be defined as:

$$\bar{D} = \frac{1}{A} \sum_{i=1}^n a_i \Delta Z_i \quad (5.4-5)$$

and the total volume V, would be equal to  $A \cdot \bar{D}$ .

If the lake were well mixed so that it were isothermal with respect to depth, and if the average depth were known, then equation 5.4-4 would simplify to:

$$C \Delta T \bar{D} = \sum_{\tau} (R_n + H + \epsilon E) \quad (5.4-6)$$

The average depth can be calculated if the areas at various depth increments,  $a_i$ , are known. Bottom contours of a lake can be obtained from historical records or from depth sounding.

The form of equation 5.4-6 lends itself to analysis of lake depth and volume from satellite remote sensed data from knowledge of surface temperature change over a given time interval, provided that the lake were well mixed so

that temperature stratification were eliminated or minimized. The change in internal energy could be calculated from change in lake temperature as indicated by changes in surface temperature.

Net radiation could be obtained by satellite as discussed in section 5.6.2.2.1, but over small lakes local measurements may be necessary.  $H$  and  $\lambda E$  could be calculated from surface temperature obtained by remote sensing.

Hicks (1975) proposed a relationship for  $H$ ,  $\lambda E$ , and the Bowen ratio,  $\beta = H/\lambda E$ , based only on water surface temperature.

$$H = 4 \epsilon \sigma T_s^3 \beta / (d\beta/dT_s) \quad (5.4-7)$$

$$\lambda E = 4 \epsilon \sigma T_s^3 / (d\beta/dT_s) \quad (5.4-8)$$

where  $\epsilon$  = water surface emissivity  
 $\sigma$  = Stefan-Boltzman constant  
 $T_s$  = surface temperature, °K.

If the air above a water surface is saturated, then  $\beta$  may be expressed as the ratio of the psychrometric constant ( $\gamma$ ) to the slope of the saturation specific humidity vs. temperature curve ( $s$ ), where  $\gamma$  is defined here as  $C_p/\lambda$ , where  $C_p$  is the heat capacity of air at constant pressure. Hicks (1975) suggested that a more reasonable form for the Bowen ratio might be:

$$\beta = (K/D)(\gamma/s) \quad (5.4-9)$$

where  $K$  = molecular diffusivity for heat  
 $D$  = molecular diffusivity for water vapor.

Bill (1978) found that equation 5.4-9 gave better estimates of  $\lambda E$  from Orange Lake, Florida, as determined from a sonic anemometer and Lyman- $\alpha$  humidimeter if  $\lambda E$  were multiplied by  $(U/U_0)^n$  where  $U_0 = 7.3$  m/s and  $n = 1.36$ . Bill et al. (1980) also suggested that a "film temperature,"  $T_f$ , e.g., a temperature intermediate between a surface temperature and the bulk fluid temperature (see Gebhart, 1971), be used to calculate heat transfer and vapor transfer from lakes. They found that equations 5.4-7, 5.4-8, and 5.4-9 could be used if the following expression for  $T_f$  were substituted.

$$T_f = 0.7 T_s + 0.3 T_{10} \quad (5.4-10)$$

where  $T_{10}$  is the air temperature at a height of 10 m.

#### 5.4.3.2 Volume of East Lake Tohopekalliga from Remote Sensed Surface Temperatures

Three thermal scanner flight scenes over East Lake Tohopekalliga were obtained and processed as 70-mm color coded film strips at 1500 EST on April 11 and at 0030 and 0500 EST on April 12. Due to low clouds at 0500 EST on April 12, the surface temperatures appeared very slightly warmer than at 0030 EST so these data were not plotted. The thermal scenes obtained from 1°F

intervals of surface temperature were extracted and plotted as isotherms on East Lake Tohopekaliga (Figure 5.4-3). Flight lines are also drawn on Figure 5.4-3. The surface temperature decreased from an average of 73.5°F to 71.2°F from 1500 EST to 0030 EST. The summation of flux energy was  $-0.54 \text{ cal/cm}^2$  over this period and  $-1.76 \text{ cal/cm}^2$  over the 1500 EST to 0500 EST period. From equation 5.4-6, this would yield depths of 0.4 m to 1.4 m for the early period and total period, respectively. Obviously, this is much too shallow based on the computation of about 2.7 m for the average depth from the real area and volume calculations (Section 5.4.2). Most of the difference in surface temperature between the two times was due to temperature decrease in the surface layers of the lake. From temperature profile data collected within the lake, we knew beforehand that these volume computations would be inaccurate because the mixed, isothermal conditions were not met. These conclusions led to the development of a stratified lake model.

#### 5.4.3.3 Lake Volume Model (LKVOL)

Calculations of mean lake depth from two sets of surface temperature data in the previous section (5.4.3.2) gave a value that was much too small (0.5 m to 1.4 m). Inspection of temperature profiles within the lake showed that the lake was thermally stratified with the water temperatures near the surface being much higher during the daytime hours due to solar heating. Hourly average wind speed during the period 1530 EST April 11 to 1530 EST April 12 ranged from 5.3 to 1.7 m/s, and averaged 3.0 m/s. This wind speed was too low to maintain adequate mixing in the lake. Therefore, a stratified lake model was developed to predict lake depth and volume from measurements of internal energy change and total flux energy exchanges as described by equation 5.4-4, which is simply solution of the energy balance of the lake. The total internal energy changes were computed by incrementing lake depths, and the total surface flux energy exchanges were computed by incrementing increasing surface areas.

##### 5.4.3.3.1 Geometry Calculations

The energy balance method used here requires some apriori relationship of lake contours, surface areas, and volumes. This is because as the lake depth is incremented from the bottom upward, the surface area increases giving rise to an increased flux of energy (i.e., flux density  $\times$  area  $\times$  time) and an increase in volume giving rise to an increased stored internal energy. A fairly accurate relationship between area and volume was needed.

An examination of the contour maps of East Lake Tohopekaliga (Figures 5.4-1 and 5.4-2) suggested a simple truncated cone model (frustrum of a cone). Cross-sectional areas as a function of elevation are shown in Figure 5.4-4. These data were then fitted to a truncated cone model and the parameters  $r_0$  (bottom radius),  $R_0$  (top radius) and  $D$  (depth, or equivalently apex angle) were determined. The values used were 1840 m, 3680 m, and 5 m, respectively.

Results of the fit are shown in Figure 5.4-4. The fit is quite reasonable near the top (where the water level usually is), but it deviates notably at the bottom. This deviation at the bottom will cause only small errors except in extreme cases of very low water levels. In the fitting procedure, the parameters were chosen to reproduce the true volume as determined from the contour map for a full (i.e., depth =  $D$ ) lake. This would further minimize errors.

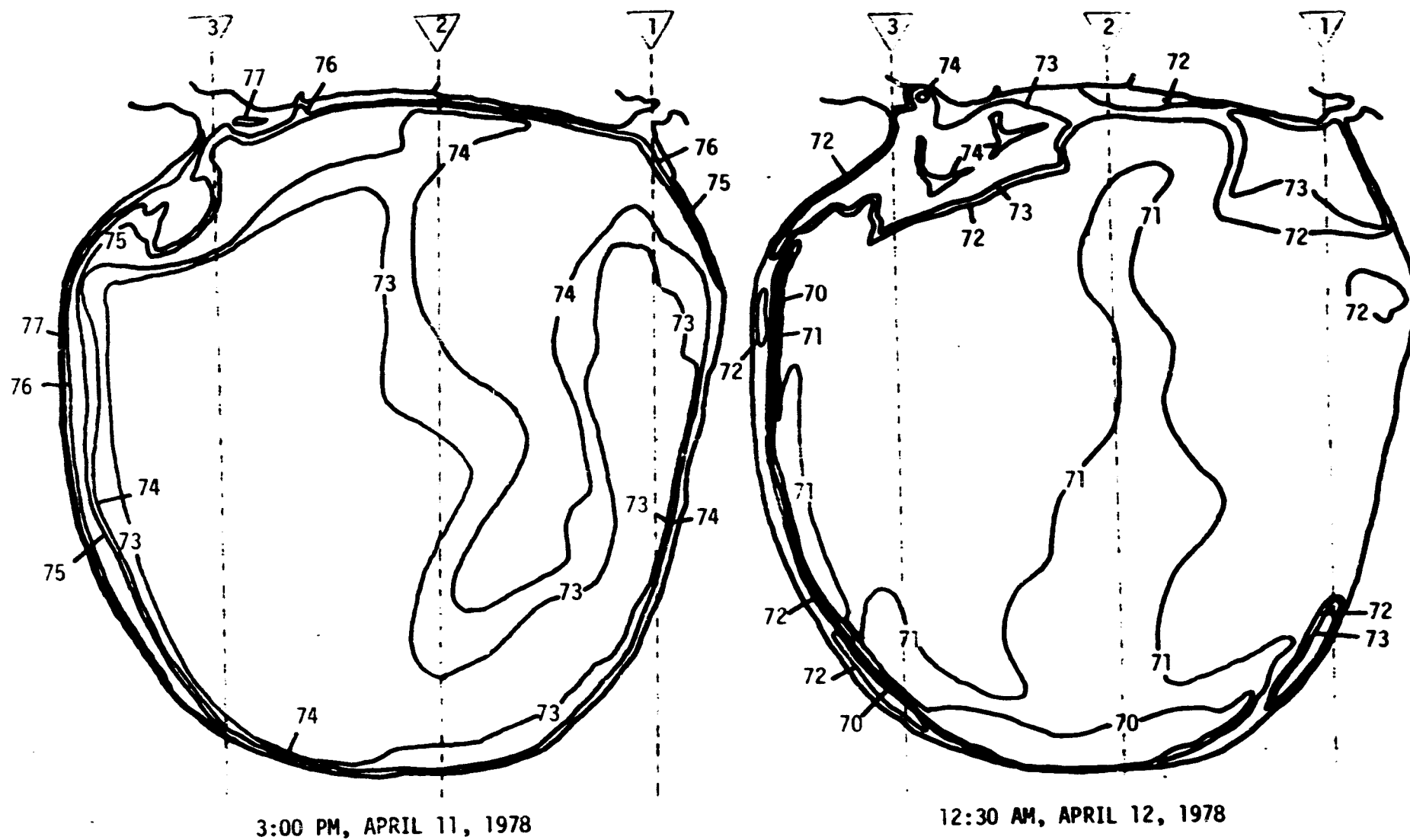


Figure 5.4-3. Surface temperature from aircraft remote sensing at two times on April 11-12, 1978.

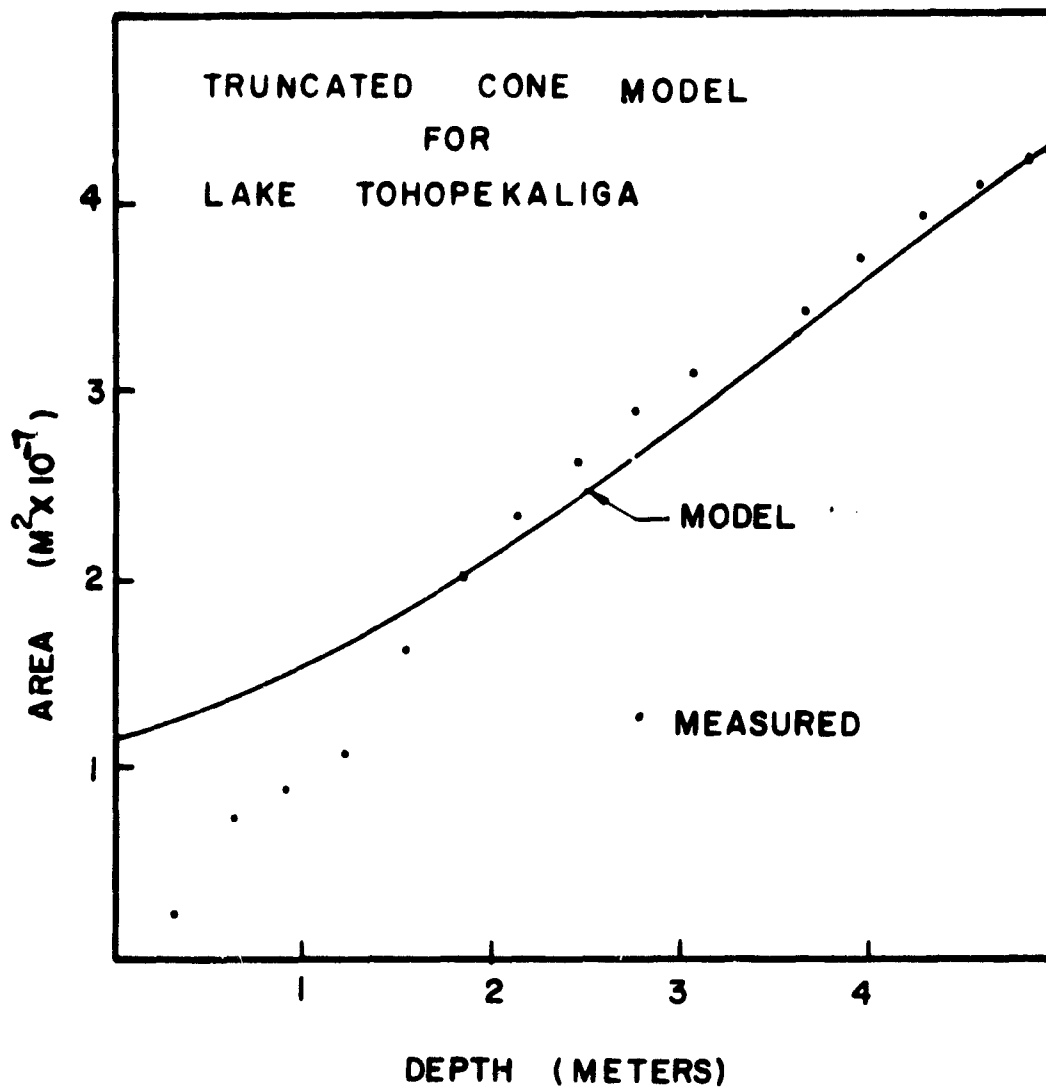
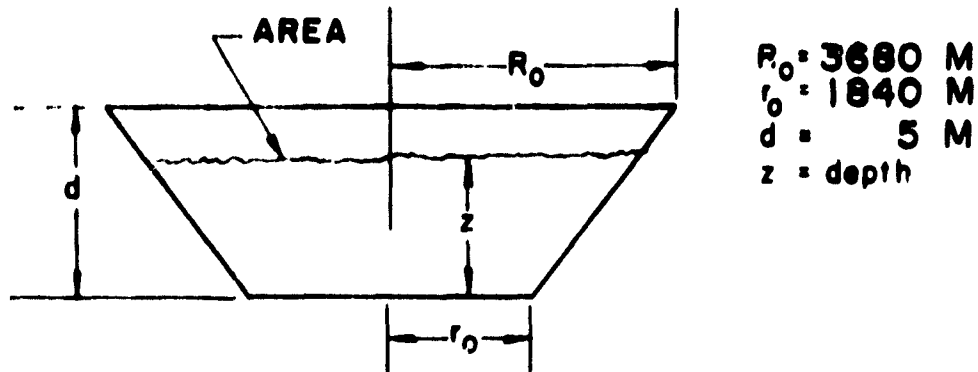


Figure 5.4-4. Geometry for lake volume calculations.  
Measured areas were from contour map.

#### 5.4.3.3.2 Lake Volume Model Description

Temperature, wind speeds, and net radiation measurements made on East Lake Tohopekaliga during April 1978 are used to estimate the lake volume by equating time-integrated fluxes of latent, sensible, and radiative heat to internally stored energy. The fluxes of sensible and latent heat are estimated via the model of Hicks (1975) as modified by Bill (1978). Modeled net radiation is used for one estimate using sun, sky, and surface radiation equations and, in another, the measured net radiation is used.

Internally stored energy is calculated with the truncated cone geometry and with the temperature profile function of Sutherland (1980) in order to account for thermal stratification.

A FORTRAN program (named LKVOL) was written which increments the lake depth until the flux energy and internally stored energy are equal. This was done in two ways, one which summed over a 24-hour period to give one single depth determination, and another which predicts lake depth based on the flux energy exchange and the internal energy change over each hourly period.

The lake volume program is attached as Appendix (I).

The input data for LKVOL include top radius (TR), bottom radius (BR), height of the truncated cone (HC), lake bottom temperature (TB), latitude (XLAT), solar declination (DEC), atmospheric attenuation coefficient (ATT), equivalent blackbody sky temperature (TSKY), hourly wind speed (U), hourly surface temperature (ST), and hourly net radiation (RN). The program has the option of computing net radiation from hourly surface temperature, equivalent blackbody sky temperature, and modeled solar radiation if net radiation is not given. The sensible heat flux and latent heat flux are calculated hourly from surface temperature and wind speed based on equations 5.4-7, 5.4-8, 5.4-9, and  $(U/U_0)^n$  as described in Section 5.4.3.1. Sensible heat flux, latent heat flux, and net radiation are then summed for each hour to give the flux energy to or from the lake. These input data and derived data are printed as output.

Internal energy stored is calculated hourly for the truncated cone model geometry and with the sinusoidal temperature profile function of Sutherland (1980). This function has lake bottom temperature and lake surface temperature as boundary condition values. Lake internal energy is calculated hourly by integrating the analytical temperature profile function.

Effective depth of the lake is calculated by determining the depth at which the internal energy change would balance the flux energy exchanges at the surface. This is done two ways. The first way requires that the sum of both flux energy exchanges and internal energy changes over the period of input data (e.g., 24 hours) be computed for each depth increment (upward direction). The internal energy changes will be a function of cumulated lake volume, and the flux energy exchanges will be a function of increasing surface area of the truncated cone model. When these values are equal, the effective depth, D, of the lake will be known.

The second method computes effective depth from hourly flux energy exchange and internal energy change. The program computes depth and volume for each hourly calculation.

### 5.4.3.3.3 Summary of Equations

The equations used in the model to describe cone geometry, to predict fluxes of H,  $\lambda E$ , and Rn, and to compute internal lake energy are described below.

#### 5.4.3.3.3.1 Truncated Cone Geometry

For the truncated cone geometry with height Z measured from the bottom upward, the cross sectional area at any height Z is:

$$A(Z) = \pi r^2 \quad (5.4-11)$$

$$r = r_0 + \frac{Z}{D} (R_0 - r_0)$$

$r_0$  = bottom radius

$R_0$  = top radius

D = height

$r_0$ ,  $R_0$ , and D are fixed numbers estimated from contour maps (Figure 5.4-1).

The volume for any height Z is:

$$V(Z) = \frac{\pi}{3} Z(r_0^2 + rr_0 + r^2) \quad (5.4-12)$$

#### 5.4.3.3.3.2 Fluxes of H, $\lambda E$ and Rn

For sensible heat (H) and latent heat ( $\lambda E$ ), the formulation of Hicks (1975) modified by Bill (1978) is followed.

$$\lambda E = \frac{4\epsilon\sigma T_\beta^3}{d\beta/dT} \left(\frac{U}{U_0}\right)^n \quad (5.4-13)$$

$\epsilon$  = lake surface emissivity (= 0.98)

$\sigma$  = Stephan-Boltzman constant (=  $0.813 \times 10^{-10}$  cal/cm<sup>2</sup> °K<sup>4</sup>)

T = lake surface temperature (°C)

$\beta$  = Bowen ratio

U = wind speed (m/s)

$U_0$  = parameter (7.3 m/s)

n = parameter (1.36).

The Bowen Ratio is calculated as:

$$\beta = (K/D) \frac{\gamma}{s} \quad (5.4-14)$$

(K/D) = ratio of thermal diffusivity and water vapor molecular diffusivity (= 0.84)

$\gamma$  = psychrometric constant (=  $6.58 \times 10^{-4}/^{\circ}\text{K}$ )

$s$  = slope of the saturation specific humidity ( $q_s$ ) vs temperature curve ( $dq_s/dT$ ) with  $q_s$  calculated as (Fleagle and Businger, 1963):

$$q_s = \frac{0.622 e_o}{p_o} e^{-(\ell/R) \frac{1}{T}} \quad (5.4-15)$$

$p_o$  = ambient air pressure ( $1.013 \times 10^6$  dyne/cm<sup>2</sup>)

$\ell/R$  = ratio of latent heat of vaporization to specific gas constant (=  $5.327 \times 10^3$ )

$e_o$  = parameter to best fit in 20-30°C range ( $e_o = 1.82 \times 10^{12}$  dyne/cm<sup>2</sup>)

with proper substitution then:

$$s = \frac{dq_s}{dT} = \frac{\ell}{R} \frac{q_s}{T^2} \quad (5.4-16)$$

$$\frac{d\beta}{dT} = -\frac{\beta}{T^2} [(\ell/R) - 2T] \quad (5.4-17)$$

Equations 5.4-11 to 5.4-15 are used to calculate the latent heat flux and Bowen ratio. The sensible heat is determined from

$$H = \beta \ell E \quad (5.4-18)$$

The net radiation, RN, if not measured, is modeled as a contribution from the sun (SUN), incoming thermal radiation from the sky (SKY), and outgoing thermal radiation from the surface (SFC) as:

$$\text{SUN} = Q_o \times e^{-a/x} \quad (5.4-19)$$

$Q_o$  = Solar constant (=  $2.0 \text{ cal/cm}^2 \text{ min}$ )

$a$  = atmosphere extinction coefficient ( $\sim 0.288$ ) and  $x$  accounts for diurnal movement of the sun calculated as:

$$x = \sin(\text{lat}) \sin(\text{dec}) + \cos(\text{lat}) \cos(\text{dec}) \cos(\text{ha}) \quad (5.4-20)$$

lat = geographical latitude of lake (degrees)

dec = solar declination (degrees  $\sim 10^\circ$  in April)

ha = hour angle of sun measured from solar noon  
 $360^\circ/24 \text{ hrs} = 15^\circ/\text{hr}$

(Actually, over water the solar radiation input should be corrected for an albedo of about 5%.)

$$\text{SKY} = \sigma T_{\text{sky}}^4 \quad (5.4-21)$$

where  $T_{\text{sky}}$  is equivalent sky temperature ( $\sim -10^\circ \text{C}$  clear;  $\sim +10^\circ \text{C}$  clouds)

$$\text{SFC} = \epsilon \sigma T^4 \quad (5.4-22)$$

where the terms are the same as in equation 5.4-13.

$$\text{RN} = \text{SUN} + \text{SKY} - \text{SFC} \quad (5.4-22A)$$

#### 5.4.3.3.3 Temperature Profile and Lake Internal Energy

The temperature profile of the lake is fitted to the surface ( $T_s$ ) and bottom ( $T_{\text{bot}}$ ) temperatures with the following function:

$$T(Z) = (T_s - T_1) + T_1 \left[ \sin \left( \frac{\pi^2}{4D} \right) + \cos \left( \frac{\pi^2}{4D} \right) \right] \quad (5.4-23)$$

where  $D$  = depth of lake (to be found by iteration) and:

$$T_1 = (T_s - T_{\text{bot}}) / [\sin(\pi/4)] \quad (5.4-24)$$

$Z$  is the vertical coordinate measured upward from the lake bottom.

The internal energy of the lake is found by integration along the  $Z$  coordinate:

$$E(D) = C \int_0^D A(Z) T(Z) dZ \quad (5.4-25)$$

where  $A(Z)$  is given by equation 5.4-11 and  $C = 1 \text{ cal/cm}^3 \text{ } ^\circ\text{C}$ .

Equations 5.4-11 and 5.4-23 are substituted and equation 5.4-25 is integrated to yield:

$$E(D) = C \left[ (T_s - T_1) V(D) + \frac{4T_1 D}{\pi} (16\Delta^2 x - 8\Delta R_0 y + R_0^2) \right] \quad (5.4-26)$$

where  $\Delta = R_0 - r$

$$x = \pi \cos(\pi/4) - 2$$

$$y = 2 \cos(\pi/4) - 1$$

#### 5.4.3.4 Results of Lake Volume Model

##### 5.4.3.4.1 Program Output Description

Table 5.4-2 is a copy of the output of the program LKVOL which was written for this study. In this particular case, 25 hourly data sets (i.e., surface temperature, wind speeds and net radiation) from 1530 EST on April 11 to 1530 EST on April 12, 1978, had been entered. The output shows:

- Column 1 depth increment in upward direction (meters)
- 2 calculated surface area at this depth
- 3 calculated volume at this depth
- 4 internal energy change over the entire 24-hour time period in calories per hour
- 5 time integrated fluxes (x area) for 24-hour time period in calories per hour
- 6 differences between column 4 and 5.

The other 24 one-element columns show the depth of which the energy balance was obtained for the individual hours (\*means balance is negative; 1 means positive). The depth determination is made by noting the depth at which the difference (column 6) changes sign and the balance depth is estimated to the nearest 0.1 m (often the halfway point between the depth where the sign changes). In this case, the depth was  $5.1 \text{ m} \pm 0.1 \text{ m}$  ( $16.7 \pm 0.3$  feet) for the summed 24-hour data.

The depth determinations at the bottom of the printouts are the individual hour determinations, essentially the same information as the last 24 columns above.

The average depth printout is based upon the individual hours and gives an idea of the spread in error of the hourly calculations. In this case, the average depth was  $4.6 \text{ m} \pm 1.4 \text{ m}$  ( $15.1 \pm 4.6$  feet) which corresponds to  $32.7 \pm 14.6$  billion gallons. In a perfect case, we would expect all determinations to agree. It should be noted from Table 5.4-2 that some of the data do not allow for a depth determination. These are the unrealistic cases where net incoming (outgoing) flux energy is accompanied with a decrease (increase) in internal energy and simply indicates errors in either measurements or flux modeling. In the program, these cases are ignored and eliminated from further computations.



Figure 5.4-5 is simply a plot of the program output demonstrating graphically the workings of the program and the geometry of the lake model. It shows that flux energy exchange increases more slowly than internal energy change. The crossover point indicates the predicted depth of the truncated cone model lake.

#### 5.4.3.4.2 Model Predictions for Lake Tohopekaliga

Data from the Tohopekaliga experiment of April 1978 were reported in two forms; one being the Bill (1978) report and the other edited set being through private communications with R. G. Bill, specifically for the hourly average inputs to the lake volume model. The Bill (1978) data contained wind speed and lake temperature profiles, but did not contain lake surface temperature or net radiation. For this reason, 10-cm depth lake temperatures from Bill (1978) were used for surface temperatures and net radiation was estimated by modeling (Section 5.4.3.3.2). This led to two data sets. The first data set (Bill, 1978) consisted of 1) unedited wind data at a height of 3 m, 2) water profile temperature data at 0.1, 0.3, 1.0, 2.0, and 3.0 m, and lake bottom temperature at 0.3 m, using copper constantan thermocouples, and 3) no net radiation. The second set of data consisted of 1) edited hourly average wind data, 2) surface temperature data from a Barnes Model No. PRT-5 precision radiation thermometer, and 3) net radiation measured with a Swissteco Model No. S-1 net radiometer. The first data set was used in the lake volume model determination shown in Table 5.4-3, and the second set used in the predictions shown in Table 5.4-4. (The precision radiation thermometer surface temperatures agreed better with the aerial IR scanner scenes (Figure 5.4-3) than did the thermocouple data.) The "a" portions of Tables 5.4-3 and 5.4-4 show the flux estimates and the "b" portions show the volume determinations. (To obtain correct EST for the TIME lists in the "a" portion of the tables, 12 hours should be added to each value. If the resultant value exceeds 24, then 24 hours should be subtracted.)

In Table 5.4-3b, the volume by the summed method yielded a depth of  $4.8 \pm 0.10$  m ( $15.7 \pm 0.3$  feet) while the hourly results were  $4.3 \pm 1.6$  m ( $14.1 \pm 5.2$  feet) with 17 realistic hours. In Table 5.4-4b, the results were  $2.3 \pm 0.10$  m ( $7.5 \pm 0.3$  feet) and  $2.4 \pm 1.8$  m ( $7.9 \pm 5.9$  feet), respectively with 23 realistic hours. The disparity in the results immediately suggested that the calculations were extremely sensitive to net flux determination as would be expected.

The depths computed in the output of Table 5.3-3 were the ones most similar to the actual lake. The area and volume ( $40.9 \times 10^6$  m<sup>2</sup> and  $116 \times 10^6$  m<sup>3</sup>) correspond closely to the actual measured values reported in Section 5.4.2 ( $43.85 \times 10^6$  m<sup>2</sup> and  $120 \times 10^6$  m<sup>3</sup>, respectively). The area and volume of the computed output of Table 5.4-3 was  $22.7 \times 10^6$  m<sup>2</sup> and  $37.4 \times 10^6$  m<sup>3</sup>, respectively. These latter areas and volumes are much too small compared with real values. This finding was unexpected, since the modeled net radiation in Table 5.3-3 were probably unrealistic (too large) compared to the measured values in Table 5.3-4.

#### 5.4.3.4.3 Sensitivity Analysis

A sensitivity analysis was then performed in an effort to determine the cause of such disparity and to determine the most significant parameters and

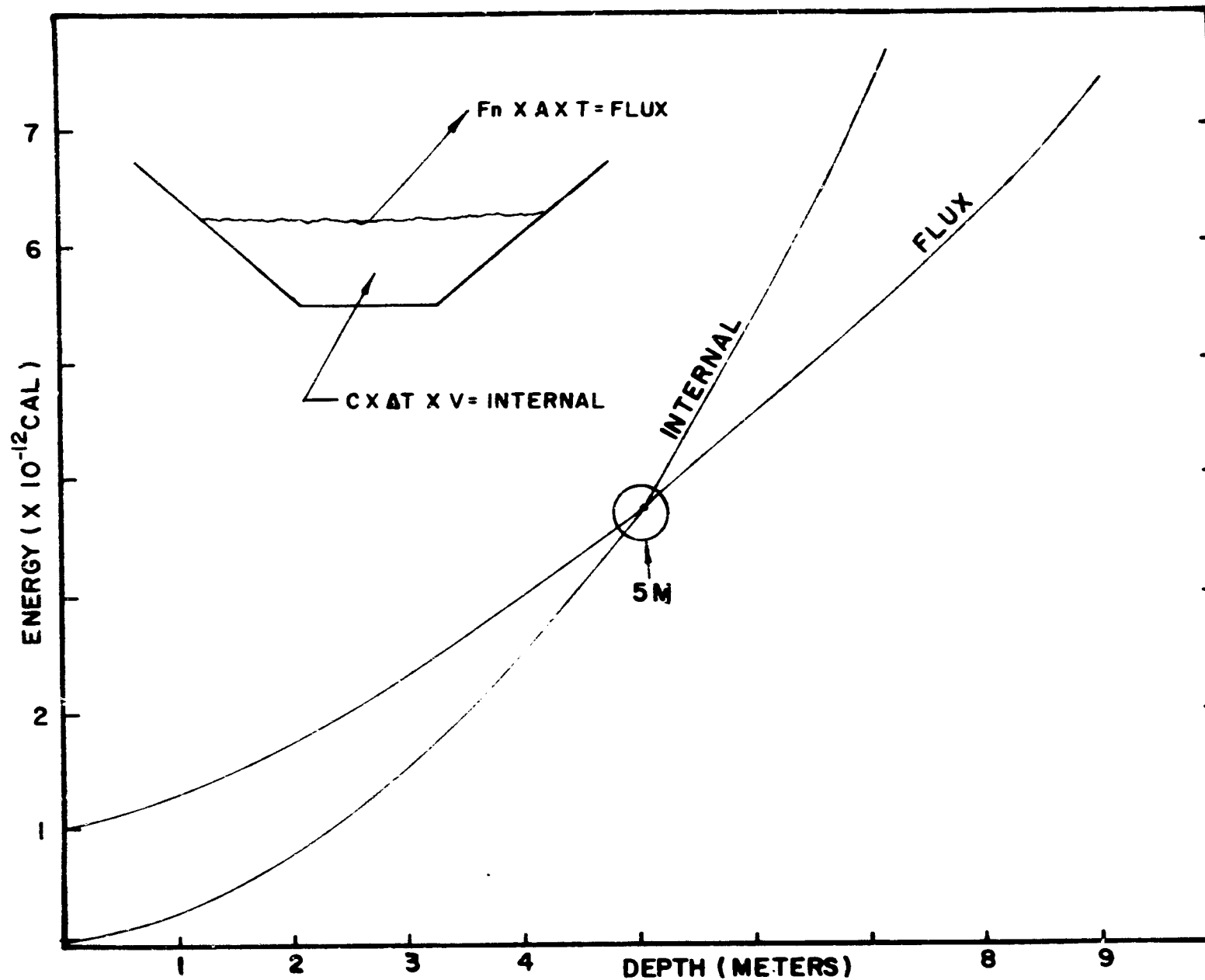


Figure 5.4-5. Plot of flux energies and stored energies from volume calculation program. Depth is incremented until two energies are equal.

Table 5.4-3 a. Input parameters, data, and fluxes from first data set for East Lake Tohopekaliga volume calculations.

INPUT DATA													
25	3	1	70	20	0.000	0.000	21.907	21.000	0.000	0.219	9.500		
3600.000	1940.000	5.000	2.0	2.6	2.6	2.4	2.2	2.1	2.0	2.1	2.0		
3.2	3.0	2.6	2.4	2.6	2.6	2.4	2.2	2.1	2.0	2.1	2.0		
3.0	3.3	3.7	4.1	4.4	4.9	5.1	3.9	3.6	2.4	2.1	1.4		
1.0													
25.8	25.5	25.3	25.0	24.9	24.3	24.7	24.6	24.5	24.4	24.3	24.2		
24.2	24.2	24.2	24.2	24.2	24.2	24.4	24.8	25.0	25.0	24.2	24.7		
27.3													
0.000	0.000	0.000	0.000	0.000	0.000	0.000	0.000	0.000	0.000	0.000	0.000		
0.000	0.000	0.000	0.000	0.000	0.000	0.000	0.000	0.000	0.000	0.000	0.000		
0.000													

RADIATION FLUXES

TIME	SUN	SFC	SPY	NEL
3.5	0.738E 00	-0.633E 00	0.501E 00	0.633E 00
4.5	0.738E 00	-0.633E 00	0.501E 00	0.633E 00
5.5	0.724E 01	-0.632E 00	0.501E 00	-0.632E 01
6.5	0.000E 00	-0.630E 00	0.501E 00	-0.124E 00
7.5	0.000E 00	-0.629E 00	0.501E 00	-0.127E 00
8.5	0.000E 00	-0.628E 00	0.501E 00	-0.127E 00
9.5	0.000E 00	-0.627E 00	0.501E 00	-0.126E 00
10.5	0.000E 00	-0.626E 00	0.501E 00	-0.126E 00
11.5	0.000E 00	-0.625E 00	0.501E 00	-0.124E 00
12.5	0.700E 00	-0.625E 00	0.501E 00	-0.123E 00
13.5	0.000E 00	-0.624E 00	0.501E 00	-0.122E 00
14.5	0.000E 00	-0.623E 00	0.501E 00	-0.122E 00
15.5	0.000E 00	-0.623E 00	0.501E 00	-0.122E 00
16.5	0.000E 00	-0.623E 00	0.501E 00	-0.122E 00
17.5	0.000E 00	-0.623E 00	0.501E 00	-0.122E 00
18.5	0.724E 01	-0.623E 00	0.501E 00	-0.623E 01
19.5	0.394E 00	-0.623E 00	0.501E 00	0.268E 00
20.5	0.738E 00	-0.623E 00	0.501E 00	0.617E 00
21.5	0.104E 01	-0.623E 00	0.501E 00	0.115E 00
22.5	0.126E 01	-0.620E 00	0.501E 00	0.113E 01
23.5	0.137E 01	-0.631E 00	0.501E 00	0.124E 01
0.5	0.137E 01	-0.635E 00	0.501E 00	0.123E 01
1.5	0.126E 01	-0.640E 00	0.501E 00	0.112E 01
2.5	0.104E 01	-0.644E 00	0.501E 00	0.097E 00
3.5	0.738E 00	-0.649E 00	0.501E 00	0.500E 00

NET FLUXES

TIME	WS	TS	H	LF	RI	FNCT
3.5	3.2	25.8	-0.0524	-0.1113	0.6030	0.4353
4.5	3.0	25.5	-0.0478	-0.1014	0.2570	0.1654
5.5	2.9	25.3	-0.0455	-0.0913	-0.0584	-0.2010
6.5	2.8	25.0	-0.0431	-0.0815	-0.1282	-0.2622
7.5	2.6	24.4	-0.0349	-0.0816	-0.1274	-0.2479
8.5	2.5	24.0	-0.0368	-0.0718	-0.1265	-0.2402
9.5	2.4	24.7	-0.0348	-0.0711	-0.1257	-0.2326
10.5	2.2	24.6	-0.0309	-0.0616	-0.1249	-0.2194
11.5	2.1	24.5	-0.0289	-0.0513	-0.1241	-0.2123
12.5	2.0	24.4	-0.0270	-0.0511	-0.1232	-0.2051
13.5	2.3	24.3	-0.0326	-0.0612	-0.1223	-0.2211
14.5	2.6	24.2	-0.0385	-0.0716	-0.1215	-0.2376
15.5	3.0	24.2	-0.0467	-0.0913	-0.1215	-0.2625
16.5	3.3	24.2	-0.0532	-0.1014	-0.1215	-0.2821
17.5	3.7	24.2	-0.0621	-0.1215	-0.1215	-0.3091
18.5	4.1	24.2	-0.0714	-0.1413	-0.0491	-0.2648
19.5	4.4	24.2	-0.0786	-0.1518	0.2679	0.0005
20.5	4.8	24.2	-0.0885	-0.1719	0.5165	0.3493
21.5	5.1	24.4	-0.0965	-0.1749	0.9152	0.8210
22.5	3.8	24.8	-0.0651	-0.1117	1.1286	0.9277
23.5	3.6	25.2	-0.0609	-0.1217	1.2384	1.0473
0.5	2.4	25.6	-0.0353	-0.0719	1.2350	1.1228
1.5	2.1	26.2	-0.0298	-0.0618	1.1167	1.0301
2.5	1.4	26.7	-0.0173	-0.0319	0.9356	0.8395
3.5	1.0	27.3	-0.0111	-0.0213	0.5902	0.4528

Table 5.4-3 b. Volume calculation results.

ORIGINAL PAGE IS  
OF POOR QUALITY

FINAL RESULTS									
DEPTH	AREA (SQ)	VOL (CU)	TL	TF	TL	TF	TL	TF	
0.20	0.1150	0.2210	0.4800	0.9320	12	-0.8610	12	0.1150	0.2210
0.40	0.1240	0.4500	0.1020	0.9320	12	-0.8610	12	0.1240	0.4500
0.60	0.1330	0.6790	0.1020	0.9320	12	-0.8610	12	0.1330	0.6790
0.80	0.1420	0.9080	0.1020	0.9320	12	-0.8610	12	0.1420	0.9080
1.00	0.1510	1.1370	0.1020	0.9320	12	-0.8610	12	0.1510	1.1370
1.20	0.1600	1.3660	0.1020	0.9320	12	-0.8610	12	0.1600	1.3660
1.40	0.1690	1.5950	0.1020	0.9320	12	-0.8610	12	0.1690	1.5950
1.60	0.1780	1.8240	0.1020	0.9320	12	-0.8610	12	0.1780	1.8240
1.80	0.1870	2.0530	0.1020	0.9320	12	-0.8610	12	0.1870	2.0530
2.00	0.1960	2.2820	0.1020	0.9320	12	-0.8610	12	0.1960	2.2820
2.20	0.2050	2.5110	0.1020	0.9320	12	-0.8610	12	0.2050	2.5110
2.40	0.2140	2.7400	0.1020	0.9320	12	-0.8610	12	0.2140	2.7400
2.60	0.2230	2.9690	0.1020	0.9320	12	-0.8610	12	0.2230	2.9690
2.80	0.2320	3.1980	0.1020	0.9320	12	-0.8610	12	0.2320	3.1980
3.00	0.2410	3.4270	0.1020	0.9320	12	-0.8610	12	0.2410	3.4270
3.20	0.2500	3.6560	0.1020	0.9320	12	-0.8610	12	0.2500	3.6560
3.40	0.2590	3.8850	0.1020	0.9320	12	-0.8610	12	0.2590	3.8850
3.60	0.2680	4.1140	0.1020	0.9320	12	-0.8610	12	0.2680	4.1140
3.80	0.2770	4.3430	0.1020	0.9320	12	-0.8610	12	0.2770	4.3430
4.00	0.2860	4.5720	0.1020	0.9320	12	-0.8610	12	0.2860	4.5720
4.20	0.2950	4.8010	0.1020	0.9320	12	-0.8610	12	0.2950	4.8010
4.40	0.3040	5.0300	0.1020	0.9320	12	-0.8610	12	0.3040	5.0300
4.60	0.3130	5.2590	0.1020	0.9320	12	-0.8610	12	0.3130	5.2590
4.80	0.3220	5.4880	0.1020	0.9320	12	-0.8610	12	0.3220	5.4880
5.00	0.3310	5.7170	0.1020	0.9320	12	-0.8610	12	0.3310	5.7170
5.20	0.3400	5.9460	0.1020	0.9320	12	-0.8610	12	0.3400	5.9460
5.40	0.3490	6.1750	0.1020	0.9320	12	-0.8610	12	0.3490	6.1750
5.60	0.3580	6.4040	0.1020	0.9320	12	-0.8610	12	0.3580	6.4040
5.80	0.3670	6.6330	0.1020	0.9320	12	-0.8610	12	0.3670	6.6330
6.00	0.3760	6.8620	0.1020	0.9320	12	-0.8610	12	0.3760	6.8620
6.20	0.3850	7.0910	0.1020	0.9320	12	-0.8610	12	0.3850	7.0910
6.40	0.3940	7.3200	0.1020	0.9320	12	-0.8610	12	0.3940	7.3200
6.60	0.4030	7.5490	0.1020	0.9320	12	-0.8610	12	0.4030	7.5490
6.80	0.4120	7.7780	0.1020	0.9320	12	-0.8610	12	0.4120	7.7780
7.00	0.4210	8.0070	0.1020	0.9320	12	-0.8610	12	0.4210	8.0070
7.20	0.4300	8.2360	0.1020	0.9320	12	-0.8610	12	0.4300	8.2360
7.40	0.4390	8.4650	0.1020	0.9320	12	-0.8610	12	0.4390	8.4650
7.60	0.4480	8.6940	0.1020	0.9320	12	-0.8610	12	0.4480	8.6940
7.80	0.4570	8.9230	0.1020	0.9320	12	-0.8610	12	0.4570	8.9230
8.00	0.4660	9.1520	0.1020	0.9320	12	-0.8610	12	0.4660	9.1520
8.20	0.4750	9.3810	0.1020	0.9320	12	-0.8610	12	0.4750	9.3810
8.40	0.4840	9.6100	0.1020	0.9320	12	-0.8610	12	0.4840	9.6100
8.60	0.4930	9.8390	0.1020	0.9320	12	-0.8610	12	0.4930	9.8390
8.80	0.5020	10.0680	0.1020	0.9320	12	-0.8610	12	0.5020	10.0680
9.00	0.5110	10.2970	0.1020	0.9320	12	-0.8610	12	0.5110	10.2970
9.20	0.5200	10.5260	0.1020	0.9320	12	-0.8610	12	0.5200	10.5260
9.40	0.5290	10.7550	0.1020	0.9320	12	-0.8610	12	0.5290	10.7550
9.60	0.5380	10.9840	0.1020	0.9320	12	-0.8610	12	0.5380	10.9840
9.80	0.5470	11.2130	0.1020	0.9320	12	-0.8610	12	0.5470	11.2130
10.00	0.5560	11.4420	0.1020	0.9320	12	-0.8610	12	0.5560	11.4420
10.20	0.5650	11.6710	0.1020	0.9320	12	-0.8610	12	0.5650	11.6710
10.40	0.5740	11.9000	0.1020	0.9320	12	-0.8610	12	0.5740	11.9000
10.60	0.5830	12.1290	0.1020	0.9320	12	-0.8610	12	0.5830	12.1290
10.80	0.5920	12.3580	0.1020	0.9320	12	-0.8610	12	0.5920	12.3580
11.00	0.6010	12.5870	0.1020	0.9320	12	-0.8610	12	0.6010	12.5870
11.20	0.6100	12.8160	0.1020	0.9320	12	-0.8610	12	0.6100	12.8160
11.40	0.6190	13.0450	0.1020	0.9320	12	-0.8610	12	0.6190	13.0450
11.60	0.6280	13.2740	0.1020	0.9320	12	-0.8610	12	0.6280	13.2740
11.80	0.6370	13.5030	0.1020	0.9320	12	-0.8610	12	0.6370	13.5030
12.00	0.6460	13.7320	0.1020	0.9320	12	-0.8610	12	0.6460	13.7320
12.20	0.6550	13.9610	0.1020	0.9320	12	-0.8610	12	0.6550	13.9610
12.40	0.6640	14.1900	0.1020	0.9320	12	-0.8610	12	0.6640	14.1900
12.60	0.6730	14.4190	0.1020	0.9320	12	-0.8610	12	0.6730	14.4190
12.80	0.6820	14.6480	0.1020	0.9320	12	-0.8610	12	0.6820	14.6480
13.00	0.6910	14.8770	0.1020	0.9320	12	-0.8610	12	0.6910	14.8770
13.20	0.7000	15.1060	0.1020	0.9320	12	-0.8610	12	0.7000	15.1060
13.40	0.7090	15.3350	0.1020	0.9320	12	-0.8610	12	0.7090	15.3350
13.60	0.7180	15.5640	0.1020	0.9320	12	-0.8610	12	0.7180	15.5640
13.80	0.7270	15.7930	0.1020	0.9320	12	-0.8610	12	0.7270	15.7930
14.00	0.7360	16.0220	0.1020	0.9320	12	-0.8610	12	0.7360	16.0220
DEPTH (METERS)	0.00	0.30	1.30	5.70	5.50	5.50	4.90	4.70	4.50
5.10	0.00	0.00	0.00	0.00	0.00	0.00	0.00	0.00	0.00
6.10	3.70	3.70	2.10						
VOL (X10-3 GAL)	0.00	0.89	4.63	41.21	38.69	36.25	31.67	29.51	27.44
33.92	0.00	0.00	0.00	0.00	0.00	33.69	31.55	33.69	
46.55	19.59	21.71	2.39						
AVERAGE DEPTH	4.3	51	0.91	1.5613					
AVG VOL	2.2780	11	4	0.1260	11	GAL			
17 VAL 10 HOURS									

Table 5.4-4 a. Input parameters, data, and fluxes from second data set for East Lake Tohopekaliga volume calculations.

INPUT DATA												
25	3	1	70	20	0.000							
3680.000	1840.000			5.000	23.900	28.000	0.000	0.208	6.500			
2.7	3.0	2.2	2.4	1.6	3.2	2.1	2.3	1.8	3.2	2.5	3.1	
3.3	3.9	3.6	1.5	4.0	5.3	5.2	4.4	3.4	1.7	2.1	1.9	
1.7												
24.5	25.2	25.5	24.3	23.6	23.2	22.9	22.6	22.4	22.1	22.2	22.1	
22.0	21.9	21.8	21.7	22.1	22.4	22.8	23.4	24.0	24.7	25.4	26.1	
26.9												
0.705	0.438	0.062	-0.066	-0.089	-0.195	-0.100	-0.352	-0.064	-0.101	-0.103	-0.105	
0.090-0.105-0.108-0.038 0.511 0.515 0.613 1.046 0.837 0.857 0.696 0.920												
0.520												
NET FLUXES												
TIME	WS	TS	H	LE	RI	FRNT						
3.5	2.7	24.5	-0.0407	-0.0335	0.7350	0.5432						
4.5	3.0	25.2	-0.0475	-0.1012	0.4380	0.2827						
5.5	2.2	25.5	-0.0313	-0.0678	0.0620	-0.0171						
6.5	2.4	24.3	-0.0345	-0.0701	-0.0660	-0.1707						
7.5	3.6	23.6	-0.0572	-0.1158	-0.0491	-0.2541						
8.5	3.2	23.2	-0.0101	-0.0952	-0.0951	-0.2411						
9.5	2.3	22.9	-0.0101	-0.0599	-0.1000	-0.1914						
10.5	2.3	22.6	-0.0317	-0.0587	-0.0920	-0.1393						
11.5	1.8	22.4	-0.0226	-0.0414	-0.0780	-0.1320						
12.5	2.2	22.3	-0.0296	-0.0547	-0.1010	-0.1047						
13.5	2.5	22.2	-0.0362	-0.0612	-0.1031	-0.2021						
14.5	3.1	22.1	-0.0471	-0.0949	-0.1050	-0.2370						
15.5	3.3	22.0	-0.0512	-0.0918	-0.0900	-0.2330						
16.5	3.9	21.9	-0.0641	-0.1144	-0.1050	-0.2935						
17.5	3.6	21.8	-0.0574	-0.1019	-0.1080	-0.2673						
18.5	3.5	21.7	-0.0552	-0.0973	-0.0980	-0.1705						
19.5	4.0	22.1	-0.0666	-0.1201	0.5110	0.3243						
20.5	5.3	22.4	-0.0782	-0.1800	0.5150	0.2369						
21.5	5.2	22.6	-0.0963	-0.1804	0.6110	0.3362						
22.5	4.4	23.4	-0.0776	-0.1500	1.0460	0.8184						
23.5	3.4	24.0	-0.0552	-0.1103	0.8370	0.6715						
0.5	1.7	24.7	-0.0218	-0.0451	0.8570	0.7901						
1.5	2.1	25.4	-0.0294	-0.0632	0.8960	0.8034						
2.5	1.9	26.1	-0.0257	-0.0579	0.8200	0.7361						
3.5	1.7	26.9	-0.0226	-0.0527	0.5200	0.4447						

ORIGINAL PAGE IS  
OF POOR QUALITY

155

measurements. The analysis showed that the volume determinations were independent of lake bottom temperature as long as the bottom temperature did not change. This is a consequence of the fact that the stored energy is based upon time differences in temperature so that a constant does not alter results. The calculations were also reasonably insensitive to cone geometry, always giving consistent volume determinations by giving varied depths. This is a consequence of the cone geometry and would be expected.

The most sensitive input is shown to be the modeling of the fluxes. Small errors in the fluxes are reflected as large errors in volume determinations sometimes causing unrealistic situations such as a net outward heat flux accompanied by an increase in lake internal energy.

The flux energy effect and the internal energy effect can be summarized as follows:

- a. Small changes in flux energy with large changes in internal energy imply a shallow lake.
- b. Large changes in flux energy with small changes in internal energy imply a deep lake.

Figure 5.4-5 illustrates how the interaction of flux energy and internal energy changes operate in truncated cone lake model.

The change in lake surface temperature from 1530 April 11 to 1530 April 12 was 1.5°C in the Table 5.4-3 data set, and 2.4°C in the Table 5.4-4 data set. Therefore, not only was the flux energy less for the second data set, but the internal energy change was larger. Both these factors led to a smaller lake depth calculation. At the depth of 5.0 m (cumulated upward), Table 5.4-3 showed an internal energy change of  $0.350 \times 10^{13}$  cal/hr and a flux energy exchange of  $0.336 \times 10^{13}$  cal/hr, whereas Table 5.4-4 showed an internal energy change of  $0.559 \times 10^{13}$  cal/hr and a flux energy exchange of  $0.287 \times 10^{13}$  cal/hr.

The lake volume model would improve in sensitivity if data were analyzed over two half-day periods, e.g., from 1530 pm to 0330 am, and from 0330 am to 1530 pm. This procedure would yield the largest values of flux energy exchanges and internal energy changes to use in predicting lake volume.

The lake volume model can also show sensitivity to sensible and latent heat transfer parameters. The input data from both data sets were run for a high wind speed (7.3 m/s), but the model failed to converge on a predicted lake depth because the flux energies were negative (loss) whereas the internal energies were positive (gain).

A sensitivity analysis was run on the input data from Table 5.4-2 to determine the effect of varying the background sky temperature from -10°C (cold-clear) to +10°C (low warm clouds) on net flux energy and on predicted depths (Table 5.4-5). Depths of 5.5 m, 5.1 m, and 4.6 m were predicted for sky temperatures of -10°C, 0°C, and +10°C, respectively. Therefore, assumptions about sky temperature do have a significant, but not overwhelming, effect on lake volume predictions.

THIS PAGE IS  
OF POOR QUALITY

TIME	TS	TS	TS	TS	TS	TS	DEPTH
3.5	2.7	25.4	-0.0416	-0.0915	0.2107	0.3536	-
4.5	3.0	25.5	-0.0474	-0.1034	0.1377	-0.0113	1.1
5.5	2.2	25.3	-0.0312	-0.0669	-0.1777	-0.2775	1.9
6.5	2.4	25.0	-0.0301	-0.0717	-0.2476	-0.3552	9.5
7.5	3.6	24.9	-0.0607	-0.1270	-0.2467	-0.4363	-
8.5	3.2	24.9	-0.0615	-0.1074	-0.2419	-0.4049	9.1
9.5	2.3	24.7	-0.0328	-0.0641	-0.2413	-0.3476	8.3
10.5	2.3	24.6	-0.0328	-0.0677	-0.2442	-0.3446	7.9
11.5	1.8	24.5	-0.0214	-0.0491	-0.2413	-0.3145	7.7
12.5	2.2	24.4	-0.0307	-0.0629	-0.2425	-0.3160	8.1
13.5	2.5	24.3	-0.0351	-0.0761	-0.2417	-0.3271	8.9
14.5	3.1	24.1	-0.0488	-0.0986	-0.2403	-0.3335	-
15.5	3.3	24.2	-0.0537	-0.1074	-0.2420	-0.4014	-
16.5	3.9	24.2	-0.0667	-0.134	-0.2430	-0.4423	-
17.5	3.6	24.2	-0.0590	-0.1209	-0.2438	-0.4215	-
18.5	3.5	24.2	-0.0571	-0.1163	-0.2434	-0.4424	-
19.5	4.0	24.2	-0.0691	-0.1397	-0.2406	-0.4500	-
20.5	5.3	24.2	-0.1013	-0.2045	0.2101	0.1914	3.5
21.5	5.2	24.4	-0.0990	-0.2022	0.2058	0.4046	3.3
22.5	4.4	24.8	-0.0795	-0.1657	1.0007	0.7041	4.7
23.5	3.4	24.2	-0.0563	-0.1200	1.1101	0.9427	5.5
0.5	1.7	25.3	-0.0221	-0.0491	1.1137	1.0455	3.3
1.5	2.1	26.2	-0.0299	-0.0668	0.9974	0.9007	3.3
2.5	1.5	26.7	-0.0262	-0.0604	0.7763	0.6097	1.7
3.5	1.7	27.3	-0.0228	-0.0541	0.4705	0.3939	-

T<sub>sky</sub> = -10 °C

Avg. depth  
5.5 m

TIME	TS	TS	TS	TS	TS	TS	DEPTH
3.5	2.7	25.4	-0.0416	-0.0915	0.2107	0.4121	-
4.5	3.0	25.5	-0.0474	-0.1034	0.1377	0.0480	0.5
5.5	2.2	25.3	-0.0312	-0.0669	-0.1777	-0.2143	1.5
6.5	2.4	25.0	-0.0301	-0.0717	-0.2476	-0.2967	7.9
7.5	3.6	24.9	-0.0607	-0.1270	-0.2467	-0.3725	8.5
8.5	3.2	24.9	-0.0615	-0.1074	-0.2419	-0.3634	7.3
9.5	2.3	24.7	-0.0328	-0.0641	-0.2413	-0.2945	6.5
10.5	2.3	24.6	-0.0328	-0.0677	-0.2442	-0.2911	6.1
11.5	1.8	24.5	-0.0214	-0.0491	-0.2413	-0.2536	5.9
12.5	2.2	24.4	-0.0307	-0.0629	-0.2425	-0.274	6.2
13.5	2.5	24.3	-0.0351	-0.0761	-0.2417	-0.2903	7.3
14.5	3.1	24.1	-0.0488	-0.0986	-0.2403	-0.3594	-
15.5	3.3	24.2	-0.0537	-0.1074	-0.2420	-0.3594	-
16.5	3.9	24.2	-0.0667	-0.1348	-0.2430	-0.3809	-
17.5	3.6	24.2	-0.0590	-0.1209	-0.2438	-0.3601	-
18.5	3.5	24.2	-0.0571	-0.1163	-0.2434	-0.3809	-
19.5	4.0	24.2	-0.0691	-0.1395	-0.2406	-0.4015	-
20.5	5.3	24.2	-0.1013	-0.2045	0.2101	0.2015	-
21.5	5.2	24.4	-0.0990	-0.2022	0.2058	0.5523	4.3
22.5	4.4	24.8	-0.0795	-0.1657	1.0007	0.5591	3.7
23.5	3.4	24.2	-0.0563	-0.1200	1.1101	0.8257	5.1
0.5	1.7	25.3	-0.0221	-0.0491	1.1137	1.0042	5.9
1.5	2.1	26.2	-0.0299	-0.0668	1.1771	1.1069	3.5
2.5	1.5	26.7	-0.0262	-0.0604	1.0598	0.9622	3.9
3.5	1.7	27.3	-0.0228	-0.0541	0.8328	0.7512	1.9

T<sub>sky</sub> = 0.0 °C

Avg. depth  
5.1 m

TIME	TS	TS	TS	TS	TS	TS	DEPTH
3.5	2.7	25.4	-0.0416	-0.0915	0.2107	0.4097	-
4.5	3.0	25.5	-0.0474	-0.1034	0.2177	0.1166	-
5.5	2.2	25.3	-0.0312	-0.0669	-0.2476	-0.1957	1.1
6.5	2.4	25.0	-0.0301	-0.0717	-0.2476	-0.2761	6.1
7.5	3.6	24.9	-0.0607	-0.1270	-0.2467	-0.3043	6.7
8.5	3.2	24.9	-0.0615	-0.1074	-0.2419	-0.2747	5.7
9.5	2.3	24.7	-0.0328	-0.0641	-0.2413	-0.2159	4.7
10.5	2.3	24.6	-0.0328	-0.0677	-0.2442	-0.2145	4.3
11.5	1.8	24.5	-0.0214	-0.0491	-0.2413	-0.1949	4.1
12.5	2.2	24.4	-0.0307	-0.0629	-0.2425	-0.2059	4.7
13.5	2.5	24.3	-0.0351	-0.0761	-0.2417	-0.2222	5.3
14.5	3.1	24.1	-0.0488	-0.0986	-0.2403	-0.2582	-
15.5	3.3	24.2	-0.0537	-0.1074	-0.2420	-0.2713	-
16.5	3.9	24.2	-0.0667	-0.1348	-0.2430	-0.3123	-
17.5	3.6	24.2	-0.0590	-0.1209	-0.2438	-0.2913	-
18.5	3.5	24.2	-0.0571	-0.1163	-0.2434	-0.3123	-
19.5	4.0	24.2	-0.0691	-0.1395	-0.2406	-0.3307	-
20.5	5.3	24.2	-0.1013	-0.2045	0.2101	0.0701	-
21.5	5.2	24.4	-0.0990	-0.2022	0.2058	0.321	5.3
22.5	4.4	24.8	-0.0795	-0.1657	1.0007	0.6247	4.1
23.5	3.4	24.2	-0.0563	-0.1200	1.1101	0.9242	5.5
0.5	1.7	25.3	-0.0221	-0.0491	1.1137	1.0755	3.9
1.5	2.1	26.2	-0.0299	-0.0668	1.1771	1.0303	3.9
2.5	1.5	26.7	-0.0262	-0.0604	1.0598	0.8113	2.1
3.5	1.7	27.3	-0.0228	-0.0541	0.8328	0.6240	-

T<sub>sky</sub> = 10.0 °C

Avg. depth  
4.6 m

Table 5.4-5. Flux and depth for different sky temperatures.

#### 5.4.3.4.4 Water Temperature Profiles

Figure 5.4-6 shows lake temperature profiles for the Tohopekaliga data along with the analytical fit (Eq. 5.4-23, section 5.4.3.3.3) for several different hours.

An examination of Figure 5.4-6 does show the lake to be stratified significantly in the daylight hours with the strong influence of the sun. This was earlier considered to be a major obstacle to the study, however, the rather good fit to the analytical function shown in Figure 5.4-6 indicates that the problem is not so difficult after all. This would be especially true if one considers errors in actual measurement which is probably near 0.25 to 0.50°C. Furthermore, it is differences in temperatures between times that is used in the internal energy calculations which tends further to decrease the effect of stratification. In fact, there is no error so long as the profile shape does not change.

It is furthermore evident from Figure 5.4-6 that at nighttime, the lake may not even actually be stratified since differences are on the order of 0.50°C, the assumed error limits. This is evident from the 2130, 0030, 0330, 0630, and 0930 profiles.

#### 5.4.3.4.5 Model Predictions for Lake Okeechobee

The above results seemed encouraging enough that a determination for Lake Okeechobee was tried. Satellite derived temperatures for the night of 22-23 February 1978 were used. Since this was a known freeze night, a sky temperature of -17.0°C was used for the radiation model. Also, since actual wind speeds were not available, the Hicks (1975) assumption that evaporation is independent of wind was used. (This was done by entering wind speeds of 7.3 m/s which is the  $U_0$  parameter in the model, Section 5.4.3.3.3). The Okeechobee surface area radius of 24 km estimated from a contour map was used for geometry, a value of 100 m for the D parameter and 20 km for bottom radius. This is a different shape from that used for Lake Tohopekaliga, but previous analysis had shown calculations to be fairly insensitive to variation of these parameters.

The results of this attempt is shown in Table 5.4-6a and 5.4-6b which yielded values of 1950 + 744 billion gallons. The volume predicted was  $5.7 \times 10^9 \text{ m}^3$  with a depth of 4.5 m (14.8 feet). This is in fair agreement with the average depth of about 12 feet at a stage of 16.5 ft msl.

If the lake were similar to a section of a cylinder rather than a truncated cone, its approximate volume would be about  $6.6 \times 10^9 \text{ m}^3$ .

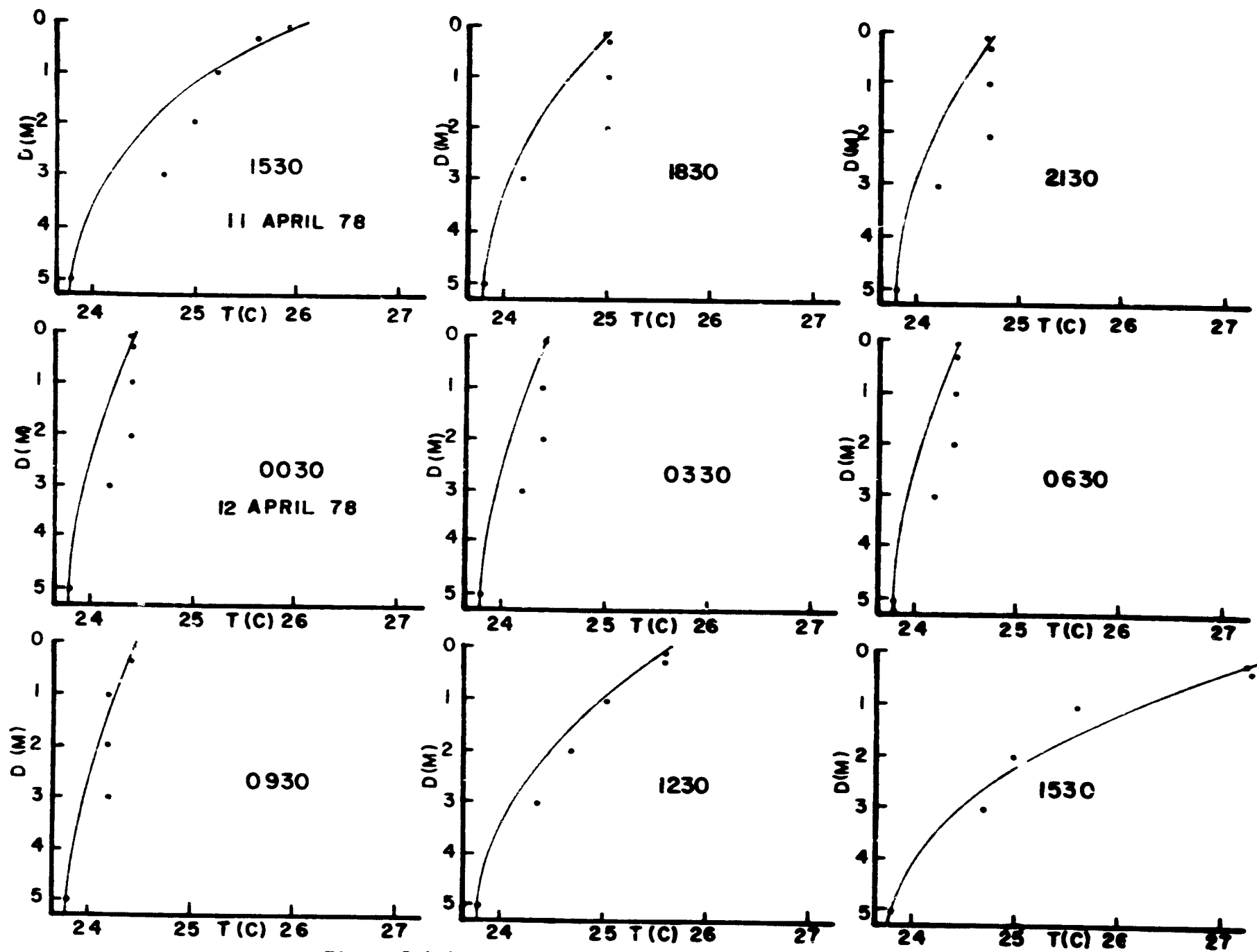


Figure 5.4-6. Plots of lake temperature profiles.  
Smooth curve is theoretical function; dots are data.

Table 5.4-6 a. Input parameters, data, and fluxes for Lake Okeechobee volume calculations from GOES satellite sensed surface temperatures.

INPUT DATA												
10	7	1	70	20	0	000	0	000	0	000	0	000
24000	000	20000	000	0	100	000	0	10	000	0	20	000
7 3	7 3	7 3	7 3	7 3	7 3	7 3	7 3	7 3	7 3	7 3	7 3	7 3
12 3	11 8	11 6	11 4	11 3	11 3	11 3	11 1	11 0	10 9	10 0	10 0	10 0
0 000	0 000	0 000	0 000	0 000	0 000	0 000	0 000	0 000	0 000	0 000	0 000	0 000

RADIATION FLUXES												
TIME	LAK		SFC		SKY		NET					
7 5	0 000E	00	-0	5291	00	0 343E	00	-0	1060	00		
8 5	0 000E	00	-0	5291	00	0 343E	00	-0	1061	00		
9 5	0 000E	00	-0	5291	00	0 343E	00	-0	1061	00		
10 5	0 000E	00	-0	5291	00	0 343E	00	-0	1062	00		
11 5	0 000E	00	-0	5291	00	0 343E	00	-0	1062	00		
12 5	0 000E	00	-0	5291	00	0 343E	00	-0	1062	00		
13 5	0 000E	00	-0	5291	00	0 343E	00	-0	1062	00		
14 5	0 000E	00	-0	5191	00	0 343E	00	-0	1062	00		
15 5	0 000E	00	-0	5191	00	0 343E	00	-0	1062	00		
16 5	0 000E	00	-0	5191	00	0 343E	00	-0	1062	00		

NET FLUXES												
TIME	WS	LS	H	LI	RI	FINET						
7 5	7 3	12 3	-0	1270	-0	1319	-0	1060	-0	4449		
8 5	7 3	11 8	-0	1269	-0	1269	-0	1061	-0	4451		
9 5	7 3	11 6	-0	1264	-0	1260	-0	1061	-0	4452		
10 5	7 3	11 4	-0	1260	-0	1261	-0	1062	-0	4454		
11 5	7 3	11 3	-0	1247	-0	1262	-0	1062	-0	4455		
12 5	7 3	11 2	-0	1245	-0	1262	-0	1062	-0	4455		
13 5	7 3	11 1	-0	1243	-0	1262	-0	1062	-0	4457		
14 5	7 3	11 0	-0	1241	-0	1262	-0	1062	-0	4459		
15 5	7 3	10 9	-0	1238	-0	1262	-0	1062	-0	4460		
16 5	7 3	10 8	-0	1237	-0	1262	-0	1062	-0	4461		

Table 5.4-6 b. Volume calculation results.

ORIGINAL PAGE IS  
OF POOR QUALITY

FINAL RESULTS									
DEPTH	AREA (MCU)	VOL (MCU)	IF	FI	FI	FI	FI	FI	FI
0.20	0.126E 10	0.251E 09	-0.143E 14	-0.321E 15	0.307E 15	1111111111			
0.40	0.126E 10	0.251E 09	-0.205E 14	-0.321E 15	0.293E 15	1111111111			
0.60	0.126E 10	0.251E 09	-0.478E 14	-0.321E 15	0.279E 15	1111111111			
0.80	0.126E 10	0.101E 10	-0.572E 14	-0.321E 15	0.265E 15	1111111111			
1.00	0.126E 10	0.126E 10	-0.715E 14	-0.321E 15	0.251E 15	1111111111			
1.20	0.126E 10	0.151E 10	-0.858E 14	-0.321E 15	0.237E 15	1111111111			
1.40	0.126E 10	0.175E 10	-0.100E 15	-0.321E 15	0.223E 15	1111111111			
1.60	0.126E 10	0.202E 10	-0.115E 15	-0.321E 15	0.209E 15	1111111111			
1.80	0.127E 10	0.227E 10	-0.129E 15	-0.321E 15	0.194E 15	1111111111			
2.00	0.127E 10	0.252E 10	-0.143E 15	-0.321E 15	0.180E 15	1111111111			
2.20	0.127E 10	0.278E 10	-0.158E 15	-0.321E 15	0.166E 15	1111111111			
2.40	0.127E 10	0.303E 10	-0.172E 15	-0.321E 15	0.152E 15	1111111111			
2.60	0.127E 10	0.328E 10	-0.187E 15	-0.321E 15	0.138E 15	1111111111			
2.80	0.127E 10	0.354E 10	-0.201E 15	-0.321E 15	0.123E 15	1111111111			
3.00	0.127E 10	0.379E 10	-0.216E 15	-0.321E 15	0.109E 15	1111111111			
3.20	0.127E 10	0.405E 10	-0.230E 15	-0.321E 15	0.950E 14	1111111111			
3.40	0.127E 10	0.430E 10	-0.245E 15	-0.321E 15	0.907E 14	1111111111			
3.60	0.127E 10	0.456E 10	-0.259E 15	-0.321E 15	0.864E 14	1111111111			
3.80	0.126E 10	0.481E 10	-0.274E 15	-0.321E 15	0.820E 14	1111111111			
4.00	0.126E 10	0.507E 10	-0.289E 15	-0.321E 15	0.776E 14	1111111111			
4.20	0.126E 10	0.532E 10	-0.303E 15	-0.321E 15	0.734E 14	1111111111			
4.40	0.126E 10	0.558E 10	-0.318E 15	-0.321E 15	0.691E 13	1111111111			
4.60	0.126E 10	0.583E 10	-0.332E 15	-0.321E 15	0.647E 13	1111111111			
4.80	0.126E 10	0.609E 10	-0.347E 15	-0.321E 15	0.603E 13	1111111111			
5.00	0.126E 10	0.635E 10	-0.362E 15	-0.321E 15	0.559E 13	1111111111			
5.20	0.126E 10	0.660E 10	-0.376E 15	-0.321E 15	0.515E 13	1111111111			
5.40	0.126E 10	0.686E 10	-0.391E 15	-0.321E 15	0.471E 13	1111111111			
5.60	0.126E 10	0.712E 10	-0.406E 15	-0.321E 15	0.427E 13	1111111111			
5.80	0.126E 10	0.737E 10	-0.421E 15	-0.321E 15	0.383E 13	1111111111			
6.00	0.126E 10	0.763E 10	-0.435E 15	-0.321E 15	0.339E 13	1111111111			
6.20	0.126E 10	0.788E 10	-0.450E 15	-0.321E 15	0.295E 13	1111111111			
6.40	0.126E 10	0.814E 10	-0.465E 15	-0.321E 15	0.251E 13	1111111111			
6.60	0.126E 10	0.840E 10	-0.480E 15	-0.321E 15	0.207E 13	1111111111			
6.80	0.126E 10	0.866E 10	-0.495E 15	-0.321E 15	0.163E 13	1111111111			
7.00	0.126E 10	0.892E 10	-0.509E 15	-0.321E 15	0.119E 13	1111111111			
7.20	0.126E 10	0.917E 10	-0.524E 15	-0.321E 15	0.075E 13	1111111111			
7.40	0.126E 10	0.943E 10	-0.539E 15	-0.321E 15	0.031E 13	1111111111			
7.60	0.126E 10	0.968E 10	-0.554E 15	-0.321E 15	0.22E 12	1111111111			
7.80	0.126E 10	0.994E 10	-0.569E 15	-0.321E 15	0.236E 12	1111111111			
8.00	0.126E 10	0.102E 11	-0.584E 15	-0.321E 15	0.252E 12	1111111111			
8.20	0.126E 10	0.105E 11	-0.599E 15	-0.321E 15	0.267E 12	1111111111			
8.40	0.126E 10	0.107E 11	-0.614E 15	-0.321E 15	0.282E 12	1111111111			
8.60	0.126E 10	0.110E 11	-0.629E 15	-0.321E 15	0.297E 12	1111111111			
8.80	0.126E 10	0.113E 11	-0.644E 15	-0.321E 15	0.311E 12	1111111111			
9.00	0.126E 10	0.115E 11	-0.659E 15	-0.321E 15	0.326E 12	1111111111			
9.20	0.126E 10	0.118E 11	-0.674E 15	-0.321E 15	0.341E 12	1111111111			
9.40	0.126E 10	0.120E 11	-0.689E 15	-0.321E 15	0.355E 12	1111111111			
9.60	0.126E 10	0.123E 11	-0.704E 15	-0.321E 15	0.371E 12	1111111111			
9.80	0.126E 10	0.126E 11	-0.719E 15	-0.321E 15	0.385E 12	1111111111			
10.00	0.126E 10	0.129E 11	-0.734E 15	-0.321E 15	0.400E 12	1111111111			
10.20	0.126E 10	0.131E 11	-0.750E 15	-0.321E 15	0.415E 12	1111111111			
10.40	0.126E 10	0.133E 11	-0.765E 15	-0.321E 15	0.430E 12	1111111111			
10.60	0.126E 10	0.136E 11	-0.780E 15	-0.321E 15	0.445E 12	1111111111			
10.80	0.126E 10	0.138E 11	-0.795E 15	-0.321E 15	0.460E 12	1111111111			
11.00	0.126E 10	0.141E 11	-0.810E 15	-0.321E 15	0.475E 12	1111111111			
11.20	0.126E 10	0.143E 11	-0.825E 15	-0.321E 15	0.490E 12	1111111111			
11.40	0.126E 10	0.145E 11	-0.841E 15	-0.321E 15	0.505E 12	1111111111			
11.60	0.126E 10	0.147E 11	-0.856E 15	-0.321E 15	0.520E 12	1111111111			
11.80	0.126E 10	0.150E 11	-0.871E 15	-0.321E 15	0.535E 12	1111111111			
12.00	0.126E 10	0.152E 11	-0.886E 15	-0.321E 15	0.550E 12	1111111111			
12.20	0.126E 10	0.155E 11	-0.902E 15	-0.321E 15	0.565E 12	1111111111			
12.40	0.126E 10	0.158E 11	-0.917E 15	-0.321E 15	0.580E 12	1111111111			
12.60	0.126E 10	0.162E 11	-0.932E 15	-0.321E 15	0.595E 12	1111111111			
12.80	0.126E 10	0.165E 11	-0.948E 15	-0.321E 15	0.610E 12	1111111111			
13.00	0.126E 10	0.168E 11	-0.963E 15	-0.321E 15	0.625E 12	1111111111			
13.20	0.126E 10	0.170E 11	-0.978E 15	-0.321E 15	0.640E 12	1111111111			
13.40	0.126E 10	0.173E 11	-0.994E 15	-0.321E 15	0.655E 12	1111111111			
13.60	0.126E 10	0.176E 11	-0.101E 16	-0.321E 15	0.670E 12	1111111111			
13.80	0.126E 10	0.179E 11	-0.102E 16	-0.321E 15	0.684E 12	1111111111			
14.00	0.126E 10	0.181E 11	-0.104E 16	-0.321E 15	0.701E 12	1111111111			
DEPTH (METERS) 1.30 3.70 5.50 7.30 9.10 10.90 12.70 14.50 16.30 18.10 VOL (X10-6 GAL) 432.68 1237.38 1170.03 932.7 273.456 902.456 902.456 902.456 902.456 902.456 AVERAGE DEPTH 5.8 5.1 5.1 5.1 5.1 5.1 5.1 5.1 5.1 5.1 AVG VOL 0.19E 13 0.744E 12 GAL 9 VAL ID HOURS									

#### 5.4.4 References

- Bill, R.G., Jr., 1978. Diurnal Variation of Latent Heat Flux on East Lake Tohopekaliga, pp v1 - v9. In: (J.F. Bartholic, R.G. Bill, Jr., and L.H. Allen, Jr.) Measurement of Evaporation from Lakes and Ponds in Florida. Publ. No. 43, Fla. Water Resources Res. Center, OWRT Proj. No. A-031-Fla., Univ. of Fla.
- Bill, R.G., Jr., A.F. Cook, L.H. Allen, Jr., J.F. Bartholic, and T. Maki, 1980. Predicting Fluxes of Latent and Sensible Heat of Lakes from Water Surface Temperatures. J. Geophys. Res. 85(C1):507-512.
- Fleagle, R.G. and J.A. Businger, 1963. An Introduction to Atmospheric Physics. Acad. Press, New York. 346 pp.
- Hicks, B.B., 1975. A Procedure for the Formulation of Bulk Transfer Coefficients over Water. Boundary-Layer Meteorol., 8:515-524.
- Sutherland, R.A., 1980. A Short Range Objective Temperature Forecasting Model. J. Appl. Meteor., 19:(in press).
- Sutherland, R.A., 1979. Climate Mapping with GOES Thermal Data, in preparation. NASA Contract NAS10-8920 Final Report, R.A. Sutherland, Principal Investigator.

#### 5.4.5 Conclusions

Wind speeds that averaged 3 m/sec were not strong enough during the April 11-12, 1978 mission to ensure sufficient mixing on East Lake Tohopekaliga to produce isothermal conditions. Temperature profile measurements showed strong temperature increases within the top meter during midday to midafternoon due to absorption of solar radiation in the top layers. Isothermal conditions were most nearly approached during the nocturnal hours from 1830 to 0630. From these observations, the best times and the best conditions for determining lake volume using isothermal, well-mixed lake assumptions would be overnight during passage of a strong cold front with high winds. Both mechanical forces and buoyant forces would tend to keep a shallow lake isothermal under those conditions. Low atmospheric temperatures and specific humidities, high winds, and clear skies would promote large flux energy exchanges which would yield measurable changes in internal energy (changes in temperature). Under these conditions, remote sensed surface temperature should accurately indicate changes in lake internal energy that could be used to estimate water volume and depth of shallow lakes by the techniques outlined in Section 5.4.3.1 and 5.4.3.2. Further experiments should be conducted under the best conditions for success.

Even under non-isothermal lake conditions, it is possible to obtain rough estimates of the lake volume of shallow lakes using the energy balance model developed in Section 5.4.3.3. Further refinements will require better lake geometry data and better flux models.

However, it does not appear that the procedures as now developed would yield volumes sufficiently accurate for operational use. On the other hand, it seems possible that the procedure could be turned around to develop better flux models. That is, from knowledge of lake volume and temperature change, the fluxes could be calculated. The program listed in the appendix, Section 5.4.6, should be modified to further investigate the possibility of determining fluxes (radiant, sensible, and latent) from lake volume and internal energy changes.

#### 5.4.6 Appendix I - Program Listing

The following program LKVOL was used to produce all of the results of this section. The major inputs are standard meteorological measurements, wind speeds, lake surface temperatures, and if available, net radiation. The second data card contains the lake geometry and bottom temperature and solar and sky temperature data which is needed if net radiation is not given.

The program is set up to take consecutive hourly data and measures time from solar noon (i.e., 1230 winter; 1330 summer). The first card reads the number of hours and starting time and other decrementing parameters. The last item on the first card is expected lake bottom temperature.

ORIGINAL PAGE IS  
OF POOR QUALITY

```

1  $JOB  DIMENSION U(25),ST(25),RN(25),FNET(25),EGY(25),E1(69),EF(99),
2      *NERR(99,24),ZC(25),V(25)
3      COMMON TR,HR,HC,TB,XLAT,XDEC,ATT,TSKY,TBC
4      C*****COMMON VARIABLES ARE TOP RADIUS,BOTTOM RADIUS,CONE HEIGHT,LAKE
5      C*****BOTTOM TEMPERATURE,LATITUDE,SOLAR DECLINATION,ATMOSPHERIC
6      C*****ATTENUATION COEFFICIENT AND EQUIVALENT BLACKBODY SKY TEMPERATURE
7
8      99 FORMAT(1X,10.3)
9      98 FORMAT(2X,12.3(2X,E14.6))
10     97 FORMAT(' STEP ',13,' Z= ',F5.1)
11     96 FORMAT(12(1X,F5.1))
12     95 FORMAT(12(F6.3))
13     94 FORMAT(2X,12.2X,E14.6)
14     93 FORMAT(' STEP ENERGY')
15     92 FORMAT(' STEP EINT EFLUX ERROR')
16     91 FORMAT(1X,F6.2,5(1X,E11.3),3X,24(1))
17     90 FORMAT(' DEPTH AREA(MSQ) VOL(MCU) IE FE')
18     89 FORMAT(' Z= ',F6.2)
19     88 FORMAT(1H1,'INPUT DATA')
20     87 FORMAT(1H1)
21     86 FORMAT(' VOL(X10-9GAL) ',10(F7.2))
22     85 FORMAT(' DEPTH(METERS) ',10(F7.2))
23     84 FORMAT(' AVERAGE DEPTH= ',F5.1,' ST DEV= ',F8.4)
24     83 FORMAT(1X,13,' VALID HOURS')
25     82 FORMAT(' AVG VOL= ',E11.3,' +- ',E11.3,' GAL')
26     81 FORMAT(' LAKE PROFILE 10CM INTERVALS ')
27     80 FORMAT(' NET FLUXES ')
28     79 FORMAT(' RADIATION FLUXES ')
29     78 FORMAT(1H1,' FINAL RESULTS ')
30     77 FORMAT(5(1X,4),1X,F10.3)
31
32 C*****NPTS=25 MEANS 25 DATA SETS
33 C*****NS=3 MEANS STARTING DATA IS 3(+1/2)HOURS FROM SOLAR NOON
34 C*****SOLAR NOON IS 1230 WINTER AND 1330 SUMMER
35
36 10 READ(5,77,END=500)NPTS,NS,NN,NM,NSTEP,TBC
37 READ(5,99)TR,HR,HC,TB,XLAT,XDEC,ATT,TSKY
38 READ(5,96)(U(I),I=1,NPTS)
39 READ(5,96)(ST(I),I=1,NPTS)
40 READ(5,95)(RN(I),I=1,NPTS)
41 WRITE(6,88)
42 WRITE(6,77)NPTS,NS,NN,NM,NSTEP,TBC
43 WRITE(6,99)TR,HR,HC,TB,XLAT,XDEC,ATT,TSKY
44 WRITE(6,96)(U(I),I=1,NPTS)
45 WRITE(6,96)(ST(I),I=1,NPTS)
46 WRITE(6,95)(RN(I),I=1,NPTS)
47
48 C*****CODES WILL SUPPRESS PRINTOUT IF 0****
49
50 17 LCCOE=1
51 18 NCCOE=1
52 19 MCCOE=0
53 20 JCCOE=1
54 21 LCCOE=0
55 22 JCCOE=0
56 23 XSTEP=0.01*NSTEP
57
58 C*****CALCULATE ALL PROFILES AT AVERAGE DEPTH***
59 IF(JCCOE.EQ.0)GO TO 15
60 WRITE(6,87)
61 WRITE(6,81)
62 DO 16 I=1,NPTS
63 TIME=1.0*(I-1)
64 CALL RSUTH(NCCOE,TIME,HC,ST(I),E,GAL)
65 16 CONTINUE
66 15 NPTS=NPTS-1
67
68 C*****CALCULATE NET RADIATION IF NOT GIVEN*****
69 IF(RN(1).EQ.0.0)WRITE(6,79)
70 DO 3 I=1,NPTS
71 TIME=1.0*(NS+I-1)+0.50
72 IF(TIME.GT.23.999)TIME=TIME-24.0
73 IF(RN(1).NE.0.0)GO TO 3
74 CALL RNET(NCCOE,TIME,ST(I),HR)
75 RN(I)=RR
76 NCCOE=0
77 3 CONTINUE
78
79 C*****CALCULATE NET FLUXES*****
80 NCCOE=1
81 WRITE(6,80)
82 DO 7 I=1,NPTS
83 TIME=1.0*(NS+I-1)+0.50
84 IF(TIME.GT.23.999)TIME=TIME-24.0
85 CALL RNET(NCCOE,TIME,U(I),ST(I),RN(I),FNET(I))
86 FNET(I)=EFLUX
87 NCCOE=0
88 7 CONTINUE
89
90 C*****START MAIN LOOP FOR DEPTH INCREMENTS***
91 DO 4 JDUM=NN,NM
92 Z=XSTEP*JDUM

```

```

72 C*****MCCODE PRINT OPTION**
73 IF(MCODE.EQ.0)GC TC 8
74 WRITE(6,91)Z
75 WRITE(6,97)JDUM,Z
76 WRITE(6,93)
77 DO 6 I=1,NPTS
78 C*****CALCULATE INTERNAL ENERGY OF LAKE***
79 TIME=1.0*(I-1)
80 CALL RSUTH(MCODE,TIME,Z,ST(1),E,GAL)
81 EGY(I)=E
82 C*****MCCODE PRINT OPTION**
83 IF(MCODE.EQ.0)GO TO 5
84 WRITE(6,94)I,EGY(I)
85 5 CONTINUE
86 SUME=0.0
87 SUMF=0.0
88 IF(LCODE.EQ.0)GO TO 13
89 WRITE(6,92)
90 C*****SUBTRACT FLUX ENERGY FROM STORED ENERGY***
91 13 DO 6 J=1,MPTS
92 EINT=EGY(J+1)-EGY(J)
93 RX=BR+(Z/HC)*(TR-BR)
94 AREA=3.14159*RX*RX*(1.0E+04)
95 EFLUX=60.0*AREA*(FNET(J+1)+FNET(J))/2.0
96 ERN=EINT-EFLUX
97 C*****SET UP SIGN PARAMETER TC FIND INDIVIDUAL ZEROCES**
98 IF(ERN.GT.0.0)GO TO 12
99 NERR(JDUM,J)=-1
100 GO TO 11
101 12 NERR(JDUM,J)=+1
102 11 SUME=SUME+EINT
103 SUMF=SUMF+EFLUX
104 C*****LCODE PRINT OPTION**
105 IF(LCODE.EQ.0)GO TO 6
106 WRITE(6,98)J,EINT,EFLUX,ERN
107 6 CONTINUE
108 EI(JDUM)=SUME/(1.0*MPTS)
109 EF(JDUM)=SUMF/(1.0*MPTS)
110 4 CONTINUE
111 WRITE(6,78)
112 WRITE(6,90)
113 DO 9 I=NN,NM
114 C*****WRITE OUT SUMMED ERRORS***
115 Z=XSTEP*1
116 RX=BR+(Z/HC)*(TR-BR)
117 AREA=3.14159*RX*RX
118 DD=RX-BR
119 VOL=(3.14159*Z/3.0)*(DD*DD+3.0*DD*BR+3.0*BR*BR)
120 ERR=EI(1)-EF(1)
121 WRITE(6,91)Z,AREA,VOL,EI(1),EF(1),ERR,(NERR(I,J),J=1,MPTS)
122 9 CONTINUE
123 C*****CALCULATE AVERAGE DEPTH AND STANDARD DEVIATION***
124 MM=NM-1
125 ZSUM=0.0
126 VSUM=0.0
127 ZNUM=0.0
128 NVAL=0
129 DO 20 J=1,MPTS
130 ZD(J)=0.0
131 V(J)=0.0
132 DO 21 I=NN,MM
133 K=I+1
134 TEST=NERR(K,J)-NERR(I,J)
135 IF(TEST.EQ.0.0)GO TC 21
136 ZD(J)=XSTEP*1-(XSTEP/2.0)
137 ZSUM=ZSUM+ZD(J)
138 ZNUM=ZNUM+1.0
139 NVAL=NVAL+1
140 RX=BR+(ZD(J)/HC)*(TR-BR)
141 DD=RX-BR
142 V(J)=(3.14159*2*4.17*ZD(J)/3.0)*(DD*DD+3.0*DD*BR+3.0*BR*BR)
143 VSUM=VSUM+V(J)
144 21 CONTINUE
145 20 CCNTINUE
146 IF(ZNUM.LT.1.0)ZNUM=1.0
147 ZAVG=ZSUM/ZNUM
148 VAVG=VSUM/ZNUM
149 VSQR=0.0
150 ERRSQ=0.0
151 DO 22 I=1,MPTS
152 VSQR=VSQR+V(I)+V(I)
153 ERRSQ=ERRSQ+ZD(I)+ZD(I)
154 XX=(VSQR/ZNUM)-VAVG*VAVG
155 IF(XX.LT.0.0)XX=0.0

```

2.000000 PAGE IS  
OF POOR QUALITY

ORIGINAL PAGE IS  
OF POOR QUALITY

```

148 VSTD= SORT (XX)
149 XX=(EHR50/ZNUM)-ZAL*ZAVG
150 IF (XX.LT.0.0) XX=0.0
151 ZSTD= SORT (XX)
152 DO 23 I=1,MPTS
153 23 V(I)=V(I)*(1.0E-09)
154 WRITE (6,85) (ZU(I),I=1,MPTS)
155 WRITE (6,86) (V(I),I=1,MPTS)
156 WRITE (6,84) /AVG,ZSTD
157 WRITE (6,82) /AVG,VSTD
158 WRITE (6,83) /VAL
159 WRITE (6,87)
160 GO TO 10
161 500 STOP
162 END

163 SUBROUTINE RNET (NCODE,TIME,TS,RR)
164 COMMON TR,HR,HC,TH,XLAT,XDEC,ATT,TSKY,TBC
165 99 FORMAT (1X,F5.1,1X,4E11.3)
166 98 FORMAT (' TIME SUN SFC SKY NET ')
167 DATA EP,SIG/0.98,0.813E-10/
168 TX=TS*273.16
169 TY=TSKY*273.16
170 X1=SIN(0.0175*XLAT)*SIN(0.0175*XDEC)
171 X2=COS(0.0175*XLAT)*COS(0.0175*XDEC)
172 XCOS=X1*X2+COS(3.14159*TIME*15.0/180.0)
173 IF (XCOS.GT.0.01) GO TO 1
174 SUN=0.0
175 GO TO 2
176 1 SUN=2.0*XCOS*EXP(-ATT/XCOS)
177 2 SFC=EP*SIG*TX*TX*TX*TX
178 SKY=EP*SIG*TY*TY*TY*TY
179 RR=SUN+SFC+SKY
180 IF (NCODE.EQ.0) GO TO 3
181 WRITE (6,98)
182 3 WRITE (6,99) TIME,SUN,SFC,SKY,RR
183 RETURN
184 END

185 SUBROUTINE BOREL (NCODE,TIME,WS,TS,RNET,HFLUX)
186 COMMON TR,HR,HC,TH,XLAT,XDEC,ATT,TSKY,TBC
187 99 FORMAT (3(2X,F5.1),4(2X,F7.4))
188 98 FORMAT (' TIME WS TS H LE RN ')
189 DATA EP,SIG,EO,PA,GMA/0.98,0.813E-10,1.82E+12,1.013E+06,6.58E-14/
190 DATA XKDD,EL,P,UO,XN/0.84,586,0.0,110.7,3.1,36/
191 C**** CALCULATE DOWN RATIO AND DERIVATIVE****
192 TX=TS*273.16
193 QSAT=(0.622*EO/PA)*EXP(-EL/(R+TX))
194 S=(EL/(R+TX))*QSAT
195 BETA=(XKDD+GMA)/S
196 DBETA=(-XKDD+GMA)/(S*TX*TX)*((EL/R)-(2.0*TX))
197 C**** CALCULATE EVAPORATIVE FLUX****
198 UR=(WS/UO)*XN
199 ELR=(4.0*EP*SIG*TX*TX*TX*UR)/DBETA
200 C**** CALCULATE SENSIBLE HEAT FLUX****
201 H=BETA*ELE
202 C**** SUM FLUXES FOR TOTAL****
203 HFLUX=H+ELE+RNET
204 IF (NCODE.EQ.0) GO TO 2
205 WRITE (6,98)
206 2 WRITE (6,99) TIME,WS,TS,H,ELE,RNET,HFLUX
207 RETURN
208 END

209 SUBROUTINE RSUTH (NCODE,TIME,Z,TS,E,GAL)
210 COMMON TR,HR,HC,TH,XLAT,XDEC,ATT,TSKY,TBC
211 DIMENSION T(101)
212 DATA PI,RHO,CP/3.14159,1.0,1.0/
213 99 FORMAT (10(1X,F7.3))
214 98 FORMAT (' ..... SOLAR TIME = ',F5.1)
215 C**** CONVERT TOP AND BOTTOM RADII TO CM****
216 RT=TR*100.0
217 RB=BR*100.0
218 DEL=RT-RB
219 RX=RB*(Z/HC)*DEL
220 DX=RX-RB
221 C**** CALCULATE TEMPERATURE PROFILE****
222 TO=TS
223 TY=TH+TBC*TIME
224 TI=(TY-TO)/(SIN(PI/4.0)+COS(PI/4.0)-1.0)
225 IF (NCODE.EQ.0) GO TO 2
226 N=100.0*Z/10.0
227 N=N+2

```

```

222      AA=PI/(4.0*100.0*Z)
223      X=-10.0
224      DO 1 I=1,N,1
225      X=X+10.0
226      T(I)=(T0-T1)+T1*(SIN(AA*(100.0*Z-X))+COS(AA*(100.0*Z-X)))
227      1 CONTINUE
228      WRITE(6,98)TIME
229      WRITE(6,99)(T(I),I=1,N)
C****CONVERT TEMPERATURE PARAMETERS TO ABSOLUTE***
230      2 TOA=T0+273.16
231      T1A=T1
C*****CALCULATE INTERNAL ENERGY WITH ANALYTICAL EQUATIONS*****
232      E1=(PI*100.0*Z/3.0)*(DR*DR+3.0*DR*NB+3.0*RE*AH)
233      E2=(16.0*DR*DR/(PI*PI))*(PI*COS(PI/4.0)-2.0)
234      E3=(6.0*DR*RX/PI)*(2.0+COS(PI/4.0)-1.0)
235      E4=RX*RX
236      E=(RHO*CP)*((TOA-T1A)*E1+(4.0*T1A+100.0*Z)*(E2-E3+E4))
C*****CONVERT VOLUME TO GALLONS***
237      GAL=264.17*E1*(1.0E-06)
238      RETURN
239      END

```

SENTRY

- 5.5-1 -

## 5.5 RAINFALL ESTIMATES FROM GOES IR DIGITAL DATA

By

Ellen Chen      Res. Assoc.

TABLE OF CONTENTS

	<u>Page</u>
5.5 Rainfall Estimates from GOES IR Digital Data . . . . .	5.5-1
5.5.1 Introduction . . . . .	5.5-5
5.5.2 Method of Scofield and Oliver . . . . .	5.5-5
5.5.3 Data Analysis . . . . .	5.5-5
5.5.4 Other Methods Using Satellite Data . . . . .	5.5-9
5.5.5 References . . . . .	5.5-12
5.5.6 Conclusion . . . . .	5.5-13

FIGURES

<u>Figure No.</u>	<u>Page</u>
5.5.2-1 Flow diagram showing steps to obtain rainfall estimates from satellite imageries, Part 1 . . . . .	5.5-6
5.5.2-2 Flow diagram showing steps to obtain rainfall estimates from satellite imageries, Part 2 . . . . .	5.5-7
5.5.4-1 Results of rainfall estimates by Follansbee (after Follansbee, 1973) . . . . .	5.5-10
5.5.4-2 Results of rainfall estimates in S. Florida (after Griffith et al., 1978) . . . . .	5.5-11

TABLES

<u>Table No.</u>	<u>Page</u>
5.5.3-1 Temperature table showing scales used and temperatures represented . . . . .	5.5-8

### 5.5.1 Introduction

Present methods of obtaining rainfall amount over large areas are unsatisfactory because rain gauges are placed far apart and their point records do not reflect true amounts received on the whole ground surface. Digitized radar data yield more representative isohyets, the area covered is larger, but the radar system is more expensive to maintain. If a good set of rainfall data is needed over a large area and through a long time period, such as for water resource research and/or conservation, then other methods need to be explored and employed. One method which has been worked out and applied by researchers is to use enhanced geostationary satellite imageries to obtain rainfall estimate. The method employed here was originally developed by Scofield and Oliver (1977). The purpose here is not to develop the method but to evaluate the feasibility of applying the method to obtain good representative rainfall for the State of Florida.

### 5.5.2 Method of Scofield and Oliver

The method developed by Scofield and Oliver (1977) is based on the empirical relationship that in convective cumulus clouds, there appears to be a correlation between 1) the cloud top brightness temperatures, 2) the area, and 3) the temperature gradient to the amount of rainfall. The method traces temperature isotherms on digitized or enhanced GOES imageries. Hourly and half-hourly data should be used for best results. Rainfall amounts are estimated according to the temperature, to the size of the area, and whether the area is increasing or decreasing in size. Lower temperatures, larger areas, and the steeper temperature gradients all indicate a larger amount of rainfall. The method can best be summarized in the following two flow diagrams (Figures 5.5.2-1 and 5.5.2-2). The inches of rainfall used in Figure 5.5.2-2 were from Scofield and Oliver and were used to estimate rainfall for both interior U.S. and in the Florida area. This set of figures should be checked carefully to insure that they apply to the atmospheric conditions of Florida. Thunderstorms in the moisture-laden subtropical climate of Florida may produce rainfall rates quite different from thunderstorms in the interior U.S.

### 5.5.3 Data Analysis

GOES IR digital data for August 30, 1978 were obtained from NOAA/NESS. The following hours were available: 0100, 0500, 0600, 0700, 0800, 0900, 1000, 1100, 1200, 1500, 1600, 1700, 2100Z (GMT time). Digitized radar rainfall data (24-hour totals) for the same date as above were obtained from NOAA at Miami for the area south of Lake Okeechobee. The purpose was to compare rainfall estimates from GOES data to the radar rainfall data. The GOES data showed that from 1500 to 1700Z clouds were developing in south Florida and areas of lowest temperatures were increasing in size. The 2100Z map showed that cloud top temperatures were not as cold and its coldest area had also diminished in size. Thus the missing hours (1800 - 2000Z) turned out to be crucial hours, therefore, no conclusion or estimates of rainfall were possible from the given set of data.

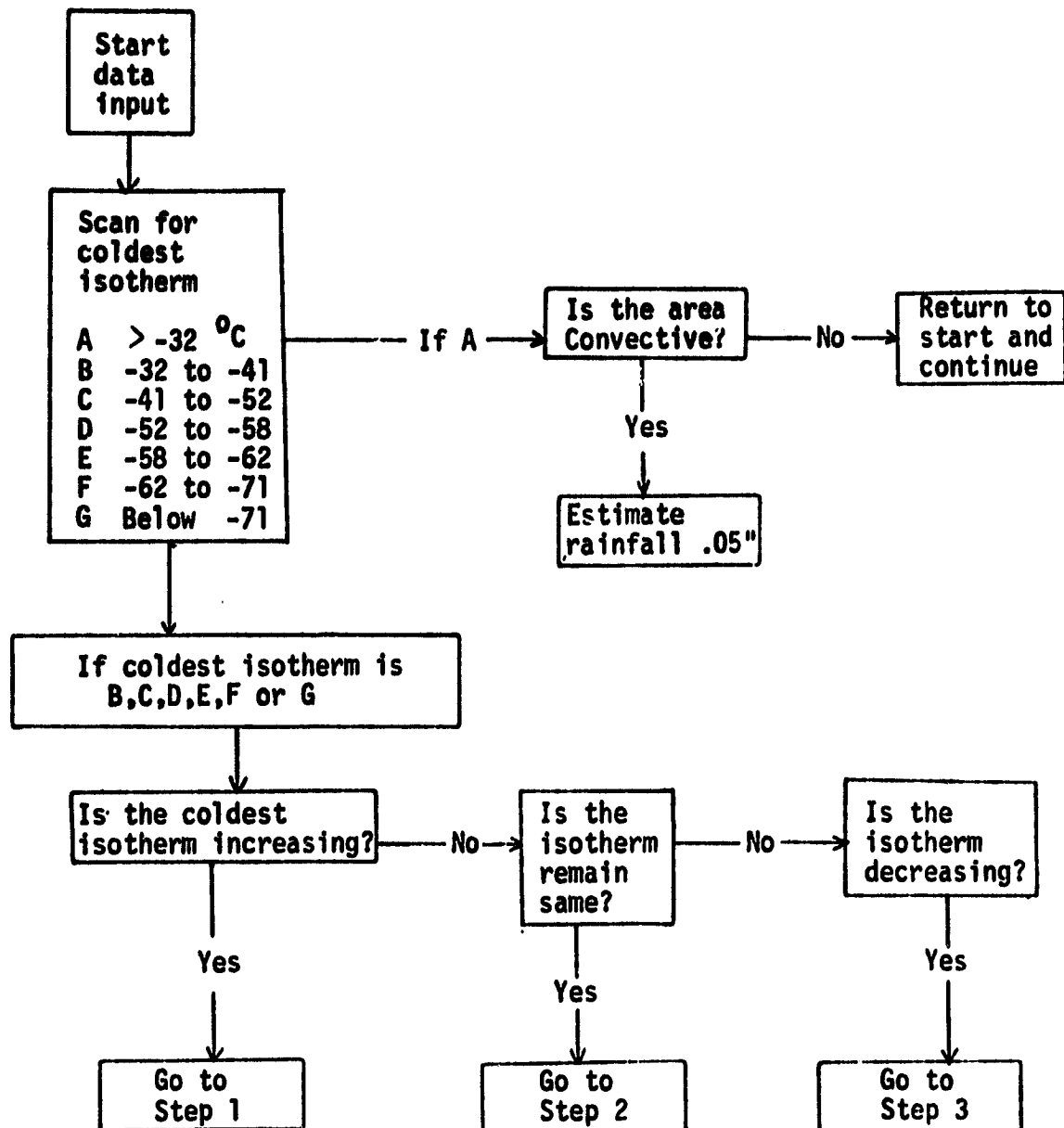


Fig. 5.5.2-1 Flow diagram showing steps to obtain rainfall estimates from satellite imagery, Part 1.

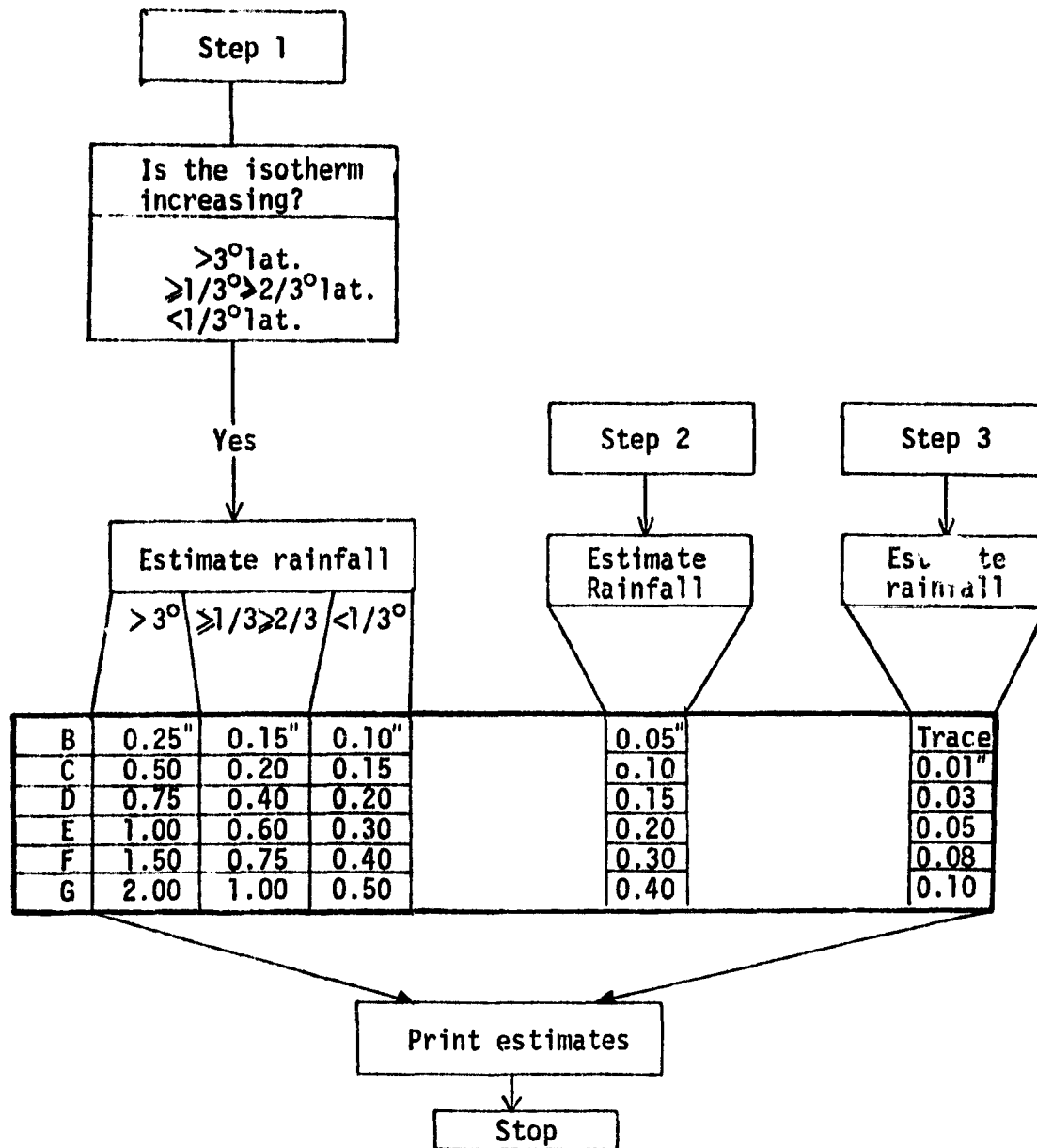


Fig. 5.5.2-2 Flow diagram showing steps to obtain rainfall estimates from satellite imagery, Part 2.

Table 5.4.3-1 Temperature table showing scales used and temperatures represented.  
TEMPERATURE ( $^{\circ}\text{C}$ )

SYMBOL	SCALE A	SCALE B	SCALE C	SCALE D
W	W	W	W	W
A	41.8	17.3	- 7.2	-32.2
B	41.3	16.8	- 7.7	-33.2
@	40.8	16.3	- 8.2	-34.2
D	40.3	15.8	- 8.7	-35.2
E	39.8	15.3	- 9.2	-36.2
F	39.3	14.8	- 9.7	-37.2
G	38.8	14.3	-10.2	-38.2
H	38.3	13.8	-10.7	-39.2
I	37.8	13.3	-11.2	-40.2
J	37.3	12.8	-11.7	-41.2
K	36.8	12.3	-12.2	-42.2
L	36.3	11.8	-12.7	-43.2
M	35.8	11.3	-13.2	-44.2
N	35.3	10.8	-13.7	-45.2
O	34.8	10.3	-14.2	-46.2
P	34.3	9.8	-14.7	-47.2
Q	33.8	9.3	-15.2	-48.2
R	33.3	8.8	-15.7	-49.2
S	32.8	8.3	-16.2	-50.2
T	32.3	7.8	-16.7	-51.2
U	31.8	7.3	-17.2	-52.2
V	31.3	6.8	-17.7	-53.2
&	30.8	6.3	-18.2	-54.2
X	30.3	5.8	-18.7	-55.2
Y	29.8	5.3	-19.2	-56.2
Z	29.3	4.8	-19.7	-57.2
1	28.8	4.3	-20.2	-58.2
2	28.3	3.8	-20.7	-59.2
3	27.8	3.3	-21.2	-60.2
4	27.3	2.8	-21.7	-61.2
5	26.8	2.3	-22.2	-62.2
6	26.3	1.8	-22.7	-63.2
7	25.8	1.3	-23.2	-64.2
8	25.3	0.8	-23.7	-65.2
9	24.8	0.3	-24.2	-66.2
0	24.3	-0.2	-24.7	-67.2
>	23.8	-0.7	-25.2	-68.2
<	23.3	-1.2	-25.7	-69.2
%	22.8	-1.7	-26.2	-70.2
*	22.3	-2.2	-26.7	-71.2
:	21.8	-2.7	-27.2	-72.2
;	21.3	-3.2	-27.7	-73.2
⊖	20.8	-3.7	-28.2	-75.2
(	20.3	-4.2	-28.7	-75.2
)	19.8	-4.7	-29.2	-76.2
=	19.3	-5.2	-29.7	-77.2
+	18.8	-5.7	-30.2	-78.2
#	18.3	-6.2	-30.7	-79.2
\$	17.8	-6.7	-31.2	-80.2
C	C	C	C	C

To obtain rainfall estimates it is necessary to read the digital magnetic tape using a program which will further separate the data into temperature ranges shown in Table 5.5.3-1. Cloud top temperatures of interest for estimating rainfalls are confined to temperature range given in scale D (-32.2 to -80.2°C). Scale C helps to define the shape of the entire cloud, scales A and B indicate surface temperatures. The change in area of lowest temperatures can be followed using scale D. The region of largest temperature gradients, corresponding to area of largest amount of rainfall, will also show up. Using guidelines established by Scofield and Oliver (Figures 5.5.2-1 and 5.5.2-2), rainfall can be estimated. This process can be done manually, but the entire procedure should be computerized. Half-hourly data stream is best suited for rainfall estimates because of the intense and short duration of summertime convective rains.

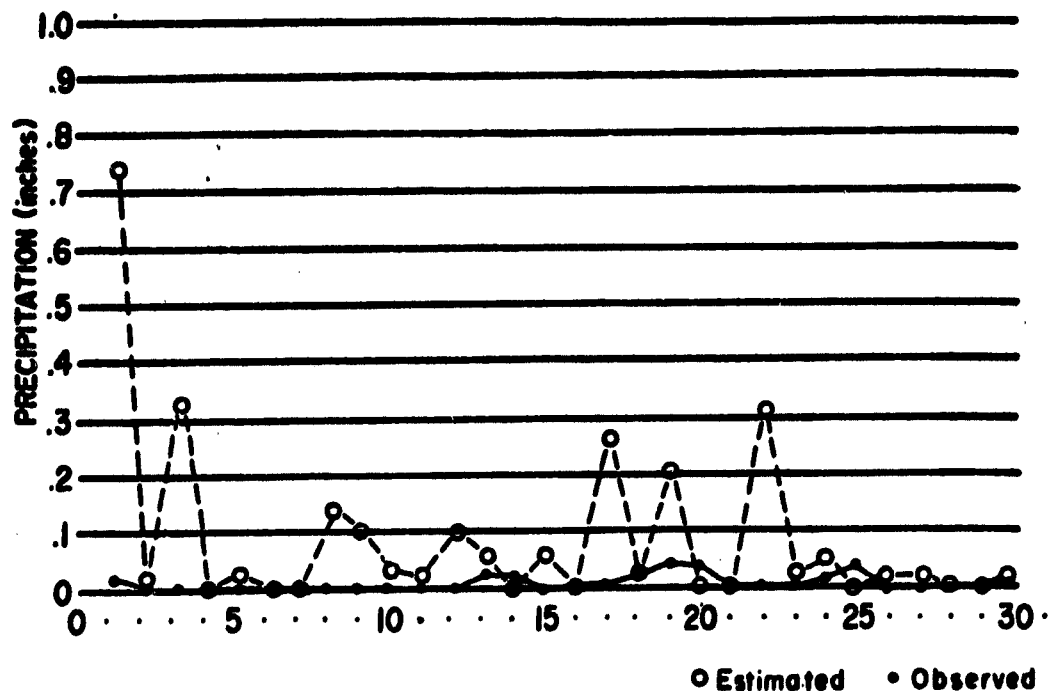
#### 5.5.4 Other Methods Using Satellite Data

Since the data obtained were inadequate to provide results, some results of estimating rainfall from GOES data obtained by other authors are shown here.

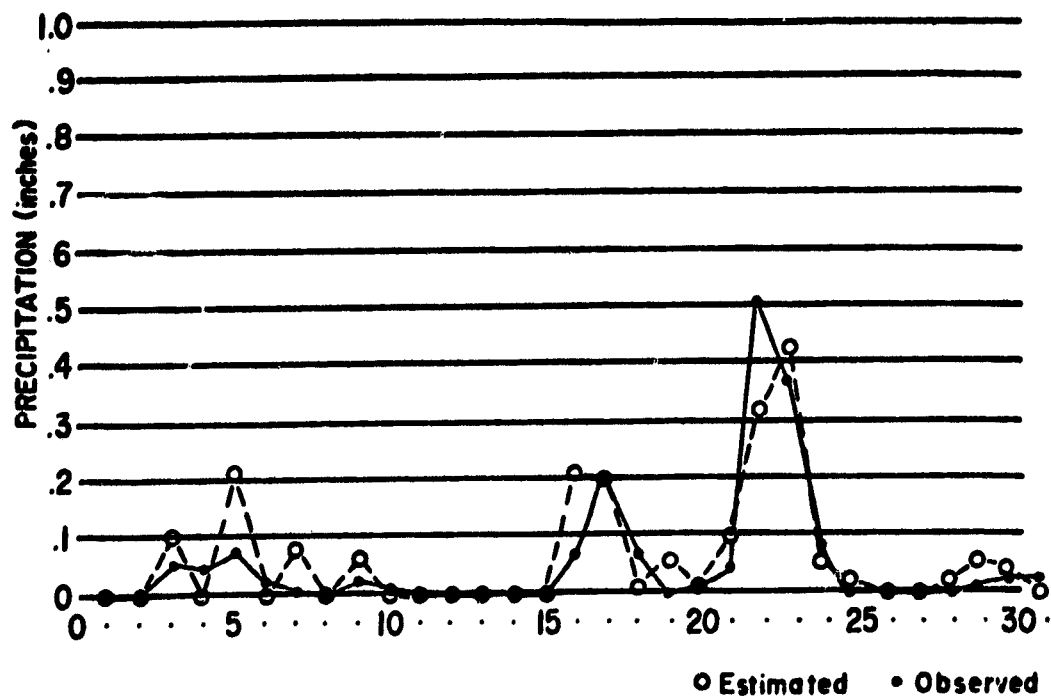
Attempts were made to estimate rainfall from remote sensing as early as the 1960s. Early results estimated for many areas of the world were reviewed by Barrett (1974). Rainfall for Florida was estimated using early satellite data (Follansbee, 1973). Figure 5.5.3-1 (after Follansbee) was included to show the result. Case a showed a generally poor estimate whereas Case b showed a generally good comparison. More recent work (Griffith et al., 1978) compared cloud size with radar echo size to obtain rainfall estimates. Cloud size and echo size were normalized to the largest cloud size/echo size in the time sequence when rainfall was to be estimated. Their method is therefore different from Scofield and Oliver where only GOES data were used.

The results of Griffith et al. (1978) showed that estimates over a small area (180 by 180 miles, Florida Area Cumulus Experiment (FACE) area) agreed better with groundtruth data than estimates over a larger area (1800 by 1800 miles, centered on Miami). Ten days were compared in the large area experiment and 8 days were used in the small area experiment. They concluded that the loss of accuracy in the larger area may be due to groundtruth data degradation of the large area. They also found that the accuracy appeared to be a function of the number of hours of estimates; individual hourly estimates showed more scatter than if hourly estimates were cumulated. Figure 9 of Griffith et al. (1978) is included to show this part of their results (Figure 5.5.3-2).

A quasi-operational method is available now to provide daily rainfall estimates for the state of Virginia (private communications, W.A. Follansbee, Wallops Island, Virginia). Quasi-operational means that rainfall estimates are provided within 48 hours of real time. The method used by Follansbee followed more closely the work of Scofield and Oliver (1978) than other methods. Much of the work has only been documented informally, so no reference is available.



a.--Estimated vs observed average rainfall over peninsular Florida for April 1967



b.--Estimated vs observed average rainfall over peninsular Florida for May 1967

Figure 5.5.4-1 Results of rainfall estimates by Follansbee (after Follansbee,1973).

MONTHLY WEA

ORIGINAL PAGE IS  
POOR QUALITY

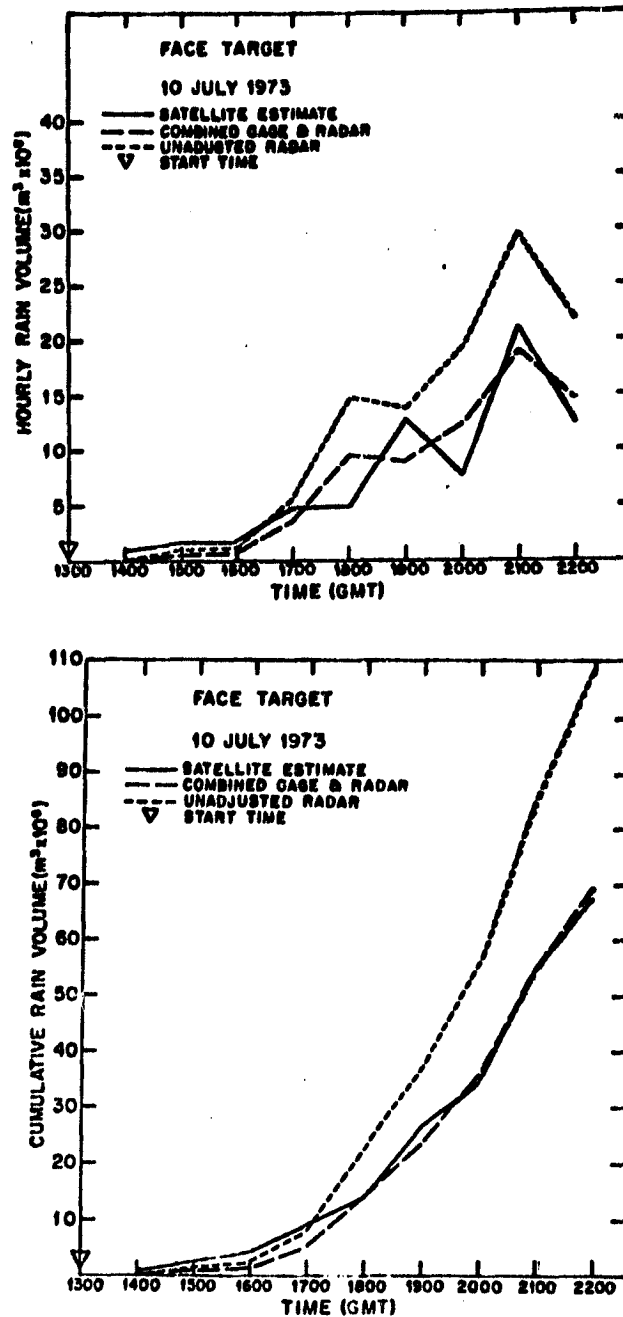


FIG. 9. Hourly (top) and cumulative (bottom) FACE target area rain results from visible data for 10 July 1973 using an 80 digital count threshold area. Satellite estimates, along with the unadjusted and gage-adjusted radar volumes, are plotted.

Figure 5.5.4-2 Results of rainfall estimates in S. Florida (after Griffith et al., 1978).

### 5.5.5 References

- Barrett, E.C. and L.F. Curtis, 1974. Environmental Remote Sensing: Applications and Achievements. Edward Arnold (Publishers), London. 309 pp.
- Follansbee, W.A., 1973. Estimation of average daily rainfall from satellite cloud photographs. NOAA Technical Memorandum NESS 44, U.S. Dept. of Commerce, Wash., D.C. 39 pp.
- Griffith, C.G. and W.L. Woodly, 1973. On the variation with height of the top brightness of precipitating convective clouds. J. App. Meteor., 12:1086-1089.
- Griffith, C.G., W.L. Woodley, and P.G. Grube, 1978. Rain estimation from geosynchronous satellite imagery - visible and infrared studies. Nom. Wea. Rev., 106:1153-1171.
- Scofield, R.A. and V.J. Oliver, 1977. A scheme for estimating convective rainfall from satellite imagery. NESS 86, 47 pp.

#### 5.5.6 Conclusions

The brief discussion of research on rainfall estimates by Follansbee (1973) and Griffith et al. (1978) using satellite data, indicate that the methods are promising but accuracies are variable. Convective rain systems frequently produce intense, localized, and short-duration rainfall. Merging of clouds also has a tendency to increase the amount of precipitation. The use of satellite data alone to interpret areas of most intense rainfall in a cloud system is difficult because there has been no work correlating rainfall amounts on the ground to areas within a cloud. The variable accuracies obtained may be related to this lack of knowledge. With a set of good groundtruth data it may be possible to deduce the area of rainfall by examining the data carefully and over a longer time period. Also, empirical relationships estimated for rainfall amounts may need further refinements. The maritime climate of Florida may need a slightly different set of parameters than continental climate. To obtain better accuracy, the estimates of rainfall may need to be evaluated on a long term basis, as is being done in the state of Virginia.

The needs to develop a program to estimate daily rainfall for Florida are 3-fold: 1) the large percentage of rainfall from scattered convective cumulus clouds during the rainy season where much of the precipitation reaching the surface will not be recorded (or possibly overestimated) due to limited number of rain gauges, 2) the dependence of shallow ground water supply on direct and timely rainfall, especially in south Florida where the problem may become more critical because of increasing population and water use, 3) the extensive agricultural areas and the need for irrigation water. The potential use for the satellite data is that the problem of accurately knowing rainfall inputs can be alleviated when a daily rainfall map is provided. The map will provide information for the hydrological cycle, water use, water management, drought, and flood prediction.

An added advantage is that major developmental work for rainfall estimates using GOES data have now been developed, much of it by W.A. Follansbee at Virginia (private communication). IFAS/UF now has the capability to receive sectorized IR GOES data directly over phone lines. Thus, real time data could be obtained and an operational system could be instituted with minimal effort and cost.

## 5.6 EVAPOTRANSPIRATION MEASUREMENTS

### Contributed by:

L.H. Allen, Jr.	Assoc. Prof. and Soil Scientist, USDA
J.F. Bartholic	Prof., PI
R.G. Bill, Jr.	Res. Assoc.
A.F. Cook	Biologist
H.E. Hannah	Electronic Tech.
K.F. Heimborg	Grad. Asst.
W.H. Henry	Phys. Sci. Tech., USDA
K. Hokkanen	Stud. Asst.
F.G. Johnson	Cmp. Sys. Anal.
J.W. Jones	Assoc. Prof.

TABLE OF CONTENTS

	<u>Page</u>
5.6 Evapotranspiration Measurements . . . . .	5.6-1
5.6.1 Remote Sensing Data Collection . . . . .	5.6-6
5.6.1.1 Equipment . . . . .	5.6-6
5.6.1.2 Test Site Location . . . . .	5.6-6
5.6.1.3 First Data Collection Mission . . . . .	5.6-6
5.6.1.4 Second Data Collection Mission . . . . .	5.6-7
5.6.2 Evapotranspiration Calculations . . . . .	5.6-7
5.6.2.1 Energy and Evapotranspiration . . . . .	5.6-7
5.6.2.2 Theory . . . . .	5.6-8
5.6.2.2.1 Proposed Method of Determining Net Radiation . . . . .	5.6-8
5.6.2.2.2 Energy Balance Partition and Evapotranspiration Mea- surements . . . . .	5.6-11
5.6.2.3 Materials and Methods . . . . .	5.6-18
5.6.2.3.1 Ground Truth Instrumentation and Measurements . . . . .	5.6-18
5.6.2.3.2 Aircraft Instrumentation and Measurements . . . . .	5.6-20
5.6.2.3.3 Other Ground Measurements . . . . .	5.6-24
5.6.2.4 Data Analysis . . . . .	5.6-27
5.6.2.4.1 Ground Truth Micrometeorology . . . . .	5.6-27
5.6.2.4.2 Aircraft Thermal Infrared Scenes . . . . .	5.6-30
5.6.2.5 Results . . . . .	5.6-32
5.6.2.5.1 Vegetative Cover Analysis . . . . .	5.6-32
5.6.2.5.2 ET by Bowen Ratio Method . . . . .	5.6-37
5.6.2.5.3 ET by Chamber Method . . . . .	5.6-52
5.6.2.5.4 Applications of Remote Sensed Data to ET . . . . .	5.6-58
5.6.2.5.5 Development of Remote Sensed ET Estimates from Stability Corrected Heat Flux . . . . .	5.6-63
5.6.2.5.6 Remote Sensed ET Estimates from Stability-Corrected Integral Profile Methods . . . . .	5.6-79
5.6.3 References . . . . .	5.6-84
5.6.4 Discussion and Conclusions . . . . .	5.6-87

# FIGURES

<u>Figure No.</u>	<u>Page</u>
5.6-1 Instruments and data acquisition system . . . . .	5.6-19
5.6-2 Portable instruments to be used over different surfaces . . . . .	5.6-21
5.6-3 Micrometeorological data acquisition system . . . . .	5.6-22
5.6-4 Upper Taylor Creek Watershed Flight Lines . . . . .	5.6-23
5.6-5 Infrared image of pasture scene in Taylor Creek Watershed . . . . .	5.6-33
5.6-6 Infrared image of citrus grove scene in Taylor Creek Watershed. . . . .	5.6-34
5.6-7 Daytime course of Bowen ratio ET - April 26, 1978 . . . . .	5.6-38
5.6-8 Daytime course of Bowen ratio ET - April 27, 1978 . . . . .	5.6-39
5.6-9 Daytime course of Bowen ratio ET - April 28, 1978 . . . . .	5.6-40
5.6-10 Daytime course of Bowen ratio ET - April 29, 1978 . . . . .	5.6-41
5.6-11 Daytime course of Bowen ratio ET - April 30, 1978 . . . . .	5.6-42
5.6-12 Daytime course of Bowen ratio ET - May 1, 1978 . . . . .	5.6-43
5.6-13 Daytime course of Bowen ratio ET - May 2, 1978 . . . . .	5.6-44
5.6-14 Daytime course of Bowen ratio ET at beginning of fall senescence. Oct. 17, 1978 . . . . .	5.6-45
5.6-15 Daytime course of Bowen ratio ET at beginning of fall senescence. Oct. 20, 1978 . . . . .	5.6-46
5.6-16 Daytime course of Bowen ratio ET at beginning of fall senescence. Oct. 26, 1978 . . . . .	5.6-47
5.6-17 Diurnal course of ET during 4 consecutive days at the beginning of spring regrowth Apr. 26, 27, 28 & 29 . . . . .	5.6-48
5.6-18 Diurnal course of ET during 4 consecutive days at the beginning of spring regrowth Apr. 30, May 1, 2 & 3 . . . . .	5.6-49
5.6-19 Diurnal course of ET 4 consecutive days beginning of fall senescence . . . . .	5.6-53
5.6-20 Diurnal course of ET 3 consecutive days beginning of fall senescence . . . . .	5.6-54

<u>Figure No.</u>	<u>Page</u>
5.6-21 Diurnal course of ET 2 consecutive days, beginning of fall senescence . . . . .	5.6-55
5.6-22 Daytime course of ET from Chamber Measurements . . . . .	5.6-57
5.6-23 Outline of temp. intervals drawn from infrared image of pasture scene in Taylor Creek Watershed Apr. 28, '78 at 1222-1225 EST . . . . .	5.6-60
5.6-24 Outline of temp. intervals drawn from infrared image of citrus grove scene in Taylor Creek Watershed, Apr. 26, '78 at 1432-1435 EST . . . . .	5.6-61
5.6-25 Bulk Aerial resistance components of turbulent resistance as a function of wind speed . . . . .	5.6-64
5.6-26 Sensible heat flux density, H, as a function of Richardson number for combination of $\Delta U$ and $\Delta T$ . . . . .	5.6-68
5.6-27 Turbulent resistance for heat transport as a function of Richardson number . . . . .	5.6-69
5.6-28 Temp. difference from surface to 0.3 m vs temp. difference from surface to 1.5 m . . . . .	5.6-73
5.6-29 ET as a function of the difference between surface temp. and air temp . . . . .	5.6-78
5.6-30 ET as a function of $Z_0$ and surface temp. (surface temp equal to 23.9° C) . . . . .	5.6-80

TABLES

<u>Table No.</u>	<u>Page</u>
5.6-1 Taylor Creek Flight Line IR Scanner Summary . . . . .	5.6-25
5.6-2 Taylor Creek Flight Line Color Infrared Photography Summary . . .	5.6-26
5.6-3 Taylor Creek Evapotranspiration Data . . . . .	5.6-28
5.6-4 Color Code and Percent Land Area for Surface Temp. Ranges from Figs. 5.6-5 and 5.6-6 . . . . .	5.6-31
5.6-5 Daytime Energy Budget Summary . . . . .	5.6-50
5.6-6 Rainfall in Inches on Taylor Creek Watershed, Apr. '78-Oct. '78 .	5.6-51
5.6-7 Daily Pan Evap. at Ft. Pierce and on Taylor Creek Watershed . . .	5.6-56
5.6-8 Regional Evapotranspiration for Pasture Scene Using Resistance Method, Apr. 28, 1200-1230 EST . . . . .	5.6-62
5.6-9 Test for Heat Flux Constancy with Stability Corrections . . . . .	5.6-71
5.6-10 ET Calculations from Different Surface Temps. for the Pasture Scene of Apr. 28, '78 (1222-1225 EST) . . . . .	5.6-76
5.6-11 ET Calculations from Different Surface Temps. for the Citrus Grove Scene Apr. 26, '78 (1432-1435 EST) . . . . .	5.6-77
5.6-12 Computations of $\lambda E$ , H, and $r_a$ from stability-corrected profile integral methods . . . . .	5.6-81

## 5.6.1 Remote Sensing Data Collection

### 5.6.1.1 Equipment

In collecting the remotely sensed data or the evapotranspiration measurements, KSC utilized the following equipment:

- a. Electronic Scanner: A Daedalus DS-1250 Scanner with two thermal channels (3 to 5 microns and 8 to 14 microns) and a ten channel head (0.38 microns to 1.1 microns).
- b. Aircraft: Twin engine Beechcraft C45H with 450 horsepower Pratt and Whitney engines and a cruise speed of 160 knots. Range is 600 nautical miles, ceiling is 12,000 feet and maximum useful equipment payload is 1079 pounds.

### 5.6.1.2 Test Site Location

The test site sampled by aircraft remote sensing lies north of Lake Okechobee and encompasses the Taylor Creek watershed. The site is 16 miles long and 5 miles wide and is defined by the following coordinates:

27°25'	27°25'	27°20'	27°20'
81°02'30"	80°47'30"	80°47'30"	81°02'30"

### 5.6.1.3 First Data Collection Mission

The first data collection mission was initiated on April 26, 1978, and concluded on April 28, 1978. The aircraft flights made during this mission are listed below with pertinent flight data.

- a. April 26: 11:45 am - 12:45 pm EST, 4500-foot altitude, 6 flight lines, IR and multispectral, black body range 70° - 106°
- b. April 26: 2:00 pm - 2:35 pm EST, 8000-foot altitude, 3 flight lines, IR and multispectral, black body range 70° - 106°
- c. April 26: 3:48 pm - 4:12 pm EST, 8000-foot altitude, 3 flight lines, IR and multispectral, black body range 60° - 96°
- d. April 28: 12:20 am - 1:06 am EST, 8000-foot altitude, 6 flight lines, IR only, black body range 30° - 66°
- e. April 28: 11:10 am - 12:04 pm EST, 4500-foot altitude, 6 flight lines, IR and multispectral, black body range 72° - 108°.

In addition to this scanner data acquired by the KSC aircraft, at KSC's request the Florida Department of Transportation covered the test site with aerial color infrared film (Kodak 2443) on May 11, 1978, to document ground cover. The flight was made at 9000 feet with 3 flight lines from 12:15 pm to 12:42 pm.

#### 5.6.1.4 Second Data Collection Mission

The second data collection mission was initiated late on October 16 and concluded on October 17, 1978 (times are converted from EDT to EST). The aircraft flights made during this mission are listed below with pertinent flight data.

- a. October 16: 11:26 pm - 12:13 am EST, 8000-foot altitude, 3 flight lines, IR only, black body range 36° - 72°
- b. October 17: 9:32 am - 10:22 am EST, 8000-foot altitude, 3 flight lines, IR and multispectral, black body range 54° - 90°
- c. October 17: 12:15 pm - 1:30 pm EST, 3500-foot altitude, 6 flight lines, IR and multispectral, black body range 64° - 100°.

As on the first mission the Florida Department of Transportation, at KSC's request, covered the test site with aerial color infrared (Kodak 2443) photography to document ground cover. The flight was made on October 26, 1978, at 12,000-foot altitude with 3 flight lines acquired from 10:14 am to 10:50 am EST.

Selected flight lines of the thermal scanner data in color film form together with color infrared aerial photography flown by the Florida Department of Transportation have been provided to IFAS for analysis. In addition, some analysis of the thermal scanner data in digital tape format has been done by IFAS on the Image 100.

#### 5.6.2 Evapotranspiration Calculations

##### 5.6.2.1 Energy and Evapotranspiration

Evapotranspiration (T) is the combined process of (a) evaporation from internal plant surfaces (and diffusion of water vapor into the atmosphere mostly through stomata) and (b) direct evaporation from the soil. Evapotranspiration from the earth's surface to the atmosphere can be regarded as both a mass flow process and an energy flow process. As a mass flow process, it depends upon the gradient of vapor concentration ( $\Delta e$ ) between two points in the water vapor flow continuum, and the resistance (r) to vapor flow between those two points.

$$\text{Flux} \propto \frac{\Delta e}{r} \quad (5.6-1)$$

As an energy flow process, the flow of water vapor from an evaporating surface presupposes that about 2.43 kJ/cm<sup>3</sup> (580 cal/cm<sup>3</sup>) of energy (at 25°C) was required to produce the vapor from liquid water. This energy could be supplied from internal storage, by radiation, or by convection from the atmosphere. As an energy flow process, evaporation is usually expressed as latent heat flux density. These two terms, evaporation and latent heat flux density, will be used interchangeably in this section (5.6).

The energy balance equation for latent ( $\lambda E$ ), sensible ( $H$ ), net radiant ( $R_n$ ), photochemical ( $\lambda P$ ), and storage ( $S$  and  $B$ ) energy flux densities over a terrestrial surface can be written as follows.

$$R_n = \lambda E + H + \lambda P + S + B \quad (5.6-2)$$

The two storage terms are actually equivalent flux densities of energy into (or from) the soil,  $S$ , and into (or from) plant biomass,  $B$ . The flux of energy into the plant biomass is usually small and can be ignored. Over a daily cycle it is negligible since the energy that flows into the plant biomass during the day flows out again at night. Likewise, the photochemical flux density of energy (photosynthesis) is usually a small part of the energy budget and can be ignored also. The most efficient plants utilize about 6% of incoming solar radiation for photosynthesis, but for most plants the percentage utilized is much lower.

For most purposes, it is adequate to use the simpler energy balance equation:

$$R_n = \lambda E + H + S. \quad (5.6-3)$$

#### 5.6.2.2 Theory

To develop a complete remote sensing technique for determining evapotranspiration over an area, we first need methods for partitioning  $R_n$  into its components of  $\lambda E$ ,  $H$ , and  $S$ .

We also need to consider the time-scale over which measurements will be taken or averaged, or the time period that a set of measurements will represent. Since evaporation, sensible heat transport, and soil heat flux are highly dependent upon "instantaneous" conditions, any estimates or measurements that cover whole-day inputs will be subject to uncertainties about how these inputs were distributed throughout the day.

Another problem is the space scale. Evapotranspiration from a large, uniformly vegetated surface can vary spatially depending on cloud cover patterns, which will affect not only the spatial net radiation inputs but also the spatial partition of the energy balance components at the ground level. When the vegetation distribution varies, the above space scale resolution becomes an even greater problem.

A procedure was outlined in the response to this proposal to develop a method for computing  $R_n$  as a function of radiation measurements by satellite. This procedure is enclosed here, although the objectives were not accomplished.

##### 5.6.2.2.1 Proposed Method of Determining Net Radiation.

The most important parameter affecting evapotranspiration is net radiation ( $R_n$ ) since energy is required to evaporate water. For a well watered surface, nearly all the  $R_n$  goes into ET.  $R_n$  is hard if not impossible to obtain over large areas with conventional ground measurement devices. Satellite data, however, can assist significantly in determining  $R_n$ .

$$R_n = Q_s - Q_{sr} + Q_a - Q_{bs} \quad (5.6-4)$$

Equation 5.6-4 shows that net radiation ( $R_n$ ) is made up of downward solar radiation ( $Q_s$ ) minus upward reflected solar radiation ( $Q_{sr}$ ) plus downward thermal radiation from the atmosphere ( $Q_a$ ) minus upward thermal radiation leaving the surface ( $Q_{bs}$ ).

**Solar Radiation ( $Q_s$ ):** Recent work has shown a good correlation for relationships between  $Q_s$  reaching the surface and cloud brightnesses determined with hourly GOES visible data. Insolation ( $Q_s$ ) is defined as the rate at which direct and scattered solar radiation is incident upon a unit horizontal surface. A clear midday value for  $Q_s$  in Florida could be  $105 \text{ mW/cm}^2$  ( $1.5 \text{ cal/cm}^2/\text{min}$ ). Daily solar radiation could be estimated to better than  $+ 1.3 \text{ MJ/m}^2$  ( $+ 30 \text{ cal/cm}^2$ ) in a Great Plains Experiment (Tarpley et al., 1979).

Visible solar radiation incident on the Earth is either reflected to space, absorbed in the atmosphere, or absorbed by the earth's surface. Surface insolation, the quantity of interest, is a function of incident solar radiation and the amounts of energy reflected to space and absorbed by the atmosphere (Tarpley et al., 1978).

The fraction of incoming radiation that is reflected to space is primarily controlled by cloud amount and cloud thickness, both of which can be estimated from satellite data. Cloud amount in an area can be computed by the two-threshold method (Shenk and Salomonson, 1972) in which the number of pixels in clear, partly cloudy, and cloudy classes are weighted to yield fractional cloud cover.

If the partly cloudy class is assumed to be 50 percent cloud covered, then the cloud fraction,  $C$ , is expressed by:

$$C = \frac{0.5N_2 + N_3}{N_1 + N_2 + N_3} \quad (5.6-5)$$

or,

$$C = \frac{N_2 + 2N_3}{2N} \quad (5.6-6)$$

where  $N$  is the total number of pixels in the target area, and  $N_1$ ,  $N_2$ , and  $N_3$  are the numbers of pixels in the clear, partly cloudy, and cloudy classes, respectively.

The brightness of a clear scene changes continually over the course of a day because of changing angles of illumination. The clear threshold is also a function of the illumination angles and can be obtained by regression. The variables in the regression equation are local solar zenith angle and the local azimuth angle between the sun and satellite.

Another cloud parameter that can be calculated is mean cloud brightness. This can be determined by averaging all pixels equal to or brighter than the cloud threshold. Mean target brightness will also be computed as another measure of reflected radiation.

The amount of incoming radiation that is absorbed in the atmosphere is controlled by cloud cover, atmospheric moisture, dust and the atmospheric mass traversed by the beam. Precipitable water and surface pressure are available from the National Meteorological Center (NMC); these two quantities, together with the satellite-derived cloud characteristics, should provide enough information to account for radiation absorbed by the atmosphere. The precipitable water and surface pressure can be accessed from NMC fields, whose resolution is about four degrees at mid-latitudes, lower than the one-half degree grid used for the Great Plains.

Reflected Solar Radiation (Qsr): Qs averages about 70 mW/cm<sup>2</sup> (1 cal/cm<sup>2</sup>/min) during much of the high ET period of the day and wavelength band ranges from 0.3 to 3.0  $\mu$ m. Some of this solar radiation is reflected from the surface. The TIROS-N and NOAA-A satellites have sensors in 2 wavelength bands which measure the reflectance in the 0.55 to 0.7 and 0.7 to 1.1  $\mu$ m intervals. Qsr can be determined by combining the energy reflected in these 2 bands. Thus, it is now possible to characterize the reflectance of large surfaces with 1 km resolution using satellite data. This characterization would only be necessary once during each season. Thus one can wait for ideal conditions under which to characterize Qsr which ranges from 5% for organic soil to between 10 to 25% for vegetation and up to 50% for sandy surfaces.

Thermal Radiation (Qa, Qbs): Thermal radiation from the atmosphere Qa and emitted from the surface Qbs is in the wavelength range of 3 to 100  $\mu$ m. Qa with tropical atmospheric conditions might average 35 mW/cm<sup>2</sup> (0.5 cal/cm<sup>2</sup>/min) during the day and night. The component can be obtained, if the sky is clear, from atmospheric sounding information obtained from satellites.

From knowledge of the air temperature profiles and water vapor profiles, the long wave radiation from the sky can be calculated. All models are based upon the methods initially outlined by Greenfield and Kellogg (1960), where the atmosphere is divided into a set of parallel slabs. The radiation coming from a slab and being attenuated by the intervening atmosphere is given by:

$$\Delta I_{\lambda}(T_{\ell}) = J_{\lambda}(T_{\ell})\tau_{\pi}(\lambda)[1-\tau_{\ell}(\lambda)] \quad (5.6-7)$$

where  $\lambda$  is the particular wavelength being considered,  $T_{\ell}$  is the temperature of the  $\ell$ th layer,  $\tau_{\pi}$  is the transmissivity of the atmosphere from the bottom of the layer to the ground,  $\tau_{\ell}$  is the transmissivity of the  $\ell$ th layer and  $J_{\lambda}$  is the Planck or Blackbody function. The air temperature profiles are needed to calculate  $J_{\lambda}(T_{\ell})$  at each layer. The water vapor profiles are needed to obtain the transmissivities.

The model must then add the contributions of each layer and then integrate over the hemispheric solid angle.

The transmissivities have been tabulated in the well-known work of Elsasser and Culbertson (1960). But several improved measurements have been made over the years (see for example Davis and Viezel, 1964).

Also, an identical calculation must be made for carbon dioxide and ozone but the CO<sub>2</sub> profiles remain fairly constant unlike those of water vapor.

There is at present significant research going on in methods for extracting these various profiles from the satellite data itself although the accuracy is somewhat questionable (see Weinreb, 1977).

If the sky is not clear, then estimates of the value of  $Q_b$ s can be obtained from methods outlined by Koberg (1958).  $Q_b$ s can be obtained from surface temperatures and has a value of  $45 \text{ mW/cm}^2$  ( $0.64 \text{ cal/cm}^2/\text{min}$ ) at  $25^\circ\text{C}$ . With just 2 clear passes during the day and a knowledge of the soil water, crop conditions, and air temperature, surface temperatures for the entire day can be estimated. Under well-watered conditions the surface temperatures of tall vegetation is seldom more than 2 to  $4^\circ\text{C}$  different than air temperature. Surface temperatures even for dry conditions under cloudy skies and low radiation loads are not greatly different than air temperature. A  $5^\circ\text{C}$  surface temperature error results in an error of  $2.8 \text{ mW/cm}^2$  ( $0.04 \text{ cal/cm}^2/\text{min}$ ).

#### 5.6.2.2.2 Energy Balance Partition and Evapotranspiration Measurements

Since the pioneering work of Penman (1948) on the physics and micro-meteorology of evapotranspiration, considerable theoretical advances have been made to refine the description of the diffusion of water vapor in plant canopies. [see e.g., Monteith (1965), Tanner and Fuchs (1968), Lemon et al. (1971), Shuttleworth (1976), and Deardorff (1978)]. These formulations differ primarily in the manner of treating the distributions of sources and sinks of water vapor with the plant canopy. Monteith treats the canopy as a single source while Shuttleworth and Lemon et al. use a multilayer concept.

In contrast to the theoretical advances, use of theoretical methods for practical prediction of ET has lagged considerably. In the hydrological model of Holtan et al. (1974), ET is predicted simply in terms of an adjustment to pan evaporation. The reliability of such coefficients is quite doubtful due to the variability of the coefficients with vegetation type, stage of growth and meteorological conditions. In Florida, Bartholic and Buchanan (1976) have shown that pan coefficients for peach trees may vary between 0.2 and 0.8.

The difficulty in using more theoretical treatments in practical situations arises from the detailed measurements necessary to implement the models. Shuttleworth (1976) has recently commented on this problem:

"It is easily seen that, even in one dimension, the general description of the vegetation - atmosphere interaction is very complex, perhaps too complex for direct practical application in any predictive sense... [This] implies that the prediction of evaporation might always have to rely on simplified and less precise treatments."

Our approach is to use evaporation techniques or models that (a) are based on physical approaches as much as possible and that (b) can use remotely sensed data for input coupled with data from a relatively sparse ground network. Remotely sensed surface temperature is the central, focal parameter. Second, we want to rely on energy balance techniques as much as possible, and, if possible, avoid aerodynamic techniques that would require complicated wind profile measurements over different terrain at different times of day. Third,

we want to avoid methods that require input of leaf stomatal resistance (or canopy resistance of water vapor) because this would require extensive observations on vegetation.

Models of ET: Two physical models are the resistance-energy balance model (e.g., Heilman and Kanemasu, 1976; and Verma et al., 1976) and the combination (Penman Type) model (e.g., Tanner and Fuchs, 1968). Common inputs to these two models are net radiation,  $R_n$ , surface temperature,  $T_s$ , air temperature at a reference height,  $T_a$ , wind speed,  $u$ , and soil heat flux,  $S$ . One form of the resistance-energy balance model was successfully tested to compute ET ( $\lambda E$ ) of sorghum, millet, and soybean as the residual in equation 5.6-3 by Verma et al. (1976) and Heilman and Kanemasu (1976). The combination model (Tanner and Fuchs, 1968) calculates ET by eliminating temperature and temperature gradients as explicit parameters. Both models are derived directly from the energy balance equation (Equation 5.6-3).

The Resistance-Energy Balance Model: The energy balance equation is (Equation 5.6-3):

$$R_n = H + \lambda E + S \quad (5.6-3)$$

where  $H$  = sensible heat flux,  $\lambda E$  (=ET) = latent heat flux, and  $S$  = soil heat flux.

The atmosphere gradient expressions near the earth's surface for  $H$  and  $\lambda E$  are:

$$H = -\rho C_p K_H \frac{dT}{dz} = -\rho C_p K_H \frac{(T_2 - T_1)}{(Z_2 - Z_1)} \quad (5.6-8)$$

$$\lambda E = -\rho \lambda \frac{M_w/M_a}{P} K_w \frac{de}{dz} = -\frac{\rho \lambda \epsilon}{P} K_w \frac{(e_2 - e_1)}{(Z_2 - Z_1)} \quad (5.6-9)$$

where the subscripts "2" and "1" refer to the heights above the ground,  $Z$ ,  $T$  is temperature,  $e$  is vapor pressure,  $K_H$  and  $K_w$  are turbulent eddy diffusivities for heat and water vapor, respectively,  $\rho$  is atmospheric density,  $C_p$  is atmospheric heat capacity,  $P$  is atmospheric pressure,  $\lambda$  is latent heat of vaporization of water, and  $M_w/M_a = \epsilon$  is the ratio of molecular weights of water vapor and dry air.

Now if the turbulent diffusivities for heat and water vapor are the same, then the ratio of  $H/\lambda E$ , the Bowen ratio,  $\beta$ , can be expressed as:

$$\beta = \frac{H}{\lambda E} = \frac{C_p P}{\lambda \epsilon} \frac{(T_2 - T_1)}{(e_2 - e_1)} \quad (5.6-10)$$

The latent heat flux density can be expressed in terms of  $\beta$  as:

$$R_n - S = \lambda E + H = \lambda E (1 + \beta) \quad (5.6-11)$$

$$\lambda E = \frac{R_n - S}{1 + \beta} \quad (5.6-12)$$

It would be desirable to use the Bowen ratio - energy balance approach directly, but there is no way to measure vapor pressure and T in the air with remote sensing. We can, however, measure leaf surface temperature,  $T_s$ , with remote sensing techniques and compute the saturation vapor pressure,  $e_s(T_s)$ .

It would be desirable to use a Bowen ratio approach indirectly with

$$\beta = \frac{C_p}{\lambda} \frac{P}{\epsilon} \frac{(T_s - T_a)}{(e_s(T_s) - e_a)} \quad (5.6-13)$$

where  $e_a$  and  $T_a$  can be measured at weathershelter height,  $T_s$  measured from remote sensing, and  $e_s(T_s)$ , the saturation vapor pressure at the canopy surface, computed from  $T_s$ . However, the leaves of the plant canopy introduce a stomatal diffusion resistance not found for bodies of water or wet soil surfaces. The energy balance for a leaf (neglecting photochemical energy of photosynthesis) can be given by:

$$R_n = \rho C_p \frac{(T_s - T_a)}{r_a} + \rho \lambda \frac{\epsilon}{P} \frac{(e_s(T_s) - e_a)}{r_a + r_s} \quad (5.6-14)$$

where the first term represents sensible heat flux, the second term represents latent heat (water vapor) flux,  $r_a$  is the aerial diffusion resistance and  $r_s$  is the stomatal diffusion resistance. This equation can be applied to a canopy of leaves.

$$(R_n - S) = \rho C_p \frac{(T_s - T_a)}{r_a} + \rho \lambda \frac{\epsilon}{P} \frac{(e_s(T_s) - e_a)}{r_a + r_s} \quad (5.6-15)$$

We will refer back to this equation later.

Actually, the boundary layer resistance component of  $r_a$  for water vapor transport is about 0.9 times that for sensible heat transport as derived by an analysis from Thom (1972), but we simplified and considered them equal in this report. Also, the values would be twice as large for vegetation with stomata on only the lower leaf surface, rather than on both leaf surfaces, since boundary layer transport of water vapor would occur on only one side.

The resistance-energy balance method could use air temperature measurements from a hygrothermograph or other instruments in standard meteorological shelters along with net radiation and surface temperature from satellite observations. The resistance-energy balance is a direct physical model derived from substitution into the energy balance equation:

$$ET = \lambda E = R_n - S - \rho C_p \frac{(T_s - T_a)}{r_a} \quad (5.6-16)$$

The sensible heat flux density equation is:

$$H = \rho C_p \frac{(T_s - T_a)}{r_a} \quad (5.6-17)$$

for transport over a surface within the surface turbulent aerodynamic boundary layer.

The aerial diffusion resistance,  $r_a$ , consists of at least two parts, the resistance across the surface of individual elements to the turbulent flow (aerodynamic boundary layer resistance),  $r_b$ , and the resistance from the lowest level turbulent flow to the reference measurement height,  $r_t$ . This latter resistance is defined by:

$$H = \rho C_p \frac{(T_o - T_a)}{r_t} \quad (5.6-18)$$

where  $T_o$  is the temperature at the roughness height,  $Z_o$ . It could be given by integrating the eddy diffusivities for heat from  $Z_o$  to a reference height,  $Z$ .

$$r_t = \int_{Z_o}^Z \frac{dZ}{K_H} \quad (5.6-19)$$

Eddy diffusivity for momentum increases linearly with height as  $K_m = kU_* Z$ , where  $k$  = von Karman's constant and  $U_*$  = friction velocity. So if  $K_H = K_m$ , then:

$$r_t = \int_{Z_o}^Z \frac{dZ}{kU_* Z} \quad (5.6-20a)$$

$$r_t = \frac{1}{kU_*} \ln \left( \frac{Z}{Z_o} \right) . \quad (5.6-20b)$$

From the logarithmic wind speed profile law for neutral conditions:

$$U_Z = \frac{U_*}{k} \ln \left( \frac{Z}{Z_o} \right) . \quad (5.6-21)$$

Therefore,

$$r_t = U_Z / U_*^2 . \quad (5.6-22)$$

Another resistance term is the resistance across the aerodynamic boundary layer defined by:

$$H = \frac{\rho C_p (T_s - T_o)}{r_b} \quad (5.6-23)$$

The values of  $r_b$  can be calculated for a single leaf surface as:

$$r_b = 1.3 \left( \frac{L}{U} \right)^{1/2} \quad (5.6-24)$$

where  $L$  is the width of the leaf in cm and  $U$  is the wind speed near the leaf in cm/sec (Monteith, 1965). For two surfaces in parallel, the coefficient is 0.65. For a canopy of leaves of leaf area index, LAI, acting in parallel,

$$r_b = \frac{SF}{LAI} 0.65 \left(\frac{L}{U}\right)^{1/2} \quad (5.6-25)$$

In actual conditions, the leaf-to-air transport of leaves interfere with each other, so the effective resistance is not as low as equation 5.6-24 would suggest. Therefore, a shelter factor, SF, must be introduced (Thom, 1971).

Heilman and Kanemasu (1976) computed an aerodynamic resistance based on  $(T_c - T_a)$ , where  $T_c$  was the canopy temperature determined from copper-constantan thermocouples attached to the underside of leaves. Their resistance term,  $r_H$ , was based on a turbulent analog which used  $T_c$  as the mean surface property. This analog was used to predict a heat transport roughness length,  $Z_H$ , that was smaller than the aerodynamic roughness length,  $Z_0$ . The turbulent component of aerial resistance  $r_t$  and the "individual element" component to aerial resistance  $r_b$  can be approximated by plotting air temperature as a function of height (on a log scale) and extrapolating to  $Z_0$ , the roughness length parameter, the height at which wind speed extrapolates to zero. This would yield a temperature,  $T_0$ . From sensible heat flux density, the defining expression for  $r_t$  is:

$$r_t = \frac{\rho C_p (T_0 - T_a)}{H} \quad (5.6-26)$$

The bulk boundary layer resistance would be defined by:

$$r_B = \rho C_p \frac{(T_s - T_0)}{H} \quad (5.6-27)$$

Here  $r_B$  is used instead of  $r_b$  to imply that this resistance would be determined for an ensemble of surfaces rather than for an individual leaf.

Values of  $r_t$ ,  $r_B$ , and  $r_a$  could be investigated under a range of conditions of wind speed, surface roughness, atmospheric instability, temperature, soil moisture, and radiation regimes, and vegetative surface conditions, to determine relevant controlling factors. For a given vegetation type,  $r_a$  could be used to compute  $H$  and hence  $\lambda E$  and evapotranspiration from equation 5.6-16 for other similar surfaces where ground truth  $H$  cannot be measured.

Another method for computing  $r_a$  depends on atmospheric stability, surface roughness,  $Z_0$ , wind speed  $U$  at height  $Z$ , and temperature,  $T$ . Atmospheric stability may be characterized through the Richardson number, Ri:

$$Ri = \frac{g \left(\frac{dT}{dZ}\right)}{\theta \left(\frac{dU}{dZ}\right)^2} \approx \frac{gZ(T_a - T_0)}{\theta U^2} \quad (5.6-28)$$

where  $g$  is the acceleration of gravity, and  $\theta$  is the absolute air temperature. Similarity theory along with empirical data for profiles of temperature and velocity in the turbulent planetary boundary-layer are summarized by Paulson (1970) and Businger (1973).

$$\frac{T_a - T_o}{T_*} = \frac{1}{k} \left[ \ln\left(\frac{Z}{Z_o}\right) - \psi_1 \right] \quad (5.6-29)$$

$$U_* = kU / \left[ \ln\left(\frac{Z}{Z_o}\right) - \psi_2 \right] \quad (5.6-30)$$

where  $\psi_1$  and  $\psi_2$  are known functions of  $Ri$ , and  $T_*$  is  $H/(\rho C_p U_*)$ . From these relations,  $r_a$  may be calculated as:

$$r_a = \frac{1}{kU_*} \left[ \ln\left(\frac{Z}{Z_o}\right) - \psi_2 \right] \quad (5.6-31)$$

Thus, if  $T_o$  and  $Rn$  are known through remote sensing and  $T_a$  and  $U$  are known from ground stations,  $r_a$  and  $H$  may be calculated. Estimation of  $S$  will be discussed below. For tall canopies  $Z$  is replaced by  $(Z - D)$  where  $D$  is the displacement height (Rosenberg et al., 1975).

**Combination Model:** Combination models are those that combine the energy balance with a bulk aerodynamic formula. They have surface temperature eliminated as an explicit variable with vapor pressure substituted through the slope of the saturation vapor pressure vs. temperature relationship. From equation 5.6-15, Tanner and Fuchs (1968) calculated ET as:

$$ET = \frac{(\gamma + \Delta)}{\Delta} E_p - \frac{\rho C_p}{\Delta r_a} (e_s(T_s) - e_a) \quad (5.6-32)$$

where,

$$E_p = \frac{\Delta}{(\Delta + \gamma)} \left[ (Rn - S) + \frac{\rho C_p}{\Delta r_a} (e_s(T_a) - e_a) \right] \quad (5.6-33)$$

where  $\Delta$  is the slope of the saturation vapor pressure,  $e_s$ , vs. temperature curve,  $\gamma$  is the psychrometric constant ( $= C_p P / \epsilon l$ ),  $e_s(T_s)$  is the saturation vapor pressure at the temperature of the surface, and  $e_a$  is the vapor pressure of the air at some reference height. In this method,  $r_a$  would be calculated as described earlier. This method requires the additional input of vapor pressure at a reference height from a ground station to provide  $e_a$ .

This combination method can be derived from equation 5.6-15 with the stomatal resistance included. This equation becomes (Monteith, 1965):

$$ET = E_p / \{ 1 + [\gamma / (\Delta + \gamma)] (r_s / r_a) \} \quad (5.6-34)$$

This equation reduces to  $E_p$  if  $r_s$  is zero.

There would appear to be no advantage in using the combination model rather than the resistance-energy balance model for remote sensing application. Indeed, both models are mathematically interchangeable, and the combination model requires bulk stomatal resistance and air vapor pressure. Bulk stomatal resistance is difficult to obtain. Also, saturation vapor pressures must be obtained. Both methods require surface temperature.

Bulk Stomatal Resistance: From equation 5.6-15 the  $\lambda E$  component is:

$$\lambda E = \frac{\rho \lambda E}{P} \frac{(e_s(T_s) - e_a)}{r_a + r_s} \quad (5.6-35)$$

Once  $\lambda E$  is determined from any model, the bulk stomatal resistance can be estimated, assuming  $r_a$  for vapor flux is the same as  $r_a$  for sensible heat flux. The  $r_t$  component should definitely be the same for both sensible heat and latent heat transfer. The  $r_g$  component may be slightly different due to leaf stomatal distribution, canopy source differences, and differences in water vapor vs. heat diffusivity.

$$r_s = \frac{\rho \lambda E}{P} \frac{(e_s(T_s) - e_a)}{\lambda E} - r_a \quad (5.6-36)$$

Bulk stomatal resistance can also be estimated from equation 5.6-34.

$$r_s = r_a \left( \frac{E}{\lambda E} - 1 \right) \left( \frac{\Delta + \gamma}{\gamma} \right) \quad (5.6-37)$$

Other models: Evapotranspiration estimates can be used to develop coefficients for the Priestley-Taylor (1972) model (i.e., Kanemasu et al., 1979).

$$ET = \alpha \left( \frac{\Delta}{\Delta + \gamma} \right) R_n \quad (5.6-38)$$

In this model, only net radiation would be needed. Actual ET is calculated as an adjustment to the ET that would occur under saturation conditions. This would be a simple, useful model if  $\alpha$  were known for each vegetation condition and each climate condition.

The Blaney-Criddle Method has been used by Rogers (1976) to estimate irrigation water requirements of crops in Florida. He has adapted the SCS Technical Release 21 approach by adjusting the period of day-length to the period of available sunshine (direct-beam solar radiation) and has improved the predictability compared to Ft. Lauderdale lysimeter studies by Stephens and Stewart. The scan of direct-beam duration (area of cloud free surface) is a remote sensing application which would be useful in applying the Blaney-Criddle technique to large areas of uniform vegetation.

Stephens and Stewart (1963) developed insolation relationships that can be compared with predicted evaporation rates.

### 5.6.2.3 Materials and Methods

Micrometeorological measurements, evaporation chamber measurements, and a vegetation survey were conducted for use in remote sensing ET calculations, and to verify remote sensed data.

#### 5.6.2.3.1 Ground Truth Instrumentation and Measurements

A site was chosen in an extensive pasture land use area in the Taylor Creek Watershed, Okeechobee County, Florida. Features of this site will be shown in maps of thermal images later in this report.

An 11-m instrumentation tower (Figure 5.6-1) was located 100 m NE of a concrete block house in a field of Pangola grass. Air temperature profiles were measured at heights of 0.3, 0.6, 1, 2, 5, and 10 m with copper-constantan thermocouples between unasperated, naturally-ventilated, white parallel disc radiation shields. Incoming global solar radiation (0.3 to 3  $\mu$ m) was measured with an Eppley<sup>1</sup> pyranometer and reflected solar radiation was measured with an inverted Eppley pyranometer (Model No. B-48). Net radiation was measured with a Swissteco net radiometer (Model No. S-1). Another Swissteco net radiometer was mounted with a bottom cover to shield upward radiation. All these radiation instruments were mounted at a height of 2 m. The net radiometers were slowly flushed with dry air that flowed from a bottle of "Drierite" (or Magnesium Perchlorate).

Wind speed and direction were measured at a height of 10 m with an R.M. Young cup anemometer and vane system (Model No. 6405). Dewpoint temperature was also recorded at this height with an Atkins dew cell (Model No. 26432-09).

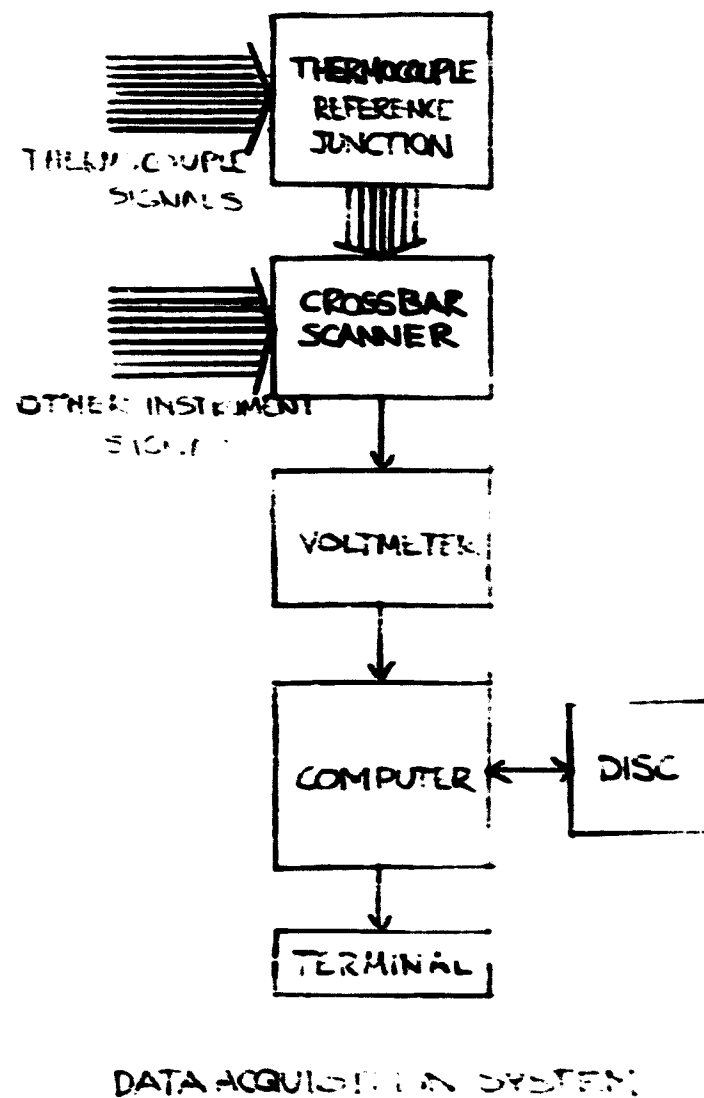
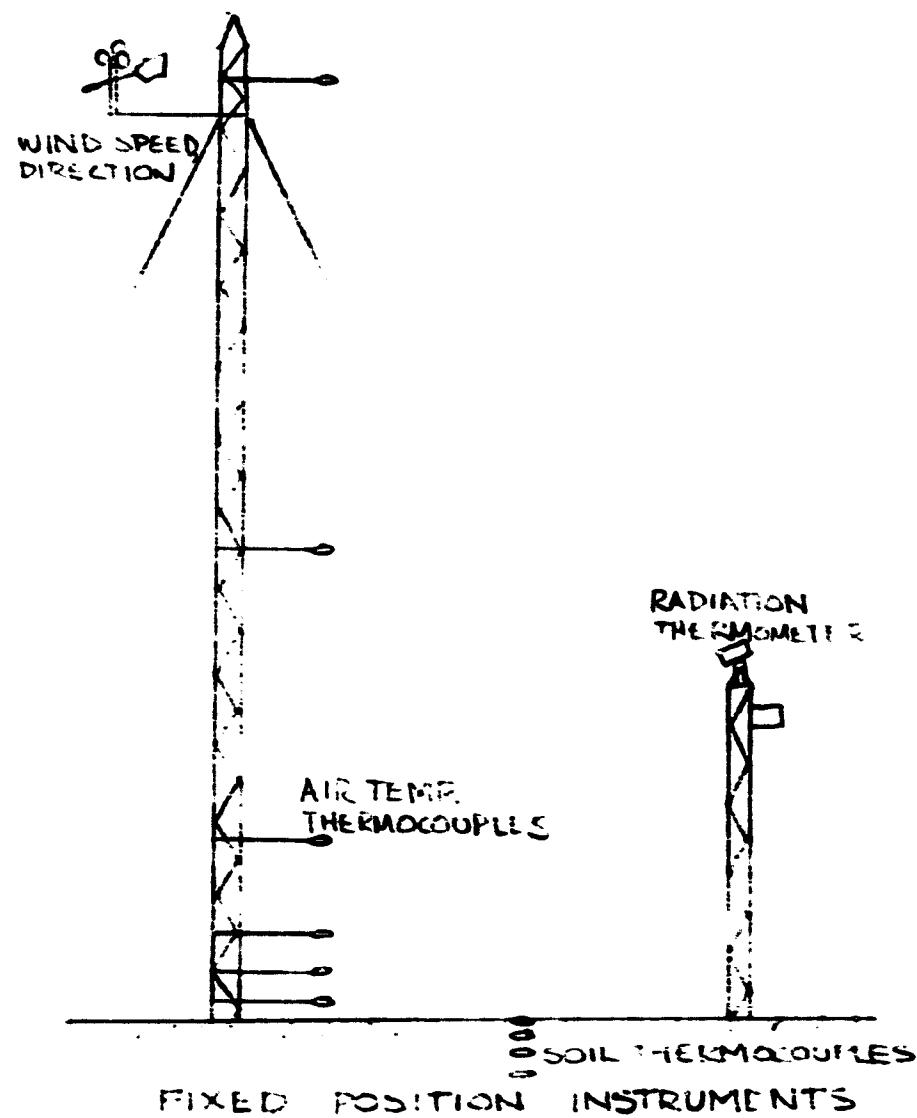
At 40 m west from the main tower, another 6-m tower was erected which held a precision radiation thermometer (Barnes Model No. PRT-5) at the top. The precision radiation thermometer (PRT) was aimed eastward at a point on the ground about 20 m away near a location where soil thermocouples were located. Soil temperatures were measured at 0, 2.5, 5, 10, 25, and 50 cm depths at 6 locations about 2 m apart.

Access tubes for a neutron soil moisture probe were located near the base of the main tower. A Troxler neutron moisture gage (Model No. 1651) was used to obtain soil moisture as a function of depth. During the experimental phase, soil samples were also taken to determine soil moisture by volume gravimetrically. Water table elevation at this site was measured with a Stevens Type F recorder. Four instrument shelters were placed at several widely spaced locations on the Taylor Creek Watershed to house max-min thermometers.

---

<sup>1</sup>Mention of proprietary products is for the convenience of the reader only, and does not constitute endorsement or preferential treatment by the University of Florida or NASA.

230



- 5.6-19 -

Figure 5.6-1. Instruments and data acquisition system.

Profile Bowen ratio inputs (air temperature and humidity) were measured with a vertical traversing sensor system (Figure 5.6-2). The sensors consisted of a fine wire (20-mil) (or 0.020") thermocouple for air temperature and a Brady Array sensor (Thunder Scientific Model No. BR 101B) for humidity (see Dill et al., 1978). This apparatus consisted of naturally-ventilated sensors mounted between two 15-cm diameter radiation shields. The sensor and shield assembly was mounted on a swivel that was attached to a V-belt that was driven by an electric motor. Each cycle of sampling of signals was triggered during each up and down traverse of the sensors by a 1.5-v pulse through a microswitch attached to the bottom of the support assembly. The signal sampling times were controlled by a data acquisition system (Figure 5.6-3). Data were sampled at the bottom of the vertical traverse, and at 1/3 height, 2/3 height, and at the top of the traverse. Additional samples were collected at the 2/3 height, and 1/3 height as the sensor system descended.

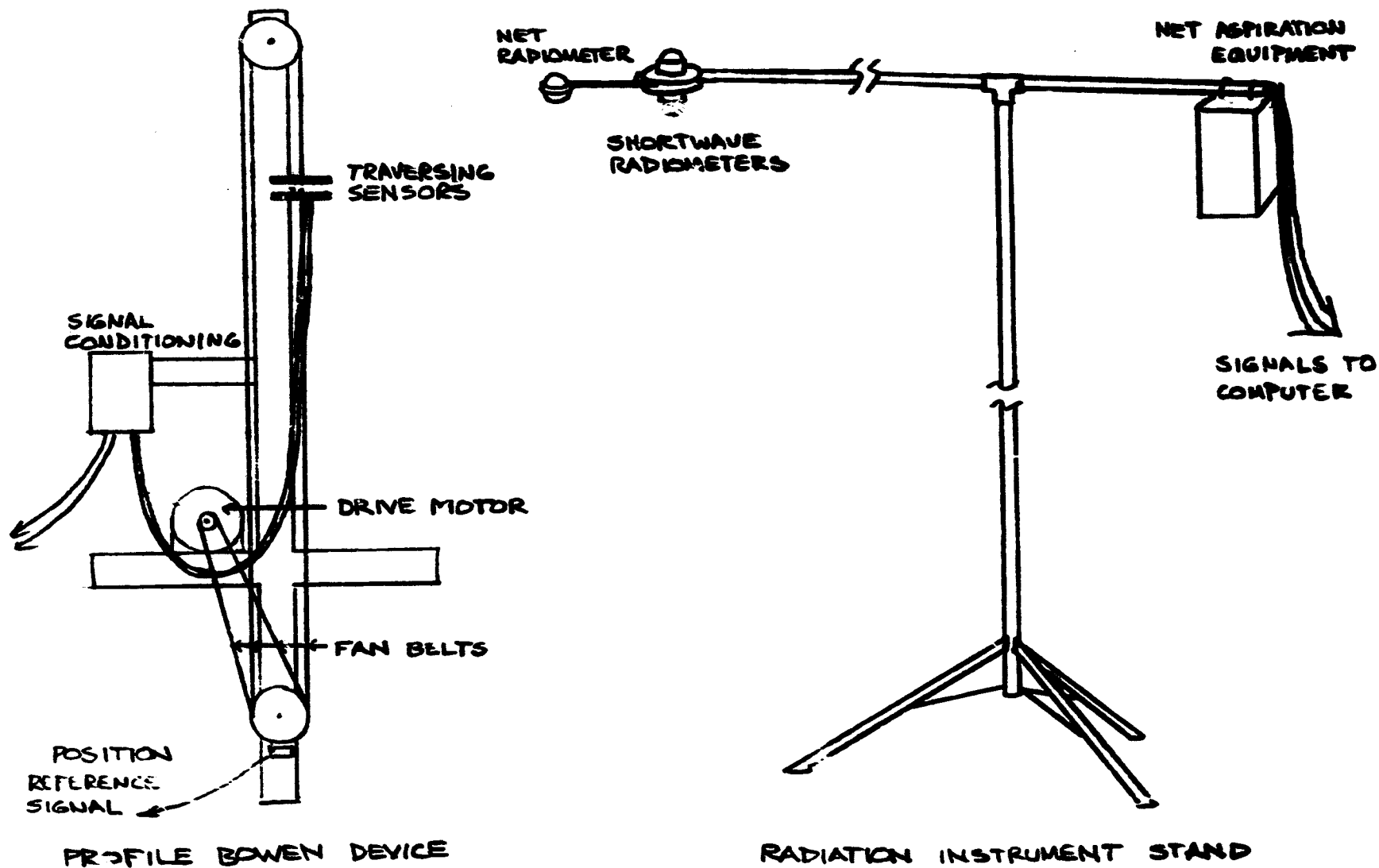
Additional routine data collected on the Taylor Creek watershed by the USDA-SEA-AR Soil and Water Unit at Ft. Pierce were rainfall and water table at 8 locations (identified as Williams, 1 through Opal, 7 on Figure 5.6-4 with the eighth location not shown), and pan evaporation and hygrothermograph records at site Raulerson, 3.

Micrometeorological data were collected and recorded by a system controlled by a Hewlett-Packard 2100 computer with 32 K memory, configured with a HP Model No. 7901A disc and HP Model No. 12960A disc drive system. The system consisted of a thermocouple reference junction system for all soil and air thermocouples. These signals, plus all other signals fed into terminal board and thence into a HP 2911A crossbar scanner. The crossbar scanner and crossbar scanner control panel were program-controlled by the HP 2100 computer. Signals were taken from the crossbar scanner through a HP 2402A digital volt meter (DVM) to the computer. Output was programmed to appear on a Texas Instruments (TI Silent 700) thermal line printer and/or the disc. The disc was used both for program storage and for data record storage.

The programs went through several stages of development. The final version consisted of a master START program which scheduled several other programs (e.g., BOWEN, for starting and executing the Bowen ratio system to compute sensible, latent (evapotranspiration), and soil heat flux on a 1/2 hour cycle, WEATH, for 1/2 hours data summaries, and WEAT3 for instantaneous summaries at 10-minute intervals beginning 5 min. after the hours). These program listings are available upon request.

#### 5.6.2.3.2 Aircraft Instrumentation and Measurements

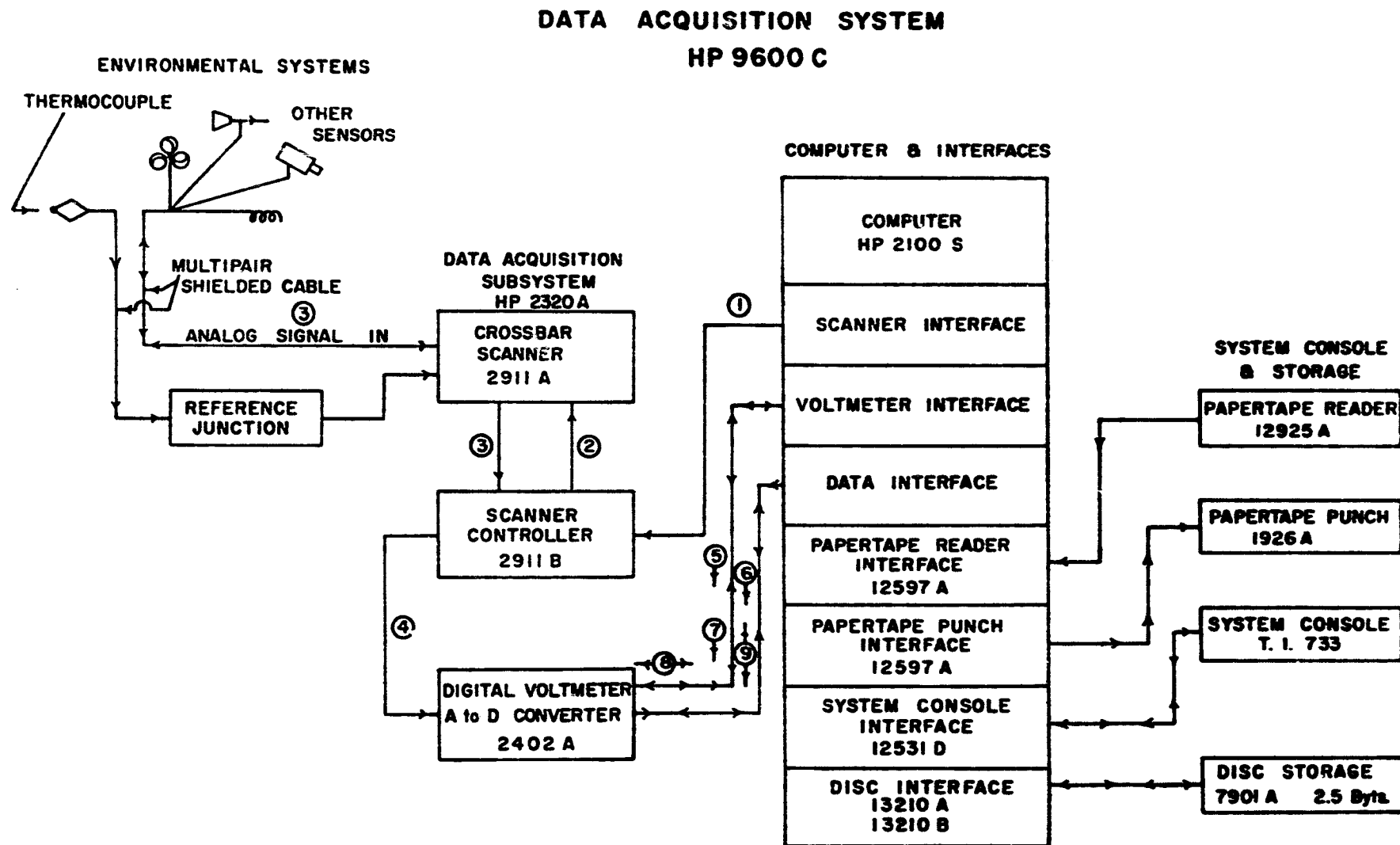
A NASA Modified Beechcraft C45H aircraft, fitted with a Multiple Spectral Sensor and thermal infrared scanner (MSS/IR), was used to obtain images along three to six east-west flight lines across the upper part of the Taylor Creek Watershed. When the aircraft flew at an altitude 4,500 ft., six flight lines were required, and when the aircraft flew at 8,000 to 9,000 ft., three flight lines were used. These flight lines were designated R-1, R-2, R-3, R-4, R-5, and R-6 for the 4,500 ft. altitudes and B-1, B-2, and B-3 for the 8,000 to 9,000 ft. altitudes as shown in Figure 5.6-4.

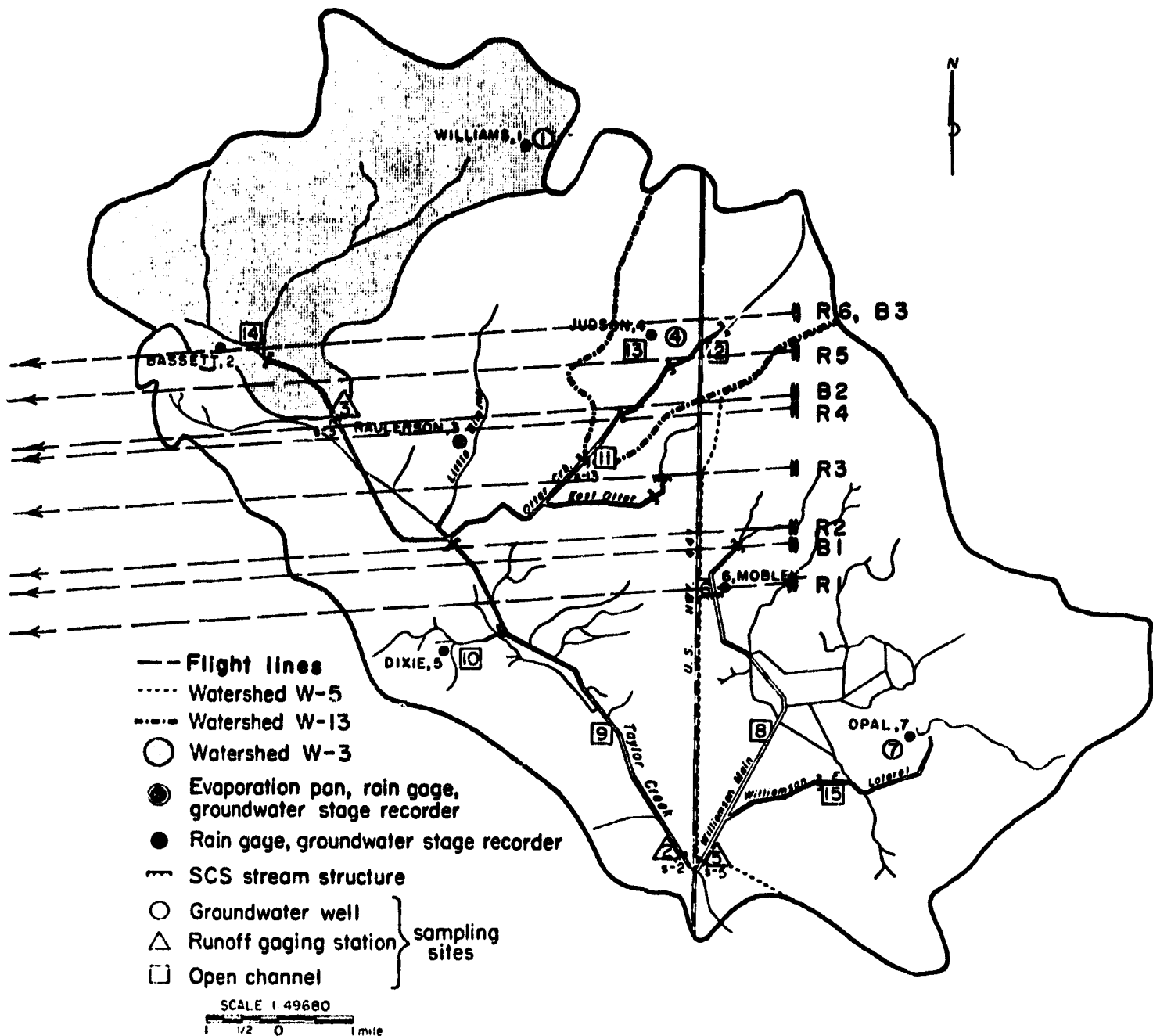


- 5.6-21 -

Figure 5.6-2. Portable instruments to be used over different surfaces.

Figure 5.6-3. Micrometeorological data acquisition system.





## UPPER TAYLOR CREEK

Figure 5.6-4. Map of Upper Taylor Creek Watershed W-2 showing watershed boundaries and locations of rain gages, groundwater stage recorders, and the evaporation pan. The micrometeorological ground truth measurement site was between Judson, 4, and U.S. Highway 441. The eastern end of the flight lines are overlaid (see Tables 1 and 2).

Flights were made in the Spring (April) and in the Fall (October) of 1978. In April 1978, 5 periods were flown. Table 5.6-1 summarizes these dates, times, and conditions, and relevant flight line data. Part of these surface temperature data that were obtained were printed on 70-mm color-coded film strips. The total temperature ranges and increments within each color code are also shown in Table 5.6-1.

On May 11, 1978, color infrared photography was flown by the Florida Department of Transportation Topographic Office along Flight lines B-1, B-2, and B-3. Table 5.6-2 summarizes the flight line information.

On October 16-17, 1978, three more flights were made with the NASA aircraft with the MSS/IR scanner (2326 to 0013 EST at 8000 ft.; 0932 to 1022 EST at 8000 ft.; and 1215 to 1335 EST at 3500 ft.). Color-coded film strips were obtained with the same temperature range as the records with temperature increments of 6°F. These aircraft scanner data are summarized in Table 5.6-1 also.

#### 5.6.2.3.3 Other Ground Measurements

On April 27 and 28, measurements of evapotranspiration from bermudagrass sod and Pangolagrass sod were obtained in the same vicinity of the meteorological tower by using an enclosed chamber technique similar to that of Reicosky and Peters (1977). A Mylar film chamber covering 1 m<sup>2</sup> in area and about 1 m<sup>3</sup> in volume was used (Jones and Boote, 1978). The chamber had a fan mounted within it to give rapid circulation inside. The base of the chamber was about 6 inches in height and was designed separately so that several bases could be placed over the sod. The bases had a narrow edge of angle metal so that it could be set into the soil or sod so that no mass-flow leaks around the bottom edges would occur. Both the top part and the base of the chamber had flat horizontal surfaces along the edges with rubber gaskets for seals. When the top section was placed on the bottom section, they could be rapidly sealed by clamping with three "vise-grip" pliers.

Two base sections were placed on bermudagrass sod and two base sections were placed on Pangolagrass sod. Evapotranspiration rates were determined by circulating air from the chamber through an EG & G Model 880 dewpoint hygrometer to measure dewpoint temperature continuously. Air temperature was monitored with a Doric 400A digital thermocouple thermometer, and recorded periodically. Since temperature and humidity rapidly rise within the chamber, the rate of evaporation was calculated from the initial time rate-of-change in the dewpoint temperature detected by the dewpoint hygrometer. The rising air temperature due to the rising plant temperature within the chamber would tend to increase the leaf-to-air vapor pressure deficits, but the rising vapor pressure as water evaporated from leaves and soil would tend to decrease the vapor pressure deficits. (These two effects would be opposite and hence be partly compensating in the first few seconds after the chambers were sealed in place.)

No chamber evaporation data were taken during the October 17 flights, but some data were taken later on October 26.

- 5.6-25 -

Table 5.6-1. Taylor Creek Flight Line IR Scanner Summary

Scanner Record									
Flight Line	Start Time (EST)	End Time (EST)	BB1 (°F)	BB2 (°F)	Alt. (Ft.)	Head	Gnd. Speed (Knots)	Temp. Range (°F)	Temp. Incr. (°F)
<u>April 26, 1978</u>									
R1	1142	1146	70°	106°	4500	090°	155	---	---
R2	1152	1159	70	106	4500	270°	125		
R3	1208	1213	70	106	4500	090°	152		
R4	1219	1226	70	106	4500	270°	125		
R5	1228	1234	70	106	4500	090°	154		
R6	1240	1244	70	106	4500	270°	125		
B1	1404	1408	70	106	8000	090°	150	70°-94°	4°
B2	1415	1422	70	106	8000	270°	115		
B3	1432	1435	70	106	8000	270°	115		
B1	1548	1553	60	96	8000	090°	150	60-84	4
B2	1558	1605	60	96	8000	270°	125		
B3	1610	1612	60	96	8000	090°	150		
<u>April 28, 1978</u>									
B1	0020	0025	30	66	8000	090°	150	---	---
B1	0032	0039	30	66	8000	270°	115		
B2	0048	0053	30	66	8000	090°	130		
B3	0102	0106	30	66	8000	270°	110		
R1	1110	1116	72	108	4500	090°	135	72-90	3
R2	1119	1125	72	108	4500	270°	132	90-108	3
R3	1128	1134	72	108	4500	090°	140	(Two strips)	
R4	1139	1144	72	108	4500	270°	136		
R5	1152	1158	72	108	4500	090°	132		
R6	1222	1225	72	108	4500	270°	135		
<u>October 16/17, 1978</u>									
B1	2326	2333	36	72	8000	090°	120	36-72	6
B2	2348	2355	36	72	8000	090°	120		
B3	0007	0013	36	72	8000	090°	120		
B1	0932	0942	54	90	8000	090°	125	54-72	3
B2	0958	1004	54	90	8000	270°	125	72-90	3
B3	1017	1022	54	90	8000	270°	125	(Two strips)	
R1	1215	1224	64	100	3500	090°	125	64-82	3
R2	1238	1244	64	100	3500	270°	140	82-100	3
R3	1247	1255	64	100	3500	090°	120	(Two strips)	
R4	1257	1303	64	100	3500	270°	125		
R5	1326	1335	64	100	3500	270°	130		
R6	1318	1322	64	100	3500	270°	130		

Table 5.6-2. Taylor Creek Flight Line Color Infrared Photography Summary.<sup>1/</sup>

Flight Line	Start Time (EST)	End Time (EST)	Drift	Flight Direc- tion	Picture No.		Frames	Expo- sure Time	Stop No.
B1	11:15	11:18	3R	WE	346	355	10	700	4
B2	11:24	11:29	3W	EW	356	366	11	700	4
B3	11:32	11:34	3R	WE	368	371	4	700	4
B2	11:37	11:42	3W	EW	372	383	12	700	4

<sup>1/</sup> Aircraft-42W, Altitude - 9,000 ft., Scale - 1" = 1500', Film type -  
Kodak 2443-214-1. Date - May 11, 1978.

On May 22-23, a vegetation survey was made of the area around the meteorological test site after thermal images were available for comparison. A vegetation survey was also made in another area containing a citrus grove.

On October 17, a Raytek Model LC814 radiation thermometer mounted at an angle on a truck was used to scan temperatures along road traverses (e.g., Chen, 1979) from east to west along the general path of the flight lines.

#### 5.6.2.4 Data Analyses

Ground truth data and thermal infrared scenes were analyzed to show the application of remote sensed data to evapotranspiration calculations.

##### 5.6.2.4.1 Ground Truth Micrometeorology

Ground truth measurements of meteorological elements and the Bowen ratio were made in the spring and in the fall on October 17-20, October 25-27, and November 2-3. Several interruptions in the records occurred during the early days of the data, and the quality of the data are described in Table 5.6-3. The Bowen ratios (ratios of sensible heat flux to latent heat flux) were computed on about a 21-min schedule during the spring. However, radiation averages and Bowen ratio calculations were eventually standardized on 30-minute periods, so we decided to standardize all the ET calculations on 30-minute periods. Most of the radiation data were for 30-minute periods except as indicated in Table 5.6-3 for the spring data. The Bowen ratio values for each 30-minute period were chosen to closely correspond (fit within the 30-min radiation average period) or were interpolated from adjacent values to give 30-minute values for use in computing ET.

The soil heat flux density part of the data reduction program in the field gave erroneous values during April and May, so we had to extract that data from 15-min interval or 30-min interval printouts of soil temperature. We found that there was some random variation in the soil temperature at 50 cm (the deepest level), presumably due to slight variation in the reference temperature controller. Therefore, we first set the soil temperature at 50 cm to a constant value (the average) throughout a daytime period, and adjusted all other temperatures in each profile up or down accordingly. Then we applied the trapezoid rule to integrate the internal energy changes in the soil profile, using a volumetric heat capacitance of  $1.26 \text{ J/cm}^3/\text{°C}$  ( $0.3 \text{ cal/cm}^3/\text{°C}$ ) for the soil (Myakka fine sand). The change in internal energy from one measurement to the next represented the soil heat flux density. There was still a lot of scatter in the resulting daily pattern of soil heat flux density (not related to radiation variations), so we then adjusted temperature differences of the bottom two points of the profile to give null heat flux between those two depths, and then recomputed soil heat flux density. The procedure was not totally justified, since from the data there appeared to be a small amount of upward (negative) heat flux in the early morning hours and a small amount of downward (positive) heat flux by mid-afternoon; however, it did smooth the daily patterns.

Soil heat flux densities were plotted as a function of time of day, and smooth curves drawn through the data, with consideration given to radiation load conditions. Values from these smooth curves were used for computing ET from the radiation balance equation.

Table 5.6-3. Taylor Creek Evapotranspiration Data. Summary of Radiation and Bowen Ratio Measurement Periods.

Date (1978)	Eastern Standard Time <sup>1</sup>			Bowen Ratio <sup>2</sup>
	10-min <sup>3</sup>	15-min <sup>3</sup>	30-min <sup>4</sup>	
Apr 26		1930-2345	0000-1730	none
Apr 27		0000-2000 2330-2345	1500-2329	1256-1424, 1616, 1734.
Apr 28		0000-1715	0001-0100 0900-1530	0931, 1053-1137, 1222-1531, 1625-1646.
Apr 29		0915-0945 1145-1915	1200-1900	0929-0950, 1239-1301, 1338-1505, 1547-1843.
Apr 30		0700-1100 1145-1200 1345-2345	0700-1100 1630-2330	0735-1057, 1204, 1419, 1905.
May 1		0000-2230	0000-1330 1430-2200	0754-1310 1351-1907.
May 2	0825-1205 1235-1755 1825-1935 2015-2355		0000-0800 0800-1930 2030-2330	0803-1249, 1411-1741, 1822-1904.
May 3	0005-1125		0000-1030	0839-1024
Oct 17	0925-2355		0930-2330	1000-1330
Oct 18	0005-2355		0000-2330	1330, 1430, 1530, 1630.
Oct 19	0005-2355		0000-2330	none
Oct 20	0005-1805		0000-1800	0900-1700
Oct 25	1135-2355		1130-2330	1330-1700
Oct 26	0005-1755		0000-2330	0730-1630
Oct 27	0805-1555		0000-1600	0730-1600
Nov 2	0805-1725		0900-2330	0900-0930, 1230, 1530, 1730.
Nov 3	0805-1705		0000-1700	0830-1700

<sup>1</sup> Times on April 30-May 3 and October 17-October 27 were converted from Eastern Daylight Saving Time to Eastern Standard Time.

Table 5.6-3. Taylor Creek Evapotranspiration Data. Summary of Radiation and Bowen Ratio Measurement Periods.

Page 2

- <sup>2</sup> Bowen Ratio data are indicated for values at the end of a 21-minute period for the April and May data, and at the end of a 30-minute period for the October and November data.
- <sup>3</sup> All 10-minute and 15-minute radiation data were instantaneous, 1-scan values.
- <sup>4</sup> 30-minute radiation was printed out as instantaneous, 1-scan values on April 26, as 1-minute averages at the end of 30-minute intervals on April 27-May 1, and as 30-minute averages of scans taken every 2 minutes on May 2-3 and October 17-November 3.

The above smoothing procedure was necessary because of lack of precise enough control of the thermocouple reference system because of electronic "noise" in obtaining the low-level signals, and because of the small temperature changes in the 15-min to 30-min data collection periods.

Wind speed at 10 m, air temperature at 2 m, soil surface temperature, and solar radiation data were also extracted at 30 minute intervals and converted to SI units.

#### 5.6.2.4.2 Aircraft Thermal Infrared Scenes

The original plan was to use several of the selected flight line thermal scenes from film strips to predict distribution of surface temperatures and distribution of contributions to watershed evapotranspiration. However, we found considerable distortion in the thermal images when they were compared with the surface maps. There appeared to be variation in ground speed across the flight lines, particularly when the flight directions were reversed on adjustment lines (e.g., 270° vs 90° heading). Also, we found a turning distortion toward the east end of flight line during one of the daytime passes.

The above distortions in the images made it difficult to "cut and paste" a continuous scene together during one of the flight periods. We next tried to transpose the color-coded temperature intervals onto another map, but this process appeared to be highly subjective and tedious. Therefore, we decided to use two smaller test scenes from Image 100 photographs that were obtained for the 1110 to 1225 EST flights on April 28 (a pasture scene including the ground truth site), and the 1404 to 1435 EST flights on April 26 (a scene including a citrus grove, scattered areas of trees with dense and sparse stands, and pastures).

The April 28 pasture scene was obtained about 1222 to 1225 EST, and the April 26 citrus grove scene was obtained about 1415 to 1422 EST. The scenes were color-coded by the Image 100 to cover cold-to-hot color scales of orange, blue, yellow, pink, aqua, and black, with tan being the out-of-range color code for the warm side. The temperature increment for the April 26 citrus grove scene was 6°F, with ranges of 70-76, 76-82, 82-88, 88-94, 94-100, 100-106, and > 106°F for the above color code sequence, respectively. The temperature increment for the April 28 pasture scene was 6°F, with ranges of 72-78, 78-84, 84-90, 90-96, 96-102, 102-108, and > 108°F for the above color code sequence, respectively.

Tracings were made of the areas represented by each color code, and areas were determined using a Hewlett-Packard Model No. 9864A digitizer system with Model No. 9830A Programmable Calculator. The actual ground area covered by each scene was determined by locating landmarks on U.S. Geological Survey 7 1/2 minute topographic maps, and determining the area within the borders. The area was 13.5 km<sup>2</sup> (5.21 mi<sup>2</sup>) for the April 26 citrus grove scene (flown at 8,000 ft.) and 3.82 km<sup>2</sup> (1.47 mi<sup>2</sup>) for the April 28 scene (flown at 4,500 ft.). Table 5.6-4 shows the actual and relative areas under each temperature range of each scene.

Table 5.6-4. Color Code and Percent Land Area for Surface Temperature Ranges from Figure 5.6-5 and Figure 5.6-6. Air Temperature at 1.5 m was 25.6°C on April 28 and 24.3°C on April 26.

APRIL 28, 1978. 1222-1225 EST				APRIL 26, 1978. 1432-1435 EST			
<u>PASTURE SCENE, 3.82 km<sup>2</sup></u>				<u>CITRUS GROVE SCENE, 13.5 km<sup>2</sup></u>			
<u>Color</u>	<u>°F</u>	<u>°C</u>	<u>% Area</u>	<u>°F</u>	<u>°C</u>	<u>% Area Tall</u>	<u>% Area Pasture</u>
Tan	>108	>42.2	23.3	>106	>41.1	0	0
Black	102-108	38.9-42.2	24.2	100-106	37.8-41.1	-	0.3
Aqua	96-102	35.6-38.9	25.1	94-100	34.4-37.8	-	10.8
Pink	90-96	32.2-35.6	16.5	88-94	31.1-34.4	-	13.9
Yellow	84-90	28.9-32.2	6.6	82-88	27.8-31.1	12.9	19.8
Blue	78-84	25.6-28.9	2.2	76-82	24.4-27.8	14.6	3.2
Orange	72-78	22.2-25.6	2.1	70-76	21.1-24.4	11.8	1.1
PK <sup>1</sup>			-	88-94	31.1-34.4	4.7	-
Y/P <sup>2</sup>			-	88	31.1	-	6.9

<sup>1</sup> PK is an unresolved mixture of small areas of Aqua, Pink, and Yellow that average within the Pink code temperature interval.

<sup>2</sup> Y/P is an unresolved mixture of borders along the Yellow-Pink temperature intervals that average near the cutoff temperature (88°F for the April 26 scene).

### 5.6.2.5 Results

Results of vegetation cover analyses, and ET by the Bowen ratio and Chamber Methods were developed and then used and compared with predictions of ET based on remote sensed  $T_s$ .

#### 5.6.2.5.1 Vegetative Cover Analysis

Two dissimilar areas were chosen for study of plant cover. One area (primarily in Section 22, T. 35S., R. 35E.), the area in which the meteorological towers and instrumentation were located, was primarily improved grass pastures used by grazing dairy cattle or improved grass utilized as a hay crop (Figure 5.6-5). The primary agricultural use in the areas was for dairying. The other area (primarily in Section 36, T. 35S., R. 34E.) in which some detailed observations of plant life were made was mostly in a citrus grove (Figure 5.6-6). Figures 5.6-5 and 5.6-6 are thermal images from an aircraft-mounted thermal scanner (8-14  $\mu\text{m}$ ) flown at heights of 1.36 km and 2.43 km, respectively. The thermal data of Figure 5.6-5 were obtained at 1222-1225 EST on April 28, 1978. The wind speed was 4.4 m/sec, the air temperature was 26.1°C, and the relative humidity was 59% (dew pt. 11.1°C). The thermal data of Figure 5.6-6 were obtained at 1432-1435 EST on April 26, 1978. The wind speed was 12.1 m/sec, the air temperature was 24.4°C, and the relative humidity was 59% (dew pt. 10.6°C). These measurements were made at a height of 10 m. The temperature code of the figures is shown in Table 5.6-4. Vegetation surveys were made on May 22-23, 1978, after thermal images were available for guidance.

Figure 5.6-5 shows U.S. Highway 441 running north-south through the image. Otter Creek, a tributary of Taylor Creek, runs northeast-southwest in the bottom right of the image. Figure 5.6-6 shows State Route 68 running east-west near the top of the image. Taylor Creek runs from northwest to southeast along the western edge of the citrus groves.

The effects of high dairy cattle population densities and associated buildings and facilities are easily seen in the thermal imagery of McArthur Dairy No. 1 indicated in Figure 5.6-5. Irregularly-shaped areas, near barns where heavy cattle traffic had eliminated plants, appear the warmest (right center of Figure 5.6-5). A mixture of sand and partially decomposed manure made up the surface and appeared greater than 42.2°C in the thermal scene. The staging area near the milking parlor had little or no vegetation and temperatures were in the highest range in those areas.

In areas of vegetation, the physical condition of a given species seemed to be differentiated in the thermal imagery. For example, Field #2 (Figure 5.6-5) is primarily Pangola (Digitaria decumbens) except for the west end which was primarily Bermuda grass (Cynodon species). Field #1 was also Pangola but was much warmer due to the poor physical condition of the grass.

Field #1 had apparently been cut for hay and then grazed heavily prior to April 28, 1978. It showed little spring growth and a high percentage of dead grass stubble. Field #2 of the same species had been cut for hay but had not been grazed. It was in a healthy growing condition and appeared cooler on the thermal image (Figure 5.6-5).



Figure 5.6-5. Infrared image of pasture scene in Taylor Creek Watershed, April 28, 1978, at 1222-1225 EST. Temperature codes are given in Table 5.6-4. Photographed from Image 100.

ORIGINAL PAGE IS  
OF POOR QUALITY

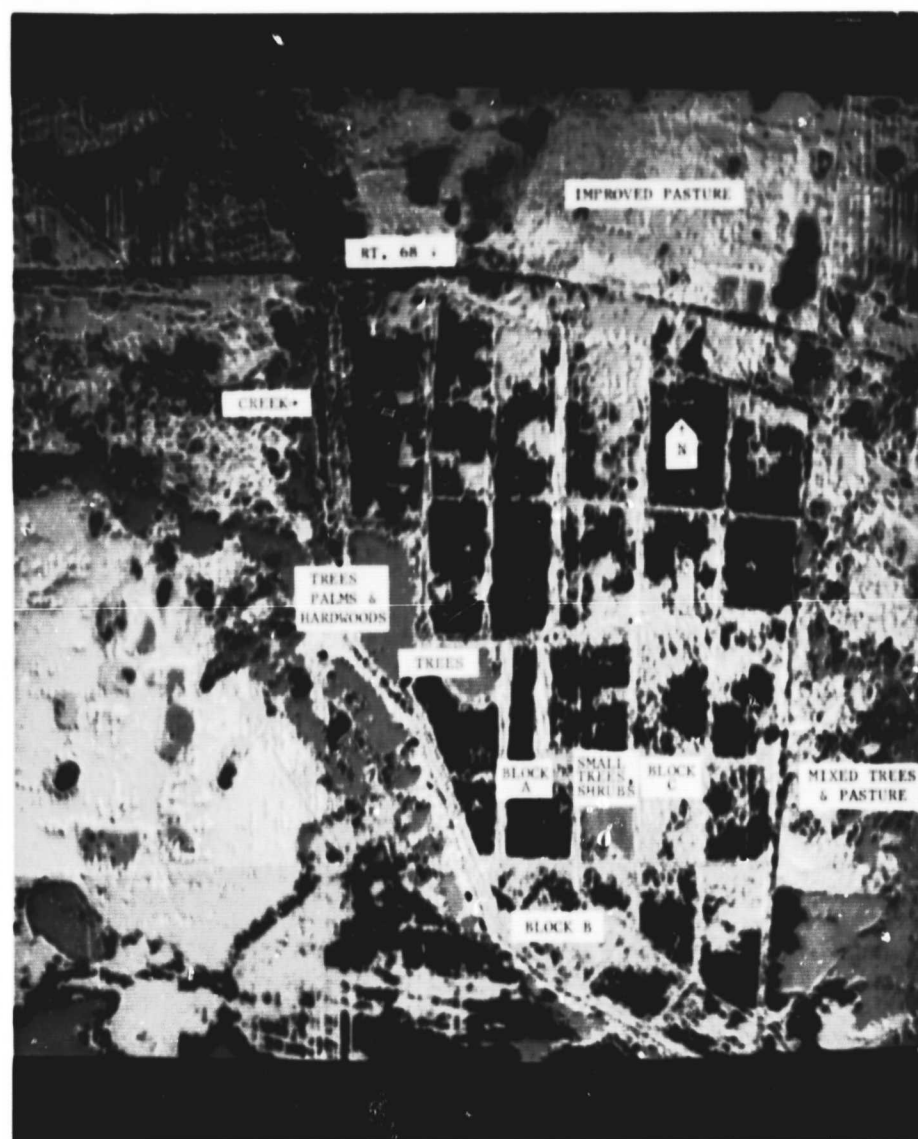


Figure 5.6-6. Infrared image of citrus grove scene in Taylor Creek Watershed, April 26, 1978, at 1432-1435 EST. Temperature codes are given in Table 5.6-4. Photographed from Image 100.

The Bermuda grass in the southwest end of Field #2 appeared cooler than the adjacent Pangola in the same field. This difference may be due in part to the more rapid spring growth of the Bermuda grass.

Field #2 also contained a depression with soil type of Placid fine sand (typical of "flag ponds" or "bayheads") in this area on the southern edge along the entrance road (Figure 5.6-5). Vasey grass (Paspalum urvillei Stuev) was the predominant species around this wet area with some sedges also present. Sedges were dominant on the southern side of the road around the depression. The eastern edge of this field (along Rt. 441) contained Vasey grass and an unknown woody shrub in a strip parallel to the highway.

Field #3 was a heavily grazed mixture of white clover (Trifolium repens), Pangola grass, carpet grass (Axonopus affinis), and Bermuda grass with a few other widely scattered species. Some of the variability in the thermal representation of this field was likely caused by higher soil moisture in slightly lower-lying areas and by heavily grazed areas. About 1.5 cm of rain had fallen on the watershed on April 23-24, 1978.

Fields 4, 5, 6, and parts of 7 were rather heterogeneous. They contained patches of grass interspersed with broadleaved weeds and thinner stands of grass. South and east of these fields was a wet area with woody shrubs as the primary ground cover.

The primary species in Field #4 and Field #6 (lying to the east parallel and adjacent to U.S. Highway 441.) was Bermuda grass which was represented as 28.6-31.1°C in the thermal scene. Patches of Bahia grass on the east side of Field #4 appeared to be warmer. Rough pigweed (Lachnanthes caroliniana) was present primarily on the west side.

Field #5 was similar to Field #4. Significant features were a small, dry depression with little vegetation created by cattle traffic around a watering trough. This area appeared as a circular area ranging from 38.9 to > 42.2°C on Figure 5.6-5. The southeast corner contained some woody shrubs. The eastern boundary of this field was a drainage ditch that no longer receives water from the barn area.

The central part of Field #7 was dense Bermuda grass sod; the southeast end progressed into a mixture of grasses and broadleaved weeds with ground cover becoming thinner.

Field #8 was a dense sod composed primarily of Bermuda grass, with a little Pangola. This turf resembled a wellkept lawn and was very homogenous. The western vegetated part had some sedges. A pond about midway on the southern boundary shows up in Figure 5.6-5 as an ellipse with a temperature of 22.2 to 28.9°C. A drainage ditch forms the northern boundary and is represented as a line (22.2 to 28.9°C) running along the middle to the eastern edge of Figure 5.6-5. At the western end of this ditch, there was culvert running into a lagoon used for effluent from a milking parlor. The lagoon shows up as an orange elongated rectangle running northwest to southeast.

Other fields in Figure 5.6-5 were given only a cursory examination from the roadside. The irregularly-shaped tan area at the top of the figure represents cattle staging areas for McArthur Dairies Barn #7 (now Barn #4). The

field to the south was Bahia and Bermuda grass. The field southeast of Barn #7 was heavily grazed, composition not determined. The field to the northeast of Barn #7 was Bahia and white clover that was not heavily grazed.

In Figure 5.6-6, thermal imagery of complex vegetative canopies associated with citrus and rangeland is shown. Taylor Creek forms the western through southern boundary of the grove, the creek forming an arc from northwest, where it flows under State Route 68, to the southeast corner. Areas where dense native tree species and woody shrubs were growing proved to be represented on the image as the coolest vegetation ( $21.1-24.4^{\circ}\text{C}$ ). Improved pastures in the surrounding fields were predominantly  $31.1-34.4^{\circ}\text{C}$  with some cooler areas ( $27.8-31.1^{\circ}\text{C}$ ) and some warmer areas ( $34.4-37.8^{\circ}\text{C}$ ). Across the top of Figure 5.6-6, the warm area (aqua) was improved pasture, the intermediate temperature area (pink) was rangeland, and the cool area (yellow) was improved pasture.

In the grove itself, Block A (Figure 5.6-6) was a mature, healthy stand of grapefruit. Vasey grass grew in the low centers between the bedded rows of trees. This block's surface temperatures appeared uniformly cool,  $24.4-27.8^{\circ}\text{C}$ .

Block B was a stand of somewhat smaller, but healthy grapefruit trees. Beds were oriented northeast to southwest. All other beds in the grove were aligned east to west. The block's warmer temperature may be due in part to bed alignment. Smaller trees also contribute to making up a smaller portion of the total surface area of the block.

Block C has a poor stand of orange trees. Some of the trees appeared to be affected by citrus blight, and many of the trees had been removed. Vasey grass made up a large portion of the ground cover. The thermal imagery for this block ( $27.8-31.1^{\circ}\text{C}$ ) would indicate a warmer surface temperature than Block A. Small spots in Block C show up as still warmer, ( $31.1-34.4^{\circ}\text{C}$ ), apparently where many trees were missing.

The trends observed in Blocks A, B and C were borne out in other blocks observed.

We also took a cursory look at some unimproved rangeland species. Palmetto (Serenoa repens) was pervasive. Some grasses indicated from Broomsedge bluestem (Andropogon virginicus L.), wiregrass (Aristida stricta), Vasey grass (Paspalum urvillei). Certainly many others were present.

Within the ecosystems observed and under the environmental conditions at the time of the study, the following may be postulated:

- 1) Physical conditions within a species affects remotely sensed surface temperatures;
- 2) Physical condition of pastures was primarily a management phenomena;
- 3) Physical condition of the grasses greatly contributed to the percentage ground cover;
- 4) Intraspecies differences seem observable, but not as clearly defined as the condition of the species of grass;

- 5) Trees and woody shrubs tend to be cooler than grasses. This may be a biased observation because these plant types were generally located in wetter environments. However, at the same site, citrus trees appeared cooler than Vasey grass. Also, windy conditions on April 26 may have enhanced cooling of the vegetation of trees and woody shrubs by convective cooling to a greater extent than the short grasses.

#### 5.6.2.5.2 ET by Bowen Ratio Method

The daytime cycle of evapotranspiration as determined by the Bowen ratio was computed and drafted as latent heat flux density for the following days: April 26, 27, 28, 29, 30, May 1, 2, October 17, 20, and 26 (Figures 5.6-7 to 5.6-16). These figures also show the daytime patterns of global solar radiation ( $R_i$ ), net radiation ( $R_n$ ), soil surface temperature (Sfc T), and air temperature at 2 m (Air T). Figures 5.6-14, 5.6-15, and 5.6-16 show the daily pattern of wind speed at 10 m (wind). Figures 5.6-17 and 5.6-18 show wind speeds for the spring (April and May) 1978 dates, as well as the whole nocturnal patterns of these parameters for April 26 - May 3.

The daily energy budget summary is given in Table 5.6-5. These data showed that the whole-day Bowen ratio (ratio of sensible to latent heat flux) ranged from 0.32 to 0.76 during the spring days. Three of these days could be classified as "high" (April 26, 27, and May 1), and the others as "low." The days with the higher Bowen ratios also were the days with the higher wind speeds (Figures 5.6-17 and 5.6-18). May 1 was also a day with somewhat lower net radiation due to intermittent cloudiness (Table 5.6-5 and Figure 5.6-18).

Surface-to-air temperature gradients tended to be larger on days with high solar radiation and low wind speed. The soil had very little vegetative cover on it in the spring. Figure 5.6-5 showed a thermal map with Field #2 containing the meteorological instrumentation. This field had Pangola grass that had been cut for hay, and had little spring regrowth. Therefore, the soil surface received a large part of the solar radiation load, and gave high surface temperatures during the day.

Prior rainfall may have influenced the surface-to-air temperature gradients, the soil heat flux, and Bowen ratio to some extent. About 1.5 cm of rain fell on April 24 (Table 5.6-6). We had no micrometeorological data on April 25, but the surface-to-air temperature gradient was somewhat smaller on April 26 than on April 27. Also, the soil heat flux increased from April 26 to April 27, and from April 27 to April 28, as the soil surface dried.

The soil moisture content measurements by the neutron probe method were unreliable. The gravimetric sampling method showed much scatter, but they did show a decreasing soil water content, especially in the upper 5 cm, from April 26 to May 1.

During the nights of April 26-27 and April 27-28, the soil surface temperature remained considerably warmer than air temperature at 2 m. The reasons for this are not clear, but some possible explanations are: (a) a cool front moved in after several days of warmer air with higher solar radiation load, (b) the surface thermocouple was actually below the soil surface sufficiently deep to be kept warm by the soil, (c) the surface thermocouple junction was receiving heat conducted by its own buried wires.

# TAYLOR CREEK APRIL 26, 1978

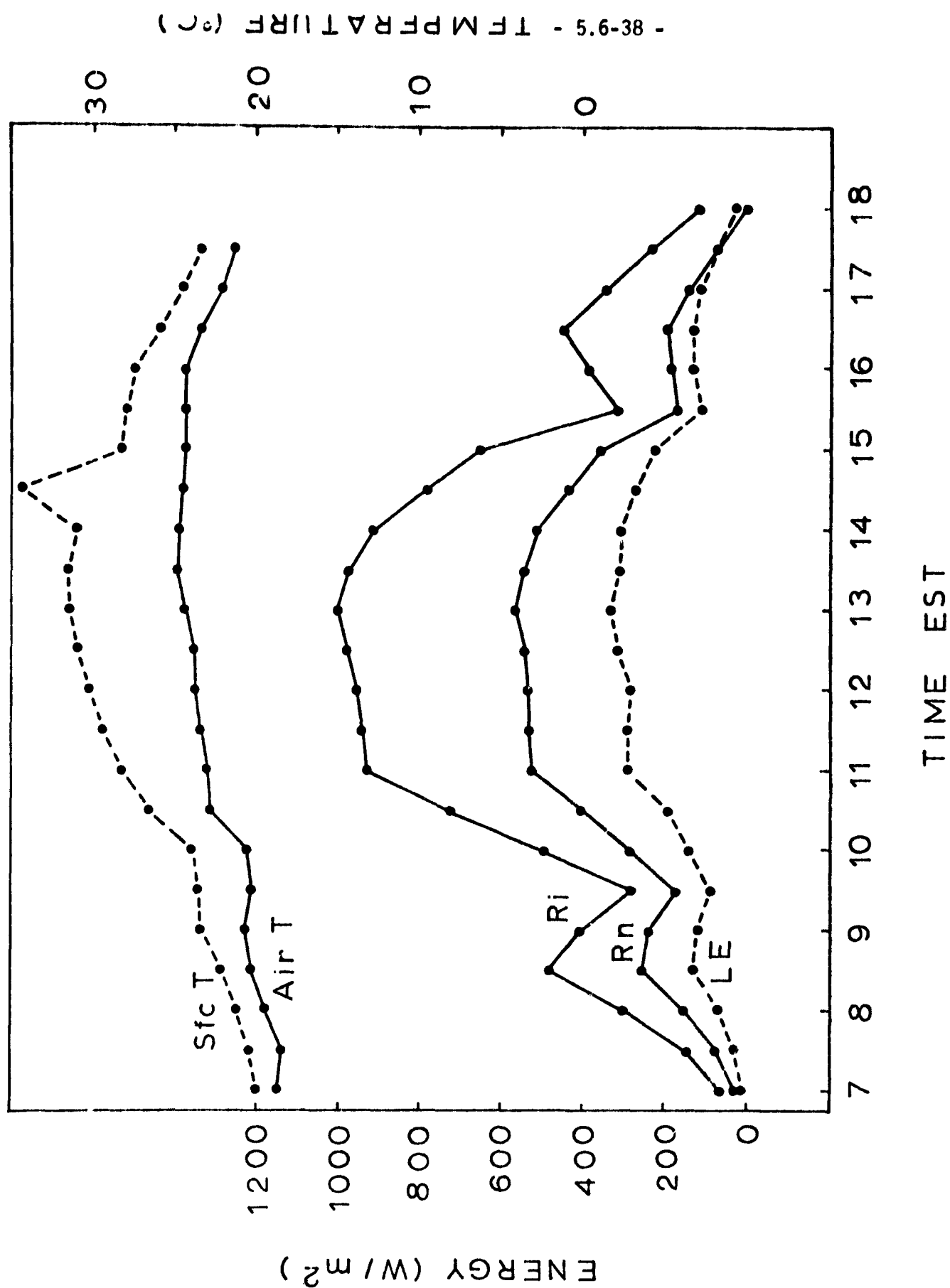


Figure 5.6-7. Daytime course of Bowen ratio ET (latent heat flux density, LE), net radiation (Rn), global solar radiation (Ri), soil surface temperature (Sfc T), and air temperature at 2 m (Air T) over Pangola grass at the beginning of spring regrowth.

# TAYLOR CREEK APRIL 27, 1978

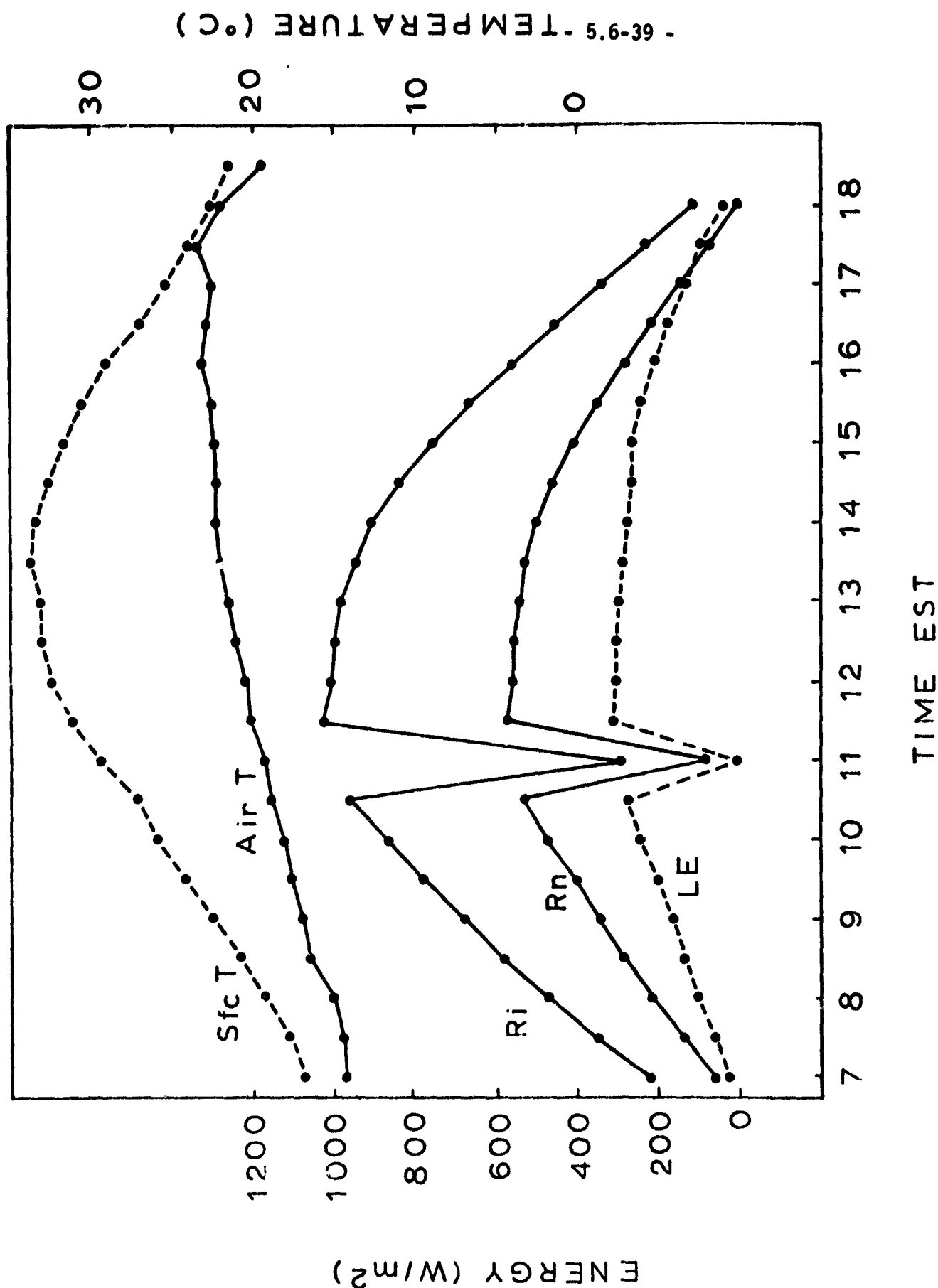


Figure 5.6-8. Daytime course of Bowen ratio ET (latent heat flux density, LE), net radiation ( $R_n$ ), global solar radiation ( $R_i$ ), soil surface temperature ( $Sfc\ T$ ), and air temperature at 2 m ( $Air\ T$ ) over Pangola grass at the beginning of spring regrowth.

# TAYLOR CREEK APRIL 28, 1978

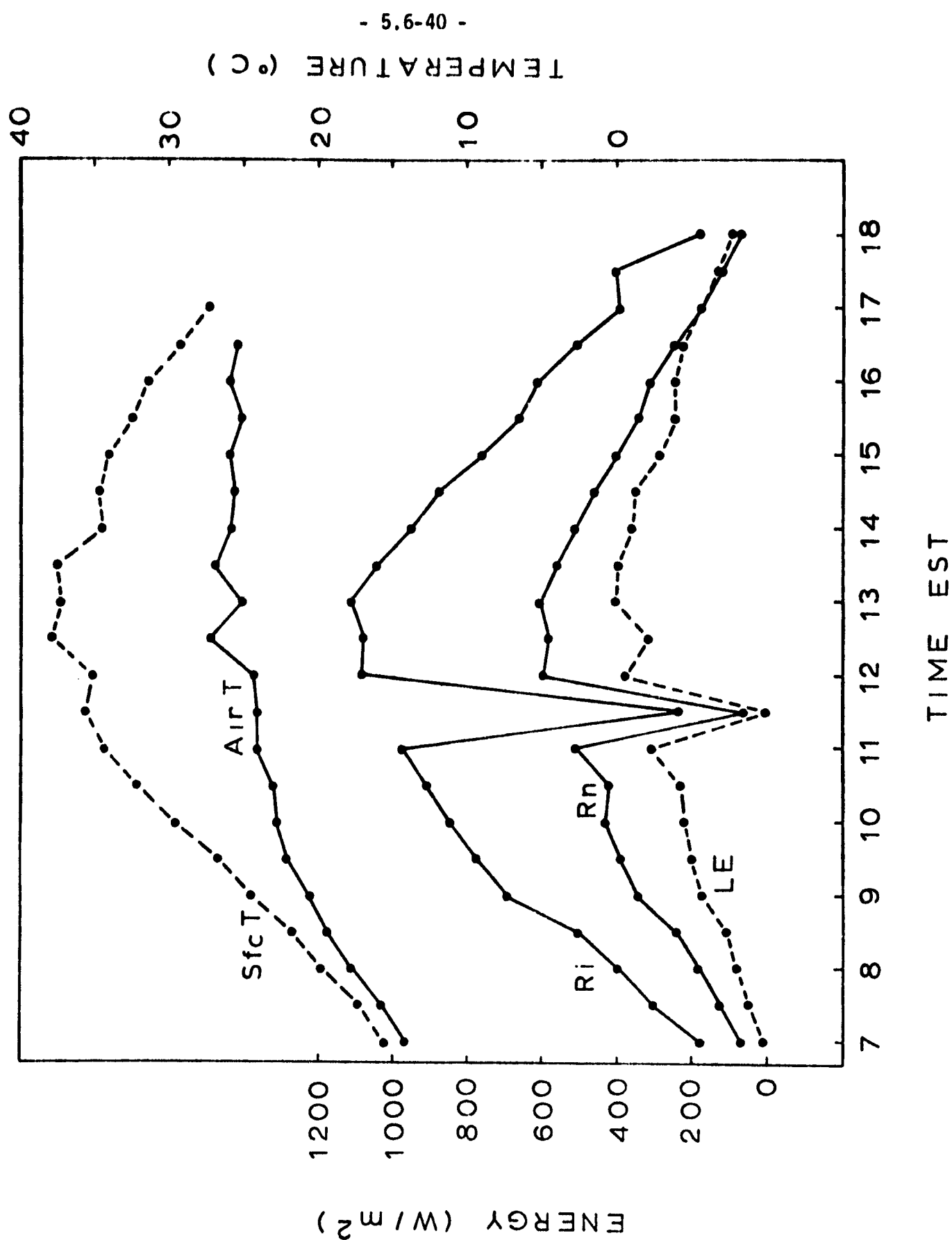


Figure 5.6-9. Daytime course of Bowen ratio ET (latent heat flux density, LE), net radiation (Rn), global solar radiation (Ri), soil surface temperature (Sfc T), and air temperature at 2 m (Air T) over Pangola grass at the beginning of spring regrowth.

# TAYLOR CREEK APRIL 29, 1978

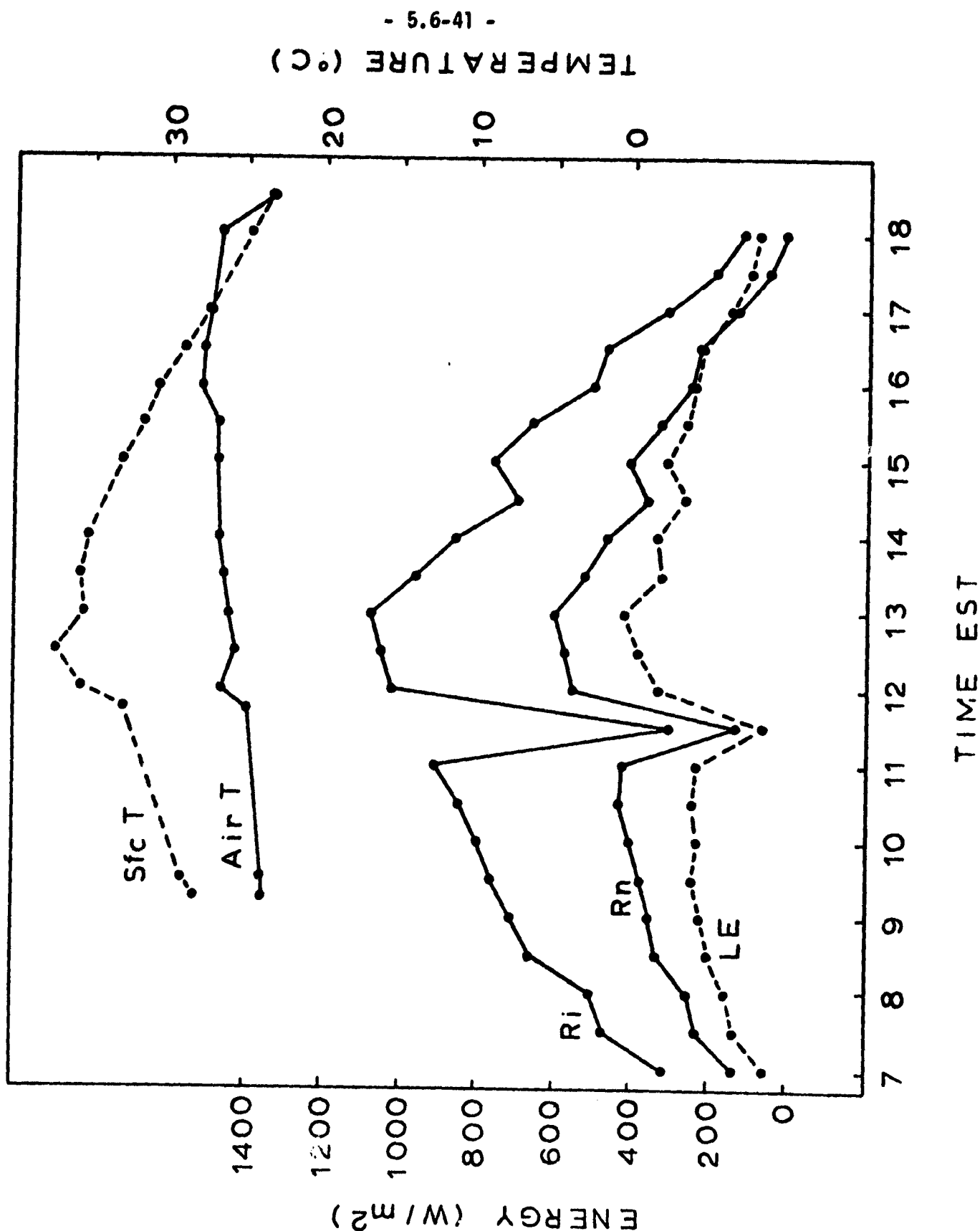


Figure 5.6-10. Daytime course of Bowen ratio ET (latent heat flux density, LE), net radiation (Rn), global solar radiation (Ri), soil surface temperature (Sfc T), and air temperature at 2 m (Air T) over Pangola grass at the beginning of spring regrowth.

# TAYLOR CREEK APRIL 30, 1978

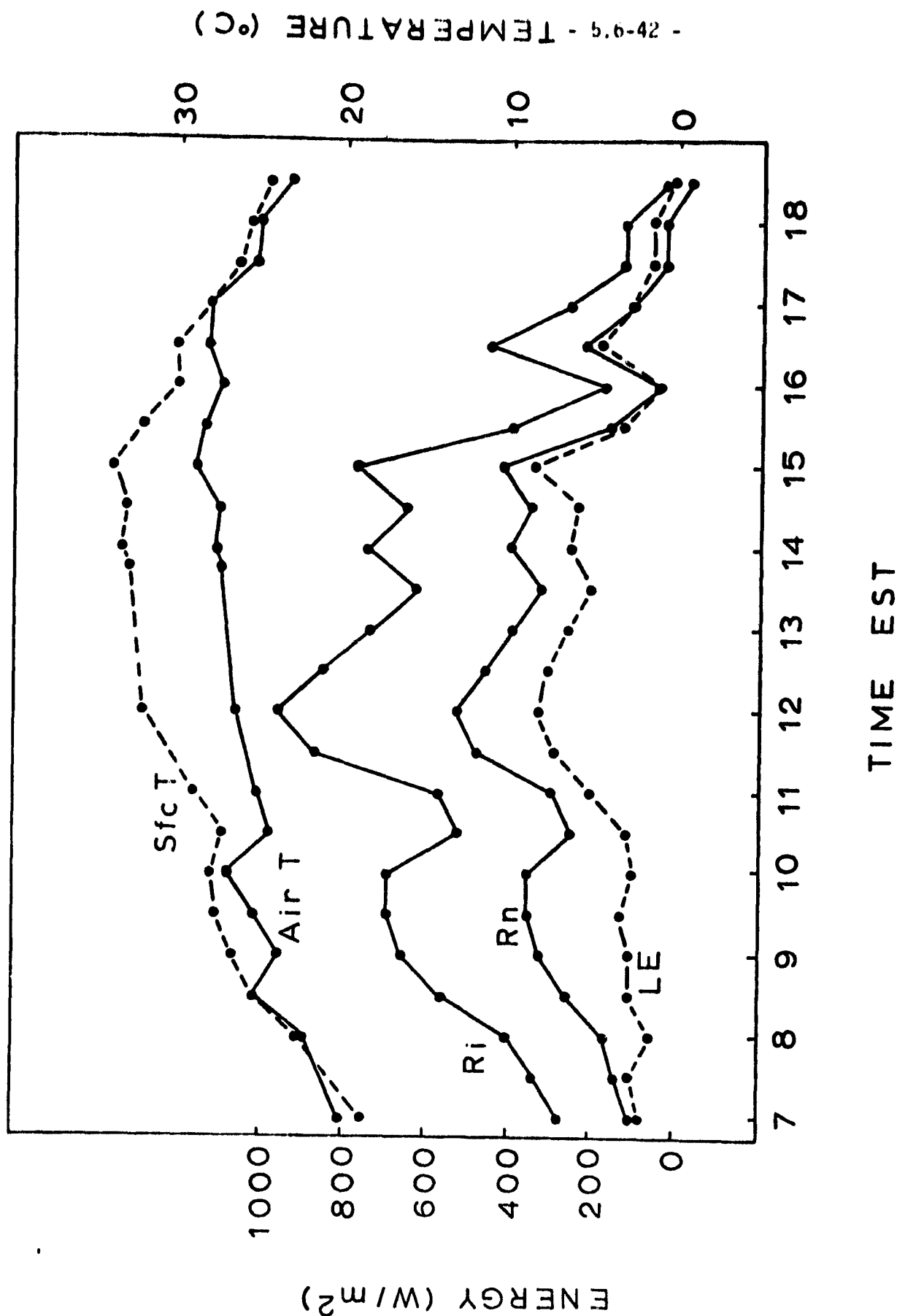


Figure 5.6-11. Daytime course of Bowen ratio ET (latent heat flux density, LE), net radiation (Rn), global solar radiation (Ri), soil surface temperature (Sfc T), and air temperature at 2 m (Air T) over Pangola grass at the beginning of spring regrowth.

# TAYLOR CREEK MAY 1, 1978

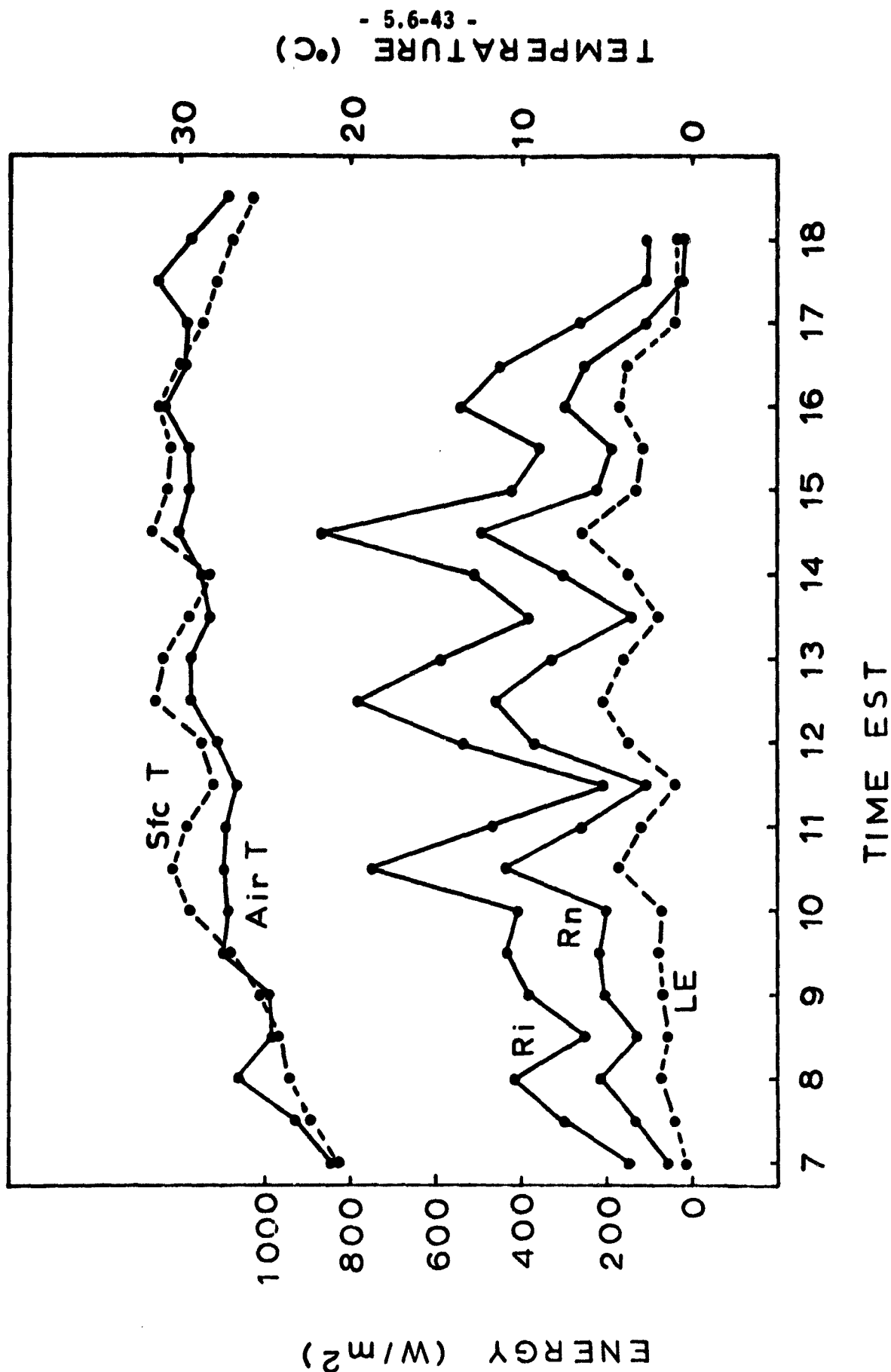


Figure 5.6-12. Daytime course of Bowen ratio ET (latent heat flux density, LE), net radiation (Rn), global solar radiation (Ri), soil surface temperature (Sfc T), and air temperature at 2 m (Air T) over Pangola grass at the beginning of spring regrowth.

# TAYLOR CREEK MAY 2, 1978

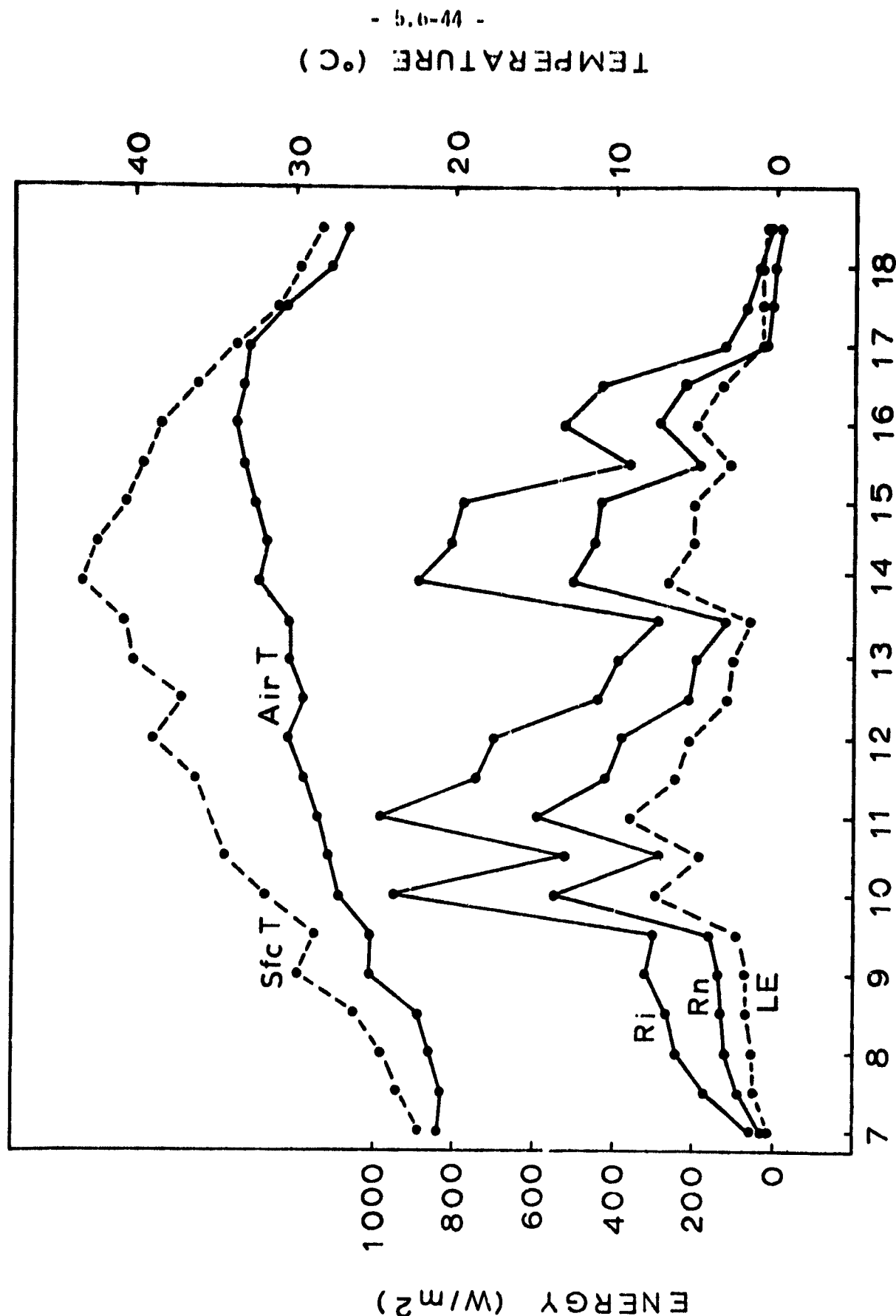


Figure 5.6-13. Daytime course of Bowen ratio ET (latent heat flux density, LE), net radiation (Rn), global solar radiation (Ri), soil surface temperature (Sfc T), and air temperature at 2 m (Air T) over Pangola grass at the beginning of spring regrowth.

# TAYLOR CREEK OCT. 17, 1978

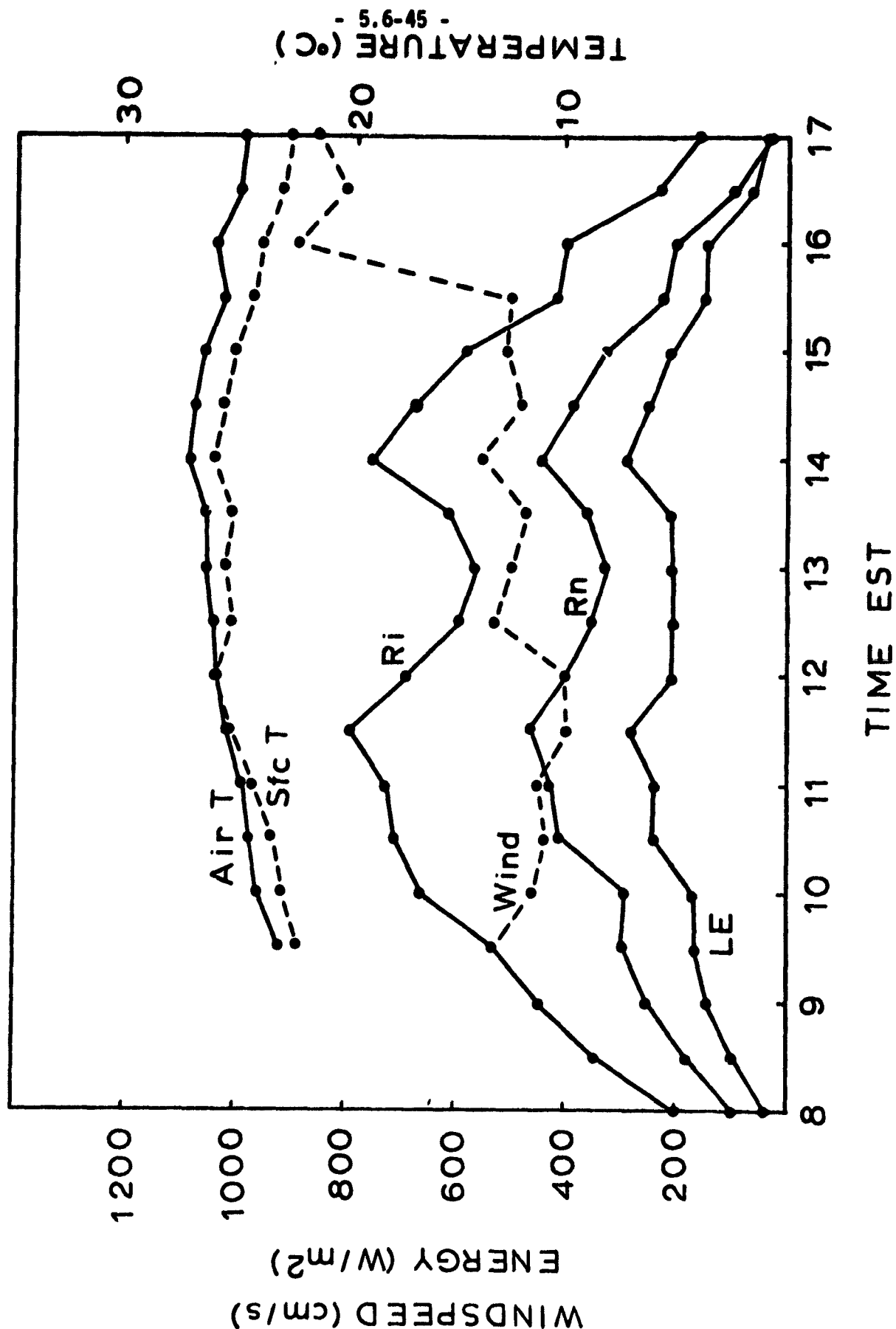


Figure 5.6-14. Daytime course of Bowen ratio ET (latent heat flux density, LE), net radiation (Rn), global solar radiation (Ri), soil surface temperature (Sfc T), air temperature at 2 m (Air T), and wind speed at 10 m over Pangola grass at the beginning of fall senescence.

# TAYLOR CREEK OCT. 20, 1978

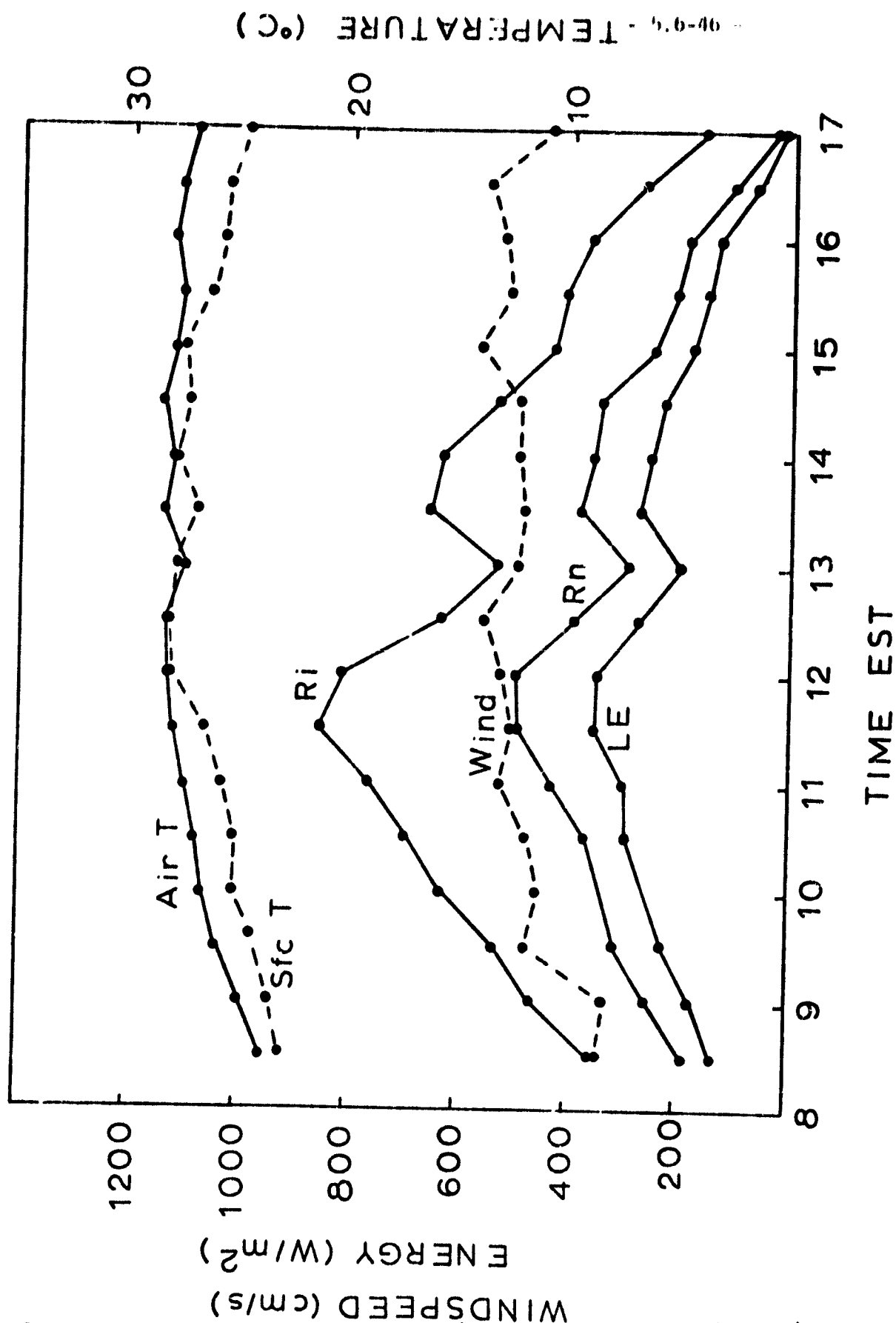


Figure 5.6-15. Daytime course of Bowen ratio ET (latent heat flux density, LE), net radiation (Rn), global solar radiation (Ri), soil surface temperature (Sfc T), air temperature at 2 m (Air T), and wind speed at 10 m over Pangola grass at the beginning of fall senescence.

# TAYLOR CREEK OCT. 26, 1978

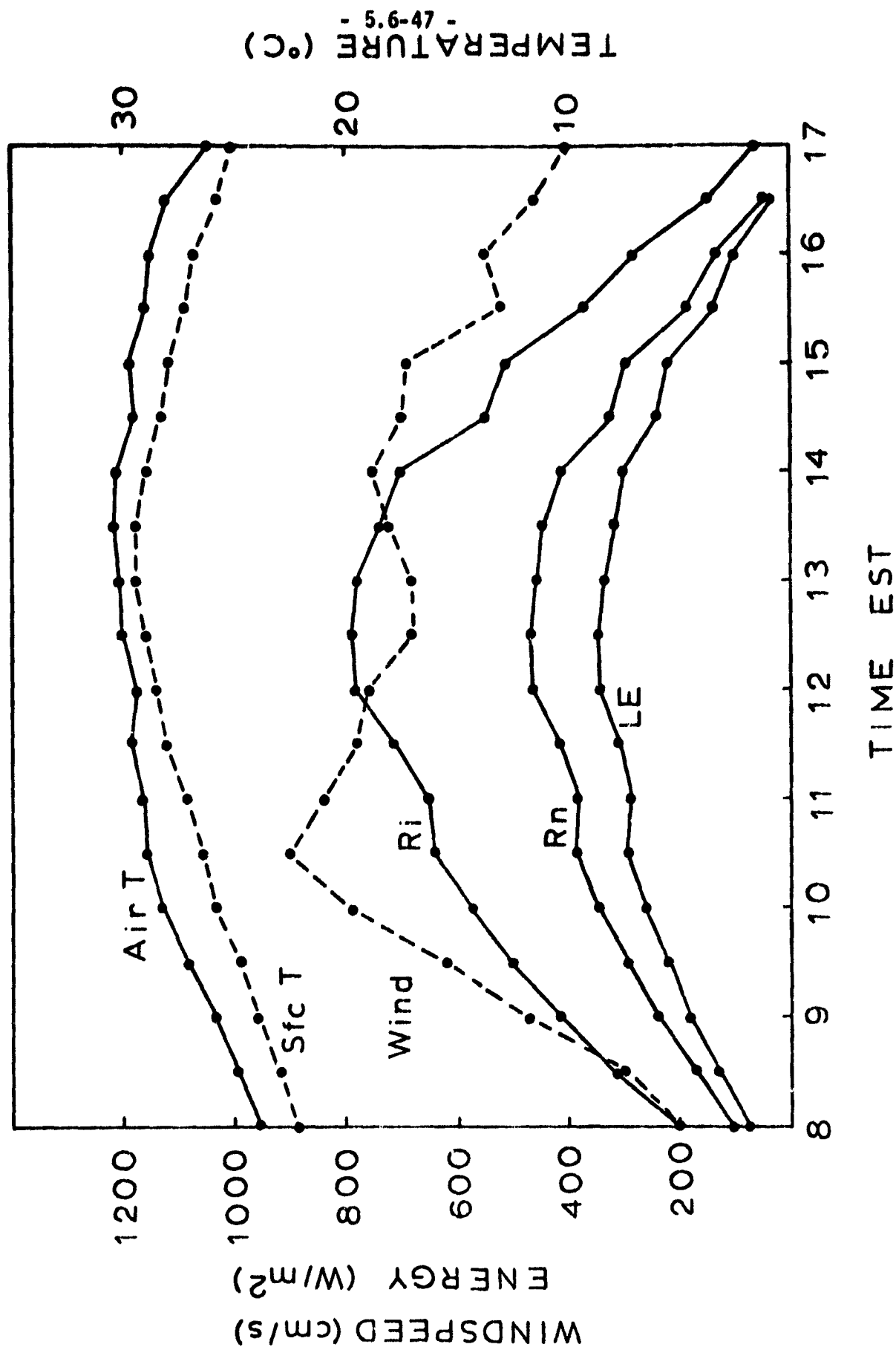


Figure 5.6-16. Daytime course of Bowen ratio ET (latent heat flux density, LE), net radiation (Rn), global solar radiation (Ri), soil surface temperature (Sfc T), air temperature at 2 m (Air T), and wind speed at 10 m over Pangola grass at the beginning of fall senescence.

# TAYLOR CREEK 1978

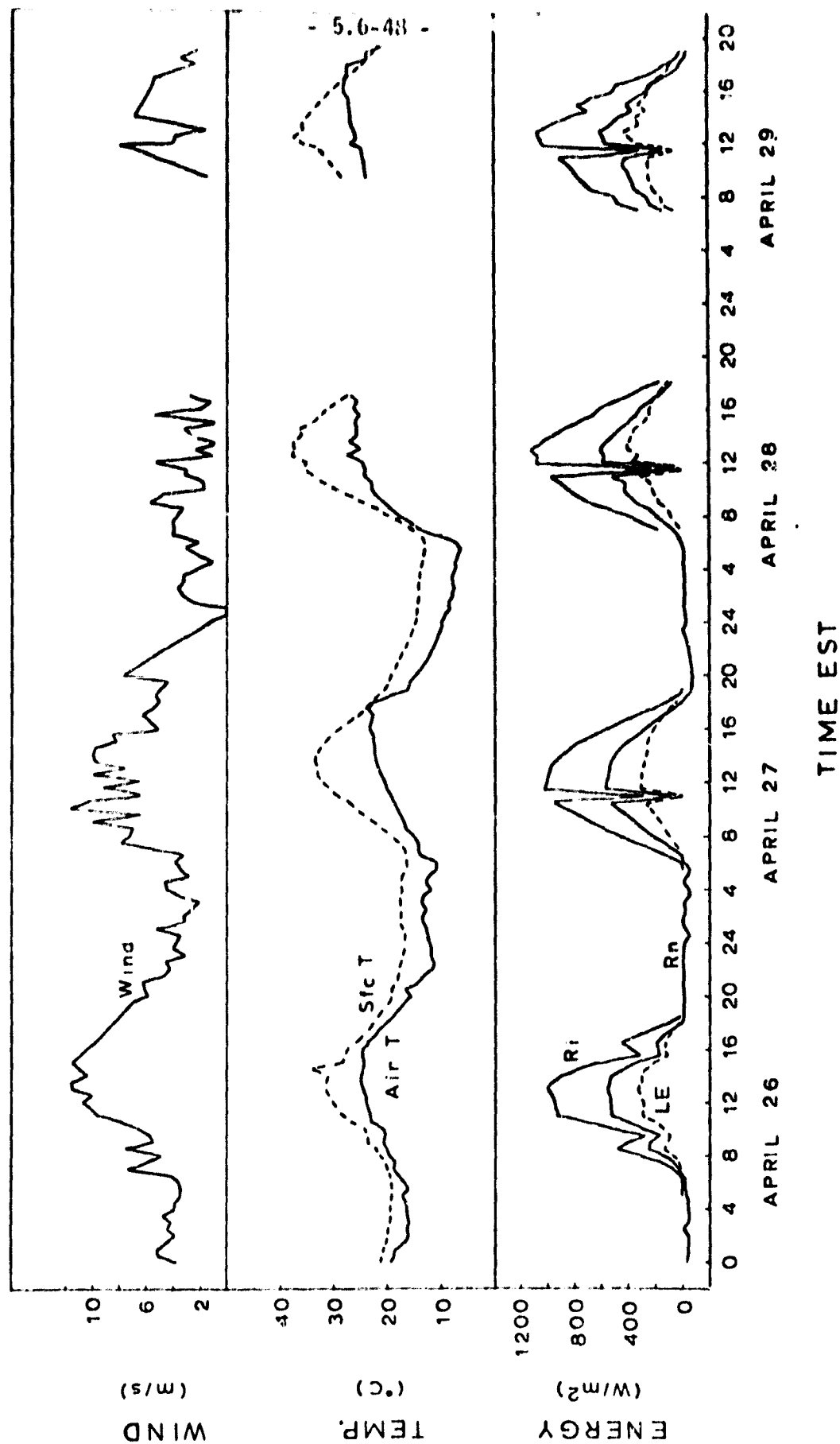


Figure 5.6-17. Diurnal course of ET (latent heat flux density, LE), net radiation (Rn), global solar radiation (Ri), soil surface temperature (Sfc T), air temperature at 2 m (Air T), and wind speed at 10 m over Pangola grass during 4 consecutive days at the beginning of spring regrowth.

# TAYLOR CREEK 1978

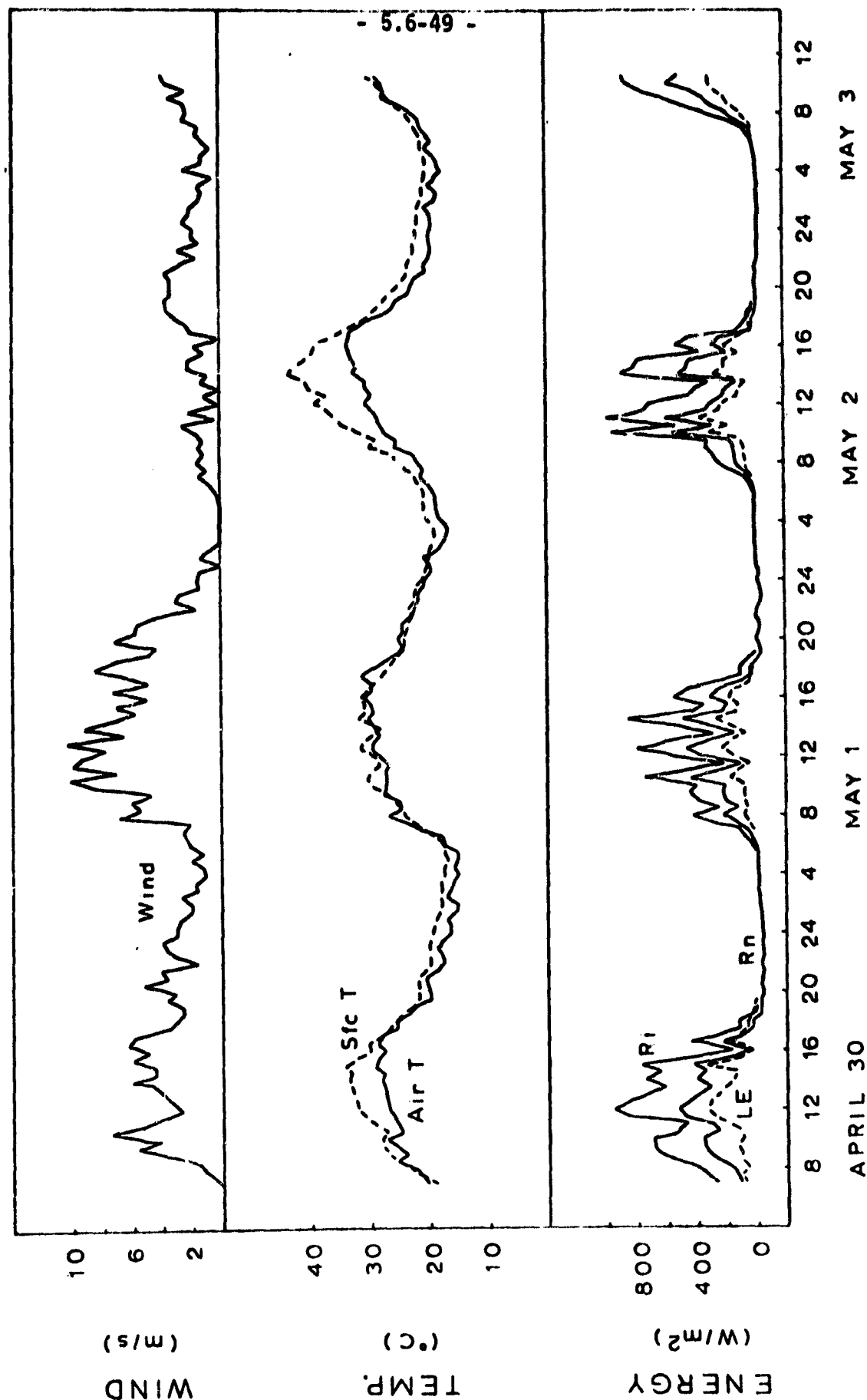


Figure 5.6-18. Diurnal course of ET (latent heat flux density, LE), net radiation (Rn), global solar radiation (Ri), soil surface temperature (Sfc T), air temperature at 2 m (Air T), and wind speed at 10 m over Pangola grass during 4 consecutive days at the beginning of spring

Table 5.6-b. Daytime energy budget summary

Date (1978)	Time Interval (EST)	←-----Energy Budget Components-----→					Bowen ratio
		Solar (MJ/m <sup>2</sup> )	Net (MJ/m <sup>2</sup> )	Soil (MJ/m <sup>2</sup> )	Latent (MJ/m <sup>2</sup> )	Sensible (MJ/m <sup>2</sup> )	
Apr 26	0700-1800	23.22	12.49	0.45	7.28	4.76	0.65
Apr 27 <sup>1</sup>	0700-1800	27.07	13.92	0.92	7.98	5.02	0.63
Apr 28 <sup>1</sup>	0700-1800	27.68	14.03	1.42	9.05	3.56	0.39
Apr 29	0700-1800	26.96	13.64	1.23	9.41	3.00	0.32
Apr 30	0700-1830	22.56	11.25	1.40	7.16	2.30	0.37
May 1	0700-1800	17.24	9.24	1.23	4.54	3.46	0.76
May 2	0700-1830	18.86	10.00	1.25	5.78	2.98	0.52
May 3	0700-1100	9.21	5.35	0.85	3.08	1.42	0.46
Oct 17	0700-1800	18.49	9.97	0.27	6.33	3.37	0.53
Oct 18	0700-1800	16.23	9.09	0.37	5.87	2.84	0.48
Oct 19	0700-1800	7.91	4.68	No Bowen Ratio Data			
Oct 20	0730-1700	17.98	10.08	0.62	6.73	2.73	0.41
Oct 25	1130-1700	11.46	6.17	0.37	4.28	1.52	0.36
Oct 26	0730-1700	17.65	10.02	0.67	7.02	2.33	0.33
Oct 27	0730-1700	17.10	9.68	0.65	6.95	2.08	0.30
Nov 2	0730-1700	17.81	9.51	0.53	6.48	2.50	0.39
Nov 3	0730-1700	16.34	8.84	0.54	6.12	2.17	0.35

<sup>1</sup> Chamber method latent heat (0700-1900 EST) for Bermuda grass and Pangola grass was 8.51 and 5.39 MJ/m<sup>2</sup>, respectively, on April 27, and 10.11 and 6.83 MJ/m<sup>2</sup>, respectively, on April 28.

**Table 5.6-6. Rainfall in inches on Taylor Creek Watershed, Okeechobee County, Florida, April 1978 and October 1978.**

Date/Rainfall - April 1978							
Location	13	14	18	19	23	24	25
Well Line "B"	0.20	0.00	0.60	0.00	0.00	0.80	0.00
Williams #1	0.04	0.00	0.03	0.14	0.00	0.45	0.00
Basset #2	0.05	0.00	0.02	0.45	0.00	0.34	0.00
Raulerson #3	0.01	0.00	0.00	0.05	0.00	0.62	0.00
Judson #4	0.19	0.00	0.00	0.27	0.00	0.68	0.00
Dixie #5	0.09	0.03	0.04	0.09	0.03	0.59	0.00
Mobley #6	0.14	0.01	0.46	0.01	0.02	0.56	0.00
Opal #7	0.24	0.00	0.70	0.02	0.07	0.70	0.01
Average	0.12	0.00	0.23	0.13	0.02	0.59	0.00

Date/Rainfall - October 1978							
Location	10	11	14	19	22	28	29
Well Line "B"	0.00	0.23	0.03	0.01	0.20	0.02	0.15
Williams #1	0.00	1.94	0.01	0.01	0.02	0.48	0.33
Bassett #2	0.00	0.25	0.05	0.26	0.11	0.38	0.13
Raulerson #3	0.00	0.23	0.04	0.18	0.02	0.20	0.06
Judson #4	0.08	0.30	0.02	0.04	0.13	0.48	0.08
Dixie #5	0.45	0.23	0.04	0.02	0.06	0.09	0.32
Mobley #6	0.00	0.15	0.03	0.05	0.12	0.02	0.36
Opal #7	0.00	0.20	0.03	0.02	0.37	0.02	0.11
Average	0.07	0.44	0.03	0.07	0.13	0.21	0.19

The Bowen ratios for the fall data, based on daytime sensible heat flux ratios, were generally lower than for the spring data (Table 5.6-5). The soil moisture contents were considerably higher during this period. The soil surface temperatures during the day were generally slightly lower than air temperatures at 2 m. The Pangola grass sod had a dense vegetative cover of both senescent and active plant material. This cover prevented most of the solar radiation from penetrating all the way to the soil surface. Also, the nocturnal air temperature was always cooler than the surface temperature (Figures 5.6-19, 5.6-20, and 5.6-21). However, this effect could be explained by the dense vegetative cover that would establish conditions for the vegetation, rather than the soil surface, to be the "surface radiator" to space. Therefore, the air in convective contact with the vegetation should be cooler than the soil surface.

In addition to surface temperature and air temperature, Figures 5.6-19, 5.6-20, and 5.6-21 also show continuous diurnal patterns of wind, global radiation, net radiation, and daytime ET (latent heat flux density). The wind speed before 1600 EST on October 16 (Figures 5.6-14 and 5.6-19) were in error by a factor of 0.6. This error also obtains for the May 2 and May 3 data (Figure 5.6-18). These errors were due to a computer program change. The values plotted for those dates should be multiplied by the reciprocal of 0.6.

Some daily pan evaporation data spanning the periods of measurement are included in Table 5.6-7 for comparison. Pan coefficients were computed for an average of six good days in April-May (April 27 - May 2), and for five good days in October (October 17, 18, 20, 26, and 27). The ratio of pan evaporation to energy budget evaporation over those days was 0.55 for the April-May days and 0.86 for the October days. Thus, the pan coefficients appear to be lower in the spring than in the fall. Long-term water balance data for the Taylor Creek Watershed suggest that the above pan coefficients (based on few data) are qualitatively correct (Knisel *et al.*, 1980).

#### 5.6.2.5.3 ET by the Chamber Method

The daytime values of ET measured by the chamber method on April 27 and April 28 agreed closely with the Bowen ratio-energy balance method (Table 5.6-5). In general, the latent heat flux density from the Bermuda grass sod exceeded the Bowen ratio-energy balance, whereas the latent heat flux density from the Pangola grass sod was less (Figure 5.6-22). On April 27, the ET in mm water was 3.51, 2.22, and 3.29 for the Bermuda grass chambers, the Pangola grass chambers, and the Bowen ratio-energy balance, respectively. On the following date, the ET values were 4.16, 2.81, and 3.73 mm water, respectively.

The evapotranspiration rates detected by the Bowen ratio-energy balance method were mainly from Pangola grass ground cover; therefore, we would have expected the rates to be closer to the chamber values for Pangola grass. Nevertheless, the chamber values did bracket the Bowen ratio-energy balance values. Overall, the results of the two methods support each other for ground truth observations.

# TAYLOR CREEK 1978

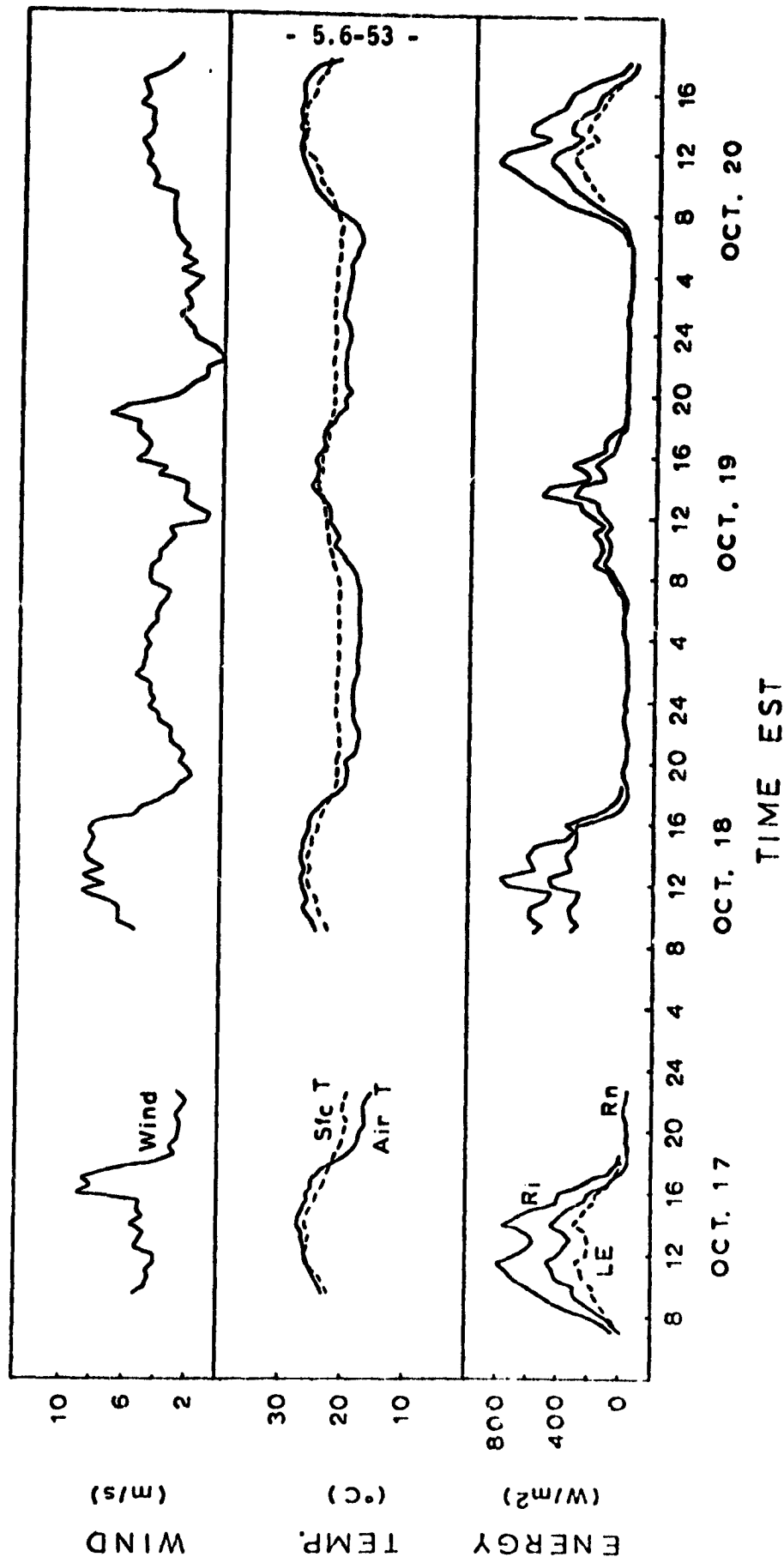


Figure 5.6-19. Diurnal course of ET (latent heat flux density, LE), net radiation (Rn), global solar radiation (Ri), soil surface temperature (Sfc T), air temperature at 2 m (Air T), and wind speed at 10 m over Pangola grass during 4 consecutive days at the beginning of fall senescence.

# TAYLOR CREEK 1978

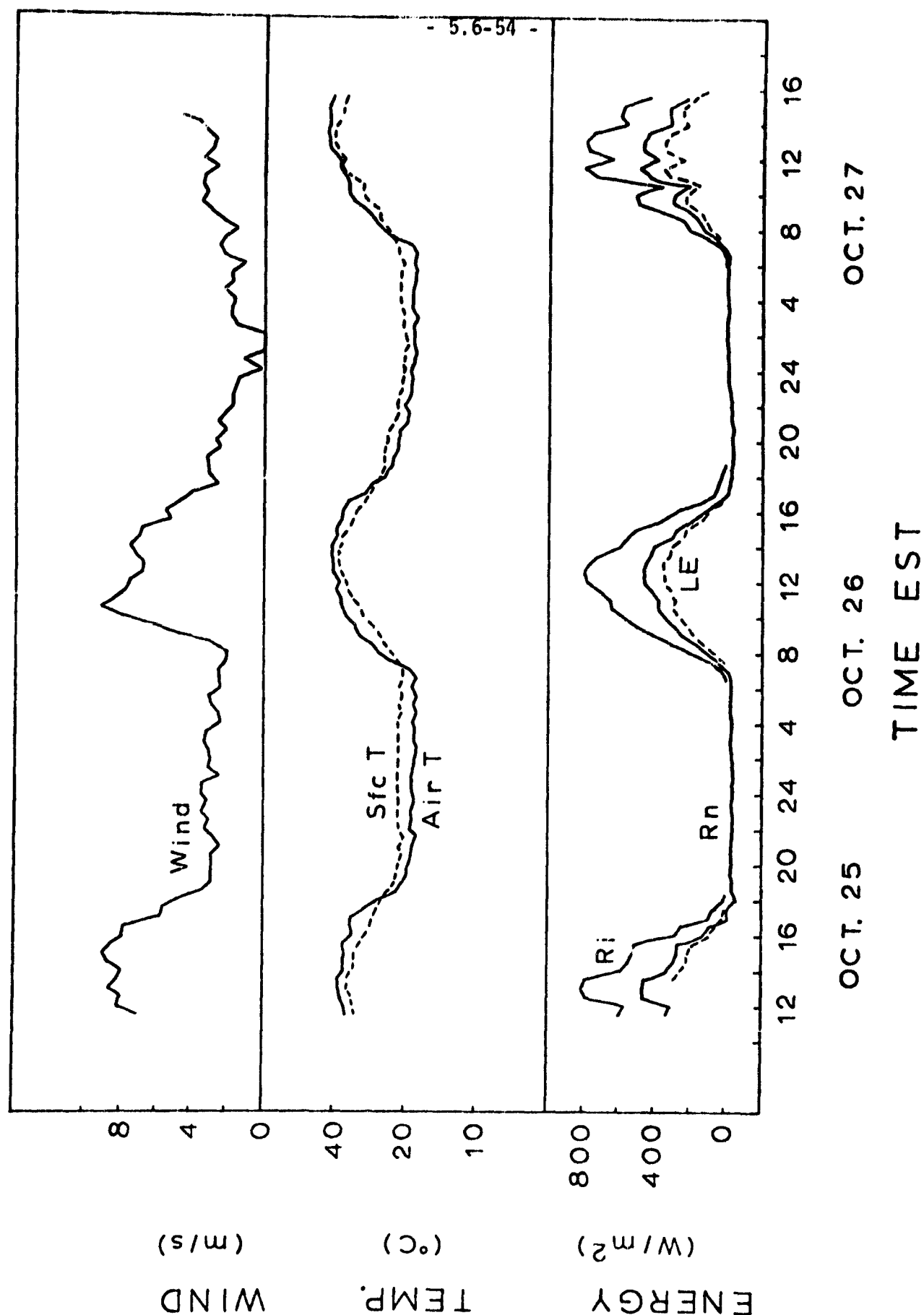


Figure 5.6-20. Diurnal course of ET (latent heat flux density, LE), net radiation (R<sub>n</sub>), global solar radiation (R<sub>i</sub>), soil surface temperature (Sfc T), air temperature at 2 m (Air T), and wind speed at 10 m over Pangola grass during 3 consecutive days at the beginning of fall senescence.

## TAYLOR CREEK 1978

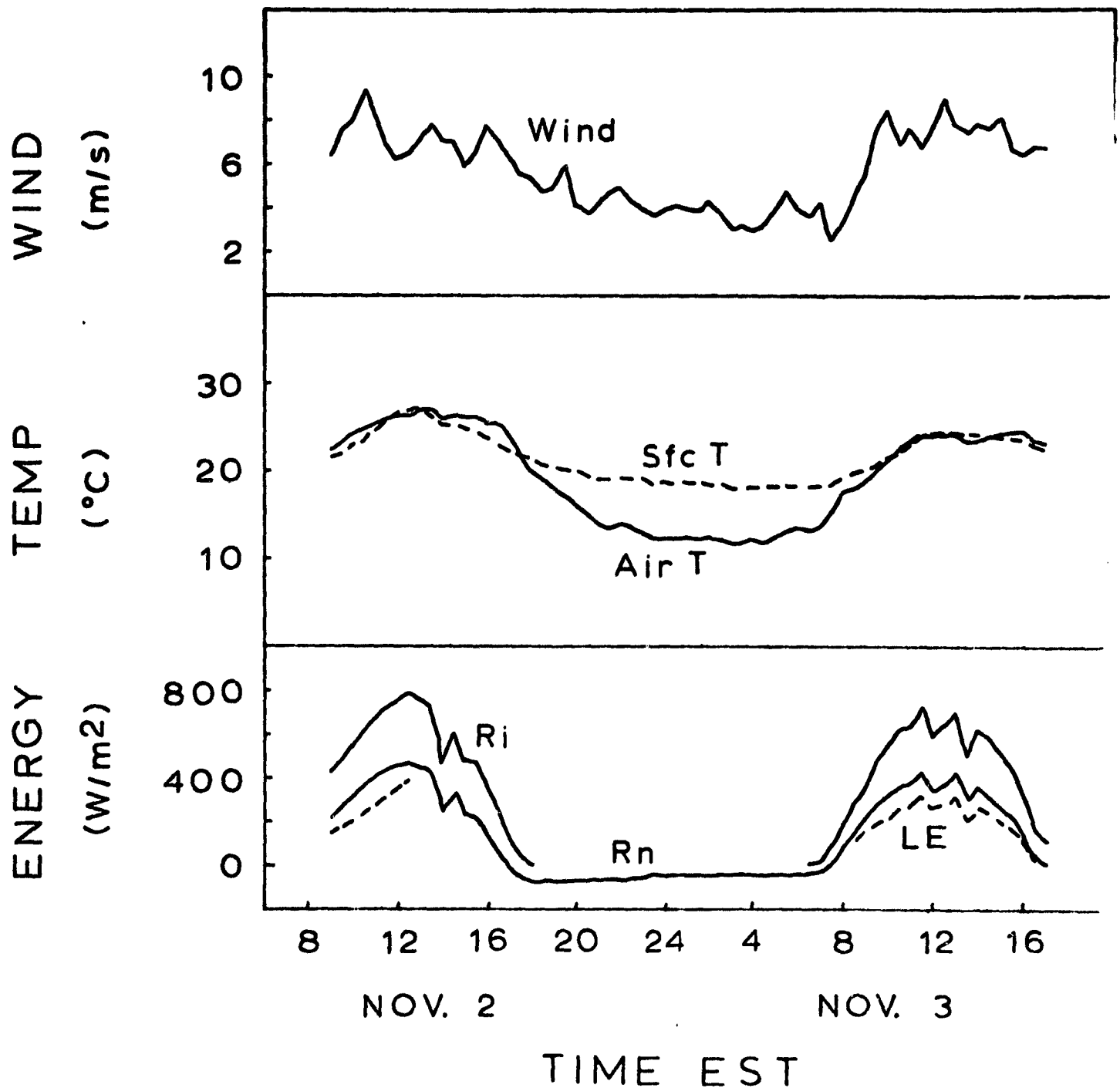


Figure 5.6-21. Diurnal course of ET (latent heat flux density, LE), net radiation (Rn), global solar radiation (Ri), soil surface temperature (Sfc T), air temperature at 2 m (Air T), and wind speed at 10 m over Pangola grass during 2 consecutive days at the beginning of fall senescence.

Table 5.6-7. Daily Pan Evaporation at Ft. Pierce and on the Taylor Creek Watershed during the period of measurements in 1978. Data supplied by USDA-SEA-AR and IFAS Ft. Pierce ARC, Ft. Pierce, Florida.

Month	Day	Ft. Pierce		Taylor Creek	
		(inches)	(MJ/m <sup>2</sup> )	(inches)	(MJ/m <sup>2</sup> )
Apr.	26	0.32	19.7	0.40	24.7
	27	0.25	15.4	0.17	10.5
	28	0.23	14.2	0.17	10.5
	29	0.24	14.8	0.22	13.6
	30	0.20	12.3	0.28	17.3
May	1	0.18	11.1	0.23	14.2
	2	0.19	11.7	0.22	13.6
	3	0.16	9.9	-	-
Oct.	17	0.24	14.8	0.12	7.4
	18	0.24	14.8	0.12	7.4
	19	0.06	3.7	0.08	4.9
	20	0.19	11.7	0.07	4.3
	21	0.16	9.9	0.13	8.0
	22	0.07	4.3	0.05	3.1
	23	0.16	9.9	0.12	7.4
	24	0.19	11.7	0.18	11.1
	25	0.24	14.8	0.16	9.9
	26	0.20	12.3	0.18	11.1
	27	0.16	9.9	0.13	8.0
	28	0.06	3.7	0.15	9.2
	29	0.10	6.2	0.04	2.5
	30	0.17	10.5	0.06	3.7
Nov.	31	0.10	6.2	0.05	3.1
	1	0.12	7.4	0.05	3.1
	2	0.22	13.6	0.05	3.1
	3	0.17	10.5	0.06	3.7

# TAYLOR CREEK

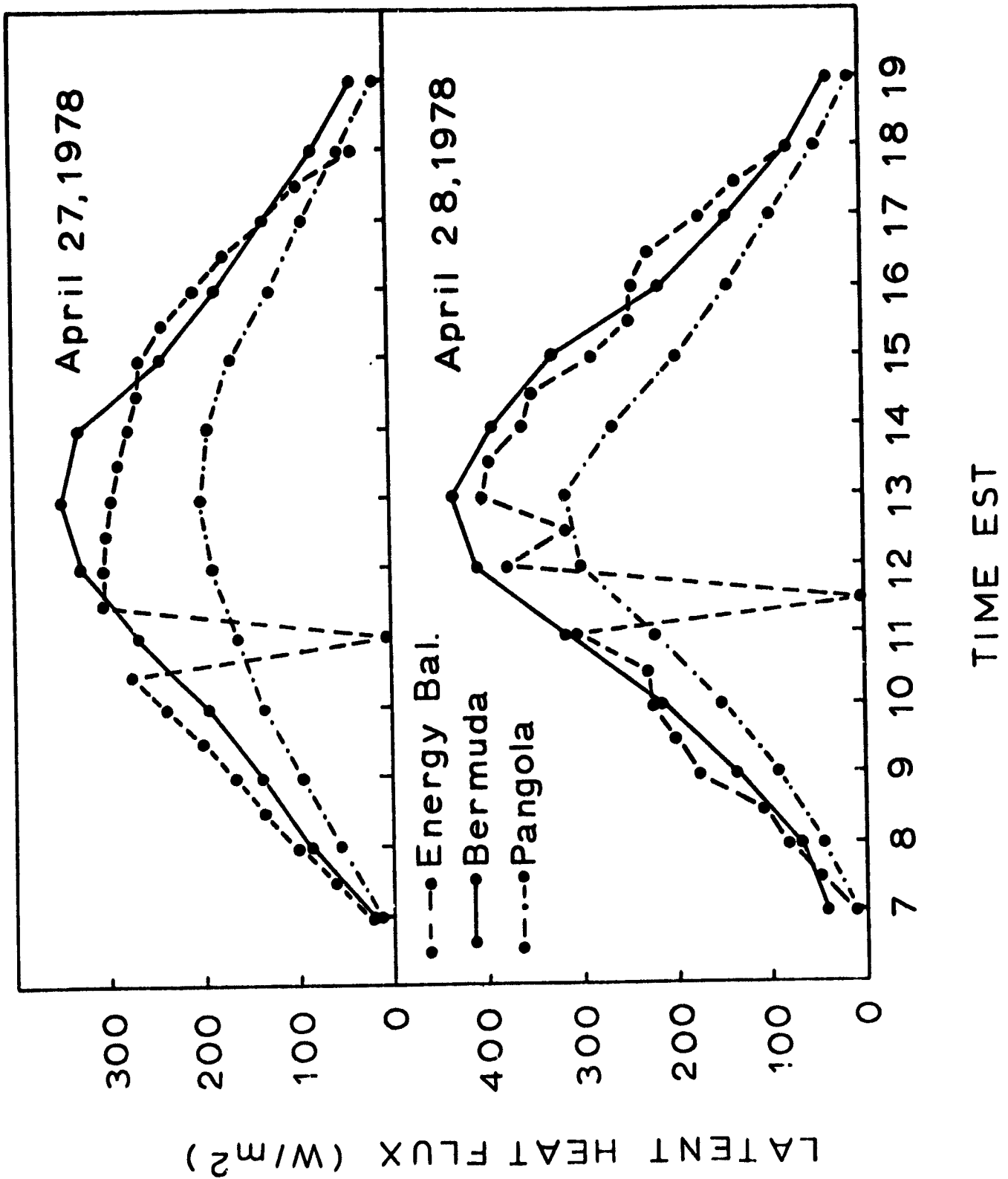


Figure 5.6-22. Daytime courses of ET (latent heat flux density) from chamber measurements over Bermuda grass and Pangola grass compared with Bowen ratio-energy balance measurements.

#### 5.6.2.5.4 Applications of Remote Sensed Data to ET

Several methods were developed to determine diffusion resistance to apply to either resistance-energy balance or combination models.

Temperature profile method: The April 28, 1978 data were used to compute the turbulent resistance component ( $r_t$ ) and the bulk boundary layer resistance component ( $r_b$ ) and the total aerial resistance to heat transfer according to equations 5.6-26 and 5.6-27. Sensible heat flux density was obtained from half-hourly Bowen ratio-energy balance measurements from 0830 to 1530 EST. Temperature profiles were plotted against the logarithm of height on semilog graph paper. The  $r_t$  values were calculated from a height of 1.5 m ( $T_a$ ) to a height of 0.02 m ( $T_0$ ) using equation 5.6-26. The 1.5 m height was chosen as representative of weather shelter height and the 0.02 m height was chosen as  $Z_0$  for this short grass surface. We assumed  $Z_H$ , the roughness length for heat transfer, to be equal to  $Z_0$ . The  $r_b$  values were calculated from equation 5.6-27 using radiation thermometer data for the surface temperature,  $T_s$ .

The average values of  $r_t$ ,  $r_b$ , and  $r_a$  were 0.36, 0.77, and 1.13 sec/cm, respectively. These values were also representative of the 1200-1230 EST values at the time of the aircraft overflights. The  $r_t$  values were smaller in the afternoon than in the morning, but the  $r_b$  values showed less difference. The  $r_a$  values were more consistent throughout the day than either  $r_t$  or  $r_b$ . The values of  $r_t$ ,  $r_b$ , and  $r_a$  were plotted as a function of wind speed for that day. The  $r_t$  values tended to decrease as a function of wind speed for the afternoon hours only.

Since the overall  $r_a$  values were more stable than  $r_t$  or  $r_b$ , then it is possible that the level of the effective  $T_0$  changed throughout the day. Also, the temperature gradient ( $T_s - T_0$ ) was about twice as large as ( $T_0 - T_a$ ). It is possible that the height for  $T_0$  is overestimated by using an estimated value of  $Z_0 = Z_H = 0.02$  m for the height of  $T_0$ . However, the  $T_s - T_0$  temperature differences are large enough to cause the height of  $T_0$  to be reduced by 3 orders of magnitude (0.00002 m). The PRT measurements at 1230 EST agree with the airborne scanner surface temperature, and are substantiated by soil surface temperature measurements. It may be possible that the surface temperature is higher because of the low ground cover, and that much of the heat and latent heat exchange involves the soil directly. However, the PRT was mounted at an angle that would view mainly the surface cover rather than the soil surface. We chose to view the transfer processes in two steps; a transfer from surface to  $T_0$  (an effective bulk boundary layer transfer) and transfer from  $T_0$  to  $T_a$  (a turbulent field boundary layer transfer).

Heilman and Kanemasu (1976) computed aerial resistance as only one component, over soybeans and over sorghum, by extrapolating the above-canopy temperature profile down to a canopy temperature,  $T_c$ , obtained either by leaf thermocouples or by infrared radiation thermometer. Their data would indicate that the ratio of  $Z_0$  to  $Z_H$  would range from 1 to 3 for the sorghum and soybean crops. If we extrapolated our temperature profiles to 0.00002 m, then we would have obtained  $Z_0/Z_H = 1000$  for our short grass surface.

This bulk aerial resistance approach assumes that net radiation, soil heat flux density, and bulk aerial resistance are uniform over the pasture area.

The method used to compute ET from the April 28 pasture scene was as follows. Sensible heat flux density for each surface temperature class of Table 5.6-4 was computed and weighted by the fractional area ( $A_i$ ) in each surface temperature class.

$$H_i = \frac{\rho C_p \Delta T_i A_i}{r_B} \quad (5.6-39)$$

where the subscript "i" refers to the values of a particular color-coded surface temperature scene (Table 5.6-4, Figures 5.6-5, 5.6-6, 5.6-23, and 5.6-24).  $\Delta T$  is the surface-to-air temperature difference. Latent heat flux density was computed by difference.

$$\lambda E_i = R_n - S - H_i \quad (5.6-40)$$

The heat flux density from the whole scene is:

$$H = \sum H_i = \frac{\rho C_p}{r_B} \sum \Delta T_i A_i \quad (5.6-41)$$

Total latent heat flux density (ET) over a scene can be also computed by summation. We did not correct for  $R_n$  or  $S$  for higher or lower surface temperatures.

This method of computation does not allow for or explain any variations in effects of atmospheric stability, boundary layer and turbulent resistance, wind, leaf area index, plant height and surface parameters ( $D$  and  $Z_0$ ) or stomatal resistance, or sensible heat and latent heat transport processes. The next section describes one approach to evaluate some of these effects on heat transport processes, and ultimately, on evapotranspiration.

On April 28, the average  $r_a$  for the day (30-minute data, 0800 to 1530 EST) was  $1.13 \pm 0.25$  sec/cm. The values for the periods ending at 1200, 1230, and 1300 EST were 1.09, 1.19, and 0.99 sec/cm, respectively. Table 5.6-8 shows the weighted  $H$  and weighted  $\lambda E$  for April 28 (1200 to 1230 EST) for the pasture scene of Taylor Creek Watershed. The values for the whole scene were 12.2 and 36.5 mW/cm<sup>2</sup>, respectively. These values compare with the ground truth measurements of 13.7 and 35.0 mW/cm<sup>2</sup> for  $H$  and  $\lambda E$ , respectively, for this time period. The value of 13.7 mW/cm<sup>2</sup> for heat flux density lies between the "Black" and "Aqua" color codes of Table 5.6-8. Figure 5.6-5 shows that the meteorological tower was located in a surface temperature area characterized by "Black," with "Aqua" (cooler) and "Tan" (warmer) area nearby.

This method demonstrates that if heat flux is known or measured, then bulk aerial resistance can be calculated for similar surfaces. If remotely sensed temperature patterns of similar evaporating surfaces are known, then the regional evapotranspiration rates can be determined. If the surface conditions are different, then a different aerial resistance would have to be determined for each surface.

Wind Speed Dependence of  $r_a$ : Wind speed would be expected to have a large effect on bulk aerial resistances under similar surface conditions. Data from



Figure 5.6-23. Outline of temperature intervals drawn from infrared image of pasture scene in Taylor Creek Watershed, April 28, 1978, at 1222-1225 EST (from Figure 5.6-5).

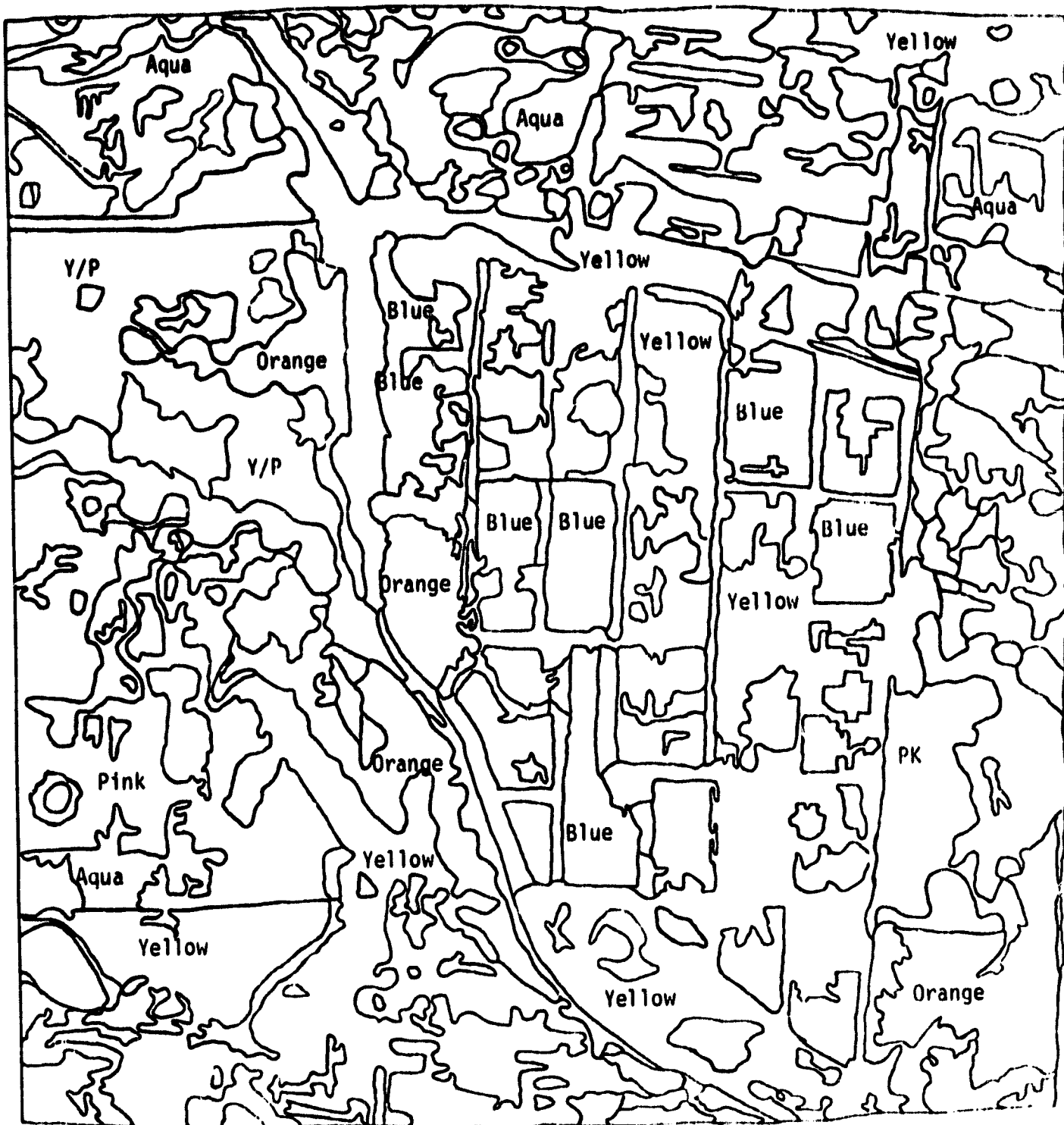


Figure 5.6-24. Outline of temperature intervals drawn from infrared image of citrus grove scene in Taylor Creek Watershed, April 26, 1978, at 1432-1435 EST (from Figure 5.6-6).

ORIGINAL PAGE IS  
OF POOR QUALITY

Table 5.6-8. Regional Evapotranspiration for Pasture Scene Using Resistance Method,  
April 28, 1200-1230 EST.

Color	$\Delta T$ (°C)	H (mW/cm <sup>2</sup> )	$\rho E$ (mW/cm <sup>2</sup> )	Proportional Area	Weighted H (mW/cm <sup>2</sup> )	Weighted $\rho E$ (mW/cm <sup>2</sup> )	B
Tan	16.5	16.8	31.9	0.233	3.92	7.43	0.53
Black	14.9	15.2	33.5	0.242	3.68	8.11	0.45
Aqua	11.5	11.7	37.0	0.251	2.94	9.28	0.32
Pink	8.2	8.3	40.4	0.165	1.38	6.66	0.21
Yellow	4.9	5.0	43.7	0.066	0.33	2.88	0.11
Blue	1.5	1.5	47.2	0.022	0.03	1.04	0.03
Orange	-1.8	-1.8	50.5	0.021	-0.04	1.06	-0.04
Totals				1.000	12.24	36.46	0.34

the fall on a high wind day (October 18), a moderate wind day (October 20), and a low wind day (October 27) were compared to determine wind speed effects.

Temperature profiles were plotted on semilog graph paper. The Pangola grass in the fall was about 0.3 m tall. Inspection of the temperature data plot from the six heights showed that a zero plane displacement height ( $D$ ) of 0.25 m gave the best straight line fits on semilog plots. We estimated  $Z_0$  at 0.03 m. When air temperature profiles were extrapolated to this small height, there was still a very large difference between the extrapolated temperature at this height, and the surface temperature measured by a precision radiation thermometer. Therefore, we calculated both a turbulent resistance component (from  $Z - D = 0.03$  m to  $Z - D = 1.5$  m) and a bulk boundary layer resistance (from the surface temperature to the temperature at  $Z - D = 0.03$  m). In most cases, the surface-to- $Z_0$  temperature difference was larger than the  $Z_0$ -to-1.5 m temperature difference, which implied that the bulk boundary layer resistance was larger than the turbulent transport resistance.

The turbulent resistance and the bulk boundary layer resistance were calculated from equations 5.6-26 and 5.6-27, respectively, for each half-hour of data on October 18, 20, and 27. Wind speed was found to be steady for 5 to 7 hour periods during those days. The turbulent resistance,  $r_t$ , and the bulk boundary layer resistance,  $r_b$ , as well as wind speeds were averaged over the steady wind periods, and standard deviations computed. These average resistance values were plotted against wind speed.

Bulk aerial resistance and the two components, turbulent resistance ( $r_t$ ) and bulk boundary layer resistance ( $r_b$ ) showed a decrease with increasing wind speed ( $U$ ) at ten meters. The values of  $r_a$ ,  $r_t$ ,  $r_b$ , and  $U_{10}$  were  $0.48 \pm 0.05$ ,  $0.20 \pm 0.04$ ,  $0.28 \pm 0.03$  sec/cm, and  $9.33 \pm 0.48$  m/sec, respectively, on October 18;  $0.70 \pm 0.06$ ,  $0.28 \pm 0.04$ ,  $0.42 \pm 0.08$  sec/cm, and  $5.80 \pm 0.35$  m/sec, respectively, on October 20; and  $0.84 \pm 0.13$ ,  $0.32 \pm 0.04$ ,  $0.52 \pm 0.13$  sec/cm, and  $3.55 \pm 0.38$  m/sec, respectively, on October 27. Figure 5.6-25 shows the component values  $r_t$  and  $r_b$ .  $r_b$  was always larger than  $r_t$ . Over the range of wind speeds, the resistances increased linearly with decreasing wind speed, however, at lower wind speeds they would be likely to increase nonlinearly with decreasing wind speed until natural convection was reached.

The  $r_b$  values were large for the short grass surface. This shows that boundary layer resistance and resistance in the low turbulence flows in short vegetation systems are very important in the overall transport processes.

These relationships of resistances to wind speed were not used further in this report, but show that linear or near-linear functions could be developed to express resistance as a function of wind speed in future remote sensing ET studies.

#### 5.6.2.5.5 Development of Remote Sensed ET Estimates from Stability Corrected Heat Flux.

The overall approach was to calculate sensible heat flux from the vegetated surface, estimate soil heat flux, and calculate evapotranspiration as the residual using a directly measured net radiation. The bulk of this effort lay

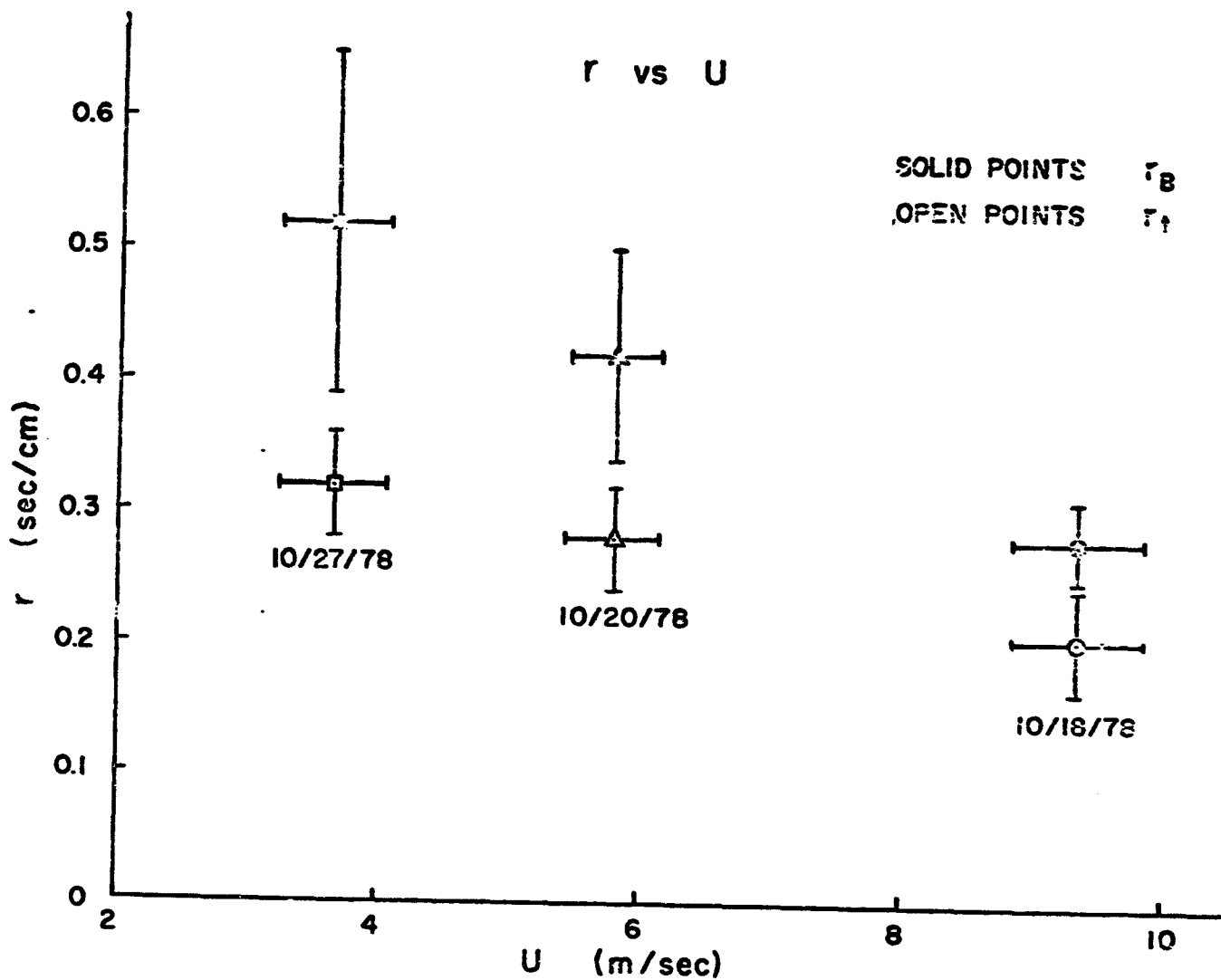


Figure 5.6-25. Bulk aerial resistance components of turbulent resistance,  $r_t$ , and bulk boundary layer resistance,  $r_B$ , as a function of wind speed,  $U$ , at 10 m on October 18, 20 and 27, 1978.

in developing means to obtain sensible heat flux from a remote surface temperature, an air temperature, and a wind speed. Key problems were exactly how to use a surface temperature and how to deal with various stability regimes.

It was decided to approach the latter problem via "diabatic influence functions"--empirical corrections to the conventional log law transport laws based on a dimensionless quantity, the Richardson number. These correction functions exist in the literature in integrated forms of equations 5.6-29 to 5.6-31 (Businger, 1973) and differential forms (Morgan, Pruitt, and Lourence, 1971). The latter form was adopted for this section.

The log law wind profile, valid when conditions are neutral, can be described by:

$$\frac{\partial U}{\partial Z} = \frac{U_*}{kZ} \quad (5.6-42)$$

where the friction velocity:

$$U_* = \frac{kU}{Z - D + Z_0} \quad (5.6-43)$$

When the air layer in question is stable or unstable, a correction  $\phi_m$  is applied:

$$\frac{\partial U}{\partial Z} = \frac{U_*}{kZ} \phi_m \quad (5.6-44)$$

analogously,

$$\frac{\partial T}{\partial Z} = \frac{H}{\rho C_p k U_* Z} \phi_H \quad (5.6-45)$$

The correction function are interrelated:

$$\phi_H = \phi_m \frac{K_m}{K_H} \quad (5.6-46)$$

The corrections used in the study were those developed by a group at the University of California at Davis (Morgan, Pruitt, and Lourence, 1971) and are listed below.

$$\phi_m = (1 + 16 Ri)^{1/3} \quad \text{STABLE} \quad (5.6-47)$$

$$\phi_m = (1 - 16 Ri)^{-1/3} \quad \text{UNSTABLE} \quad (5.6-48)$$

$$\frac{K_H}{K_m} = \frac{K_w}{K_m} = 1.13 (1 + 95 Ri)^{-0.11} \quad \text{STABLE} \quad (5.6-49)$$

$$\frac{K_H}{K_m} \approx \frac{K_W}{K_m} = 1.13 (1 - 60 Ri)^{.074} \quad \text{UNSTABLE} \quad (5.6-50)$$

The approximation in the second set of relationships is based on the near equality of  $K_H$  and  $K_W$  documented by Dyer (1967). The Richardson number is the ratio of bouyant and turbulent momentum transport influences:

$$Ri = \frac{g}{\theta} \frac{\partial T}{\partial Z} / \left( \frac{\partial U}{\partial Z} \right)^2 \quad (5.6-51)$$

The equation used to calculate heat fluxes was developed from the basic turbulent transport equations:

$$H = \rho C_p K_H \frac{\partial T}{\partial Z} \quad (5.6-52)$$

$$\tau = \rho K_m \frac{\partial U}{\partial Z} = \rho U_*^2 \quad (5.6-53)$$

to make use of the empirical relationships for  $\phi_m$  and  $\frac{K_H}{K_m}$ .

The first may be rewritten:

$$H = \rho C_p \left( \frac{K_H}{K_m} \right) K_m \frac{\partial T}{\partial Z} \quad (5.6-54)$$

Solving the second for  $K_m$ , the eddy diffusivity of momentum,

$$K_m = \frac{U_*^2}{\frac{\partial U}{\partial Z}} \quad (5.6-55)$$

Solving  $\frac{\partial U}{\partial Z} = \frac{U_* \phi_m}{kZ}$  for  $U_*$  and substituting:

$$K_m = \frac{k^2 Z^2}{\phi_m} \frac{\partial U}{\partial Z} \quad (5.6-56)$$

and

$$H = \rho C_p k^2 Z^2 \left( \frac{K_H}{K_m} \right) \left( \frac{1}{\phi_m} \right) \frac{\partial U}{\partial Z} \frac{\partial T}{\partial Z} \quad (5.6-57)$$

In difference form:

$$H = \rho C_p k^2 \left( \frac{Z_{gm}}{\Delta Z} \right)^2 \left( \frac{K_H}{K_m} \right) \left( \frac{1}{\phi_m} \right) \Delta U \Delta T \quad (5.6-58)$$

where  $\Delta Z = Z_2 - Z_1$  and  $Z_{gm}$  is the geometric mean of  $Z_1$  and  $Z_2$ . The corresponding Richardson number is:

$$Ri = \frac{g}{\theta} \frac{\Delta Z \Delta T}{(\Delta U)^2} \quad (5.6-59)$$

The behavior of equation 5.6-57 is shown in Figure 5.6-26. The relatively rapid increase in sensible heat transport with increasing temperature gradients is as expected. However the changes in heat transport with respect to increasing wind gradients is not so obvious; apparently, at very low wind speeds air movement may actually suppress the buoyant rising of warm air. At Richardson numbers below 0.1 heat transport rises gradually with increasing wind speed.

Transport relationships like equation 5.6-57 may also be cast in terms of  $r_t$ , the resistance to heat transport in the turbulent boundary layer. This is shown in Figure 5.6-27 as a comparison to Figure 5.6-26 and because resistance methods were also attempted.

The usefulness of these equations was tested in two stages. First, in order to establish the applicability of the empirical results, heat fluxes were calculated between the various levels at which temperatures had been measured. Since the site was uniformly vegetated, met fetch requirements, and could be considered near a steady state during a given half-hour period, the calculated fluxes should have been equal (indicating the same heat flux at all levels). Second, to determine the absolute accuracy of the calculated fluxes they were compared to heat fluxes obtained via the ground truth Bowen ratio method.

All quantities in the equations were physical constants or measured directly except  $\Delta U$ , since no wind profile was measured. A stability corrected  $\Delta U$  was calculated iteratively. First, a friction velocity was calculated from the 10 meter wind speed measurement according to equation 5.6-43. The displacement height  $D$  and the roughness parameter  $Z_0$  were obtained graphically from temperature profiles, assuming  $Z_H = Z_0$  and  $D_H = D_m = D$ . Heilman and Kanemasu (1976) assumed the latter equality, but obtained  $Z_H$  by extrapolation. Then, assuming  $U_*$  constant over the profile,  $\Delta U$  was approximated by:

$$\Delta U = \frac{U_*}{k} \frac{\phi_m \Delta Z}{(Z - D)_{gm}} \quad (5.6-60)$$

(difference form of equation 5.6-44) by first using a guess for  $\Delta U$  to compute  $Ri$ , which in turn was used to calculate  $\phi_m$ , and a new  $\Delta U$  was then used as a new guess, and the procedure repeated. Generally this procedure converged on a  $\Delta U$  of three significant figures in four to five iterations.

Figure 5.6-26. Sensible heat flux density,  $H$ , as a function of Richardson number for combinations of  $\Delta u$  and  $\Delta T$ .

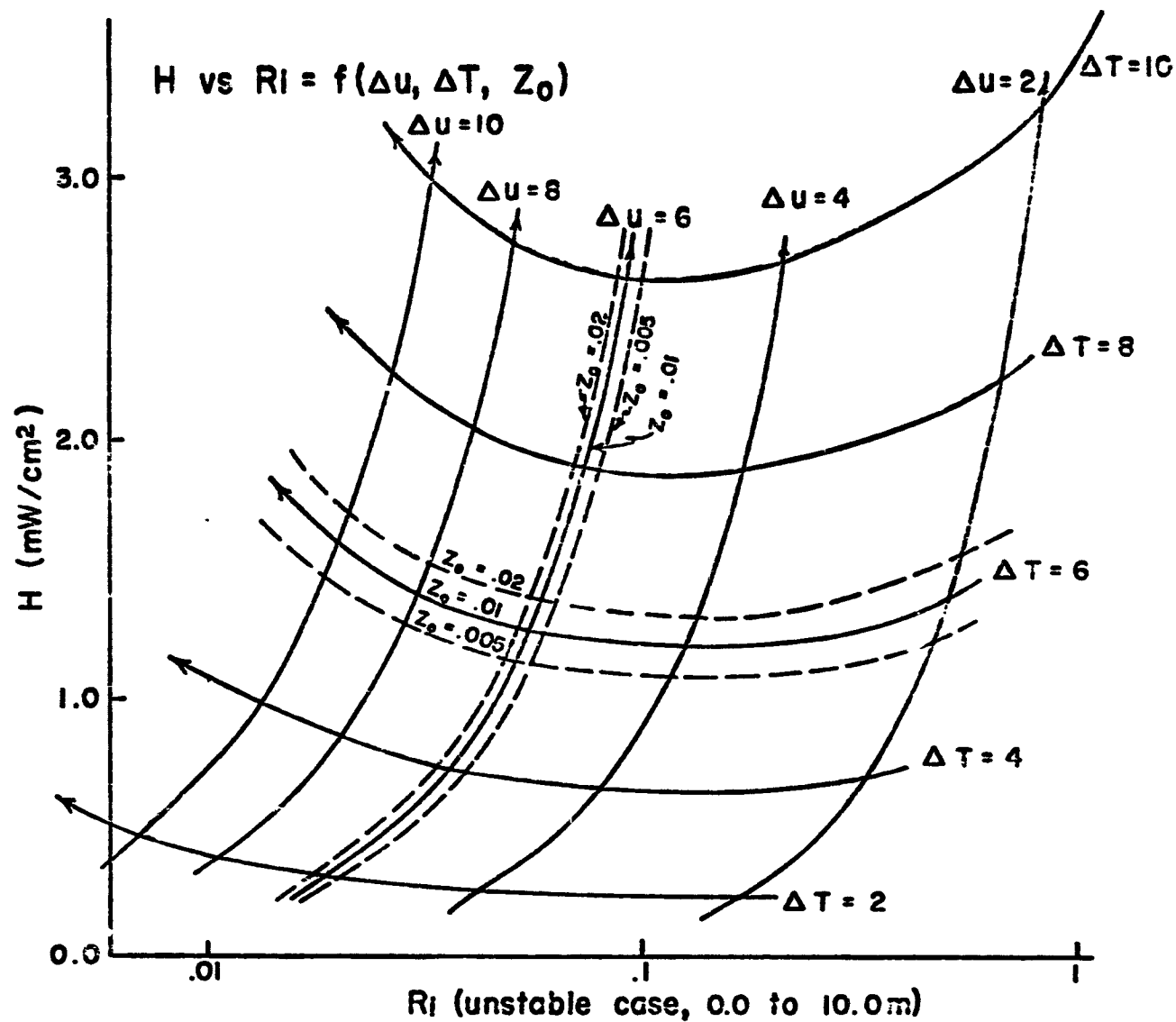
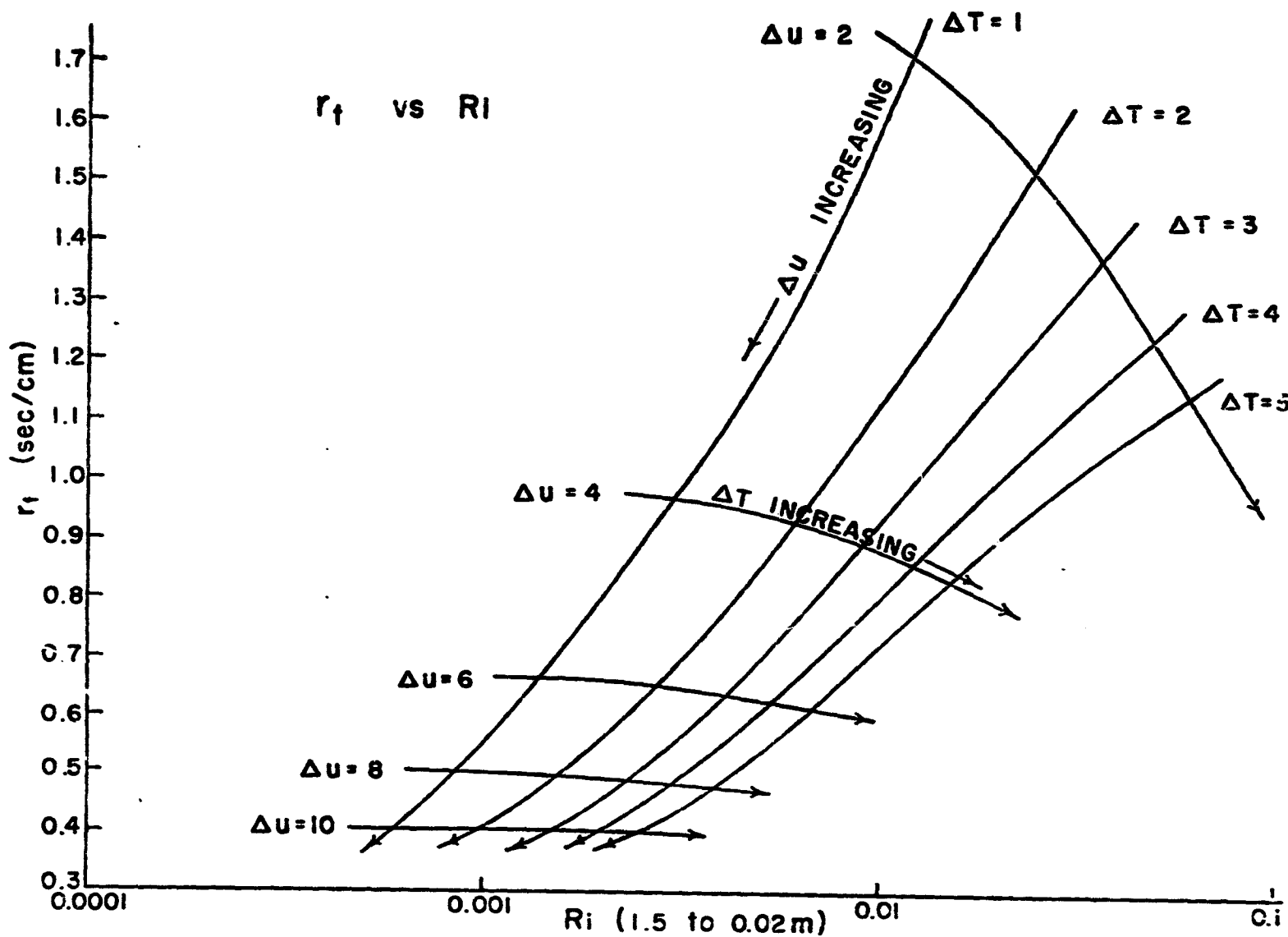


Figure 5.6-27. Turbulent resistance for heat transport,  $r_t$ , as a function of Richardson number for combinations of  $\Delta u$  and  $\Delta T$ .



The flux constancy test (Table 5.6-9) showed several problem areas in the stability corrected heat flux calculation method. These are 1) relatively high heat fluxes calculated for surface and near surface layers 2) relatively low heat fluxes calculated for layers extending from very low to very high levels and 3) relatively high heat fluxes for layers high in the profile. In general, reasons for these departures from constant flux can be traced back to wind and temperature profiles at levels outside the 0.35 to 2.0 meter layer studied at Davis (for which stability corrections were determined).

Calculated heat fluxes are high in air layers bounded on the bottom by the vegetation surface because of the extremely high temperature gradients immediately at the surface. As well as increasing  $\Delta T$  directly, high temperature gradients force up the iteratively calculated  $\Delta U$ , sometimes to physically unrealistic levels. The dominance of  $\Delta T$  in the heat flux equation 5.6-58 continues from the surface to the 2.0 m level. At this point the second problem area begins--heat fluxes become relatively lower because of the increasing importance of  $Z_{gm}$  in the equation. The geometric mean of  $Z_1$  and  $Z_2$  is intended to be the point on the profile at which  $\Delta U/\Delta Z$  or  $\Delta T/\Delta Z$  is the slope of the wind or temperature profile; this holds only approximately when the profiles are not truly logarithmic. Since the stability corrected wind profile is calculated as a correction to a log profile, the geometric mean height will effectively underestimate the point at which a gradient calculated by differences holds in the unstable case, and overestimate in the stable case. These effects are most noticeable when geometric mean heights are calculated over heights more than an order of magnitude apart. The final problem area is calculations made between upper levels. Here  $\Delta T$ 's are small leading to unreasonably small  $\Delta U$ 's, which in turn lead to very high Richardson numbers and corresponding very high stability correction factors.

Thus, to stay on the safe side, it was decided to restrict our calculations to the Davis study layer of 0.35 to 2.0 m (Morgan et al., 1971).

Since many temperature profile data were available for pasture surfaces, regressions relating the difference in surface and air temperatures to the difference in air temperature over the air layer in which the empirical relationships hold were developed.

$\Delta T_T = T_s - T_{1.5}$  temperature difference between surface and 1.5 meters

$\Delta T_{BL} = T_s - T_{0.3}$  difference between surface and 0.3 meters

$\Delta T_t = T_{0.3} - T_{1.5}$  difference between 0.3 and 1.5 meters.

First temperatures at  $Z - D = 0.3$  and 1.5 meters were tabulated from graphs of the temperature profiles. The  $\Delta T_T$  was graphed versus  $\Delta T_{BL}$  for all profiles, a line with zero intercepts was fit to the data by eye, and slope of the line, computed.

$$\Delta T_{BL} = C \Delta T_T \quad (5.6-61)$$

Table 5.6-9. Test for heat flux constancy with stability corrections. <sup>1/</sup>

$Z_1 \backslash Z_2$	9.3	0.6	1.0	2.0	5.0	10.0
0.0	76.1	31.9	25.9	16.0	11.20	8.34
0.3		15.4	13.2	10.8	8.19	6.74
0.6			14.4	13.8	12.00	10.00
1.0				15.6	14.40	10.70
2.0					17.90	16.80
5.0						22.00

<sup>1/</sup> Heat fluxes, in  $\text{mW/cm}^2$ , are calculated for an average temperature profile and 10-m wind speed measured between 1500 and 1530 EST on October 27, 1978.  $Z_2$  and  $Z_1$  are the upper and lower bounds of the air layer for which the heat flux was calculated.

The equation used to calculate  $\Delta T_t$  was

$$\Delta T_t = \Delta T_T - \Delta T_{BL} \quad (5.6-62)$$

$$\Delta T_t = (1 - C) \Delta T_T \quad (5.6-63)$$

Figure 5.6-28 shows the basis of the  $\Delta T_{BL}$  vs.  $\Delta T_T$  regressions. These were plotted for spring and fall data, or short grass and long grass and suggest that in the future generalized relationships involving parameters like vegetation height may be developed such that these relationships need not be measured for all surfaces that may be encountered.

For taller vegetation (forest trees, citrus trees, shrubs, and palmetto), the transport processes and aerial resistances would be much different than for short grasses. Since no ground truth measurements were made over this type of vegetation, we had no way of calculating or estimating the bulk aerial resistance directly. A leaf-to-air heat transport resistance equation developed by Thorpe and Butler (1977) and Landsberg and Powell (1973) was adapted. The type of equation was developed for leaves in an apple orchard where shelter or interference effects among leaves were evident. The generalized equation was

$$r_a = 2.7 \left( \frac{L}{U} \right)^{1/2} \quad (5.6-64)$$

For an assumed leaf dimension (L) of 6 cm, the above equation reduces to

$$r_a = 6.6 U^{-1/2} \quad (5.6-65)$$

where U is in cm/sec.

The wind speed at the top of the tall vegetation was estimated to be one-half of the measured wind speed (over pasture) at 10 m. Many examples in the literature show that this is a reasonable approximation (e.g., Allen, 1968).

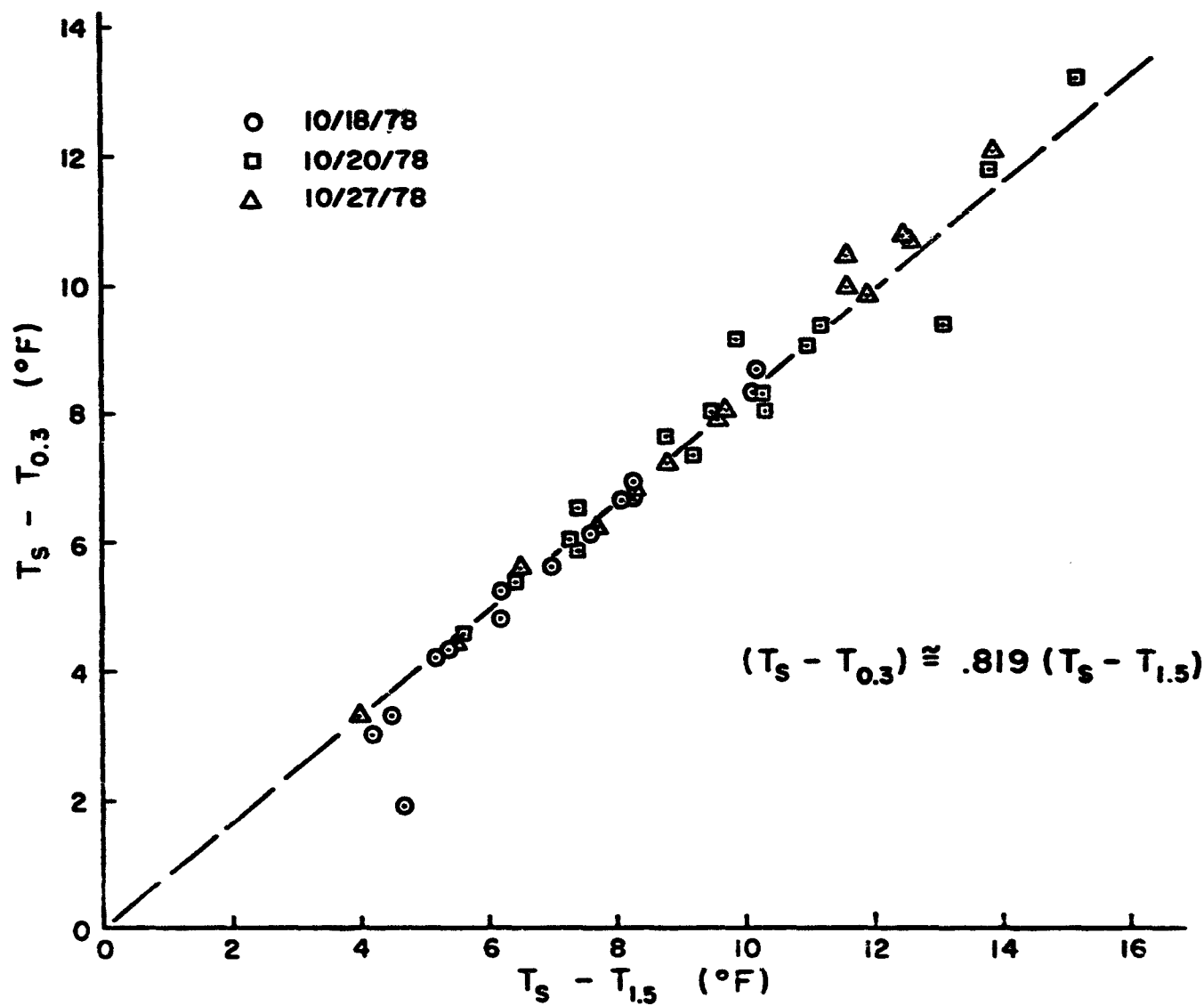
General Procedure for Converting Thermal Scene Into a Regional ET Estimate: To summarize the technique developed and show its application to thermal scenes, the entire calculation procedure is outlined below. It is assumed that for the area in question roughness length and displacement height are known, air temperature and wind speed are known from auxiliary ground measurements, and surface temperature is available from satellite data.

(1) Divide the range of vegetation roughness lengths ( $\bar{Z}_0$ ) and surface temperature ( $\bar{T}_s$ ) into suitable increments. Determine the area of each  $\bar{Z}_0$ ,  $\bar{T}_s$  combination and compute the percentage of total area in each combination as  $P(\bar{Z}_0, \bar{T}_s) = A(\bar{Z}_0, \bar{T}_s)/A(\text{total})$  (in the most complex scene on April 26, two roughness conditions, corresponding to short and tall vegetation, in seven temperature increments were considered).

(2a) For short vegetation ( $Z_0 = 0.01$  m,  $D = 0.0$  m)

A. Use  $\Delta T_T$  vs.  $\Delta T_{BL}$  regressions to calculate  $\Delta T_t$  in ( $^{\circ}\text{C}$ ) for each  $\bar{T}_s$ .

Figure 5.6-28. Temperature difference from surface to 0.3 m vs. Temperature difference from surface to 1.5 m.



B. Calculate friction velocity  $U_*$  in (m/sec)

$$U_* = \frac{k U_{10}}{\ln\left(\frac{Z - D}{Z_0}\right)} = 0.0579 U_{10} \quad (5.6-66)$$

C. Calculate  $\Delta Z$ ,  $(Z - D)_{gm}$ ,  $\frac{(Z - D)_{gm}^2}{(\Delta Z)^2}$ , where

$$(Z - D)_{gm} = \exp\left[\frac{\ln(Z_1 - D) + \ln(Z_2 - D)}{2}\right] \quad (5.6-67)$$

$$\Delta Z = Z_2 - Z_1 \quad (5.6-68)$$

D. Use iterative technique to calculate  $\Delta U$

a) guess at  $\Delta U$

$$b) \text{ calculate } Ri = \frac{g}{\theta} \frac{\left(\frac{\Delta T}{\Delta Z}\right)}{\left(\frac{\Delta U}{\Delta Z}\right)^2} \quad (5.6-28)$$

where  $\theta$  is absolute temperature ( $^{\circ}K$ )

c) calculate a new  $\Delta U$

$$\Delta U_{new} = \frac{U_* \Delta Z \phi_m}{k (Z - D)_{gm}} \quad (5.6-60)$$

(from difference form of  $\phi_m$  definition equation 5.6-60)

$$\phi_m = (1 + 16 Ri)^{+1/3} \quad (\text{See Equations 5.6-47 and 5.6-48})$$

d) go to b) using  $\Delta U_{new}$  to calculate  $Ri$ .

E. Calculate heat flux in ( $mW/cm^2$ ) for each  $\Delta T_t$

$$H = \rho C_p k^2 \left(\frac{K_H}{K_m}\right) \left(\frac{1}{\phi_m^2}\right) \frac{(Z - D)_{gm}^2}{(\Delta Z)^2} \Delta U \Delta T \quad (5.6-58)$$

(2b) For tall vegetation, use special resistance technique to calculate  $H$  for each  $T_s$ .

$$r_a = 6.6 (U)^{-1/2} \quad (5.6-65)$$

$$H = \frac{\rho C_p (T_s - T_a)}{r_a} \quad (5.6-17)$$

(3) Calculate ET for each  $Z_0$ ,  $T_s$  combination

A. Estimate soil heat flux (in estimates presented here measured S was used for short vegetation, and S was considered negligible under tall vegetation)

B.  $ET(Z_0, T_s) = R_n$  (measured or remote) -  $H(Z_0, T_s)$  - S (estimate)

(4) Calculate regional ET flux.

$$ET = \sum_{Z_0} \sum_{T_s} P(Z_0, T_s) ET(Z_0, T_s) \quad (5.6-69)$$

Tables 5.6-10 and 5.6-11 summarize regional evapotranspiration rates arrived at using the preceding procedure on two thermal scenes. The results are reasonable judging from a comparison to the ground truth measurement, and demonstrate that this approach is workable.

A better insight into the effect of the diabatic influence function stability treatment can be gained from Figure 5.6-29, which shows ET as a function of surface-to-10 m air temperature for two different wind speeds. As the surface-to-air temperature difference increases, atmospheric instability increasingly enhances sensible heat transport leaving less energy for ET, resulting in a curve that is concave downward. With an increase in wind speed, stability effects are damped and the relationship becomes more linear. Without a stability correction, these curves would be exactly linear.

The bottom line on any technique making use of remotely sensed surface temperatures is how close the resulting estimates fit ground truth measurements. On this score our results are still somewhat inconclusive since our remote sensed estimates average 30 to 50 percent higher than our ground truth measurements.

There are a variety of possible reasons for this discrepancy. The method for remote heat flux estimates was found to be extremely sensitive to parameters such as the displacement height and the geometric mean height. Without consideration of the displacement height, heat flux estimates bore little relation to ground truth values; the grass surface at Davis, California was short enough not to require its use.

Also, since the differential version of the diabatic influence functions was used, no explicit use of the roughness length  $Z_0$  was made. It is possible that even if actual profiles over clipped grass and profiles over pasture (with or without displacement height corrections) are nearly the same, heat transport would be affected by the roughness of the underlying surface.

Besides the particular sensitivity of the method to some parameters and questions about the applicability of dimensionless empirical expressions, the

#### 5.8.4.5 Data Base Management System

A flexible computer oriented data base to provide timely data for the various models, etc., discussed above, was defined by all of the Water Management Districts as a prime need. The development of the Water Resources Management Information System (WRMIS) data base was started through the meetings with the various WMD's and through the remote sensing techniques developed tasks. Studies of existing NASA data base management systems: e.g., AOIPS and IBIS, were started to determine if an existing system could be used or if a new system would need to be developed due to the extensiveness of the data base and the need for it to include remote sensing data and ancillary data of point source type, areal type, and time series variable. One of the major areas of study proposed for FY 1979 through an effort by a Kennedy Space Center contractor, Computer Sciences Corporation, was a continuation of this effort to develop a Data Base Management System. This effort would have included the review of all applicable commercial data management systems; e.g., Hydrocomp's HSPII, COMAC, etc.; as well as other systems developed through NASA. The study would have also included the evaluation of applicable computer hardware for operation of the data base including main-frame systems versus multi-mini systems. The study would include an evaluation of existing and proposed expansion of each WMD's computer system to assure that the data base could be used by all districts.

#### 5.8.5 Long Range Plan Conclusions

The above results of the meetings and studies concerning the development of the Long Range Plan consist of a status report on this task. As mentioned in the introduction to this report, the carry over FY 1979 and subsequent year's efforts on the project were not funded by NASA Headquarters, therefore the effort to develop the Long Range Plan was brought to a close in August of 1978.

Table 5.6-10. ET calculations from Different Surface Temperatures for the Pasture Scene of April 28, 1978 (1222-1225 EST) using Stability Corrected Heat Flux Densities that were Derived from Temperature Profiles.

Color	$T_s^1$ (°F)	$\Delta T_t^2$ (°C)	$\Delta U_t^3$ (m/sec)	$Ri^4$	$\{ \}^5$	$H^6$ (mW/cm <sup>2</sup> )	$ET^7$ (mW/cm <sup>2</sup> )	$P^8$ (%)
Tan	110	2.21	0.743	-0.158	57.6	29.6	19.1	23.3
Black	105	1.86	0.800	-0.115	48.8	22.7	26.0	24.2
Aqua	99	1.44	0.870	-0.0721	40.1	15.7	33.0	25.1
Pink	93	1.03	0.943	-0.0458	33.2	10.1	38.6	16.5
Yellow	87	0.61	1.02	-0.0231	27.5	5.36	43.3	6.6
Blue	81	0.19	1.10	-0.0062	22.8	1.49	47.2	2.2
Orange	75	-0.22	1.17	+0.0064	18.6	-1.50	50.2	2.1

$$\text{Regional ET} = \frac{1}{100} \sum ET_{(\text{color})} P_{(\text{color})} = 30.3 \text{ mW/cm}^2$$

$$\text{Ground Truth ET (measured in a black/aqua field)} = 35.0 \text{ mW/cm}^2$$

Constants used in calculations:

$$T_a = 25.6^\circ\text{C}, U_{10} = 4.37 \text{ m/s}, U_* = 0.253 \text{ m/s}, D = 0.0 \text{ m}, Z_0 = 0.01 \text{ m}, \Delta Z = 1.2 \text{ m},$$

$$Z_{gm} = 0.671 \text{ m}.$$

<sup>1</sup> Midpoint of temperature range of color on thermal scene.

<sup>2</sup> Calculated from regression:  $\Delta T_t [^\circ\text{C}] = 0.125 (T_s - T_a) [^\circ\text{C}]$ ; signs chosen so upward heat flux is positive.

<sup>3-4</sup> Calculated iteratively:  $Ri = \frac{g}{\theta} \left( \frac{\Delta T}{\Delta Z} \right) / \left( \frac{\Delta U}{\Delta Z} \right)^2$ ;  $\Delta U = \frac{U_*}{k} \frac{\Delta Z (1-16Ri)^{-.333}}{Z_{gm}}$ , unstable case,  
 $\theta = \text{absolute temperature } [^\circ\text{K}], g = 9.8 \text{ m/s}^2$ .  $\Delta U = \frac{U_*}{k} \frac{\Delta Z (1+16Ri)^{-.333}}{Z_{gm}}$ , stable case

<sup>5</sup> Stability correction factor  $\{ \} = 20.9 (1-60Ri)^{.074} (1-16Ri)^{.667}$ , unstable case,  
 $\{ \} = 20.9 (1+95Ri)^{-.11} (1+16Ri)^{-.667}$ , stable case.

<sup>6</sup>  $H = \{ \} ((Z_{gm}/\Delta Z)^2) \Delta U \Delta T.$

<sup>7</sup>  $ET = Rn - S - H = 58.2 - 9.5 - H = 48.7 - H.$

<sup>8</sup>  $P = \frac{100 \text{ Area}_{(\text{color})}}{\text{Total Area}}$

C-4

Table 5.6-11. ET calculations from Different Surface Temperatures for the Citrus Grove Scene of April 26, 1978 (1432-1435 EST). Stability Corrected Heat Flux Densities that were Derived from Temperature Profile Data were used to Calculate ET from Short Vegetation, and a Leaf-to-Air Resistance Model was used to Calculate Sensible Heat Flux, and then ET, from Tall Vegetation.

Short Vegetation:

Color	$\bar{T}_s^1$ [°F]	$\Delta T_t^2$ [°C]	$W_t^3$ [m/s]	$R_t^4$	( ) <sup>5</sup>	$H^6$ [mW/cm <sup>2</sup> ]	$ET^7$ [mW/cm <sup>2</sup> ]	$p^8$ [%]
Tan	108	2.24	2.98	-.00993	23.9	49.9	4.7	0.0
Black	103	1.89	3.01	-.00825	23.4	41.6	3.2	0.3
Aqua	97	1.47	3.04	-.00630	22.8	31.9	12.9	10.8
Pink	91	1.06	3.06	-.00446	22.3	22.6	22.2	13.9
Y/P	88	.854	3.08	-.00356	22.0	18.1	26.7	6.9
Yellow	85	.639	3.09	-.00264	21.7	13.4	31.4	19.8
Blue	79	.222	3.12	-.00090	21.2	4.6	40.2	3.2
Orange	73	-.194	3.15	+.00077	20.6	3.9	48.7	1.1

Tall Vegetation:

Color	$\bar{T}_s^1$ [°F]	$\Delta T_T^3$ [°F]	$H^{10}$ [mW/cm <sup>2</sup> ]	$ET^7$ [mW/cm <sup>2</sup> ]	$p^8$ [%]
PK	91	15.2	36.3	8.5	4.7
Yellow	85	9.2	22.0	22.8	12.9
Blue	79	3.2	7.65	37.2	14.6
Orange	73	-2.8	-6.70	51.5	11.8

Regional ET

$$ET = \frac{1}{100} \sum_{\text{Vegetation heights}} \sum_{\text{colors}} ET(\text{height, color}) P(\text{height, color}) = 29.2 \text{ mW/cm}^2$$

Constants used in calculations:  $T_a = 24.3^\circ\text{C}$ ,  $U_{10} = 12.1 \text{ m/s}$ ,  $U_* = 0.701 \text{ m/s}$ ,  $D = 0.0\text{m}$ ,  $Z_0 = 0.0\text{ m}$ ,  $\Delta z = 1.2\text{m}$ ,  $Z_{gm} = 0.671 \text{ m}$ .

1-6 Calculated in the same way as for pasture scene, Table 10.

$$7 \quad ET = R_n - S - H = 43.5 - (-1.26) - H$$

$$3 \quad p = \frac{100 \text{ Area (color, height)}}{\text{Total Area}}$$

$$9 \quad \Delta T_T = \bar{T}_s - T_a$$

$$10 \quad H = \frac{\rho C_p (5/9) \Delta T_T}{r_a} \text{ where } r_a = 6.6 (U_{10}/2)^{1/2} = 0.268 \text{ s/cm}$$

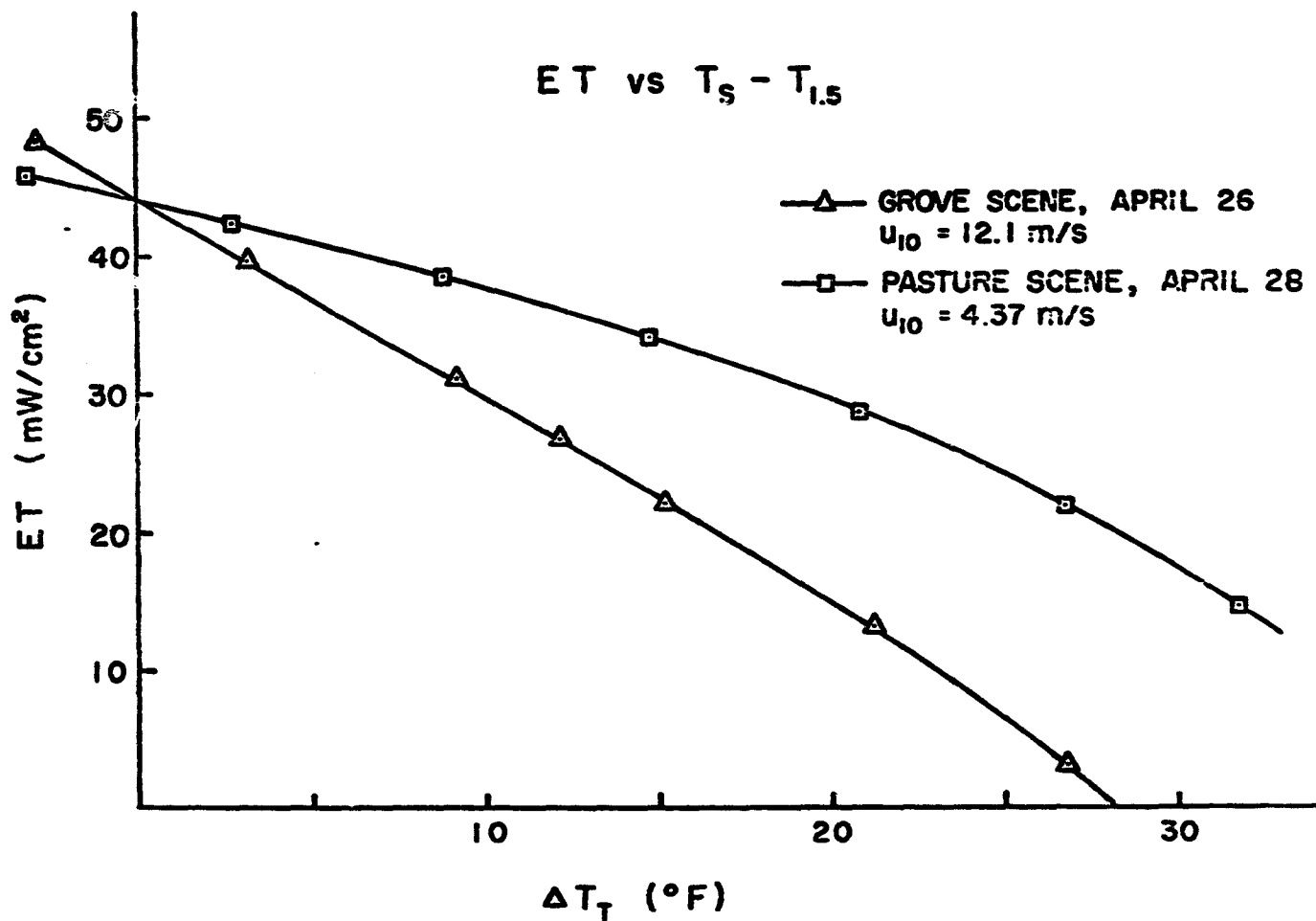


Figure 5.6-29. ET as a function of the difference between surface temperature and air temperature at 1.5 m for short vegetation for the conditions on April 28 (1222-1225 EST), square symbols (□) and on April 26 (1415-1422 EST), triangle symbols (△).

temperature profiles may have been unreliable. Accurate temperature profiles were particularly hard to obtain in the spring, when the data acquisition system was still being modified in the field. Also, very large differences in surface temperature were observed in different fields around the micrometeorological test site (Figures 5.6-5 and 5.6-23) that appeared to cause warmer eddies to occasionally flow past the 2, 5, and 10 m levels of the temperature mast.

#### 5.6.2.5.6 Remote Sensed ET Estimates from Stability-Corrected Integral Profile Methods

Mean meteorological data acquired from the micrometeorological tower were obtained at an instantaneous readout at 1245 EST. These data were:  $T_a = 23.9^\circ\text{C}$ , Dewpoint temperature =  $11.0^\circ\text{C}$ ,  $R_n = 64.1 \text{ mW/cm}^2$ ,  $S = 9.5 \text{ mW/cm}^2$ , wind =  $5.07 \text{ m/sec}$ , and Bowen ratio =  $0.47$ . These data were input into the models shown in equations 5.6-28 to 5.6-31 with the surface temperature (Black) shown in Table 5.6-4 and Figures 5.6-5 and 5.6-23. Stability parameters  $\psi_1$  (momentum) and  $\psi_2$  (heat) were computed according to the integration of Paulson (1970). Aerial resistance can be computed from equation 5.6-31 for use in the resistance-energy balance model of equation 5.6-16 or the combination model of equation 5.6-32. The roughness length parameter,  $Z_0$ , is required to compute  $r_a$ . Webb (1965) indicated that  $Z_0$  for open grassland is about 0.02 to 0.04 m. According to Szeicz et al. (1969), this would correspond to grass heights of about 5 to 10 cm. Some of our pasture vegetation was estimated to be 4 cm, so 1 cm or less may be a more representative  $Z_0$ . The sensitivity of equation 5.6-16 and equation 5.6-32 to  $Z_0$  was tested for values between 0.5 cm to 4 cm (Figure 5.6-30).

Both stability ( $R_i$ ) and roughness ( $Z_0$ ) had an effect on the computed  $r_a$  values. At a  $Z_0$  of 1 cm, the ratio of  $r_a$  in the most unstable case ( $\Delta T = 17.2^\circ\text{C}$ ) to  $r_a$  in the neutral case ( $\Delta T = 0^\circ\text{C}$ ) was  $0.476/0.587$ , or  $0.81$ . In the neutral stability case ( $\Delta T = 0^\circ\text{C}$ ), the relative values of  $r_a$  decreased with increasing  $Z_0$  ( $0.712$ ,  $0.587$ ,  $0.477$ ,  $0.416$ , and  $0.376$ , for  $Z_0$  of  $0.5$ ,  $1$ ,  $2$ ,  $3$ , and  $4$  cm, respectively). Table 5.6-12 shows values of sensible heat and latent heat flux densities as a function of Richardson number (equation 5.6-28). The temperature gradient shown in this table was  $T_s - T_a$  where  $T_a$  was at 10 meters. The sensible heat flux density and latent heat flux density is shown in Table 5.6-12. Total fluxes were computed based on proportional areas (shown in Tables 5.6-8, 5.6-10, and 5.6-11). These computations showed much higher values of  $H$  and lower values of  $\lambda E$  for the April 28 pasture scene than computed in Table 5.6-8. The computed overall Bowen ratio was  $1.47$ , as compared to  $0.34$  in Table 5.6-8. In general, the  $r_a$  values were about  $1/2$  of the bulk aerial resistance,  $r_b$ , computed by using equation 5.6-27. As discussed in Section 5.6.2.5-D, the aerial resistance should be considered in two parts, especially for this type of short grass vegetation. The  $r_a$  values computed by assuming  $Z_H = Z_0 = 1 \text{ cm}$  are really turbulent transport values, and do not include the bulk boundary layer resistance.

Half-hourly data on April 28, 1978, were used to compute  $Z_H$  values. Temperature profiles were smoothed by plotting air temperature vs. log height.

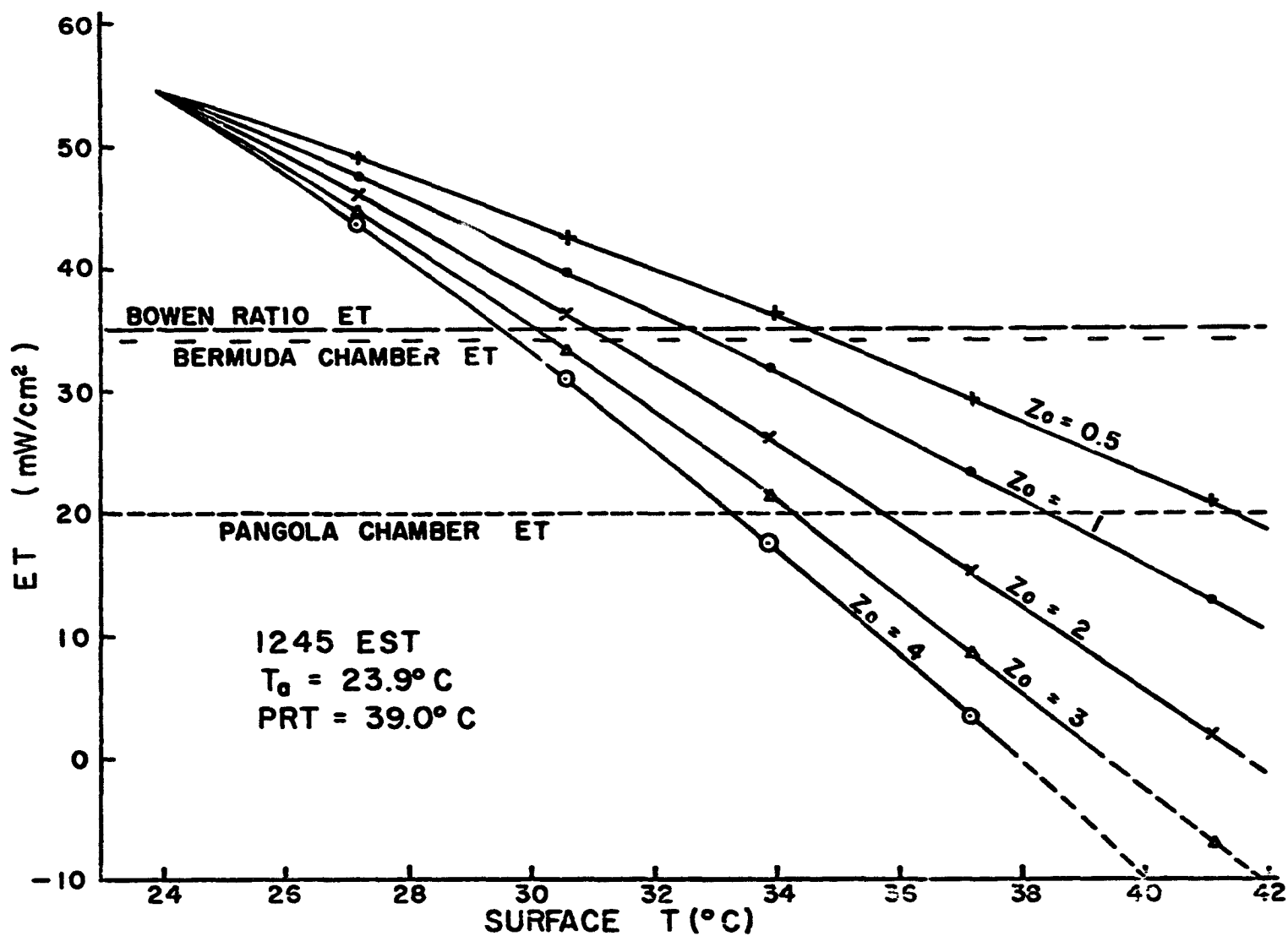


Figure 5.6-30. ET as a function of  $Z_0$  and surface temperature (surface-to-air temperature difference) for measurements at 1245 EST on April 12, 1978. Chamber ET and Bowen ratio ET are also shown. (Also see Table 12.)

391

Table 5.6-12. Computations of  $\lambda E$ ,  $H$ , and  $r_a$  from stability-corrected profile integral methods using meteorological input data from April 28, 1978 at 1245 EST with the thermal scene obtained at 1222-1225 EST.

Color	$\Delta T$ (°C)	Ri	$\Psi_1$	$\Psi_2$	$U_*$ (cm/s)	$Z_H = Z_0 = 1 \text{ cm}$				$Z_H = 0.01 \text{ cm}$			
						$r_a$ (s/cm)	$H$ (mW/cm <sup>2</sup> )	$\lambda E$ (mW/cm <sup>2</sup> )	$\beta$	$r_a$ (s/cm)	$H$ (mW/cm <sup>2</sup> )	$\lambda E$ (mW/cm <sup>2</sup> )	$\beta$
Black (Tan)	17.2	-0.219	0.488	0.889	31.6	0.476	41.7	12.9	3.23	0.841	23.6	31.0	0.76
Aqua	13.3	-0.169	0.409	0.770	31.2	0.492	31.2	23.4	1.33	0.861	17.8	36.8	0.48
Pink	10.0	-0.127	0.337	0.630	30.9	0.508	22.7	31.9	0.71	0.881	13.1	41.5	0.32
Yellow	6.7	-0.085	0.251	0.478	30.5	0.527	14.7	39.9	0.37	0.904	8.6	46.0	0.18
Blue	3.3	-0.042	0.142	0.273	30.0	0.553	6.9	47.7	0.14	1.000	4.1	50.5	0.08
Orange	0	0	0	0	29.4	0.587	<u>0</u>	<u>54.6</u>	<u>0</u>	1.033	<u>0</u>	<u>54.6</u>	<u>0</u>
Totals							32.5	22.1	1.47		18.5	36.1	0.51

Values at  $z = 10$  m and  $z = 0.3$  m were extracted and  $T_*$  computed from the following equation (see Kanemasu et al., 1979).

$$T_* = \frac{k (T_{0.3} - T_{10})}{[\ln(10) - \ln(0.3) - \psi_{2,10} + \psi_{2,0.3}]} \quad (5.6-70)$$

The stability functions at 10 m and 0.3 m were taken from Table 5.6-12, depending upon the  $T_s - T_{10}$  temperature difference. The value of  $Z_H$  was determined by substituting values of  $T_s$  (surface temperature from radiation thermometer data) into the above type of equation:

$$Z_H = \text{EXP} [\ln(10) - \frac{k}{T_*} (T_s - T_{10}) - \psi_{2,10}] \quad (5.6-71)$$

The arithmetic mean of fifteen profile determinations of  $Z_H$  was 0.0178 cm, the geometric mean was 0.00273 cm, and the mode was 0.00286. The values computed ranged from 0.0919 on to  $0.516 \times 10^{-6}$ . This wide scatter was likely due to the fact that temperature profiles and surface radiation temperatures were read only each 15 minutes (see Table 5.6-3).

Since wind speed profiles were not measured, there was no way to determine  $Z_0$  directly. However, through the definition of  $T_* = H/(\rho C_p U_*)$ ,  $Z_0$  could be calculated from  $T_*$  values obtained from air temperature profile data, from  $H$  values obtained from the energy balance - Bowen ratio apparatus, and from wind speed measured at 10 m. Rearranging equation 5.6-29 gives:

$$Z_0 = \text{EXP} [\ln(10) - \frac{K U_{10}}{U_*} - \psi_2] \quad (5.6-72)$$

Fourteen profiles from 830 to 1530 EST on April 28 were analyzed. The arithmetic mean value of  $Z_0$  was 4.16 cm, the geometric mean value was 0.161 cm, and the mode was 0.412 cm. The values ranged from 32.5 cm to  $3.5 \times 10^{-12}$  cm. Here again, low frequency of observations, including wind speed at 10 m, probably contributed to the scatter of data (see Table 5.6-3).

From the above analyses, a value of  $Z_H = 0.01$  cm was selected to recompute  $r_a$ ,  $H$ , and  $\lambda E$  by the integral profile stability corrected method (equation 5.6-31). Computations were made for  $Z_0$  values of 0.5, 1, 2, 3, and 4 cm, but only the values of  $Z_0 = 1$  cm are shown in Table 5.6-12. Computations were made for the whole scene of April 28, 1978. The values of  $r_a$  based on  $Z_H = 0.01$  were approximately twice as large as those based on  $Z_0 = 1$  cm. They should correspond more nearly to the sum of  $r_t$  and  $r_b$ , the turbulent resistance, and the bulk boundary layer resistance. The values ranged from 0.841 sec/cm at  $Ri = -0.219$  to 1.033 for  $Ri = 0$ , and compare well with the value of 1.13 obtained from  $T_s - T_{10}$  and  $H$  measurements.

The total scene (April 28)  $H$ ,  $\lambda E$ , and  $\beta$  values were 18.5 mW/cm<sup>2</sup>, 36.1 mW/cm<sup>2</sup>, and 0.51, respectively. These values compare well with those of Table 5.6-8. Therefore, this method looks promising when accurate values of  $Z_H$  can be obtained.

Another alternative approach of computation of  $H$  and  $\lambda E$  by the integral profile stability corrected method would be to determine  $T_0$ , an air temperature at  $Z_0$ , by some method, and then compute  $T_0 - T_a$ , Richardson number,  $\psi_1$ ,  $\psi_2$ , and  $r_a$  based on these temperature and height differences. However, this method does not have the advantage of using surface-derived temperatures directly.

The surface temperatures measured by the airborne scanner and the radiation thermometer are probably not the theoretical temperatures at  $Z_H$ , but they appear to be suitable for use in computing fluxes of sensible heat and latent heat.

### 5.6.3 References

- Allen, L.H., 1968. Turbulence and Wind Speed Spectra Within a Japanese Larch Plantation. *J. Appl. Meteorol.*, 7:73-78.
- Bartholic, J.F. and D.W. Buchanan, 1976. Disposition of Water from Fruit Crops and Approaches to Increase Water Use Efficiency. Water Resource Research Center, University of Florida, Gainesville, Florida, Number 33.
- Barton, I.J., 1979. Parameterization of the Evaporation from Nonsaturated Surfaces. *Jour. Appl. Meteorol.*, 18:43-47.
- Bill, R.G., Jr., R.A. Sutherland, J.F. Bartholic, and E. Chen, 1978. Observations of the Convective Plume of a Lake Under Cold-Air Advective Conditions. *Boundary-Layer Meteorol.*, 14:543-556.
- Businger, J.A., 1973. Aerodynamics of Vegetated Surfaces. Heat and Mass Transfer in the Biosphere (D.A. de Vries and N.H. Afgan, ed.). *Scripts Book Co.*, Washington, D.C., 594 pp.
- Chen, E.Y., 1979. Estimating Nocturnal Surface Temperature in Florida Using Thermal Data from Geostationary Satellite Data. Ph.D. Dissertation, University of Florida, Gainesville, Florida, 280 pp.
- Davis, P.A. and W. Viezee, 1964. A Model for Computing Infrared Transmission Through Atmospheric Water Vapor and Carbon Dioxide. *J. Geo. Res.*, 69:3785.
- Deardorff, J.W., 1978. Efficient Prediction of Ground Surface Temperature and Moisture with Inclusion of a Layer of Vegetation. *J. Geo. Res.*, 83:1889-1903.
- Dyer, A.J., 1967. The turbulent Transport of Heat and Water Vapour in an Unstable Atmosphere. *Quart. J. R. Met. Soc.*, 93:501-508.
- Elsasser, W.M. and M.F. Culbertson, 1960. Meteorological Monographs. 4, 43 pp.
- Greenfield, S.M. and W.W. Kellogg, 1960. Calculations of Atmospheric Infrared Radiation as Seen From a Meteorological Satellite. *J. Appl. Met.*, 17:283.
- Heilman, J.L. and E.T. Kanemasu, 1976. An Evaluation of a Resistance Form of the Energy Balance to Estimate Evapotranspiration. *Agron. J.*, 68:607-611.
- Holtan, H.N., G.V. Stiltner, W.H. Hensor, and N.C. Lopez, 1974. USDA HL-74 Revised Model of Watershed Hydrology. USDA, ARS, Plant Physiology Report, Number 4.
- Jones, J.W. and K.J. Boote, 1978. Personal Communication.
- Kanemasu, E.T., M.L. Wesely, B.B. Hicks, and J.L. Heilman, 1979. Techniques for Calculating Energy and Mass Fluxes. In: Modification of the Aerial Environment of Crops (B.J. Barfield and J.F. Gerber, eds.). Ch. 3.2, pp. 156-182, ASAE Monograph Number 2, Amer. Soc. Agr. Eng., St. Joseph, Michigan.

- Knisel, W.G., P. Yates, J.M. Sheridan, T.K. Woody, III, L.H. Allen, Jr., and L.E. Asmussen, 1980. Hydrology and Hydrogeology of Taylor Creek Watershed, Okeechobee County, Florida: Data and Analysis. USDA Technical Bulletin (In Press).
- Koberg, Gordon E., 1958. U.S. Geological Survey, Energy - Budget Studies. Water-Loss Investigations: Lake Mead Studies, Geological Survey Professional Paper 298, Pages 20-29.
- Landsberg, J.L. and D.B. Powell, 1973. Surface Exchange Characteristics of Leaves Subject to Mutual Interference. Agric. Met. 13:169.
- Lemon, E., R.W. Stewart, and W.R. Shawcroft, 1971. The Sun's Work in a Cornfield. Science, 174:371-378.
- Morgan, D.L., W.O. Pruitt, and F.J. Lourence, 1971. Analysis of Energy and Mass Transfers Above Vegetative Surfaces. Res. & Devel. Tech. Rept. ECOM 68-G10-F by Univ. of Calif. (Davis) for U.S. Army Electronics Command, Atmos. Sciences Lab., Ft. Huachuca, Arizona. AD 721-301. 128 pp.
- Monteith, J.L., 1965. Evaporation and Environment. Symp. Soc. Expl. Biol., 19:205-234.
- Paulson, C.A., 1970. The Mathematical Representation of Wind Speed and Temperature Profiles in the Unstable Atmospheric Surface Layer. J. Appl. Met., 9:857-861.
- Penman, H.L., 1948. Natural Evaporation from Open Water, Bare Soil and Grass. Proc. Roy. Soc. A, 199:120-145.
- Priestley, C.H.B. and R.J. Taylor, 1972. On the Assessment of Surface Heat Flux and Evaporation Using Large-Scale Parameters. Mon. Weather Rev., 100:81-92.
- Reicosky, D.C. and D.B. Peters, 1977. A Portable Chamber for Rapid Evapotranspiration Measurements on Field Plots. Agron. J., 69:729-732.
- Rogers, J.S. and J.F. Bartholic, 1976. Estimated Evapotranspiration and Irrigation Requirements for Citrus. Soil Crop Sci. Soc. Florida Proc., 35:111-117.
- Rosenberg, N.J., 1974. Micro-Climates, The Biological Environment. John Wiley and Sons, New York, 315 pp.
- Rosenberg, N.J., B.L. Blad, S.B. Verma, and M.W. Baradas, 1975. Great Plains Evapotranspiration by a Resistance Model Using Remotely Sensed Thermal Imagery. Nebraska Water Resources Research Inst., Project B-028.
- Shenk, W.E. and V.V. Solomonson, 1972. A Simulation Study Exploring the Effects of Sensor spatial Resolution on Estimates of Cloud Cover from Satellites. J. Appl. Met., 11:214-220.
- Shuttleworth, J.W., 1976. A One-Dimensional Theoretical Description of the Vegetation-Atmosphere Interaction. Boundary-Layer Met., 8:81-99.

- Stephens, J.C. and E.H. Stewart, 1963. A Comparison of Procedures for Computing Evaporation and Evapotranspiration. Public 62, Intern. Assoc. of Sci. Hydrol., Trans. Intern. Union of Geodesy and Geophysics, Berkeley, Calif. pp. 123-133.
- Szeicz, G., G. Endrod, and S. Tajchman, 1969. Aerodynamic and Surface Factors in Evaporation. Water Resources Res., 5:380-394.
- Tanner, C.B. and M. Fuchs, 1968. Evaporation from Unsaturated Surfaces: A Generalized Combination Method. J. Geo. Res., 73:1299-1304.
- Tarpley, J.D., 1979. Estimating Incident Solar Radiation at the Surface from Geostationary Satellite Data. J. Appl. Met., 18:1172-1187.
- Tarpley, J.D., S.R. Schneider, J.E. Bragg, and M.P. Waters III, 1978. NOAA Tech. Memorandum NESS-96, Satellite Data Set for Solar Incoming Rad. Studies Wash., D.C., May 1978, 36 pp.
- Thom, A.S., 1971. Momentum Absorption by Vegetation. Quarterly J. R. Met. Soc., 97:414-428.
- Thom, A.S., 1972. Momentum, Mass and Heat Exchange of Vegetation. Quarterly J. R. Met. Soc., 98:124-134.
- Thorpe, M.R. and D.R. Butler, 1977. Heat Transfer Coefficients for Leaves on Orchard Apple Trees. Boundary Layer Met., 12:61-73.
- Verma, S.B. and B.J. Barfield, 1979. Aerial and Crop Resistances Affecting Energy Transport. In: Modification of the Aerial Environment of Crops (B.J. Barfield and J.F. Gerber, eds.). Ch. 3.5, pp. 230-248, ASAE Monograph Number 2, Amer. Soc. Agric. Eng., St. Joseph, Michigan.
- Verma, S.B., N.J. Rosenberg, B.L. Blad, and M.W. Baradas, 1976. Resistance-Energy Balance Method for Predicting Evapotranspiration: Determination of Boundary Layer Resistance and Evaluation of Error Effects. Agron. J., 68:776-782.
- Webb, E.K., 1965. Aerial Microclimate. In: Agricultural Meteorology, Meteorological Monographs, Vol. 6, Nr. 28, Ch. 2, pp. 27-58. Amer. Meteorol. Soc., Boston, Mass.
- Weinreb, M.P., 1977. Sensitivity of Satellite Retrievals of Temperature to Errors in Estimates of Tropospheric Water Vapor. J. Appl. Met., 16:605.

#### 5.6.4 Discussion and Conclusions

Measurements of surface radiation temperature from a thermal radiation scanner were obtained during aircraft overflights on April 26 and 28 and on October 17, 1978. Micrometeorological measurements (including net radiation and surface radiation temperature) were obtained at a test site during those time periods. The objectives were to develop methods for predicting regional evapotranspiration (ET) using remote sensed data. Specifically, several approaches using remotely sensed surface temperature were investigated.

Measurements for several daily periods in the spring and fall of ET were obtained from an energy balance Bowen ratio method. ET was also determined by a chamber method utilizing rates of change of humidity immediately after placement. Differences in ET were due mainly to differences in stage of development between Bermuda grass and Pangola grass.

A vegetation survey compared midday surface thermal images with ground cover. The differences in thermal patterns of pasture appeared to be more correlated with density of ground cover than species of vegetation. For tall vegetation, wild stands of palm and hardwood were significantly cooler than citrus groves. Bare soil areas were hottest. Short grass surfaces were observed that were much warmer than air (up to 15°C). Only shallow water, marshes, and tall trees were at or slightly below air temperature.

Two thermal pattern scenes (pasture on April 28, 1222-1225 EST and citrus on April 26, 1415-1522 EST) were analyzed for the percentage of land area in seven 6°F temperature intervals. The percentages of the scenes were used to compute ET from each component. Also, the citrus grove scene was further divided into tall vegetation and short vegetation.

Three methods were investigated for calculating ET on a regional basis. All computed sensible heat flux density first, and then computed ET from the energy balance equation. The first was to compute a bulk aerial resistance ( $r_b$ ) from the ground truth sensible heat flux measurement, and from remote sensed surface temperature, and from air temperature. The values of  $r_b$  were applied to the surface-to-air temperature differences to compute H, and then regional ET.

The second method was to develop atmospheric stability-corrected heat transport coefficients to apply in the turbulent boundary layer above the grass surfaces. It was found that the temperature difference in the turbulent layer ( $\Delta T_t$ ) could be accurately calculated from the surface temperature to air temperature difference ( $\Delta T$ ). This  $\Delta T_t$  was then used in calculating ET by first calculating the sensible heat flux (H). The above procedure was applied directly to the April 28 pasture scene to compute ET from the ensemble of surface temperatures. For the citrus grove scene, a leaf-to-air resistance term from the literature was adapted for the tall vegetation.

The third method used integrated profile stability corrections. Accurate predictions from this method require the ability to determine the effective height of the heat source ( $Z_H$ ) to apply to the effective source temperature. Once this value was determined, the regional ET calculations were made for the pasture scene.

All three methods appeared to give consistent results. The first method is the simplest, but it does require sensible heat flux density measurements from a surface type to get bulk aerial resistance values. These values cannot be applied to other surface-types.

The second method and third method both require temperature profile measurements, and preferably, wind profile measurements.

In this study, we did not test methods for predicting net radiation,  $R_n$ , by remote sensed methods.

The methodology was tested only over short grass surfaces. The same type of methods should apply over other vegetated surfaces, but the specific parameters would have to be determined. One effect that we saw was that the temperature gradients near the short grass surfaces were very large, much larger than for tall vegetation (e.g., row crops and trees).

For this report we have not compared our results and data with simple predictive ET models. This comparison could be done in the future.

Future work is needed on other types of vegetated surfaces to better define effects of wind speed, stability, surface roughness, plant height, leaf area index, and soil moisture conditions on aerial resistances (and bulk stomatal resistance).

The use of remotely sensed surface temperatures does appear to offer a reasonable way to calculate regional ET from surfaces with a variety of temperatures. In the future, comparisons should be made between ET computed by relatively detailed surface temperature measurements and relatively large-scale pixel temperature measurements.

- 5.7-1 -

## 5.7 THREE-DIMENSIONAL AQUIFER MODEL

TABLE OF CONTENTS

	<u>Page</u>
5.7 Three-Dimensional Aquifer Model . . . . .	5.7-1

TABLES

<u>Table No.</u>	<u>Page</u>
5.7-1 Surface Flow model Parameters . . . . .	5.7-4
5.7-2 Groundwater Model Parameters . . . . .	5.7-6

SFWMD plans to develop a three-dimensional aquifer model to simulate the movement of water beneath Florida's southwest coast. In the first year effort under the Water Resources Management Project, this model was to be examined and its development guided to take maximum advantage of the latest remote sensing technology. This was to include a detailed examination of the various input parameters and identification of those amenable to measurement by remote sensing.

To date this model is still in the most preliminary stages of development. The basic equations describing surface and groundwater flow have been selected, but the actual model development is still in progress and the necessary parameters are only vaguely defined. Consequently, a detailed examination of the input parameters and a precise identification of those amenable to measurement by remote sensing could not be made. Instead, a somewhat limited evaluation of the application of remote sensing to the parameters already identified is presented. This brief treatment should be useful in guiding the development of the model to take maximum advantage of the latest remote sensing technology.

The basic equations and parameters for the Surface Flow Model and Groundwater Model are presented in Tables 5.7-1 and 5.7-2, respectively. These models will describe primarily horizontal movement of water over the surface and within the groundwater aquifer. Specific terms in the Surface Flow Model equations allow water to enter and leave the surface flow (e.g., rainfall, known flows, and pumpages) and to migrate from the surface to groundwater (e.g., infiltration rate). In the Groundwater Model, water entering and leaving the aquifer is described in a term  $W$ , which includes well withdrawals, rainfall recharge, evapotranspiration, and leakage to lower of higher aquifers.

Remote sensing is most applicable in defining parameters which follow the movement of water on the surface, in describing the areal extent of surface conditions (e.g., geology, drainage, vegetation) which might affect both surface flow and flow between surface and groundwater, and in locating direct evidence of links between groundwater and surface water (e.g., free-flowing wells, areas of good drainage). Radar sensors currently under development may soon extend this range below the surface.

The individual parameters amenable to remote sensing are indicated in Tables 5.7-1 and 5.7-2, together with the applicable remote sensing measurement and an evaluation of the feasibility of using the remote measurement as a substitute for the present data base. Since the Surface Flow and Groundwater Models are in a very preliminary stage, the feasibility rating must be considered quite tentative.

The feasibility evaluation contains three possible rankings. Only near-term feasibility is considered because of the great uncertainty in predicting long-term developments and because of the immediacy of SFWMD's need for this data. Near-term is taken to mean within the next decade. A ranking of one (1) indicates that the technique is presently available and need only be applied to this particular case. A ranking of two (2) means that the technique is currently under development, has shown considerable promise, and is expected to be widely available in the near future. Three (3) indicates that developing the technique will require substantial additional research, but is quite possible.

Basic Equation:

$$\frac{d(Av)}{dt} + \frac{d(BAv^2)}{dx} - B_r r \wedge T \cos \theta_r - B_L v q_L = gA \sin \theta_x - g \frac{d(Ah)}{dx} \cos^2 \theta_z - g A S_f$$

Parameters	Remote Sensing Measurement	Feasibility	Present Data Base
A Flow cross-section	area (water)	1	Maps or design diagram
v Velocity			Direct measurement: flowmeter
T Flow width	length (water)	1	Maps
h Flow depth	water depth/vegetation historical flooding	2 1	Stage records, topographic maps
S <sub>f</sub> Friction slope	a function of n, v and the hydraulic radius		Computed from n
g Gravitational acceleration			Known constant
n Manning's friction factor	vegetation	2*	Estimate based on vege- tation, soil, and other factors
B Momentum correction factor			Estimate based on geo- metry, usually 1.0
d Raindrop diameter			Estimate

1 - current 2 - highly probable (new sensors, some research)

\*Ancillary data required

3 - possible (new sensors,  
extensive research)

Surface Flow Model Parameters

Table 5.7-1

Parameters	Remote Sensing Measurement	Feasibility	Present Data Base
0 Angle of inclination			Field measurement or estimated from topographic maps
L Flow length	length (water)	1	Maps
K Roughness size	vegetation	2*	Estimate based on vegetation, soils, and flow depth
i Infiltration rate	vegetation, land cover, soil soil moisture	2* 3	Lysimeter, estimated from vegetation, soil, and landcover
Y Kinematic viscosity of water	temperature	2	Ground temperature measurements, interpolated
Λ Terminal velocity of raindrops			Estimate
r Rainfall intensity	cloud top temperature	2	Simulated from historical or statistical events
q Inflow or outflow rate			Known flows and pumpages

Surface Flow Model Parameters (cont'd)

Table 5.7-1

$$\text{Basic Equation: } \frac{d}{dx} \left( K_{xx} b \frac{dh}{dx} \right) + \frac{d}{dy} \left( K_{yy} b \frac{dh}{dy} \right) + \frac{d}{dz} \left( K_{zz} b \frac{dh}{dz} \right) = S \frac{dh}{dt} + W$$

Parameters	Remote Sensing Measurement	Feasibility	Present Data Base
K Hydraulic conductivity	soils	2	Analysis of field pumping tests, estimate
b Saturated thickness of aquifer	geology	1*	Borehole measurement, radioactive test, or geological information
h Head of groundwater		3	Direct measurement
x, y Coordinates of aquifer	geology	1	Maps
S Storage coefficient	geology	1*	Core sample or field pumping test
W Well withdrawal	free-flowing wells (water depth/vegetation)	2	Estimate based on measured water use
	free-flowing wells (temperature)	2	
Rainfall recharge	cloud top temperature	2	Estimate based on rainfall and soil
	soil moisture, soils	3	
Evapotranspiration	vegetation, temperature	3*	Pan evaporation
Leakance between aquifers	geology	2*	Estimate based on geology

\*Ancillary data required

1 - current    2 - highly probable (new sensors, some research)    3 - possible (new sensors, extensive research)

#### Groundwater Model Parameters

Table 5.7-2

- 5.7-7 -

If it appears that remote sensing could not be used to measure a parameter, a feasibility rating is simply not indicated. This material, including the selected parameters and feasibility ratings, will be provided to SFWMD to aid and guide them in developing the Three-Dimensional Aquifer Model.

- 5.8-1 -

## 5.8 LONG RANGE PLAN

TABLE OF CONTENTS

	<u>Page</u>
5.8 Long Range Plan . . . . .	5.8-1
5.8.1 Introduction . . . . .	5.8-4
5.8.2 Study Team Functions . . . . .	5.8-4
5.8.3 Team Meeting Results . . . . .	5.8-9
5.8.3.1 South Florida Water Management District - Study Meeting Results . . . . .	5.8-9
5.8.3.2 Southwest Florida Water Management District - Study Meeting Results . . . . .	5.8-10
5.8.3.3 St. Johns River Water Management District - Study Meeting Results . . . . .	5.8-10
5.8.3.4 Suwannee River Water Management District - Study Meeting Results . . . . .	5.8-11
5.8.4 General Findings . . . . .	5.8-11
5.8.4.1 Hydrology . . . . .	5.8-11
5.8.4.2 Water Use . . . . .	5.8-11
5.8.4.3 Environmental . . . . .	5.8-13
5.8.4.4 Climatological . . . . .	5.8-13
5.8.4.5 Data Base Management System . . . . .	5.8-14
5.8.5 Long Range Plan Conclusions . . . . .	5.8-14

FIGURES

Figure No.	Page
5.8.2-1 Major Study Meeting - South Florida Water Management District . . . . .	5.8-5
5.8.2-2 Major Study Meeting - Southwest Florida Water Management District . . . . .	5.8-6
5.8.2-3 Major Study Meeting - St. Johns River Water Management District . . . . .	5.8-7
5.8.2-4 Major Study Meeting - Suwannee River Water Management District . . . . .	5.8-8

### 5.8.1 Introduction

The final goal of the project was to develop a complete Water Resources Management Information System based on the latest state-of-the-art remote sensing and data processing technology and to demonstrate and then implement this system on the various Water Management Districts' computer hardware. To accomplish this goal, it was obvious that an indepth study would need to be made of several factors. First, the requirements for water resources data and existing as well as planned capabilities for storing and manipulating such data within all of the five Florida Water Management Districts would have to be documented. This effort would identify the needs for water resources data; the methods of gathering, storing, and using such data; as well as the identification of data needs that were not being supplied through the present system or being supplied inadequately. The IFAS would need to complete an academic study of the identified data and data processing needs to define the areas where IFAS expertise could be applied to help satisfy these needs along with a definition of an academic approach to the development of the Water Resources Management Information System. The NASA personnel would need to complete a review of all state-of-the-art remote sensing and data processing technology, existing and planned, to determine their applicability to satisfying the data needs previously identified. The results of these studies would be melded into a complete long range plan that would define the steps required to develop the Water Resources Management Information System. The plan would delineate the applicable remote sensing technology being developed, how it would be phased into the long range goals, and those remote sensing research or applications development tasks needed to supply the defined data needs.

### 5.8.2 Study Team Functions

The NASA and IFAS study teams, depicted in Figure 3.2-1, met with the various Water Management District personnel to define their data needs. Figures 5.8.2-1 through 5.8.2-4 depict the dates of the major planning meetings, the key Water Management District personnel involved, and the technical disciplines represented. After these major planning meetings between NASA/IFAS teams and the key Water Management District representatives, many other meetings took place between the individual NASA/IFAS team members and other representatives from the various technical disciplines within the Water Management Districts. Establishing, completing, and documenting the results of these various meetings was the responsibility of the Team Captains. The team captains kept their respective Project Coordinators apprised of these meetings and provided them with Memorandums for the Record documenting their meeting results.

It can be noted from the meeting dates shown in Figures 5.8.2-1 through 5.8.2-4 that all of the major meetings took place before June 1978. The early completion of meetings was required to provide information needed to develop the follow-on FY 1979 studies which were due to NASA in June and July. Since the IFAS contractual obligations did not begin until March 3, 1978, it was impossible to complete an indepth study of the Water Management Districts' needs in this short time. It will be noted that the Northwest Florida Water Management District was not included in the meeting results. Again this was due to the limited time available to complete the planning meetings.

## MAJOR STUDY MEETING

### SOUTH FLORIDA WATER MANAGEMENT DISTRICT

MEETING DATE: MARCH 6, 1978

#### KEY SFWMD PERSONNEL

B. Branner

J. Crews

W. Dineen

F. Davis

S. McCormic

J. Marban

A. Kreitman

B. Jenkins

J. Lynch

#### DISCIPLINE REPRESENTED

Operational Field Data

Permitting

Environmental Sciences

Water Chemistry

Land Resources (Mapping)

Water Resources (Hydrology)

Groundwater (Hydrology)

Data Management

Data Processing

Figure 5.8.2-1

## MAJOR STUDY MEETING

### SOUTHWEST FLORIDA WATER MANAGEMENT DISTRICT

MEETING DATE: MAY 5, 1978

#### KEY SWFWMD PERSONNEL

J. Butler  
Z. Palmer  
J. Wehle  
J. Thompson  
B. Perry  
H. Nguyen  
T. Holton  
B. Evans  
C. Miller  
E. Comer  
M. Johnson  
P. Hubbell  
B. Courser  
T. Rochow  
L. Bartos  
K. McKenney

#### DISCIPLINE REPRESENTED

Planning and Regulation  
Planning  
Water Resources  
Water Resources  
Technical Information  
Hydrology  
Program Development  
Permitting  
Resources Development  
Aerial Mapping  
Aerial Mapping  
Aerial Mapping  
Environmental  
Environmental  
Environmental  
Special Projects

- 5.8-6 -

Figure 5.8.2-2

## MAJOR STUDY MEETING

### ST. JOHNS RIVER WATER MANAGEMENT DISTRICT

MEETING DATE: MARCH 21, 1978

#### KEY SJRWMD PERSONNEL

J. Kubal  
B. Moresi  
C. Tai  
D. Winegardner  
K. Dennehy  
J. Barker  
L. Shapiro  
E. McCuller  
T. Owens

#### DISCIPLINE REPRESENTED

Water Resources  
Water Resources  
Hydrology  
Hydrology  
Hydrology  
Environmental  
Resources Planning  
Resources Planning  
Data Systems

5.8-7

Figure 5.8.2-3

**MAJOR STUDY MEETING**

**SUWANNEE RIVER WATER MANAGEMENT DISTRICT**

**MEETING DATE: MAY 12, 1978**

**KEY SRWMD PERSONNEL**

D. Morgan

R. Musgrove

K. Webster

D. Fisk

**DISCIPLINE REPRESENTED**

Executive Director

Planning

Water Resources

Hydrology

- 5.8-8 -

### 5.8.3 Team Meeting Results

The following sections depict the specific areas of interest as defined by each of the four Water Management Districts. The topics listed represent the basic information from which the FY 1979 follow-on studies were developed. They encompass primarily the remote sensing techniques development tasks, and/or studies that would lead to such tasks, that would eventually lead to techniques that would be able to provide data into the Data Base Management System. There were other general areas of discussion resulting in more common needs defined by the Water Management Districts that will be discussed in subsequent section of this report.

#### 5.8.3.1 South Florida Water Management District - Study Meeting Results

The following list depicts the results of the IFAS/NASA team meetings with the SFWMD in the definition of specific tasks to be undertaken during the FY 1979 period of the study.

##### a. Lake Okeechobee Volume Measurements

This need was a carry over from the FY 1978 study and was included to verify findings accomplished during that study. For a description of this task, see Section 5.1.

##### b. Improvement of Conservation Area Water Storage Information

This need was a carry over from the FY 1978 study and was included to test the algorithms developed during that study in the Conservation Areas 1 and 2. For a description of this task, see Section 5.2.

##### c. Overland Flow Measurements

This need was a carry over from the FY 1978 study and was included to allow IFAS to continue collecting flow data for a complete hydrologic season and to run the models with a complete newly developed Manning's N data set. For a description of this task, see Section 5.3.

##### d. Three-Dimensional Aquifer Model

This need was a carry over from the FY 1978 study and was included to develop and test remote sensing techniques in the actual Three-Dimensional Model. For a description of this task, see Section 5.7.

##### e. Land Use Mapping

The SFWMD is in the process of placing all of their land use data on a new Computer Vision digital mapping system. This task was to determine if LANDSAT could provide a viable means for economically updating this data base.

##### f. Data Collection Platforms

Many of the data parameters required by agricultural, hydrological, and environmental models cannot be supplied from the present state-of-the-art

remote sensing techniques. Therefore, a study was going to be undertaken to determine which of these parameters could be provided through DCP's.

g. Floridan Aquifer Study

The Floridan Aquifer provides the majority of the aquifer fresh water supply within Florida. However, little is known about this aquifer. During FY 1979, the USGS planned to begin an indepth study of the Floridan Aquifer. NASA and IFAS, through the SWFWMD, planned to cooperate with the USGS to determine how remote sensing could help define parameters concerning the Floridan Aquifer.

5.8.3.2 Southwest Florida Water Management District - Study Meeting Results

The following list depicts the results of the IFAS/NASA team meetings with the SWFWMD in the definition of specific tasks to be undertaken during the FY 1979 period of the study.

a. Flood Plain Extrapolation

A major requirement of the SWFWMD is to define the flood plains of water bodies within their district. At the present time about 30% of their district has been mapped using aerial photography at a very high cost. They were interested in determining if LANDSAT data could be used to map such flood plains to an adequate resolution.

b. Well Field Drawdown

Saltwater intrusion into the aquifer from extensive well field drawdown is a continuing problem in coastal zones. The SWFWMD has extensive historical well field drawdown data from which data could be derived to complete a study to determine if there would be a relationship between temporal LANDSAT land cover maps and the drawdown data.

5.8.3.3 St Johns River Water Management District - Study Meeting Results

The following list depicts the results of the IFAS/NASA team meetings with SJRWMD in the definition of specific tasks to be undertaken during the FY 1979 period of the study.

a. Upper St. Johns River Basin Study

This task involved the testing of a remote sensing data base in the newly developed Upper St. Johns Basin decision making model. Final expansion of this model would include environmental constraints, planning constraints, water supply functions and a hydrological model. It seemed like a good development test bed for the Water Resources Management Information System.

b. Oklawaha Hydrological Model

During FY 1979 the SJRWMD planned to develop a specific hydrological model for their Oklawaha River Basin. During this development stage NASA and IFAS would work with them to determine the data base requirements of the model and define techniques for supplying this data base.

#### 5.8.3.4 Suwannee River Water Management District - Study Meeting Results

The following depicts the results of the IFAS/NASA team meetings with the SRWMD in the definition of specific tasks to be undertaken during the FY 1979 period of study.

##### a. Floridan Aquifer Recharge

In the SRWMD the Floridan Aquifer is recharged through some of the lakes in the area due to the low piezometric head. Some of the lakes in the area perform a recharge function and others do not. Existing data indicates that there is a correlation between rainfall, lake level change, and recharge rate of the various lakes. Mapping of the lake surface areas from satellite data may be correlated with available rainfall data and lake stage data to develop a technique wherein satellite data alone may be used to determine which lakes recharge the aquifer and perhaps the recharge rate.

#### 5.8.4 General Findings

Aside from the specific remote sensing data base development and related study factors defined in the previous section, there were five major areas of concern that tended to be common to all Water Management Districts. These major areas of concern were the areas wherein the Long Range Plan would concentrate in developing means for meeting all of the common needs of the Water Management Districts which would culminate in a complete Water Resources Management Information System. A general discussion of these areas, including the findings to date, is included in the following sections.

##### 5.8.4.1 Hydrology

The most developed area of concern defined by the Water Management District is the area of Hydrology. This area would include surface water hydrologic models; aquifer water hydrologic models; water storage balance models for lakes, reservoirs, marshland storage areas, etc. These models and algorithms are used by the Water Management Districts to develop data concerning available water for water resources planning, operations, and regulation functions within their districts. The level of maturity of development in this area varies with respect to the age of the various districts. That is, some districts have well developed models that are currently being run on their own computers while other districts have not yet found a real need for hydrological models. The plan was to develop an area of commonality among the districts so that a general set of hydrologic models and algorithms could be used by all districts. The data gathering techniques to support these models and equations would be developed in parallel to the model development. Examples of such data support development can be seen in the previous section wherein the proposed FY 1979 tasks are described. These remote sensing data sources and other data sources, defined to support the hydrological models and algorithms, would then be included in the Data Base Management System, discussed in a subsequent section.

##### 5.8.4.2 Water Use

During the IFAS/NASA team meetings with the Water Management Districts, it was found that one of the major areas of need was information (i.e., data

and models) in the area of water use and/or water demand. The area of water use encompasses agricultural, urban, and industrial water needs. The importance of information in these various areas will depend upon the specific Water Management District's needs. However, in all cases it was obvious that there was a competition for water among these various groups with the agricultural water use area being one of the most critical areas in which information was lacking. This being the case, a proposed NASA/IFAS study, beginning in FY 1979, was defined to begin research to develop water balance, water demand, crop yield, and economic models for agricultural crops in Florida that are highly dependent upon water to provide a viable crop. Even though the need for data, models, etc., in the areas of urban and industrial water needs was not as great, it was obvious that further development was required in these areas to provide a complete water use inventory system. One of the more complex, and least known, areas of need concerning water use was found to be the ability to define the economic value of water in the three major areas of use: i.e., agricultural, urban, and industrial. To provide such information, it was obvious that an indepth study would be needed in each of these areas to develop economic models that could be used in conjunction with the water use models being developed.

An example of what would be involved in developing information for water use and economic data to model water was for one agricultural crop; i.e., pasture, is as follows:

a. Pasture Water Use

(1) Determine pasture water demand components by measuring rainfall, irrigation, runoff, drainage, and soil moisture status.

(2) Determine evapotranspiration rates, as function of atmospheric demand, forage species, soil water status, and management practices.

(3) Determine the relationship between evapotranspiration and forage yield and quality.

(4) Develop a predictive model for evapotranspiration and yield as functions of atmospheric demand, forage species, soil water status, and management practices.

b. Economic Models

(1) Determine the decision making strategies of individual irrigators in a study area regarding choice of particular systems and operation of those systems.

(2) Determine the investment and variable cost of irrigation system type.

(3) Determine, in quantitative manner, the impact of other cultural practices and input levels on the level of irrigation and irrigation strategies.

(4) Evaluate the impact of current institutional rules and regulations on water use.

Such a study would be required on each major irrigated crop within the state of Florida. However, within the IFAS organization a large amount of such data exists and more is being developed through their on-going water program which has been greatly expanded for FY 1979.

#### 5.8.4.3 Environmental

One of the least defined areas where information is required concerns the environmental area. Much of the water storage of surface freshwater for use within the state involves marshland areas. The storage of water in these areas cannot only affect the quality of water stored therein, but the storage of water in such areas can have a dramatic effect on the ecosystem of the marshlands. Therefore, research needs to be completed to develop environmental models that could be used to determine in advance what water storage in marshlands would do to the ecosystems. The University of Florida Center for Wetlands, through work with the St. Johns River Water Management District (SJRWMD), has begun to define an environmental study. This task involves a study area called the Jane Green Swamp, a presently un-impounded marshland area, with an existing impounded area, the Taylor Creek marshland area. Plans are for the University of Florida to accomplish a one-year study of these areas. After this time they felt that they would have enough information to define a joint University of Florida/NASA study for the development of a marshland environmental model that could use remote sensing as a major portion of its data base.

There were other areas within the scope of environmental data and model needs identified that required further study to better define the needs. These include water quality modeling which would be attached to the current hydrological models. These models could be used to determine the impact of urban development, industry, and agriculture on water runoff and storage quality. Proposed studies in this area include examining the Hydrocomp, Hydrologic Simulation Program FORTRAN, water quality model developed for EPA to determine if it could be used to model water quality for typical Florida runoff and storage conditions.

Another area of environmental study identified was the impact of well field drawdown. An initial effort in this area was defined in the well field drawdown study defined in the task described in a previous section.

#### 5.8.4.4 Climatological

Two climatological factors, evapotranspiration and rainfall, were identified as the most critical in all of the modeling efforts and for which present data sources provide a very inaccurate data base which produces poor results in water balance and water use equations. The development of remote sensing techniques to provide an improved data base for these two important factors was started under the FY 1978 study project. However, these efforts were considered only a feasibility study phase and a more indepth study for these areas was proposed for the FY 1979 study period.

A description of these important areas of research will not be included in this section since they are adequately discussed in subsequent sections concerning the results of the FY 1978 studies.



#### 5.8.4.5 Data Base Management System

A flexible computer oriented data base to provide timely data for the various models, etc., discussed above, was defined by all of the Water Management Districts as a prime need. The development of the Water Resources Management Information System (WRMIS) data base was started through the meetings with the various WMD's and through the remote sensing techniques developed tasks. Studies of existing NASA data base management systems: e.g., AOIPS and IBIS, were started to determine if an existing system could be used or if a new system would need to be developed due to the extensiveness of the data base and the need for it to include remote sensing data and ancillary data of point source type, areal type, and time series variable. One of the major areas of study proposed for FY 1979 through an effort by a Kennedy Space Center contractor, Computer Sciences Corporation, was a continuation of this effort to develop a Data Base Management System. This effort would have included the review of all applicable commercial data management systems; e.g., Hydrocomp's HSP11, COMAC, etc.; as well as other systems developed through NASA. The study would have also included the evaluation of applicable computer hardware for operation of the data base including main-frame systems versus multi-mini systems. The study would include an evaluation of existing and proposed expansion of each WMD's computer system to assure that the data base could be used by all districts.

#### 5.8.5 Long Range Plan Conclusions

The above results of the meetings and studies concerning the development of the Long Range Plan consist of a status report on this task. As mentioned in the introduction to this report, the carry over FY 1979 and subsequent year's efforts on the project were not funded by NASA Headquarters, therefore the effort to develop the Long Range Plan was brought to a close in August of 1978.